UNIVERSITY OF CAPE TOWN

Department of Mechanical Engineering

RONDEBOSCH, CAPE TOWN
SOUTH AFRICA

Dissertation Presented for the Degree of Masters

MAY 2022

Flexible Media Polishing Machine for Ti-6Al-4V Components

Quintin Oliver de Jongh, BsC(Eng) - UCT

SUPERVISOR: *A/Prof Ramesh Kuppuswamy*

Body Word Count: 40030

Plagiarism Declaration

1. I know that plagiarism is wrong. Plagiarism is to use another's work and pretend that it is one's own.
2. I have used the IEEE (The Institute of Electrical and Electronic Engineers), convention for citation and referencing. Each significant contribution to, and quotation in, this report / project from the work(s) of other people has been attributed and has been cited and referenced.
3. This report/project is my own work.
4. I have not allowed and will not allow anyone to copy my work with the intention of passing it off as his or her own work.
5. I know the meaning of plagiarism and declare that all the work in the document, save for that which is properly acknowledged, is my own. This thesis/dissertation has been submitted to the Turnitin module (or equivalent similarity and originality checking software) and I confirm that my supervisor has seen my report and any concerns revealed by such have been resolved with my supervisor

Signature: _____

Declaration of Free License

I hereby:

(a) grant the University free license to reproduce the above thesis in whole or in part, for the purpose of research.

(b) declare that:

(i) the above thesis is my own unaided work, both in conception and execution, and that apart from the normal guidance of my supervisor, I have received no assistance apart from that stated below;

(ii) except as stated below, neither the substance or any part of the thesis has been submitted in the past, or is being, or is to be submitted for a degree in the University or any other University.

(iii) I am now presenting the thesis for examination the thesis for examination for the Degree of Masters.
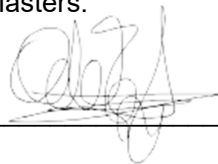
Signature: _____

Table of Contents

Table of Figures

Table of Tables

Definitions, Acronyms & Nomenclature

Acicular – needle shaped crystallites or grains

Analytical – derived purely through mathematical reasoning (scientific or on historic results)

Asperities – rough, sharp or rugged surface projections

Ductile Regime Polishing – flattening of asperities in ductile conditions (no brittle fracture or failure of asperities occurs)

Empirical – obtained from data and observations (current results)

Fatigue Life – number of stress cycles a specimen can sustain before fatigue failure occurs

Flexolap – mechanical polishing by use of a constant stream/jet of flexible abrasive media impinging upon a workpiece over time (the shortened name for flexible abrasive assisted polishing process).

Friability – tendency of a solid substance to break into smaller pieces under contact

Martensitic – containing a large amount of hard steel crystalline structure (martensite)

Porosity – amount of void space in a material

Radius of Curvature – radius of circular arc that best approximates the curve at that point

Rapid Prototyping – fast fabrication of assembly/part, often by use of 3D modelling and Additive Manufacturing

Residual Stress – stresses remaining in a solid material after the original cause of stress has been removed

Shear Modulus – material response to shear deformation, the ratio of shear stress and shear strain

Viscoelastic – property of materials that exhibit viscous and elastic characteristics when undergoing deformation

Acronyms and Definitions

Al-Cr-N – Aluminium – Chromium – Nitrogen (alchrona)

AM – Additive manufacturing

ANOVA – Analysis of variance: statistical method seprating observed variance data into different components to use for additional tests

AWJSM – Abrasive water jet slurry machining: a machining process using a low-pressure jet of abrasive slurry to machine features such as holes and channels

BSE – Back scatter electrons: high-energy electrons from the electron beam (in microscopy) that are reflected out of the specimen volume by elastic scattering interactions with specimen atoms

CFD – Computational fluid dynamics: a branch of fluid mechanics using numerical analysis and data structure to solve problems involving fluid flow

DMA – Dynamic mechanical analysis: a technique where a small deformation is applied to a sample in a cyclic manner and allows for the study and characterization of materials

FEA – Finite element analysis: a mathematic, numerical technique to solve differential equations arising in engineering and mathematical modelling

FRL – Filter – regulator - lubricator

H2O2 – Hydrogen peroxide

HV – Hardness (Vickers)

KV – Kelvin Voigt

MAB – Micro abrasive blasting: a refined form of sandblasting where air and abrasives are mixed and projected in a focussed stream

MEMS – Micro electro-mechanical systems

MRR – Material removal rate
FEM – Finite element method: defined as FEA above

NNS – Near net shape: the initial manufacturing technique of a product is close to the final shape and the part requires less post processing/finishing to achieve dimensional accuracy

PA6 – Polyamide 6 (plastic)

PCD – Polycrystalline diamond
CVD – Chemical Vapor deposition: a widely used processing technology where thin films are formed on a heated substrate via a chemical reaction of gas-phase precursors

PCM – Planetary centrifugal mixer: a device causing agitation of materials without using agitator blades

Ra **– Mean of all absolute profile deviations from centreline**

$Rymax$ - **Largest peak height or lowest valley depth**

Rz – **Absolute peak to valley average of five highest peaks and five lowest valleys**

SEM – Scanning Electron Microscopy: using a focussed beam of electrons to scan a sample surface and produce a high-resolution image showing information on material surface composition and topography

SiC – Silicon Carbide

SLM – Selective Laser Melted (additive manufacturing process): a 3D printing technique using a high-power density laser to fully melt and fuse metallic particles

SLS – Selective Laser Sintered (additive manufacturing process): similar to SLM but particles are sintered and parts are more commonly polymer-based

TEM – Transmission Electron Microscopy: similar to Sem but uses transmitted electrons rather than reflected or 'knocked-off' electrons

EM – Electron Microscopy: comprising of all electron microscopy techniques

OHL – Overhung Load

Ti-6Al-4V – Alloy of 90% Titanium, 6% Aluminium and 4% Vanadium

Ti-Al-N – Alloy of Titanium, Aluminium and Nitrogen

UV - Ultraviolet

WC-Co – Tungsten Carbide

Nomenclature

δ - **deformation**

ω - **deformation**

σ – **contact stress**

F_{imp} – **impinging force**

R – **abrasive radius**

m_{abr} – **abrasive mass**

ρ - **density**

t – **contact time**

H_R – **hardness ratio**

v – **Poisson's ratio**

S_y – **Yield Strength**

d_c – **depth of cut**

E – **Elastic modulus**

$\omega(V)$ – **deformation as a function of velocity**

V – **impinging velocity**

α – **arc angle**

$\emptyset$ - **diameter**

C_B – **centre-centre distance**

L_B – **belt length**

c – **damping coefficient**

k – **spring stiffness**

x – **deformation in the x axis**

ω_n – **natural frequency**

ω_d – **damped frequency**

ξ – **damping ratio**

Acknowledgments

Abstract

New-age components (notably those in the bio-medical and aerospace industries) are often manufactured from hard to machine materials such as Ti-6Al-4V and tungsten carbide and have extreme surface finish requirements. Flexolap polishing offers a technique to achieve these requirements, and minimizes the disadvantages encountered by other polishing techniques. The aim of this dissertation is that of designing and developing a working Flexolap polishing machine (and associated abrasive compound) suitable for the South African manufacturing industry (and any industry with a lack of financial means and skills for advanced manufacturing). This aim was affirmed by developing models to characterize the Flexolap polishing process, as well as by using experimental analysis to verify the process viability and compatibility with Ti-6Al-4V (and subsequently, other easier to machine materials).

A thorough literature review is presented with the most important conclusions of optimal polishing conditions (high hydration, high media impinging velocity and a 45º polishing angle) and applicable modelling methods (momentum, critical values, and vibrational analysis).

Two models (empirical and analytical) and a supporting simulation model are presented for force control and stipulation of required conditions for ductile regime polishing to occur. A third model is presented later in the dissertation and classifies the viscoelastic nature of the designed abrasive as well as its damping effect as the compounded media is hydrated (the media-workpiece interaction becomes more underdamped). The results of all modelling processes provide proof that effective polishing can be achieved at designed working conditions (times of less than 10 minutes to desired surface roughness and contact stresses less than that for brittle failure but greater than that required to induce ductile regime polishing).

The process of creating/building the Flexolap machine is described through design and development. Process calculations to support design include belt and pulley calculations, bearing calculations, steady abrasive/air flow calculations and weld strength calculations.

Experimental techniques include gathering force data (using a dynamometer) and finding surface properties (using a profilometer and various microscopes). This led to gathering a large set of results which were used to study the process viability. Analysis is based on surface roughness and texture change over time (or change over other parameters), as well as the changes in force over parameters such as media hydration, media diamond concentration and media velocity.

Experimental results display trends of polishing forces decreasing with an increase in hydration, while surface roughness decreases in a logarithmic manner (with a great initial decrease before reaching a convergence point). Surface texture is also shown to improve with

a lesser presence of asperities and a more uniform texture overall (with greater hydration levels). Higher impinging velocities lead to lower surface roughness being achieved quicker while higher diamond concentration tends to create higher roughness at higher impinging velocities. Medium-high media hydration (30%), higher impinging velocities (31.4 m/s) and a polishing angle of 45º are proven to be the most effective polishing conditions.

The study was successful in proving the viability and effectiveness of the Flexolap polishing technique while also providing pertinent experimental and theoretical data towards the further study of the process.

The expected benefits the outcomes of this study provide to industry are: an easy to learn finishing process that can easily integrate into a finishing or manufacturing workshop (thus upskilling operators), an efficient and cost effective means of polishing hard to machine materials (reducing cycle time and cost), and a framework of polishing machine that can be easily adjusted to meet industry needs for example: size/shape of workpiece and automation of the process. This study was embarked on due to the lack of inexpensive and easy to operate polishing methods available in South Africa, particularly because raw titanium is often exported for processing due to the low availability of advanced manufacturing equipment for the material in South Africa as well as the low level of operator experience in advanced manufacturing machinery.

Keywords: Polishing, Flexible Abrasives, Finishing Operations, Advanced Manufacturing

List of Publications

Throughout the course of this dissertation, a significant number of publications were produced. These are listed below in the form of journal papers and conference papers.

Journal Papers:

- A study on intelligent grinding systems with industrial perspective (International Journal of Advanced Manufacturing Technology) doi: 10.1007/s00170-021-07315-9 - published

- Polishing of a Selective Electron Beam Melting Processed Tungsten Carbide Punch through High Velocity Impinging of Flexible Media (Journal of the Brazilian Society of Mechanical Sciences and Engineering) doi: 10.1007/s40430-022-03543-6 – published

- Spring-Dashpot Vibrational Model for the Investigation of Viscoelasticity in Gelatinous Abrasive Media and Subsequent Control of Parameters for the Flexolap polishing of Ti-6Al-4V Alloy (International Journal of Advanced Manufacturing Technology) doi: 10.1007/s00170-022-09863-0 - published

Conference Papers:

- A Force Controlled Polishing Process Design, Analysis and Simulation Targeted for the Selective Laser Sintered Aero-Engine Components (COMA 22)

- Research Endeavours Towards Development of an Intelligent Grinding System (COMA 22)

- Towards configuration and development of an AR enhanced IGS for Ti-6Al-4V alloy (COMA 22)

Chapter 1 - Introduction

1.1. Background

In a rapidly evolving engineering world where components require finer tolerances and higher precisions than ever before, manufacturing sciences are required to keep pace with expectations. These stringent requirements are put in place so that components can be used in critical assemblies with the longest life possible. The most notable industries requiring such great precision are that of the biomedical, aerospace, and automotive industries. A key step in achieving the correct dimensions are the finishing processes associated with advanced manufacturing (plating, grinding, and polishing, to name a few). Of these, the polishing process is often the last, as it is possible to achieve surface roughness levels of less than 0.1 µm [1] with a mirror finish and smooth surface texture.

The requirement for near net-shape (NNS) manufacturing leads to additive manufacturing (AM), which allows for rapid evolutionary prototyping and testing as well as producing complex shapes out of materials that are notoriously difficult to machine by conventional methods. Material wastage is minimal and post manufacturing can be greatly reduced through AM. This does not come without its detriments though, as AM techniques can leave undesirable features such as porosity, relatively poor surface finish and a relatively high roughness. Multiple challenges exist in the control of AM/SLS produced components with some of the main challenges on geometrical deviation and surface quality come from STL (stereolithography) file quality and powder layer thickness [2]. Powder layer thickness is directly related to what is commonly known as the 'staircase effect' on side wall surfaces [2]. Using thinner layers can aid in better surface integrity but this extends manufacturing time. Low quality 3D models can cause chordal deviation to the STL file and a bad quality print [2]. Other settings and errors such as process parameter settings, machine errors and material shrinkage bring deviations in geometric consistency as well as surface finish [2].

Ti-6Al-4V, a common component used in aero-engine components, is often produced by SLS/SLM followed by a polishing process [3], and is a great example of AM used in industry where post processing is required. The additional process (polishing) is required to meet the stringent criteria of dimensional and form accuracy, as well as surface integrity [4]. Materials used in the above state industries are often of high hardness and strength. This presents unlimited challenges to the polishing process, which need to be overcome by scrutinous process design and experimentation.

Various polishing techniques exist and while most allow for fine tolerances to be achieved, they are either notably high in cost, require a large amount of operator experience, can only polish simply shaped surfaces, are limited in workpiece-material compatibility, or the process

parameters are not easily controllable. Methods of polishing Ti-6Al-4V include electrolytic, chemical, and mechanical polishing. Chemical polishing involves the use of a chemical liquid to dissolve the oxide layer on the surface and can achieve a surface roughness of less than 1 μm, however, it is difficult to control the process [5]. Electrolytic polishing can achieve a surface roughness of less than 10 nm, but it too is difficult to control, and it is hard to find the exact process parameter values suitable for specific materials. Mechanical polishing is commonly used in industry as the process is simple to implement and does not require an in-depth background in engineering/materials science. Many mechanical polishing processes do not allow for the polishing of complex shapes though.

1.2. Problem Statement

This dissertation concerns the design, development, and characterisation of a flexible abrasive assisted polishing process (Flexolap) for polishing SLS/SLM manufactured Ti-6Al-4V components, and endeavours to produce predictable process outputs by controlling polishing forces through the easily adjustable parameters of media impinging velocity, media hydration levels, size of diamond abrasives in polishing media, and polishing time.

A recently developed polishing technique, known as "Aerolap" (or Flexolap) polishing, has the favourable advantages of low abrasive cost (abrasives can also be reused), fast processing time, ability to polish any complex surface, and a quick learning curve for the operator (minimal operator experience is required). However, many of the process parameters and polishing mechanisms have not been fully investigated yet. To provide a viable finishing technique to industry, it is vital that the process be characterized, and a model created, so that the process can be implemented assuredly and so that workpiece polishing will result in a uniform low surface roughness (mirror finish of less than 0.1 μm) over a short period of time (20 minutes or less) [4]. Notably, this will allow operators to spend much less time on determining the correct process settings to achieve the ideal surface roughness/finish [1].
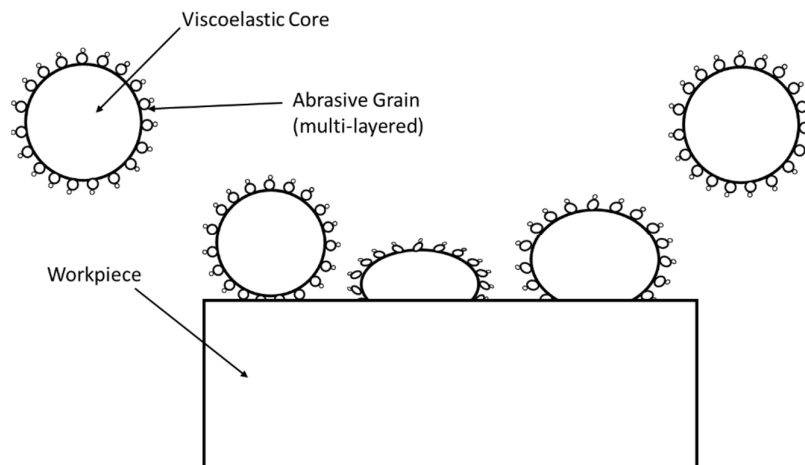
Figure 1 - *Flexolap Polishing Simplified Overview*

Aerolap/Flexolap polishing references the process of firing a viscoelastic core coated in an abrasive grain towards a workpiece (whereas conventional blasting methods use only an abrasive as the polishing media, which is often not viscoelastic). Figure 1 shows a brief (magnified and non-proportional) overview of the Flexolap polishing process. The use of viscoelastic abrasive cores is advantageous since controllable and elastic deformation occurs when media impacts workpiece. The ability to have a large deformation upon impact allows for a distribution of force over a greater area meaning less contact stress (allowing for more strenuous process conditions to be designed without damaging the workpiece) as well as a greater occurrence of micro-interactions between abrasive grains and workpiece asperities (improving polishing time) [6]. The elastic nature of deformation means that the media retains its shape and size after impact and can thus be recycled without redesign of the process parameters.

The foundations allowing for the continued development and specialized research into process were laid by the studies of Kuppuswamy, Ozbayraktar and Saridikmen [4], who investigated the Flexolap polishing of poly-crystalline diamond inserts; and separately by Razali [1], whose outputs of polishing stand-off distance and impinging angle as well as investigations into abrasive media types and abrasive hydration, have allowed for a focused scope of research. Flexolap polishing is a relatively new process (with first mentions of the process appearing in literature between 2004 and 2006) and literature is limited to an extent. However, more detail into the process and insight from previous studies and researchers is presented in the Chapter 2: Literature Review, Flexolap Polishing Background and Previous Developments.

This project research includes but is not limited to design, development, experimentation, analysis, and simulation, has taken place at the Advanced Manufacturing Laboratory (AML) and Centre for Materials Engineering (CME), both located at the University of Cape Town, South Africa. Data acquisition equipment and experimental equipment were provided by both AML and CME.

1.3. Project Impact

Understanding the significance of project outputs is vital to the determination of research objectives and scope, as well as to how research should be made available. This project is multi-faceted in the manner of how results are measured and observed, influencing both the advanced manufacturing (AM) and industrial manufacturing industries. In addition to these industries, results directly impact research into materials (notably Ti-6Al-4V) and the implementation of these materials into advanced sectors.

South Africa is the second largest producer of titanium bearing minerals in the world (after Australia), standing at 22% of the world's production [7], but much of this is not manufactured directly into usable goods in South Africa (in turn hurdling economic growth). Lack of processing/manufacturing equipment for Titanium (slow structural transformation) as well as the lack of skilled, qualified, and experienced individuals accounts for the decision to export materials [8]. It should also be noted that markups in South Africa are considerably higher than those of other comparable industries worldwide and they do not appear to be declining [9].

The South African precision engineering and advanced manufacturing industry is a fraction of the size it could be with a constant deterioration since 2001, particularly due to the inadequate use of information and communication technology and the lack of skilled workers in the industry [10]. Advancing industries that will directly allow the country to produce complex components from raw materials will benefit economic growth and aid in the development and subsequent retention of skilled workers. Research into Flexolap polishing and manners of implementing it in industry are important in achieving the economic growth desired from manufacturing.

As stated previously, additive manufacturing techniques of producing Ti-6Al-4V are becoming more common in industry. Ti-6Al-4V is biocompatible with bone and gingival tissues and most notably, it is capable of osseointegration, allowing the alloy to be used as a dental implant for lost teeth [11]. Titanium alloys, due to their high strength-to-weight ratios (strengths as high as steel with a density of 40% that of steel [12]) and high corrosion resistance (it can serve up to 15 times longer in seawater than steel) [13], are very desirable in engineering applications. Studying the effects of polishing AM produced Ti-6Al-4V samples will allow for a better understanding of the mechanical properties, how they can be manipulated to produce desired components and how microstructural changes are affected due to manufacturing techniques (both surface grinding and Flexolap polishing in this case).

1.4. Objective and Scope

This dissertation aims to show completion of the following objective:

Designing, and subsequently developing, a Flexolap polishing process (along with its associated media and machine) to complete characterization experiments on SLM produced Ti-6Al-4V components, to further research in the Flexolap polishing field.

The scope of the project (means of achieving the main objective) includes the following tasks:

- To characterize and build a model for the Flexolap polishing process (specifically for the polishing of the Ti-6Al-4V material), by use of process modelling tools (analytical and empirical), simulation and the fundamentals of contact mechanics.

- To determine a suitable abrasive media that is effective at carrying out the polishing process (sufficient flexibility and stiffness at working impinging velocities) and is both economical and environmentally sustainable.

- To design and develop a machine that can carry out the Flexolap polishing process and impart ductile regime polishing conditions upon Ti-6Al-4V samples. This machine should also be easily incorporable to the manufacturing industry.

- To develop and implement an experimental procedure to determine the effects of impinging velocity, polishing time, media water content, and media diamond concentration on the surface roughness, surface texture and microstructure of Ti-6Al-4V while being polished.

- To highlight the effects of the previously stated input parameters on in-process variables (notably polishing force and residual stress).

- To compare the Flexolap polished surface of Ti-6Al-4V samples to that of surface ground Ti-6Al-4V and to that of SLM manufactured Ti-6Al-4V.

- To develop an empirical model for process outputs (notably surface roughness and media flexibility) based on obtained experimental results.

The above stated scope can be summarised as follows: modelling, simulation, and characterization of the process; design and development of a Flexolap polishing machine and associated media mixing device; abrasive media characterization and selection; design of experiments to determine the above-mentioned effects; conducting the designed experiments; analysing results and creating conclusions; adding more detail to the model based on empirical findings.

1.5. Project Organisation

This dissertation contains nine chapters, each of which are introduced and summarised below.

- Chapter One (Introduction) – The dissertation and project details are described, and the Flexolap polishing process is briefly introduced. The impact the project has on research/academia and industry is stated along with the objective of the project and what the scope is limited to. The dissertation format/organisational structure is described and finally the relevant research questions are shown.

- Chapter Two (Background and Literature Review) – A thorough background to the process and related processes/research is detailed in this chapter alongside a detailed literature review. Previous and current research describing the details pertaining to Flexolap polishing, machine design, contact mechanics, abrasive media selection, additive manufacturing, Ti-6Al-4V, and methods of process modelling are the focus of this chapter.

- Chapter Three (Process Modelling) – The different methodologies of Flexolap polishing process design and modelling are elaborated in this chapter. The three methods (analytical, empirical and simulation) used for characterization are explicitly defined and initial results are presented.

- Chapter Four (Machine Design and Development) – The process of machine element design for individual components and the entire assembly is detailed in this chapter. The machine development, value additions, and process of assembly/building is explained in this chapter too.

- Chapter Five (Abrasive Media Selection) – The choice of abrasive compound is described in this chapter by means of engineering design, logical reasoning, and suitability to the process. Other available choices are specified, and comparisons are made.

- Chapter Six (Experimental Design, Set-Up, and Procedure) – The manner in which experiments were designed (DOE) is elaborated in this chapter. The physical set-up of experimental conditions and data collection as well as the designed procedure and carrying out of experiments is described too.

- Chapter Seven (Pre-Experimental Results) - Initial process characterization and affirmation of design.

- Chapter Eight (Experimental Results) – In this chapter, a comprehensive set of results is shown, describing the outcomes of polishing force, surface roughness, surface texture and optimal polishing conditions, and their relationships to controllable polishing parameters (impinging velocity, diamond grit size, polishing time, and media hydration levels).

- Chapter Nine (Vibrational Model) – A model developed for the characterization of abrasive media flexibility and how media hydration affects the interaction between abrasive and workpiece.

- Chapter Ten (Discussion) – Additional remarks relating expected results from process modelling and design to experimental results as well as information that is drawn from the project overall, is described in this chapter.

- Chapter Eleven (Conclusions) – The deductions of the overall dissertation and a summary of key results is presented in this chapter.

- Chapter Twelve (Recommendations) – In this final chapter, recommendations on how the project and process can be further improved are detailed as well as prospects and where the project may lead.

The figure below (Figure 2) provides a summary and roadmap to the content of this dissertation.
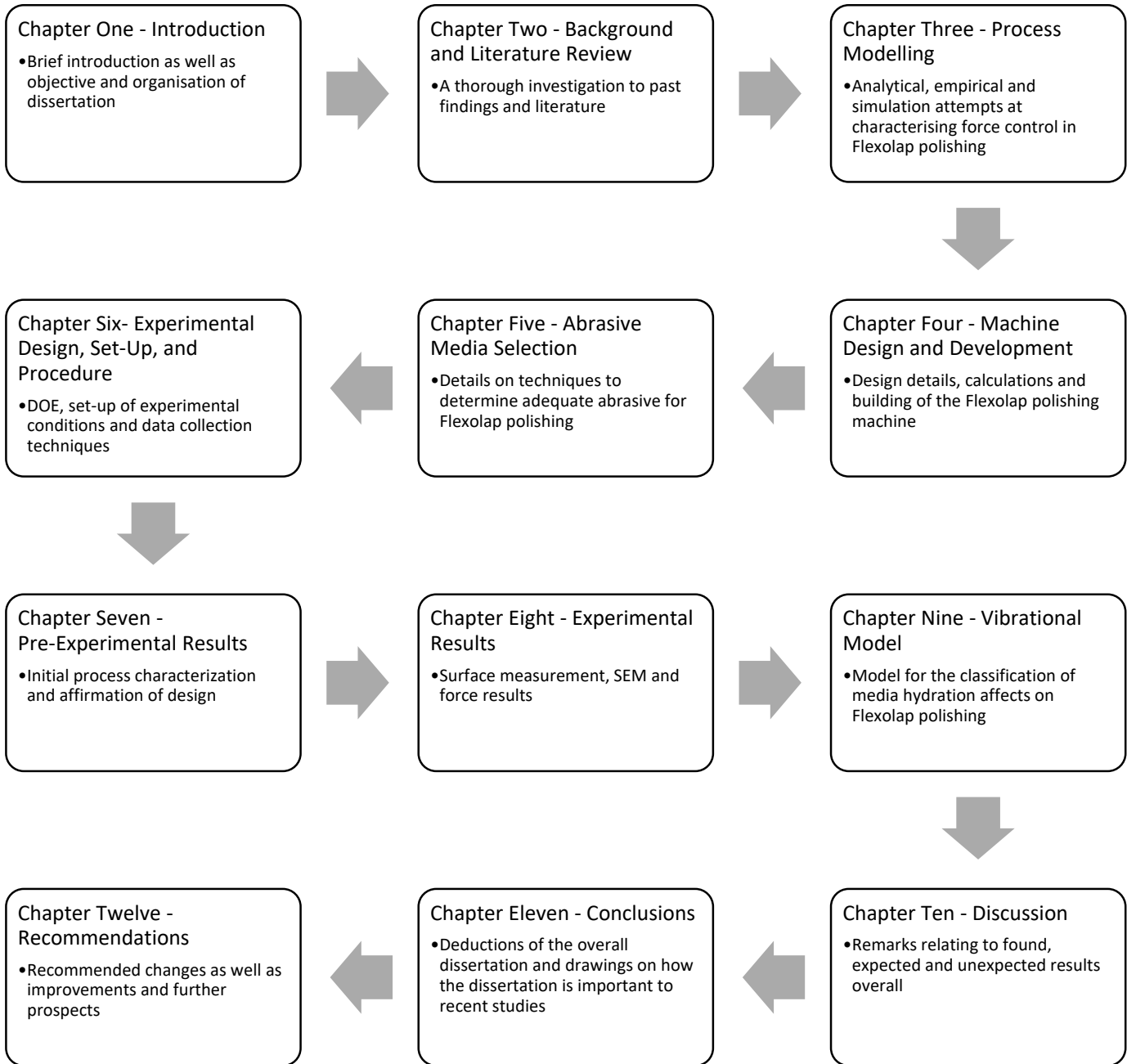
Figure 2 - Project Organisation Flowchart

Chapter 2 – Background and Literature Review

2.1. Flexolap Polishing Background and Previous Developments

Flexolap polishing uses media consisting of a viscoelastic core, coated with abrasive grain materials (often diamond and SiC) [14] [15] [16] [17]. The polishing media is projected towards the workpiece by the centrifugal force of a spinning impeller combined with compressed air. The abrasive media exits the impeller at a specified velocity and travels a short distance before colliding with the workpiece. At this collision point, the media deforms and mitigates its impact energy as the media slides along the work piece surface [1]. After a certain number of collisions, a mirror finished surface is produced. The process is considered clean because the media is hydrated and thus dust and chips adhere to the media. If the polishing is completed successfully, the surface roughness of the component will be much less than that of a surface ground component. Figure 3 below shows a schematic diagram of the described Flexolap polishing system with recycling of media.

Figure 3 – Basis of Flexolap Polishing and Recycling Method

Traditional lapping and polishing techniques, where the workpiece must be kept still or contain uncomplex shapes and profiles [18], are not desirable in industry, while techniques such as electropolishing induce tensile residual stresses on the components (in turn, reducing fatigue life) [19].

The Flexolap/blast polishing process is not restricted by workpiece shape or profile and does not require a high level of operator skill or a large amount of time. These are all attractive characteristics for a mainstream industrial process. Importantly though, the process has not been fully characterized yet, condition optimization (as well as process prediction) has not been completed. Nickel powder blast polishing is already being used to finish aero-engine components, as it allows for controlled polishing forces (by the induction of repelling charges from nickel present on the workpiece), however, the polishing media cost for this process is high [4].

Razali [1] has done a substantial amount of research regarding Aerolap polishing, namely how the controllable attributes of the polishing process: media injection speed, media injection angle and media water content, affect the surface being polished. This includes effects on surface roughness and surface morphology. Surface hardening as well as polishing characteristics were investigated as well. Razali's research focussed mainly on the polishing of a drill flute surface. It should also be noted that Razali [1] describes the method of adding water to polishing media and the subsequent methods of measuring the media's associated mass and modulus of elasticity. In addition to this, the polishing experimental setup is described (as well as the intricacies of the process) and how the injection speed, impact force and polishing conditions are measured.

Significantly, Razali [1] concluded that if the only output required from the process is a smooth surface (a low value of surface roughness), this can be achieved easily by blasting abrasives at the highest output velocity (56 m/s in his case), most force balanced impact angle (45 degrees) and with the middle level of water content (30%). However, to achieve optimal surface parameters, such as desirable surface texture and minimal residual stress values, the process needs to be individualized and optimized for each specific surface purpose. As stated by Razali, the rake face requires a more textured surface while the flank surface should be as smooth as possible. Much of Razali's work is included in the three reports submitted to the Journal of the Japan Society for Abrasive Technology, which are described in detail in this literature review.

Based on the notion of sandblasting and shot peening, Flexolap polishing, or "Aerolap" polishing become popular around 2005. Kitajima and Yamamoto [20] detailed deburring methods and their trends in Japan around this time. They noted that edge standards in workpieces were not introduced until the year 2000 (ISO13715) and this did not precisely define edge quality either. JISB0721, a standard for "edge quality and its grades for material removal parts" [21] was only implemented in 2004. This explains the notable increase in demand for deburring/polishing technologies around that time, as well as the rapid development of blast polishing and its widespread dissemination in the manufacturing community. It should be noted that JISB0721 defines edge quality by three characteristics: surface texture, surface integrity and edge size. Surface texture includes the surface contour, macro effects and geometry of the edge. Surface contour can be further divided into size and form accuracy as well as roughness, while macro effects include laps and folds, craters and pits and other imperfections. Geometry of the edge is defined as its tolerance. Surface integrity has more to do with the material properties of the workpiece, including residual stress, plastic deformation, micro-structural transformations, micro cracks, and material inhomogeneity [20]. Kalpakjian and Schmid [22] elaborate on surface texture in a similar manner to this.

Kitajima and Yamamoto also noted the difficulty in selecting an appropriate deburring method (with workpiece size/shape/material, desired edge/surface quality, and machining and equipment cost all factoring into decision making). After some research they showed that blast polishing removes the unevenness in the cutting edge, forming a sharp tool and of course, creating a mirror finish on the adjacent tool surface. In a separate paper they also showed that blast polishing deburring performance and sharp edge creation is outstanding compared to other conventional deburring techniques [16].

Minaki et al. [23] studied the effects of dry blasting on the improvement of stainless-steel surface texture in 2006 and used a blasting machine very similar to the Aerolap polishing machines developed later. This machine was developed for plating base treatment before the workpiece would undergo high vacuum ion plating. Figure 4 is a diagram of the device, which shows many similar characteristics to the blast polishing devices seen today. The blasting process was used to improve fatigue and wear resistance. They found significant results in how the blasting process affects the plating process; noting that adhesion work increases as injection time and distance is increased and as injection distance is decreased. Adhesion work generally increases as surface roughness (Ra) decreases and thus the above stated findings show a decrease in surface roughness as those variables are respectively changed.
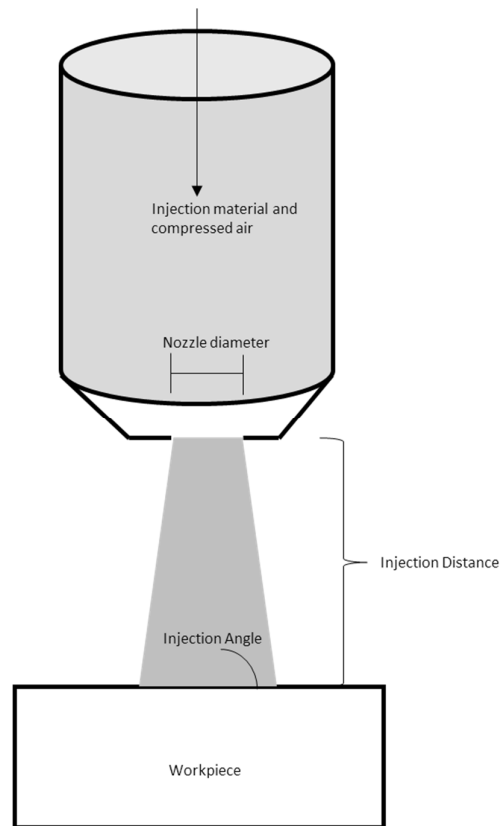
Figure 4 - Blasting Device for Pre-Treatment of Plates

Three reports were produced for the Journal of the Japan Society for Abrasive Technology [6] [24] [25], wherein the authors studied various different polishing factors influencing the surface condition of cemented carbide. The objectives of the studies were to describe and clarify the controlling process parameters for the Aerolap polishing process, with the aim of improving process efficiency and optimizing the process conditions (such as polishing time, surface roughness and operator experience). The clarification of parameters was important as the process had been implemented in industry at the time without an in-depth knowledge of process control. The researchers used multi-cone (a viscoelastic core of similar nature to gelatin) mixed/coated with multi-powder (#3000 mesh SiC and #3000 mesh diamond powder) as their abrasive for the studies. The multi-cone can absorb and retain water, allowing for the control of viscoelasticity by adjusting media hydration levels [24]. The Aerolap polishing machine they used is the same as that of Razali [1] (who is a contributing author to this report). See Figure 5 below, showing the Aerolap polishing system used by the researchers (and Razali's relevant description of the Aerolap polishing process against the conventional blasting process). It should also be noted that the workpiece was mounted on a stage that allowed for a change in angle (injection angle) and stand-off distance (distance from the nozzle output). The device also allows for the control of media injection rate (by changing conveyor belt speed) as well as control of impeller speed (by selecting the appropriate inverter value).

Figure 5 - Flexolap Polishing Device and Process
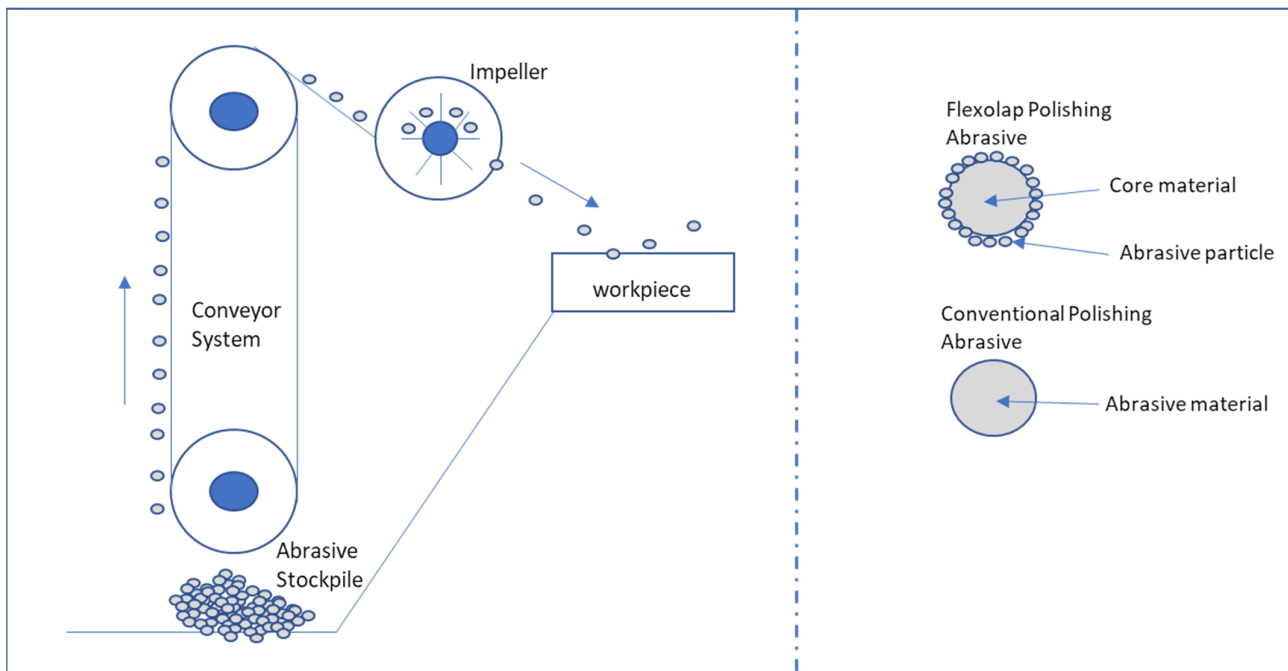
The first report, prepared by Takai et al. [24] in 2013, describes the effects of injection angle and polishing time on the surface roughness of cemented carbide components. In this study, the water content was kept constant at 30%. They used a high-speed camera (FASTCAM SA1) with a frame rate of 50000 frames/second and computational software (Dipp-flow) to measure projection speed of the polishing media. They found that the projection speed was very similar to the inverter value of speed (i.e., the media speed can be assumed similar to that of the output velocity of the impeller). They measured the surface roughness for various values of projection speed (from 12.3 m/s to 59.5 m/s) and found that the higher the projection speed, the lower the final surface roughness (Ra) will be. They also found that higher projection speeds result in more rapid rates of surface roughness decline (smoothening) i.e. less required polishing time. They found that after a 16.6 m/s impinging velocity, surface roughness values converged at a certain polishing time (with higher velocities resulting in lower values of surface roughness convergences). In turn they could draw the following: the higher the kinetic energy from the projected polishing media, the lower the value of surface roughness convergence (opposing that of conventional blasting). Figure 6 shows the polishing time versus surface roughness, showing the clear reasoning for drawn conclusions by the researchers.
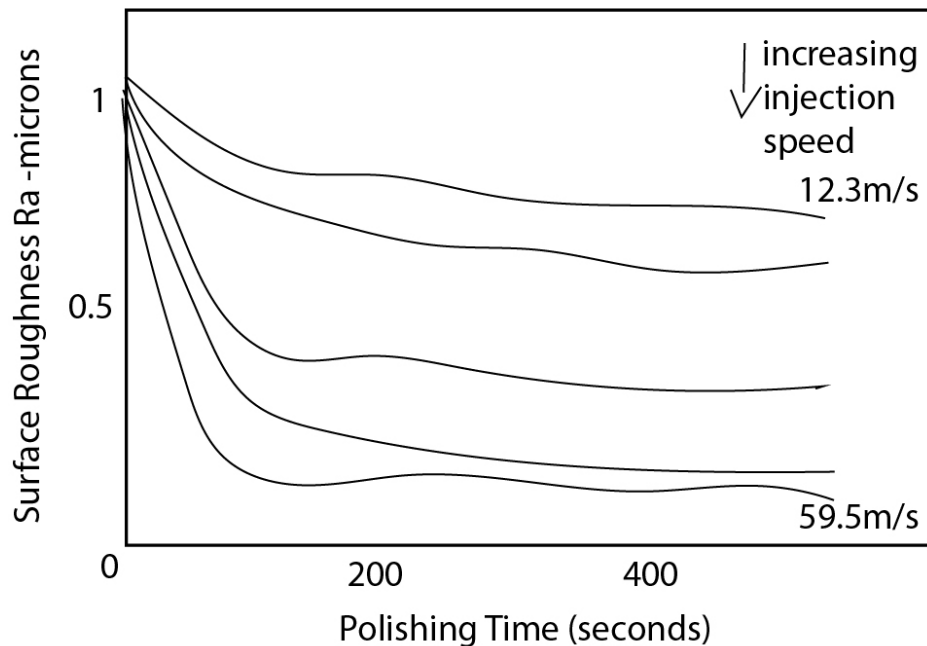
Figure 6 - Surface Roughness vs Time, adapted from [1]

This report highlighted the importance of high impinging velocity to the efficiency and effectiveness of the blast polishing process (and for lower impinging velocities, polishing time is notably important).

Takai et al. produced a second report in 2014 [25], showing their findings on the effect of abrasive media injection angle and kinetic energy (directly related to water content) on the surface condition of cemented carbide. Figure 7 below shows the method in which the impinging angle and standoff distance could be changed (the workpiece is mounted onto a stage which can be moved by translation in three axes and rotate in one axis). Angles of 15º, 30º, 45º, 75º and 90º were studied, while standoff distance was kept at a constant 20 mm (with previous research showing that lower standoff distances are more efficient [20]).
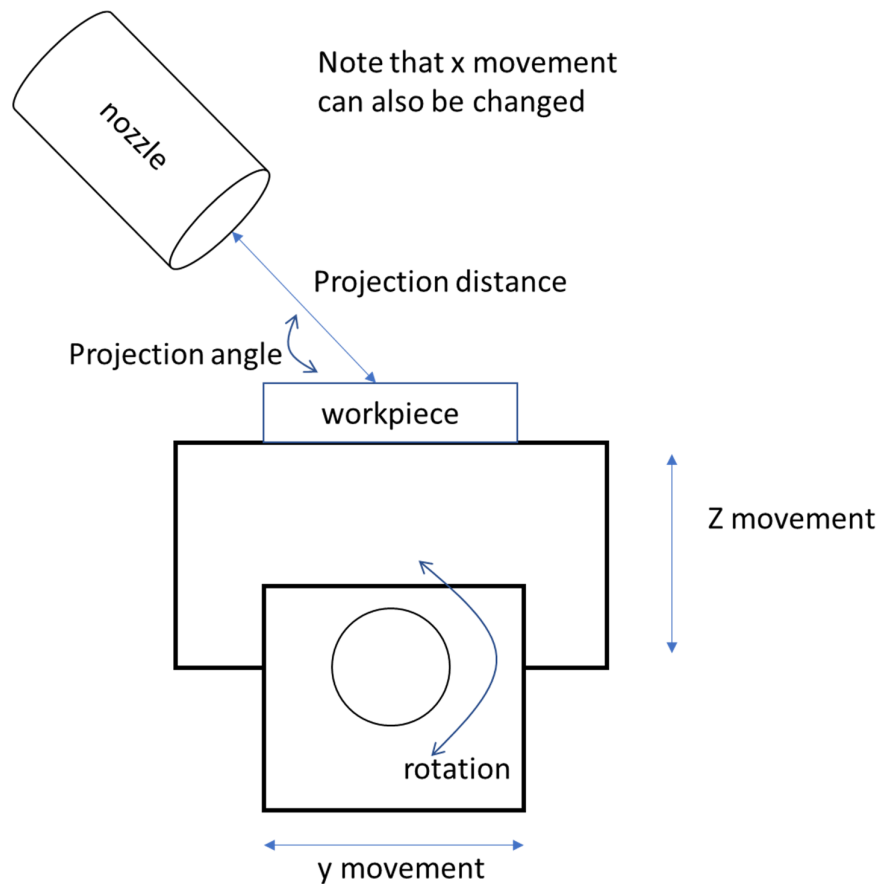
Figure 7 - Method of Changing Injection Angle and Standoff Distance, adapted from [25]

It was determined that the most effective polishing angle for achieving the lowest possible surface roughness at the fastest rate possible is 45º, followed by 15º, 75º and then 90º. The increase in efficiency from 15º to 45º is drastic and it was thus drawn that the only viable polishing angle for an optimal process, is 45º.
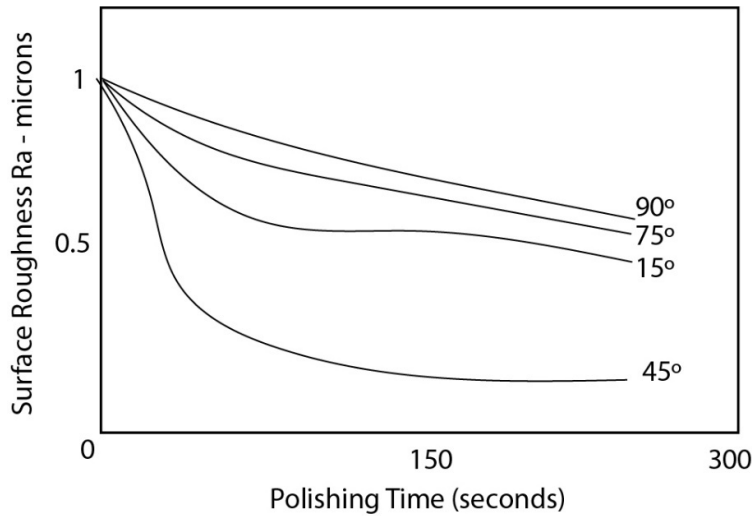
Figure 8 - Polishing Angle vs Surface Roughness, adapted from [1]

Figure 8 shows the findings of the study. It was concluded that the horizonal component of impinging force (removal force) contributes much more to surface roughness reduction than that of the vertical component (biting force) [25]. However, as the greatest rate of surface roughness decrease was at 45°, they noted that the balance between biting force and removal force is important. They also found that at 90°, no surface flattening was observed (as the biting force is the only contributor to material removal). At the other angles, flattening occurred due to the presence of the horizontal contributor: removal force.

In this study the authors also investigated the relationship between water content and mass of polishing media, finding that the mass of polishing media increased by nearly triple as water content was increased from 0% to 50% (see Figure 9 below).
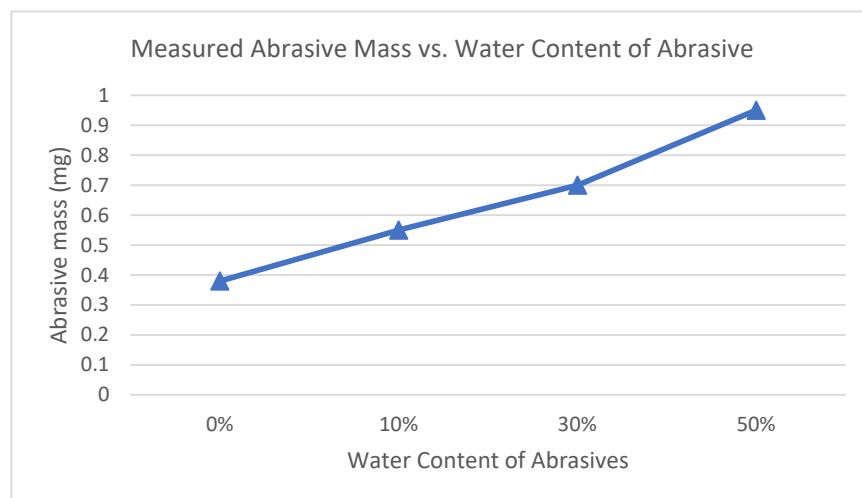
Figure 9 - Abrasive Water Content vs. Mass, adapted from [25]

The impinging velocity for different water contents was measured and it was found that there is no notable change in impinging velocity as water content is increase (a slight decrease in velocity was noted) [25]. Importantly, it was noted that kinetic energy increased significantly as water content and velocity was increased. Importantly, the authors noted that as water content increased, the time for surface roughness saturation increases, but the value of the surface roughness saturation (limit) becomes lower (a lower surface roughness can be acquired with a higher water content, but it will take a longer time). See Figure 10 for a visual description of this conclusion.

Finally, it was reported that larger and more apparent scratch/grinding marks were present at lower water contents and the presence/size of these decreased as water content was increased.
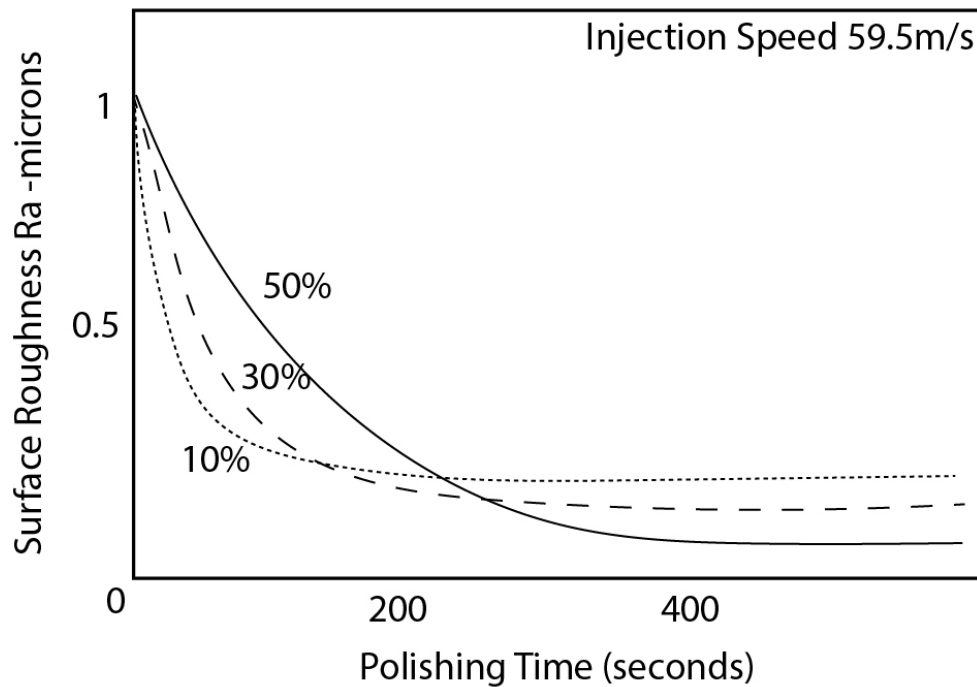
Figure 10 - Saturation of Surface Roughness vs Water Content

In 2016, Fukumoto et al. (in their third report on the topic) [6] studied the influence that media hydration levels (water content levels) have on the mechanism of polishing. They note that the trend seen in Figure 10 may be due to the elasticity/flexibility of the polishing media, which is directly related to hydration levels, which they measured as approximately 7 kN/m at 10% water content, 0.5 kN/m at 30% water content and 0.5 kN/m at 50% water content. Notably, the authors calculated particle impact force by using the conservation of momentum (with time taken as the amount for a single abrasive media to come into contact and then separate from the respective workpiece). They found that higher impact forces were found at lower water contents.

The authors also noted that lower hydration levels result in higher work hardenings and vice versa. They attributed this to media elasticity as well. Finally, the authors conclude that higher water contents result in a shallower, yet more extensive, polishing action (with lower values of final surface roughness). Lower water contents result in a deeper, yet more local, polishing action, with a higher final surface roughness value (see Figure 11 below)

low hydration

Less deformation of abrasive

Larger values of surface roughness
Deep and local action

high hydration

More deformation of abrasive

Lower values of surface roughness
Shallow and extensive action
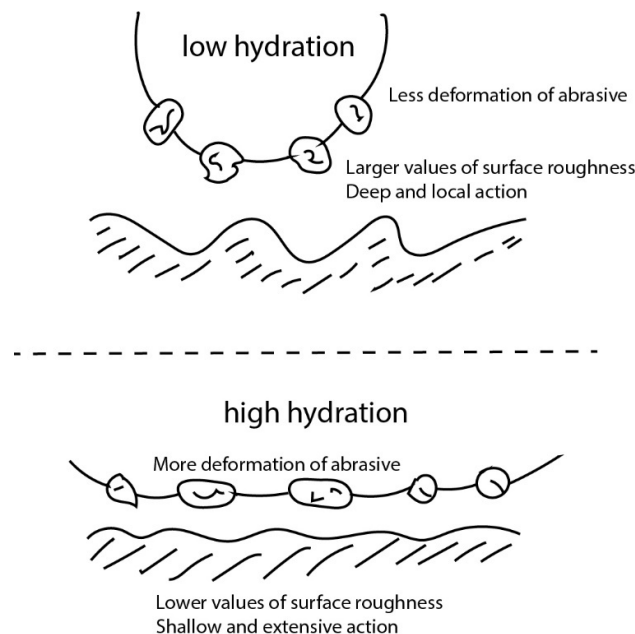
Figure 11 - Comparison of low and high-water content abrasive in contact with workpiece

In a study by Nizar et al. [26], grinding mark micro textures on the surface of WC-Co cutting tools was controlled via the Aerolap polishing process. Note that WC-Co tools are often used to cut aluminium alloys, which have the infamous property of chips adhering to the cutting tool surface (causing deterioration of chip evacuation, leading to cutting force increase). It was proposed that blast polishing would aid in allowing dry machining to be performed by the cutting tool on aluminium allows (by controlling the grinding mark textures). They found that

after polishing, cutting forces during initial use of the tool were reduced. However, as the tool was continually used, the forces become lesser than if the tool had not been polished. They noted that grinding mark textures improve anti-adhesion and provide lubricant storage. Too much polishing removes grinding textures and can thus reduce performance of the cutting tool. This study highlights the importance of controlling the Flexolap polishing process and not over-polishing workpieces that require textural markings.

Cheon and Pyoun [27], evaluated the tool life of Ti-Al-N coated carbide hobs before and after Aerolap polishing (using multi-cone media). Their results were found to be excellent in terms of machinability, wear, and life, with a 2.5 X reduction in wear and a 1.42 X greater tool life.

2.1.1. Other Polishing and Abrasive Blasting Techniques Used in Industry

To gain a full and in-depth understanding of the micro-polishing techniques (surface smoothening by material removal) it is important to understand other polishing techniques and their respective mechanics. In the previous chapter, the advantages of Flexolap polishing have been discussed in comparison to other techniques. However, the intricacies of other polishing methods which may help in process design have not been discussed. This sub-chapter aims to fill that gap by providing a basis of previous implementation of polishing techniques.

Kubota et al. [28] describe a technique of polishing PCD materials with that of iron-plate H_2O_2 chemical reactions. To achieve the polishing set-up, they filled a bath with an H_2O_2 solution and placed an iron plate inside the bath. The bath spins on a rotary table while the sample is held by a separate holder that submerges the sample and rotates in the opposite direction. Note that the sample is pressed against the surface of the plate. A notable issue with this technique is that it took over 15 hours to polish the sample. Afterwards, the sample must then be cleaned using an ultrasonic cleaner for at least 15 minutes. An acid solution could also be used (more effective). They also had the issue of only achieving localized polishing due to the different material removal rates (diamond grains vs metal binder).

Watanabe et al. [29] used UV irradiated polishing methods to polish PCD workpieces and managed to reduce surface roughness from 0.3 µm to 0.052 µm. They describe the process as a "mechanochemical polishing process combined with a UV-induced photochemical reaction". Their removal rate varied between 0.14 µm/hour to 7 µm/hour [29]. In a similar process, Ramesham and Rose [30] used thermomechanical methods (hot nickel plate in ambient hydrogen and achieved rates of 38.6 nm/min. The set-up of these polishing devices is comparatively expensive, and the skill required is quite high (making it a hard process to implement in industry). Size of specimen is limited as well.

Thermochemical polishing for chemical vapor deposition (CVD) PCD films was performed in a study by Zaitsev et al. [31]. This process was completed by securing the polishing sample on a plate in a polishing chamber with a very specific gas mixture of high purity. High temperatures are required in this process as well as high degrees of accuracy regarding time and temperature control. Purity of gas mixture is of utmost importance too. The designed process is novel in the sense that very thin films can be polished (a very specific application).

Chen et al. [32] produced a study on the dynamic friction polishing of PCD (simple explanation shown in Figure 12). This method is abrasive free and utilizes the thermo-chemical reaction between a metal disk and a diamond sample to remove material. Diamond is converted into carbon (non-diamond type carbon). An issue with this method is that as polishing time increases, carbon concentration and deposition on the rotating metal plate increases, and this results in a decrease in polishing rate. MRR also decreases with increased plate speed.
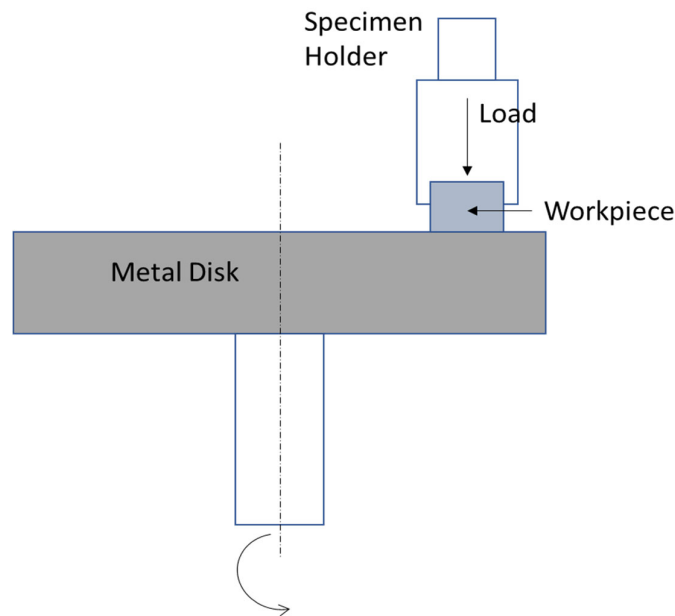
Figure 12 - Dynamic friction polishing, adapted from [32]

Carvalhao and Dionisio [33] studied two methods of cleaning graffiti (namely alkyd-paint aerosols) on calcareous stone (in Portugal). They studied the effectiveness of chemical cleaning methods and of more interest: soft-abrasive blasting. The first method used sponge like urethan-polymer with a calcium carbonate abrasive composite (used to minimize levels of abrasion and dust). The second method only involved the use of pure calcium carbonate particles. Both particles were spherical in shape, however method one used particles between 27 µm – 100 µm and the second method used particles varying between 70 µm – 200 µm [33]. Of interest in this study (in comparison to the conventional use of blasting) is that a smooth

surface is not desirable, and the outputs required are related to low reduction in Ra and Rz as well as low change of various colour factors. They concluded that both the chemical cleaning method and the blasting methods are both effective at cleaning graffiti off stone and allow for enough control over the process to ensure that the damage thresholds are not reached.

Hansel [34], categorizes abrasive blasting processes into three categories (surface cleaning and finishing, surface preparation and shot peening). He describes various blasting machines (suction and pressure), the safe operation of blasting machine and the implementation of various blasting techniques. It is stressed though, that whichever process is used, careful design and development (or selection) of the process must be undertaken to achieve the correct outcome.

Table 1 shows a summary of polishing techniques described in this sub-chapter.

Table 1 - Summary of Other Polishing Techniques

Technique	Benefits	Detriments
Iron plate H202	Polishing was achieved and the operator does not have to supervise the device for the entire polishing time.	Long polishing times (over 15 hours) and only localized polishing achieved. Materials can be costly and size limitations
UV irradiated polishing	Very low surface roughness achieved with reasonably high MRR rates (0.14 µm/hour to 7 µm/hour)	High operator skill required and very high set-up and material costs. Limitation on workpiece size.
Thermochemical polishing for CVD	Ability to polish very thin films.	Specific to thin films and requires high skilled operators.
Dynamic Friction Polishing	Abrasive free polishing technique and operator skill does not have to be high.	As polishing time increases, a decreasing MRR occurs due to deposition on rotating metal plate.

2.2. Factors Influencing the Flexolap Process

This sub-chapter is directly related to the previous chapter: "Flexolap Process and Background". Some studies and reports have greater focus on the process factors and their effects, and to adequately highlight their importance, these papers have been reviewed and are discussed below.

In a report by Okamoto [35] (a leading producer of grinding equipment and the greatest producer of Aerolap polishing machines), it is noted that water content adds viscoelasticity to the polishing media and that when the media collides with the workpiece, the projection is converted to a frictional force and moisture is evaporated from the media at the same time. During development and testing of their machine, they found that a mirror finish will be achieved when the media is hydrated to between 17% and 30% (depending on the workpiece to be polished) and that media with a low water content will still be effective at providing improved surface roughness, however, a mirror finish should not be expected. Another notable fact to draw is that due to the fact the moisture evaporates by frictional heat, water must be consistently added to the media as it recirculates, to ensure adequate water content in each individual media.

Draganovska et al. [36] in their creation of a regression model for abrasive blasting found that the most important factors affecting the application of blasting technology are:

- Choice of abrasive media. With desired attributes being high durability, accurate size and shape and minimal side effects on the surface due to the particles.
- Choice of blasting device. The device should be able to work automatically with a programmed blasting process (with blasting nature occurring in a similar fashion to that calculated and designed).
- Optimization of blasting process parameters. Choosing the correct impinging velocity, impinging angle, optimal abrasive type, stand-off distance and area of contact (nozzle output) are just some of the technological parameters that can be optimized.
- Secondary impacts of blasting. This can include surface hardening, the undesirable or desirable changing of mechanical properties of both the surface and sub-surface layers and roughening/smoothening of the surface.
- Optimization of blasting economy (efficiency of blasting). Including: optimization of blasting time and service life of abrasives and equipment.

As stated by Draganovska et al. [36], large abrasive medias create a large concentration of energy on the impact area, resulting in large deformation of impurities and base layers (resulting in surface hardening). Smaller particles (less kinetic energy) cause less microplastic deformation but do allow for a rise in the distribution of pressure strain. They also state that sharp particles penetrate the surface and will either become embedded in the surface or create an undesirable surface finish, meaning spherical shaped (or smooth shaped) particles will create preferable markings, and due to tension on the surface of the workpiece, impurities will disintegrate and easily peel off the material.

When selecting the appropriate grit size for abrasives, Draganovska et al. state the relationship between the ratio of abrasive particle hardness to the workpiece particle hardness (with larger ratios allowing for a higher removal rate but also a greater surface roughness). Processes with notably hard particles (steel shot peening), blasting for a long time, mean that hardening must be accounted for. Flexolap polishing is significantly shorter in nature than these and uses abrasives that are flexible in nature and are a lot less hard than the workpiece, meaning that surface fatigue and hardening is of lesser concern.

When accounting for shape, the two most common shapes are shot (spherical shaped) and grit (irregular sharp shape). These shapes result in surfaces with either rounded small peaks (shot) or with sharp notches (grit) [37].

Concluding their study of blasting properties, Draganovska et al. stated that the evaluation of blasted surfaces can occur by measuring the surface topography, microhardness, changes in mechanical properties, residual stress/tension, structural changes, and the change in physical/chemical properties.

Klusner et al. [38] studied the influence of surface topography on steel galling of coated WC-Co metals. To investigate the effects, the samples they acquired were polished down to a mirror-like finish (under Ra 10 microns) using Aerolap polishing and then wet blasted. These were then coated with a thin layer of Al-Cr-N. Finally, three variants of post-treatments were used for the study. The first method was a manual wet-blasting technique, the other two were: mild Aerolapping and a more thorough Aerolapping. They found that the thorough Aerolapping process resulted in a great reduction in Ra compared to the other processes and the ratio of peaks to valleys was also significantly less in this process (in comparison to the other processes). See Table 2 for a comparison of results.

Table 2 – Klusner [38] Results of Various Finishing Methods on Surface Topography of WC-Co metals

Coating/post-treatment	Ra (µm)	Rz (µm)	Rpk/Rvk
Uncoated/wet blasting	0.117 +- 0.002	1.14 +- 0.02	1.21
AlCrN/wet blasting	0.108 +- 0.001	1.01 +- 0.06	1.27
AlCrN/mild Aerolapping	0.105 +- 0.007	0.83 +- 0.15	1.63
AlCrN/Aerolapping	0.046 +- 0.006	0.71 +- 0.15	0.51

Klusner et al. [38] concluded that more research would be required to determine the influence of process parameters but stipulated that some important factors could be: impinging angle, stand-off distance, blasting pressure (impinging velocity) and polishing time.

Podgornik et al. [39] studied the influence of surface roughness on galling properties and found significant correlations, stating that polishing of coatings is more effective than substrate polishing. He noted that diminishing of galling can be achieved by reduction in Ra (by use of polishing methods).

2.3. Contact Mechanics & Tribology

The interaction between abrasive and workpiece requires in-depth analysis to understand how material removal (and associated processes) take place. Modelling can be done from a macro-lens as well as a micro-lens and it is often a good idea to do both to acquire a complete understanding of what is happening in the system.

To model any process where particle interaction (or any interaction for that matter) takes place, a solid understanding of contact mechanics and tribology is required.

Greenwood and Tripp [40] produced a model in 1967 (one of the earliest analytical models available) to describe the elastic contact of rough spheres, extending the Hertzian theory of elastic contact between two spheres. Greenwood produced a basic elastic asperity-based model in 1966 with Williamson [41] and the model with Tripp was extended from this. They defined the model as a discrete number of microcontacts where the heights of asperities are distributed using a Gaussian probability law. They assumed the contacts occurred between a finite number of asperities, in which they could then calculate forces due to asperity deformation. The forces were assumed equivalent to a continuous pressure, and this allowed them to calculate macroscopic deformation. This macroscopic deformation changes the forces between asperities and so they used an iterative loop to find pressure distributions and self-consistent displacements [40]. They found notable differences to the classic Hertzian model, notably: increased contact region size, but less total area of contact. They also stated that the Hertzian model is the high-load limit for rough surfaces (where their updated model can account for high and low loads).

Chang, Etsion and Bogy [42] followed up on this model (and many others after) by presenting a model for the elastic-plastic contact of rough surfaces. The model is based on volume conservation of an asperity during plastic deformation. Their model was found useful even if a large percentage of the true contact area is plastic. Importantly, they showed that singular asperity contact area for this condition can be found by:

$$\bar{A} = \pi R \omega \left(2 - \frac{\omega_c}{\omega} \right) \tag{1}$$

Where R is the sphere radius, ω is deformation and ω_c is critical deformation. They proved that the lower limit of this expression is the asperity model for elastic contact while the upper limit of this expression is given by the surface microgeometry model for pure plastic contact [42]. They noted that after taking all mentioned aspects into consideration, the variation from the initial model by Greenwood and Williamson [41], is not significant.

Kogut and Etsion [43] presented a similar model for the elastic-plastic contact of a sphere and a rigid flat. However, they developed their model using FEM and showed the model with three

distinct stages varying from fully elastic to fully plastic (with elastic-plastic being the middle stage). This model has the important outputs of dimensionless contact load, contact pressure, and contact area expressions. This model was used extensively in this dissertation to develop a new empirical model for the prediction of polishing parameters (used in parallel to the presented analytical model).

The fundamentals of contact mechanics, as discussed well in the textbooks of Stolarski [44] are essential in developing a model for polishing or any other manufacturing/engineering process where contact takes place. For contact in polishing, the simplification of contact between a convex sphere and a plane is made (starting initially with point contact and then transforming into a surface area of contact). The contact area generally begins as an ellipse, from which many solutions for deformation, contact area, contact stresses, and pressure distribution, can then be found. Most of the models also assume low enough deformation that the radii can be taken as constant. Derivations can be made to achieve the solutions described by using sphere geometry, elastic properties of materials and algebraic calculus. See Figure 13 for derived equational solutions.

The figure shows a sphere in contact with a plane. Labels: P — Contact force (arrow pointing down onto sphere); Sphere; D_1 — Sphere Diameter; $2a$ — $2 \times$ contact radius; Plane.

Associated equations:

$$a = 0.721\sqrt[3]{P(\eta_1 + \eta_2)D_1} \qquad contact\ radius$$

$$P_o = \frac{1.5P}{\pi a^2} = -\sigma_{cmax} \qquad contact\ stress$$

$$\delta = 1.04\sqrt[3]{\frac{P^2(\eta_1 + \eta_2)^2}{D_1}} \qquad deformation\ of\ sphere$$
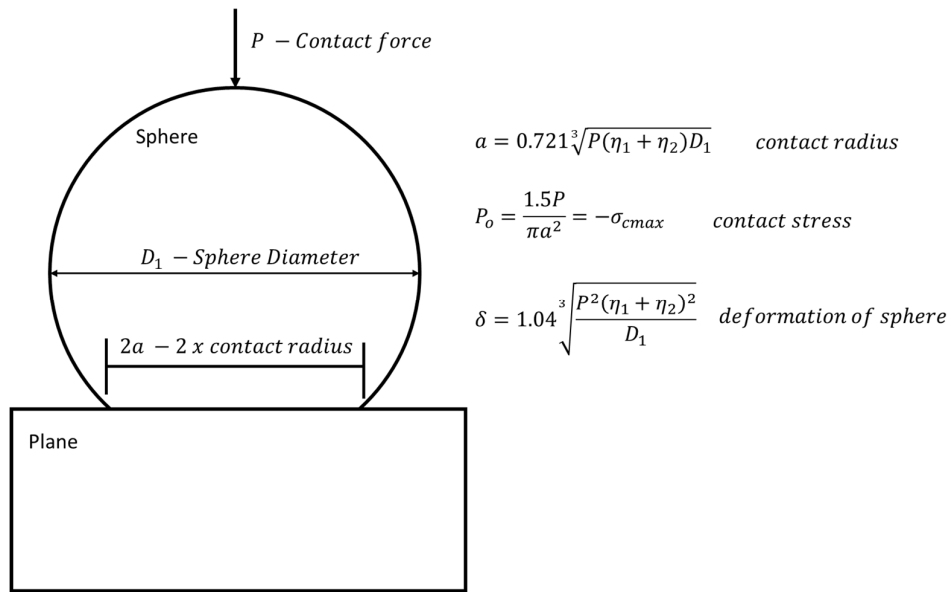
Figure 13 - Contact between sphere and plane and associated equations

Where the material property η is found by:

$$\eta_1 = \frac{1 - v_1^2}{E_1} \tag{2}$$

v is Poisson's ratio, E is the elastic modulus of the material. a is the half length of contact (radius of contact), P is the contact force, D_1 is the diameter of media P_o is the maximum contact pressure/stress, δ is the contact deformation.

Viscoelasticity is an important aspect to consider when examining the interaction of flexible abrasives (notably with a gelatin core) to a harder surface (that of Ti-6Al-4V). Naghieh et. al [45] provide a mathematical formulation that aids in studying the contact mechanics of viscoelastic layered surfaces, where the effects of different Poisson's ratios and elastic models on typical contact mechanic properties (Hertzian contact stress, deformation, pressure distribution with time) are explored. They use a standard linear solid model as seen in Figure 14 - Zener Model KV (Zener model with a spring in series to a Kelvin-Voigt model) to model the viscoelasticity of materials.
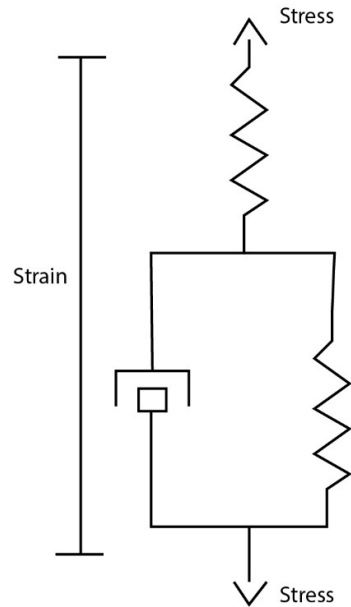
Figure 14 - Zener Model KV

They found the contact pressure for a viscoelastic layered material (with Poisson's ratio of 0.5) to be:

$$p(r,t) = \frac{E_o a^4}{16 d^3 R} \left\{ \begin{array}{l} e^{-\frac{t}{\tau_2}}(1 - \left(\frac{r}{a_o}\right)^2)^2 + ((2 - e^{\frac{-t}{2\tau_2}})^{\frac{1}{3}} - \left(\frac{r}{a_o}\right)^2)^2 \\ e^{-\frac{t}{\tau_2}} \int_{f(0)}^{f(t)} [2 - (\xi^{\frac{1}{2}} + \left(\frac{r}{a_o}\right)^2)^3]^{-2} \, d\xi \end{array} \right. + \tag{3}$$

Where:

$$f(t) = [(2 - e^{\frac{-t}{2\tau_2}})^{\frac{1}{3}} - (\frac{r}{a_o})^2]^2 \tag{4}$$

And t is time, a is the contact radius, d is the layer thickness, τ is the relaxation time, r is the distance in the x axis, R is indenter radius, E is elastic modulus, ξ is a substituted variable. Note that $f(t)$ is a non-parametric time function.

2.4. Methods of Modelling the Process

Various methods exist that aid in characterising manufacturing processes. Analytical methods, empirical methods, numerical methods, a mixture of these or simulation tools (which often involve a combination of the above stated methods to solve a problem) can be used.

The methods currently used to characterize the Aerolap/Flexolap polishing process are mostly analytical and empirical, and the literature surrounding those will be focussed on. Numerical methods are available, and these are briefly described too. Simulation tools and relevant literature is discussed in the following sub-chapter.

The Flexolap polishing process can be thought of as a series of micro-indentations in a workpiece from many polishing media impacting the workpiece surface [46]. This decreases the overall surface roughness and other surface values e.g., largest peak and valley heights. The surface peaks are plastically deformed by the media and are then deformed to fill in the valleys. This improves the surface texture. Figure 15 below shows a micro-scale view of how the polishing media interacts with the workpiece. Contact of asperities and modelling with asperity contact in mind (as per the previous sub-chapter) provides the most insight into the process, and from previous studies, it seems to provide the most reliable and accurate results.
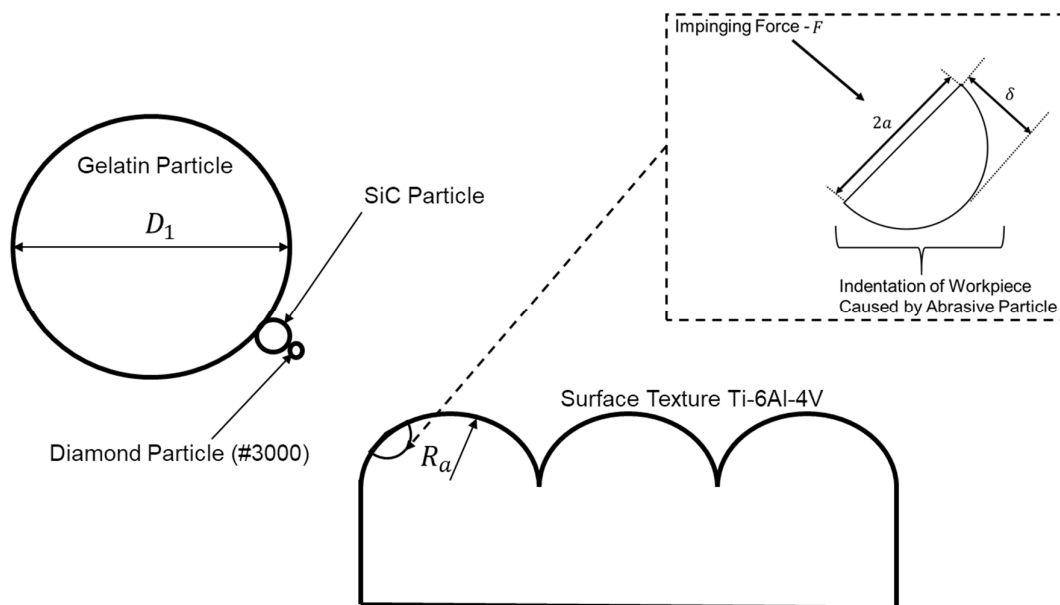
Figure 15 - Micro-View of Flexolap polishing Process [46]

In an article by Zhao, Maietta and Chang [47], a model was presented regarding (rough) asperity microcontacts and the transition from elastic deformation to fully plastic flow. They studied the contact between two nominally flat surfaces and used the fundamentals of contact mechanics (as previously discussed) as well as the continuity of variables across different modes of deformation. Fourth-order polynomial functions and logarithmic functions were used

to model the relationship between asperity-interface contact area and average contact pressure, with this relationship then used as the basis for the elastic to plastic contact. Importantly, this allows for the area of contact to be calculated based on contact load and plasticity index. The modelling process and outputs of by Zhao, Maietta and Chang are particularly applicable to the characterization of the Flexolap polishing process and the fundamentals they have set out are used extensively in this dissertation. Note that a model accepting contact load (which translates to polishing forces/pressures) as inputs allows for the characterization of a force-controlled process, which is crucial to manipulating the Flexolap polishing process.

A notable and popular method of modelling the Flexolap polishing process is to use the conservation of momentum as a foundation [1] [4] [24]. From this, popular Hertzian contact models (as stated in previous chapters) can be used to find values such as contact area, contact pressure, pressure distribution etc.

Achtsnick et al. [48] provided a model and evaluation techniques of the micro abrasive blasting process (MAB). The MAB finishing process is most notably for MEMS (micro-electro-mechanical systems), which include devices such as tire pressure sensors, microphones, accelerometer airbag sensors and biosensors. MAB is based on the material removal of mask-protected substrates with an air jet shooting abrasives toward the substrate. Note that for their designed process, the air pressure used varies between 2 bar and 9 bar (very similar to that of typical Flexolap polishing processes). The process model, in addition to a developed material model, provides the description of the interaction between substrate surface and impinging abrasive particles. Indentation fracture mechanics was used as the basis of modelling (with the simplifying assumption of perpendicular impingements). As per previous models, kinetic energy is translated to impact plastic work and the model transition from plastic deformation to brittle fracture is dependent on material properties. Their model of material removal is of notable interest, with much of it being derived from Marshall et al. [49] (who created a fracture system for the elastic-plastic behaviour of the substrate material). As is noted, and agreed by both models, the abrasive hardness must be harder than workpiece (or in this case, substrate) hardness for material removal to occur. The derived formula for peak impact load (derived from the plastic work done during impact, indentation volume and indenter force) is given by:

$$P_{max} = \sqrt[3]{\frac{36 HV U_{kin,p}{}^2 \tan^2 \alpha}{\sin \alpha}} \qquad (5)$$

Where HV is the material's Vickers hardness (indenter force divided by indentation area).

α is the half plane angle of the indenter. a is half the indentation diagonal length and the kinetic energy of indenter force and corresponding indenter force are given by:

$$U_{kin,p} = \frac{2}{3} \frac{a^2 HV}{\sqrt{2} \tan \alpha} \tag{6}$$

$$P(h) = \frac{2HV a^2(h)}{\sin \alpha} \tag{7}$$

These derived formulae allow for the development of a more in-depth model (relating to material erosion rate, crack size and a roughness model for various nozzle configurations).

Karpuschewski et al. [50] produced a study on the simulation and further improvement of the micro-abrasive blasting (MAB) process (note that this study is directly linked to the study by Achtsnick et al. [48]). This study investigated how the MAB process could be made more controllable and efficient so that it is of greater interest to industry (the same interest of study as this dissertation).

They created a set of models containing further sub-models. The model focusses were: MRR, blast profile and particle beam. Figure 16 below shows the MAB process, which is very similar to the Flexolap polishing processes described in previous chapters (with the noticeable absence of a driving impeller).
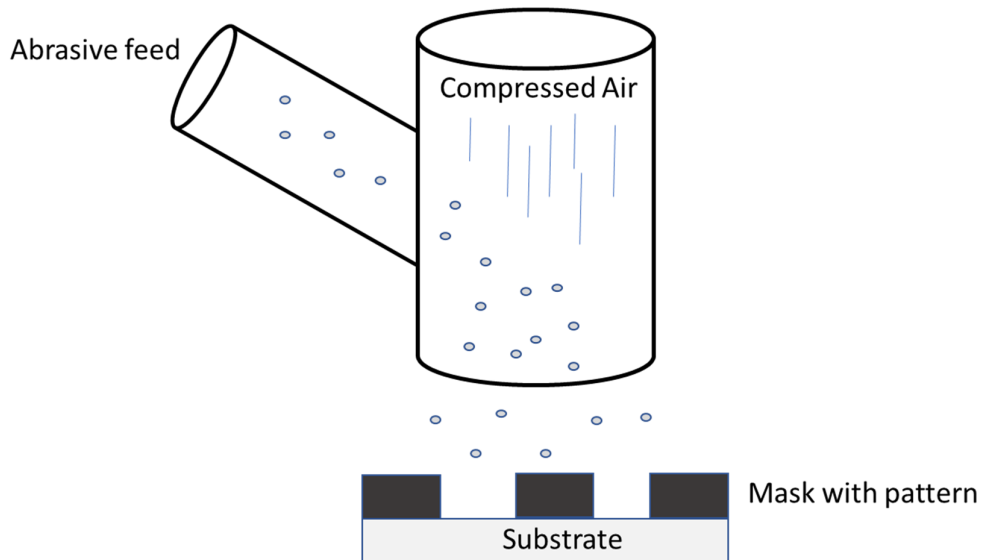
Figure 16 - MAB on MEMS, adapted from [50]

Similarly, to other models (such as that of Kuppuswamy's momentum model [4]), Karpuschewski et al. related material erosion (removal) to abrasive particle velocity by the power function:

$$Er \propto v_p^k \tag{8}$$

Where Er is dimensionless erosion, v_p is particle velocity and k is an empirical velocity coefficient e.g. 2.2 for stainless steel and 1.6 for copper [50]. Although this is for mask materials, it relates well to the surface removal of metals in other processes (blast polishing). Karpuschewski et al. extended their previous computational models [51] based on the modelling of loose abrasive processes to analyse the effect of nozzle configuration in MAB. The sub-models contained and related to this model are of particle velocity, airflow velocity profile, particle mass and distribution and beam expansion. From this they describe the interaction between impinging blast particle and the substrate surface. With note that the change from plastic deformation to brittle fracture of the surface is controlled by substrate material properties [50]. The secondary model they created was a jet model (modelling the airflow velocity and particle acceleration with fluid mechanic formulae). Using these two adjacent models, they then simulated particle velocity, energy intensity distribution and finally the evolution of a blasted hole. This allowed the authors to develop a nozzle that allowed for a 40% increase in particle velocity compared to their initial nozzle design [52].

Draganovska et al. [36] produced a regression model allowing for the prediction of surface topography following the abrasive blasting of surfaces. Their study focusses namely on the relation between singular roughness parameters (using correlation analysis). After measuring roughness values (from different blasting devices), a correlation matrix was created and statistic importance of correlation between the chosen and measured process parameters was determined. Important regression models were then found and created with the use of ANOVA, with results of roughness parameters finally allowing for the overall assessment of blasted surfaces.

For their blasting process, they used steel grit, steel slag, and corundum, all with particle sizes of around 0.9 mm. Blasting pressure was 6 bar, impinging angle was 75º and stand-off distance was 200 mm.

A correlation analysis between roughness parameters was completed using Statistica and regression models were then put in place, where they found that the strongest relationship between roughness parameters was that of Rz to Rt [36].

The above discussed study is particularly helpful to the empirical model that is developed after collection of experimental results.

Other important models are that of vibrational (spring damper) and viscoelastic (spring damper as well) models. These range in implementation but are often used to determine the displacement (strain), stress and vibrational (spring constant and damping constant)

properties of materials under a force or stress. This is incredibly helpful when attempting to model the effects of hydration on the viscoelasticity of multi-cone/gelatin.

The viscoelastic models are all based on a time dependant variant of Hooke's Law [53]:

$$\sigma = \eta \frac{d\varepsilon}{dt} \tag{9}$$

Feldmann et al. [53] presented a model to determine the fractional Zener model parameters from low frequency DMA (dynamic mechanical analysis) measurements and found that they could acquire the elastic properties of PA6 for a broad range of frequencies based on the time-temperature superposition.

Schiessel et al. [54] presented a paper with generalized viscoelastic models and their fractional equation solutions which aided greatly in solving more complex problems and defining their response.

Bulicek and Malek [55] presented a paper relating to the Kelvin-Voigt model and its generalizations, using both elastic and dissipative Cauchy stresses to solve non-homogenous, mixed boundary value problems.

Assie et. al. [56] presented a notably interesting FEM model that solved the problems pertaining to the contact-impact of viscoelastic materials (at velocities lower than 30 m/s). Using the standard linear solid model and Newmark time integration (method), they found solutions in one dimensional, two dimensional and three-dimensional space for the contact force and velocity upon impact of the materials.

Many other viscoelastic models and vibrational models exist and are of use to the vibrational chapter shown later in this dissertation. Those models are presented in that chapter.

Modelling relates directly to the following chapter: 'Modelling of Contact Processes using Simulation Tools' with many factors helping to influence the parameters and metrics of one another. The process of simulation and modelling is often a repetitive one and finding the harmony between both allows us to represent the process as truly as possible, where errors can be found more easily, and corrections made more efficiently.

2.5. Modelling of Contact Processes using Simulation Tools

If done correctly, simulation can be a powerful tool in predicting process behaviour and forecasting results. It is thus a useful aid in affirming process models and for providing information to help process/machine design.

Kurcharski et.al [57], produced one of the earlier finite element models (1994) for the contact of rough surfaces. They too set the basis of their model off well-known contact mechanic asperity models (such as Greenwood and Tripp's model [40]). However, the introduction of an elastoplastic deformation law (like Zhao, Maietta and Chang [47]), allowed for a more realistic study on singular asperity deformation. The study is conducted numerically by examining a single asperity's deformation by using the finite element method.

Yastrebov et.al [58] created a more recent model (2011) similar to that of Kurcharski et.al but more detailed, using computer aided tools and possessing the ability to run models much quicker (due to higher available computer processing speed). In their study, they presented a full-scale FEA model and a reduced model for the frictionless contact of an elastoplastic material and a rigid plane. They create surface roughness using experimental measurement and representative surface elements. They noted that the full FEA model took days to complete the solution while the reduced model took a matter of seconds and could produce predictions of the real contact area, the load-displacement curve and the free volume between the plane and material [58]. An important output found was that the interaction between asperities when predicting results/producing a model, has a notable impact on the predicted outputs.

Although FEM and FEA are not used directly in the simulation-based models in this dissertation, studying the literature related to them can provide valuable ways of thinking and can aid in the understanding of how simulation tools (such as ANSYS and SolidWorks) produce model outputs. It also allows for the understanding and more efficient manipulation of these tools to achieve the desirable outputs.

Maliaris et.al [59] produced a simulation in 2021 that is of noticeable interest to the study of Flexolap polishing. They created a simulation (and qualitative assessment) of the shot peening process (which in its mechanical nature of material removal and process design, is very similar to Flexolap polishing). It is important to note that shot peening is used as a surface treatment to increase the fatigue performance of engineering components. Maliaris et al. [59] used a two-dimensional FEM model to generate the geometry condition of impacting shots (with slightly varying diameters). They used the classic mathematical Voronoi algorithm (where a plane is split into n convex polygons with each polygon containing a single unique point and so that each point is as close to its generating point as any other).

Using various FEA meshes and constraints for certain elements (the top layer, core layer and the transitional layer in between the two), they could predict the residual stress accumulation at different impacting velocities for rigid and elastic-plastic shots. Their final model provides a valuable alternative to analytical-empirical equations and accounts for all process parameters in a realistic fashion. This study shows first-hand the benefit of computer-generated simulations being used in conjunction with analytical and empirical models.

In a review by Hashmi et al. [60], simulation techniques for loose abrasive-based machining processes were examined. They examined the following techniques: computational fluid dynamics (CFD), finite element methods (FEM), molecular dynamic simulation (MDS), discrete element method (DEM), multivariable regression analysis (MVRA), artificial neural networks (ANN), response surface analysis (RSA), and data-dependant systems (DDS) [60]. MVRA, ANN, DDS and RSA are appropriate as experimental based statistical techniques for mathematical process modelling while CFD and FEM are available on most commercial simulation software, and some make these methods simple for a user to implement. They found that DEM and MDS provided the most accurate results but require the largest computational power while statistical methods provide an easy determination of process parameters.

Dallinger and Hubler [61] used the DEM (discrete element method) to calculate stresses and contact forces on bottles moving on a conveyor system (using particle analysis), showing an efficient method of implementing simulation system for a high number of bodies.

The above stated simulation-based models (and results) are not only important when concerning the direct implementation of simulation to the Flexolap polishing process investigated in this dissertation but also to the analytical and empirical models developed and machine development/process design.

2.6. Media Materials and Properties

The determination of an appropriate abrasive material or compound is critical to achieving a successful process design with inherent efficiency. As described in previous sub-chapters, some important abrasive factors include: size of the abrasive (larger abrasives result in higher forces/depths of cut but less abrasives hit the surface per second, meaning a less even coverage of the surface), hardness ratio between the workpiece and media (harder medias generally result in higher rates of material removal, while softer abrasive allow for a more controlled process) and shape (with spherical shapes generally resulting in better surface finishes and sharp shapes result in a larger presence of embedded media and higher localized pressures/forces). Shape is also directly related to imparted surface topography [62].

Although not a polishing process, the implementation of gelatin which Amar and Tandon [63] used to enable their abrasive water slurry jet machining (AWJSM) is of interest to this dissertation. Note that gelatin is favoured as a media core due to the ability to change its viscoelasticity by means of hydration without the need for temperature increases, which makes the process less energy intensive than the other typical choice of a thermoplastic core. The objective of AWJSM is on high rates of (accurate) material removal, however, the choice and implementation of abrasive is just as critical in this process as it is in Flexolap polishing. Amar and Tandon used gelatin and water as a liquid polymer solution to increase the efficiency of energy transfer of abrasive (garnet in this case) to the workpiece. Gelatin was used due to its favourable characteristics to act as a polymer and its economic cost. Gelatin in this case also allowed for a more uniform mixing of abrasive than typical polymeric solutions. The outputs of the above stated research imply that gelatin is an appropriate choice of media for Flexolap polishing.

Hansel [62], produced a report regarding abrasive blasting systems, their operation and a section describing common abrasive categories and materials, as well as their associated benefits and/or disadvantages. Friability (breakdown) of media is stated as an important factor because it determines the number of reuses (recyclability of the media). The friability of media is directly related to hardness, composition, and brittleness. Density of material is also important as different kinetic energies will be imparted upon the workpiece (resulting in application of stress in some cases). Hansel separates abrasives into three categories: natural, by-product and manufactured.

Microblast (garnet), aluminium oxide, steel grit, steel shot, platinum grit, glass beads, glass grit and sodium bicarbonate are just some of the abrasive blasting medias used in industry and that can be purchased in South Africa [64].

Above descriptions have shown separate abrasives but have not explored compounding media to achieve the most desirable properties possible. While researching Flexolap/blast polishing, one will find that animal proteins (gelatin and agar agar) are a very common media core [1] [4] [14] [15] [16] [35] [24]. Gelatin can absorb a great content of water (meaning that its viscoelasticity can be controlled as well as its mass and thus its kinetic energy upon impact) [1]. This level of control allows for a versatile process that can be changed based on material/process requirements. To impart a great level of abrasive action, SiC and diamond are coated onto the protein core (see the properties of multi cone in Table 3). SiC and diamond are the hardest available abrasives in industry, but as a singular abrasive, they are very expensive and not particularly re-usable. However, when these materials are coated onto the animal protein, a much lesser quantity is required (due to only surface coating being required) and the ability for re-use becomes an option. Higher mesh levels (smaller sizes) of diamond and SiC are often more expensive but allow for better adhesivity to the protein [6].

Table 3 - Multi-cone properties compared to others

Material	Mesh Size	Shape	Density	M. Hard.	Friab.	In. Cost.	Cycles	Per Use Cost
Gelatin	10	Round	1300	2.5<	Medium	Low	200+	Low
SiC	3000	Square	3210	9	High	Low	2	High
Diamond	5000	Square	3500	10	Medium	High	2	High
Overall	10 - Complex	Round	Complex	Complex	Medium	Low	200+	Low

Schwarz et al. [65] investigated the mechanical properties of hydrogel (gelatin) using vibrational analysis and laser-doppler vibrometry. They were able to deduce the Young's Modulus of the materials from the resonance frequencies of the first mode (root of Young's modulus increases as the frequency of the mode increases). They also found that the damping constant increased with gelatin concentration. This is useful to the vibrational analysis done in this dissertation.

The most important conclusion to be drawn from this section is that for the Flexolap polishing process, the abrasive used should be visco-elastic in nature and thus should allow for high levels of water absorption and retention. This leads to the use of animal proteins, which although minorly abrasive in nature, have the beneficial property of high adhesion and allow for the bonding of materials with better abrasive properties (SiC and diamond) to the surface.

2.7. Workpiece Materials – Namely SLS Ti6Al4V

Developing an understanding of the properties (mechanical and chemical) of the material that is to be worked upon is vital in developing a process that is efficient and non-damaging to the workpiece. Although the developed polishing process is designed to be used on a large variety of materials, the dissertation presented focuses on the finishing of SLS produced Ti-6Al-4V (as this allows more scientific outcomes to be produced). Of the available titanium alloys, Ti-6Al-4V is the most used (accounting for 45% of exported titanium alloys in the world [66] [67]).

Dhansay [68] shows visually and textually the large variation in properties and microstructures of Ti-6Al-4V depending on production and heat treatment methods (with yield strengths varying from 758 MPa to 950 MPa, elongation from >8% to 14% and ultimate tensile strength from 860 MPa to 1020 MPa). There are three different microstructures that Ti-6Al-4V can exist in: fully lamellar, fully equiaxed and bi-model). These are achieved by use of different heat-treatment processes.

The microstructure is very sensitive to temperature changes. In SLS produced Ti-6Al-4V, and due to great temperature gradients, there exists a non-equilibrium phase consisting of a fine, acicular martensitic structure. Because of the martensitic structure achieved, the SLS produced alloy has a higher yield stress but lower ductility (due to residual stress, microcracks and martensite) compared to the conventional wrought method of manufacturing the alloy.

Residual stress accumulates in the SLS process due to the large thermal gradients present [69] and these need to be relieved after manufacturing so that restriction of use is not a problem. The samples polished in this dissertation have been relieved of residual stress through temperature gradient mechanisms and this portion of study does not form part of the scope of this dissertation.

Harada et al. [3] studied the mechanical properties of SLS Ti-6Al-4V compared to conventional cast SLS Ti-6Al-4V and produced the following SEM images (which help to serve as reference for desirable outputs of the designed process in this dissertation)

The following properties (see Table 4) for typical SLS Ti-6Al4V have been drawn from [3] and [70] and help in classification for the models built in this dissertation:

Table 4 - SLS Ti-6Al-4V Properties

Property	Symbol	Value
Density	$\rho_{Ti6Al4V}$	$4410\ kg/m^3$
Hardness	$H_{Ti6Al4V}$	$2270\ MPa$
Modulus of Elasticity	$E_{Ti6Al4V}$	$114\ GPa$
Fracture Toughness	$K_{cTi6Al4V}$	$75\ MPa\sqrt{m}$
Yield Strength	$\sigma_{yTi6Al4V}$	$900\ MPa$
Poisson's ratio	$\nu_{Ti6Al4V}$	0.342

As stated by Atzeni et al. [71], AM produced Ti-6Al-4V components are increasingly used in industry but have the main structural weakness of fatigue life. Fatigue life is affected by surface quality, where micro-cracking occurs due to the small surface defects incurred in manufacturing. The authors of this journal studied the effects of Abrasive Fluidized Bed and Laser finishing as methods of surface finishing the Ti-6Al-4V alloy with the studies focusing on internal porosity, mechanical properties, and fatigue properties. They found that both processes lead to an increase in measured fatigue life (257793 cycles for AFB and 961523 cycles for LF) also noting that LF has a low environmental impact compared to AFB. Surface morphology was found to be smoother over time for both techniques, but overall surface roughness Ra did not significantly decrease and was not close to a mirror finish even after 10 hours (this was not the goal of the study). Although both techniques are useful for reducing porosity and increasing fatigue life, post finishing is required to achieve a mirror finish and the associated attributes of low surface roughness.

Lizzul et al. [72] noted that the surface finish of AM produced Ti-6Al-4V alloys after ball end milling are better than that of wrought alloys due to the presence of alpha phase colonies which favour material removal by lowering the material's resistance to cutting.

Bagehorn et al. [73] studies the finishing method of milling, blasting and electrochemical polishing in order to reduce surface roughness and found that all increased the fatigue performance compared to the as built part, with all processes showing significant improvement in surface roughness too (up to 93% reduction).

2.8.　Summary of Literature Review

Many topics have been reviewed to provide all the necessary knowledge and relevant tools applicable to this project. A summary of the review, with a highlight on the key research outputs from previous studies, is provided below.

2.8.1.　Abrasive Media

While deciding on abrasive media, the ability to control the viscoelasticity of the abrasive media allows for the ability to impart a large variety of polishing conditions that can be used to polish multiple materials. The simplest way in which viscoelasticity can be control is through the retention of water in a media. If choosing an abrasive media as a compound, the core must have high adhesivity for the outside abrasive layers to stick to the core effectively.

2.8.2.　Polishing Conditions

When designing for polishing conditions, the ability to control injection speed, injection angle, number of abrasives per second, hydration level of abrasives and stand-off distance (distance between output nozzle and workpiece surface) are most critical to achieving desired outputs and to create a process that caters for force control. Polishing outputs can be measured by: surface topography, microhardness, changes in mechanical properties, residual stress/tension, structural changes, and the change in physical/chemical properties. Other outputs that are more abstract in measurement are the measure of applied forces, deformations, and contact areas/stresses

Previous Flexolap designs show that the lowest stand-off distance possible combined with an impinging angle of 45º, provides the most efficient and effective results, fastest reduction in Ra with the least possible damage and markings to the surface. Higher water contents are more preferential and surface damage reduces significantly with higher hydration conditions. Higher hydration conditions will result in a surface roughness that is lower overall, but the polishing time to achieve it will be longer. Lower hydrations achieve lower surface roughness quicker, but their limit is higher. Higher polishing speeds are more desirable in Flexolap polishing, however if higher velocities cannot be achieved easily, change in hydration will result in kinetic energies that will accommodate the loss of velocity.

2.8.3.　Process Modelling

When concerning modelling of the process, the simple method of conservation of momentum in combination with contact mechanics equations allows for an accurate technique to analytically model the Flexolap polishing process. An empirical method, based on the transitional and critical values of contact mechanics between a sphere and plane, allows for another method of modelling as well as a technique of verifying the first model.

2.8.4. Simulation

FEM and CFD models are the most easily accessible for simulating the process before running experiments while statistical simulation methods are easier and more applicable after experiments have been run.

2.8.5. Vibrational Model

Vibrational models and viscoelastic models are notably useful when modelling the effects of hydration and the Kelvin-Voigt model is of particular interest to the abrasive used in this dissertation. These researched models aid greatly in the development of a model for the flexibility of abrasive media.

2.8.6. Polishing Material

SLS produced Ti-6Al-4V has higher yield stresses but lower ductility than other conventional manufacturing techniques for the alloy. This means that residual stress, microcracks and martensite are more present in the alloy. As shown by previous studies, this implies that fatigue life in AM produced parts can be significantly less than that of conventionally (typically wrought) produced parts. If the correct choice of surface finishing technique/s are selected, the effects of surface fatigue due to porosity and other defects can be mitigated. It should also be noted that due to the presence of alpha phase colonies, material removal is easier to achieve on AM produced Ti-6Al-4V than on wrought components. Some surface finishing techniques include Abrasive Fluidized Bed and Laser finishing. The samples used in this dissertation have been treated so that residual stress has been relieved before reaching our laboratory. A basis on which to compare final polishing results has been provided as well.

2.8.7. Gaps in Flexible Abrasive Polishing Addressed by this Research

Multiple opportunities for research have become apparent in the studied literature. Firstly, the development of process models that determine polishing time and polishing forces is lacking, particularly models that are not based on the notion of momentum. A developed semi-analytical-empirical model with verifiable results is presented to address this gap. Published studies into the full development of a blast polishing machine and process are lacking and the Flexolap research presented intends to highlight the detail on how to design both the machine and process to implement blast polishing effectively at various conditions. The experimental results presented study the effect of diamond concentration on polishing outputs (this has not been studied before) and the effects of this in addition to the varying combinations of polishing time, impinging velocity and hydrational level of abrasive media allow for the study of a multitude of unresearched outcomes. The behaviour of abrasive media when hydrated is not widely understood and the vibrational spring-dashpot model presented in this dissertation provides concrete values of damping ratio, damping coefficient

and contact parameters (time, stress, and force) to characterize the hydrated media's properties in the Flexolap polishing process.

2.8.8. Concluding Statement

All the above research and collected information is used throughout the project and dissertation to achieve valuable results that contribute to the advanced manufacturing sphere.

Chapter 3 – Process Modelling (Pre-Development)

The presented models below were developed to aid with machine element design as well as the polishing process design. Developing a force-controlled process is useful in all manufacturing processes as it allows an operator to control other related outputs, such as development of residual stress, crack development, ensuring that ductile regime processes occur and optimizing work time. By studying the contact mechanics (and the interaction between abrasive and workpiece), predictions can be made that can stop various modes of failure, including fatigue, wear, yielding and fracture [74]. By using multiple methods of modelling (analytical, empirical and simulation), verification on outputs and results can be made with a high degree of confidence. These calculations are vital in ensuring that the correct polishing conditions can be imparted and aid greatly in the machine design and development.

3.1. Process Inputs and Description

Table 4 in the literature review chapter provides the typical values for the workpiece to be polished (important material property inputs). The material properties of the abrasive are as follows (see Table 5):

Table 5 - Material properties of abrasive constituents

Material	Density (ρ) kg/m^3	Poisson Ratio (v)	Modulus of Elasticity (E) Pa	Hardness (H) GPa	Yield strength (S_y) GPa
Gelatin	680	0.5	43200	-	1.07e^{-4}
Diamond	3020	0.148	1180x10^9	105	35
SiC	3500	0.14	330x10^9	28	21

The abrasive consists of 97% gelatin, 2.9% SiC and 0.1% diamond (mesh 5000). The velocity inputs for the model were taken at steps varying from 6.28 m/s to 31.4 m/s (these are the minimum and maximum velocities that the designed polishing process can provide).

3.2. Analytical Method – Notion of Momentum

3.2.1. Methodology

The analytical method of modelling proves to be superior to other models when considering the entire abrasive and its interaction with the workpiece. It also provides a greater understanding of what is happening at the macro level. The method (and corresponding equations) used in this subsection have been presented in "A Force Controlled Polishing Process Design, Analysis and Simulation Targeted for the Selective Laser Sintered Aero-Engine Components" for the conference: COMA 22. These equations are also presented in a

study by Kuppuswamy et al. [4]. Modelling a multi-layered asperity without empirical data can prove complex in nature. Researchers [4] studying the nature of polishing have started with kinetic energy models and the principle of momentum conservation:

$$F = \frac{m_1 v_1 - m_2 v_2}{\Delta t} \tag{10}$$

Where F is the particle's force upon the workpiece, m_1 and m_2 are the particle's mass before and after collision respectively, and v_1 and v_2 are the particle's velocity before and after collision, respectively. Δt is the time needed to cover the stand-off distance d:

$$\Delta t = \frac{d}{v} \tag{11}$$

Abrasive mass is calculated by multiplying the combined abrasive volume (which has an assumed diameter of 2 mm) by the combined abrasive density:

$$\frac{1}{\rho_C} = \frac{\%vol_{gel}}{\rho_{gel}} + \frac{\%vol_{SiC}}{\rho_{SiC}} + \frac{\%vol_{diamond}}{\rho_{diamond}} \tag{12}$$

The combined density of all becomes very similar to the density of gelatin due to the small percentage by volume of SiC and diamond.

Velocity v_1 is changed as the inputs given above change while v_2 is assumed as 0 m/s because as the abrasive media changes shape and deforms, it becomes stagnant and falls off the workpiece target (all energy is absorbed by the workpiece).

Contact force is the input for many fundamental contact mechanics equations and the following values can be acquired (assuming contact between a sphere (the abrasive) and a plane (the workpiece)):

$$a = 0.721[F(\eta_1 + n_2)\frac{D_1 D_2}{D_1 + D_2}]^{\frac{1}{3}} \tag{13}$$

$$P_o = \frac{1.5F}{\pi a^2} \tag{14}$$

$$\delta = 1.04\left[(\eta_1 + n_2)^2 F^2 \frac{D_1 D_2}{D_1 + D_2}\right]^{1/3} \tag{15}$$

Where a is the contact radius, P_o is the hertzian contact stress/pressure and δ is workpiece deformation. The input parameter D_1 is the abrasive diameter (assumed as approximately 2 mm) and D_2 is the grain diameter of the workpiece (assumed as 10 µm for Ti-6Al-4V). η is a material parameter, which is the difference of Poisson's ratio for the material divided by its Young's modulus (η_1 represents the workpiece and η_2 represents the abrasive).
The formula is given as:

$$\eta = \frac{1-v}{E} \tag{16}$$

v is respective Poisson's ratio and E is respective Young's modulus.

Separately to this, the area of contact (as described in contact mechanics) is found as:

$$A = \pi a^2 \tag{17}$$

Where a (the contact radius) is found using (13).

Abrasive deformation is found by multiplying the acquired deformation (15) by the hardness ratio of the two materials, where H_1 is $H_{gelatin}$ (simplified due to the hardness effect of gelatin overcoming the combined hardness) and H_2 is $H_{Ti6Al4V}$ (workpiece hardness).

$$\delta_w = H_R \delta \qquad (H_R = \frac{H_1}{H_2}) \tag{18}$$

A desirable process output is that of polishing time from an initial surface roughness (R_{a1}) to the finished surface roughness (R_{a2}). This is found by:

$$t_{polishing} = \frac{\text{Total impingments to acheive desired surface roughness}}{\text{Number of impingments per second}} \tag{19}$$

$$t_{polishing} = \frac{\frac{2\pi}{3}(R_{a1}^2 - R_{a2}^2)}{\frac{\pi n}{6}(3a^2 + \delta_{vol}{}^2)\delta_{vol}} \tag{20}$$

Where n is the amount of abrasive particles colliding with the workpiece per second and δ_{vol} is the indentation volume [75] of the abrasive on the workpiece:

$$\delta_{vol} = \frac{\pi}{6}(3a^2 + \delta^2)\delta \tag{21}$$

Where a and δ are as mentioned previously. To ensure that the process is occurring in ductile regime conditions, contact stress evaluations were used. The Bifano equation for critical depth of cut [75] was used to accompany this and is calculated by:

$$d_c = 0.15\frac{E_{Ti6Al4V}}{H_{Ti6Al4V}}\left(\frac{K_{cTi6Al4V}}{H_{Ti6Al4V}}\right)^2 \tag{22}$$

For the Ti-6Al-4V alloy, the critical depth of cut was found to be 2.513 mm. As mentioned previously, all other depths of cut can be assumed as indentation depth (workpiece deformation).

It is also important to note the theoretical maximum shear stress for no deformation to occur:

$$\tau_{max} = \frac{G}{2\pi} \tag{23}$$

Where G is shear modulus (45 GPa for Ti-6Al-4V). τ_{max} was calculated to be 7.2 GPa for Ti-6Al-4V. Note that τ_{max} is the minimum theoretical contact stress to induce ductile regime polishing conditions.

It is important to note that surface roughness is not directly calculated in this model and the initial and final surface roughness are used as inputs to the model. An initial surface roughness of 2.2 μm was assumed (assuming a semi-finished SLS Ti-6Al-4V part) and a final desirable surface roughness of 0.1 μm (approximately the value whereby mirror finish is achieved) was assumed. These inputs can be adjusted as desired to determine polishing time for each specific case. Table 6 below shows the acquisition of polishing time results using the model. Steps of 0.2 μm are assumed and the volume of asperity is calculated by finding the spherical volume using R_{ai} (where i is the iteration number of calculation from 0 (2.2 μm) to 10 (0.1 μm)). Once the spherical asperity volume is calculated, the difference in volume between steps is stated and the number of hits can be calculated by dividing the difference in volume by the indentation volume per abrasive as per (21). Polishing time is then found by dividing the number of hits required by the number of particles impacting per second. The acquisition of this result is summarised in (20).

Table 6 - An example of polishing time calculation for a polishing condition of 31.4 m/s

Impeller Velocity	Equivalent RPM	Ra	Volume of sphere (μm^3)	Difference in Volume (μm^3)	Difference in Volume (m^3)	Number of hits required to achieve volume difference	Polishing time to achieve number of hits (seconds)	Polishing time (min)
31.4	83.29109	2.2	22.30112			0	0	0
		2	16.75516	5.545958	5.55E-18	1.94E+04	12.38	0.062296
		1.8	12.21451	10.08661	1.01E-17	3.54E+04	22.52	0.113307
		1.5	7.068583	15.23254	1.52E-17	5.34E+04	34.02	0.171118
		1.2	3.619115	18.682	1.87E-17	6.55E+04	41.72	0.20987
		1	2.094395	20.20672	2.02E-17	7.08E+04	45.12	0.226999
		0.8	1.07233	21.22879	2.12E-17	7.44E+04	47.41	0.238482
		0.6	0.452389	21.84873	2.18E-17	7.66E+04	48.79	0.245446
		0.4	0.134041	22.16708	2.22E-17	7.77E+04	49.50	0.249023
		0.2	0.016755	22.28436	2.23E-17	7.81E+04	49.76	0.25034
		0.1	0.002094	22.29902	2.23E-17	7.82E+04	49.80	0.250505

3.2.2. Results

The most important output is that of force which shows an exponential increase when related to impinging velocity; impinging force was calculated to be 0.0056 N (per media) for a velocity of 6.28 m/s and increased to a value of 0.1403 N (per media) for a velocity of 31.4 m/s. It should also be noted that the polishing depth of cut grows slightly as impinging velocity is increased but it is always far below (by a factor of over 10000) the critical depth of cut for Ti-6Al-4V (2.53 mm as described in the previous section). The results also show that all impinging velocities are high enough to induce ductile regime polishing conditions and are below the maximum value of contact stress to induce surface damage to the workpiece (45 GPa, the shear modulus of Ti-6Al-4V). Shear modulus (a material's resistance to shearing deformation) in terms of contact stress, is the point at which asperities plastically deform instead of elastically deform and is a lower measure of material failure than Young's Modulus. Figure 17 shows a visual representation of the above discussed results.
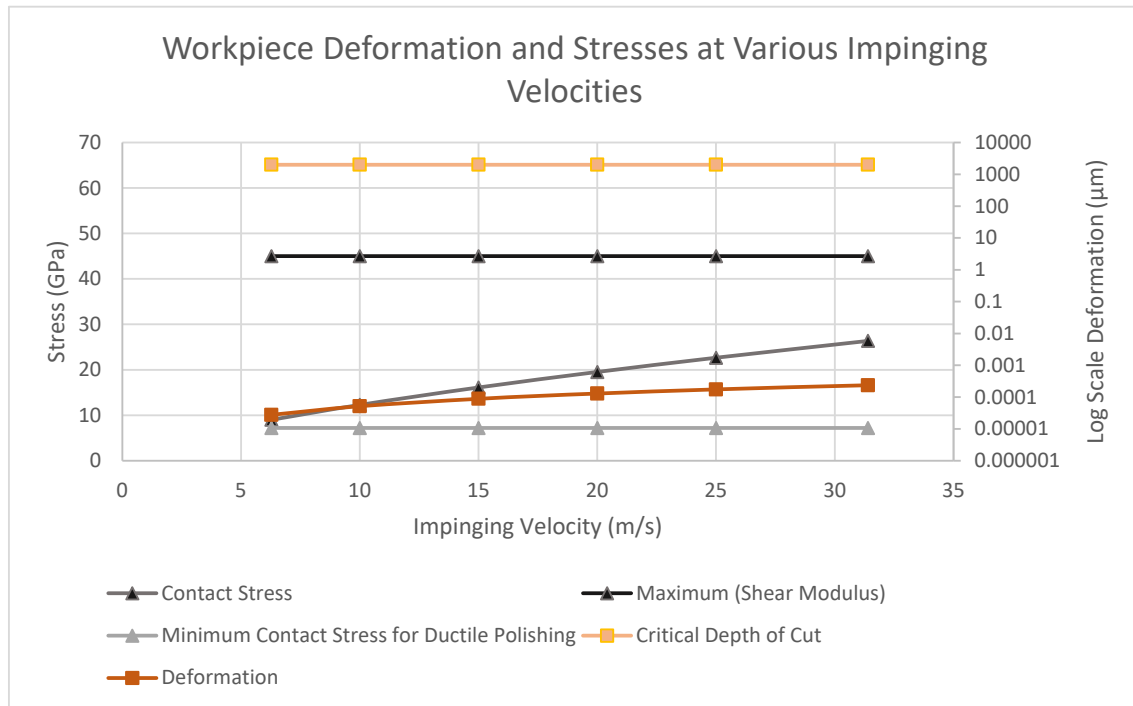
Figure 17 - Analytical Method Notable Results

The two figures below (Figure 18 and Figure 19) show the relationship between impinging velocity and time to polish. At an impinging velocity of 6.28 m/s, the polishing time is calculated to be 91.46 minutes. This decreases exponentially to the next value of 16.6 minutes for an impinging velocity of 10 m/s. Polishing time then decreases to 3.75 minutes at 15 m/s and further decreases to 0.25 minutes at 31.4 m/s.
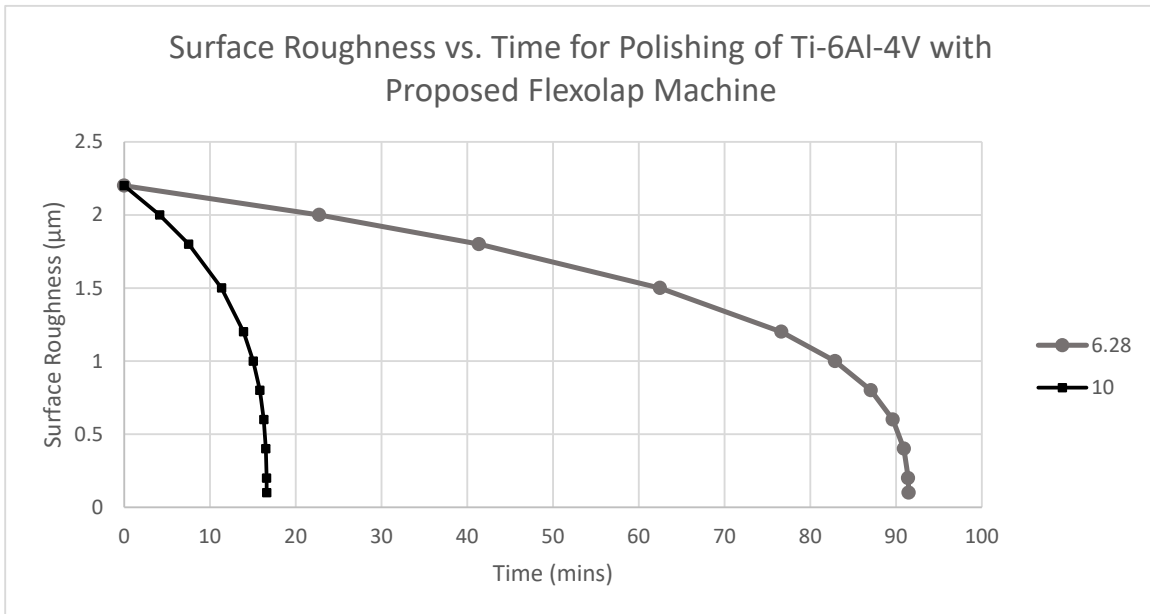
Figure 18 - Polishing times for 6.28 m/s and 10 m/s
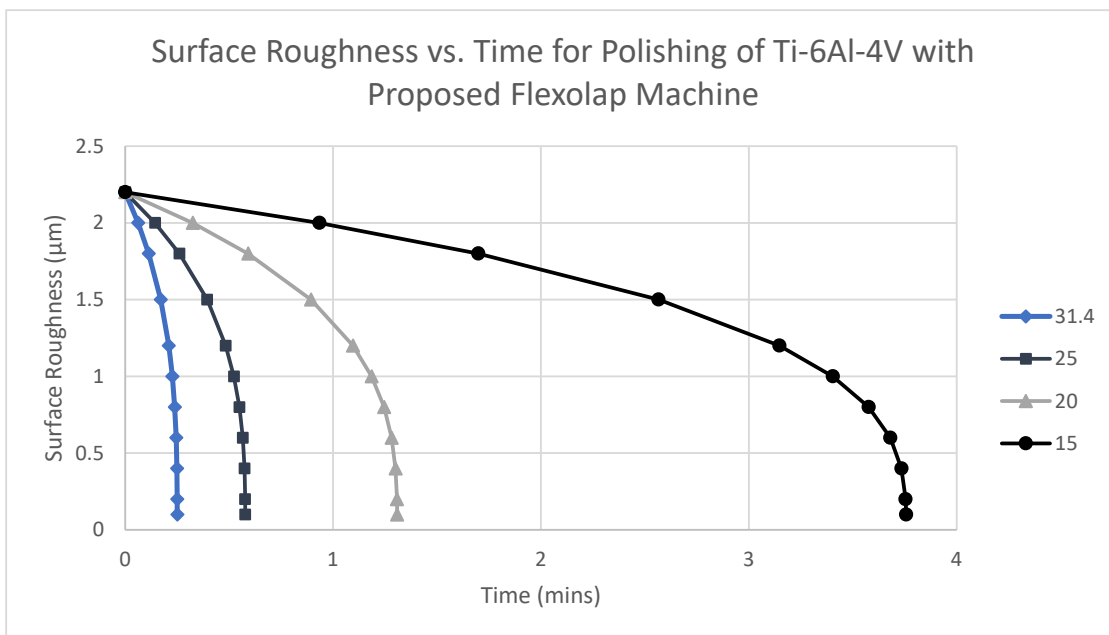
Figure 19 - Polishing Times for velocities: 15 m/s, 20 m/s, 25 m/s and 31.4 m/s

3.3 Empirical Method

3.3.1. Methodology

The method described below uses derived empirical formulae as well as scientific formulae and analytical methods. This methodology is based on the notion of parameters relating to their critical values (where critical values have been obtained using hertzian contact mechanics and sets of developed and more importantly, verified, empirical formulae). The method was formulated with both the macro-perspective and the micro-perspective in mind. The micro-perspective methodology assumes that a single #3000 mesh diamond particle impinges upon a single Ti-6Al-4V asperity, while the macro perspective assumes the combined media (gelatin, SiC and diamond) contacts the Ti-6Al-4V surface (the visualisation of this is made clearer in the simulation section as well as in previously displayed diagrams). FEM developed models [43] [76] have been used to improve previous models that were pioneering for parameter prediction in polishing [42] [47]. The basis of modelling was that of von Mises yield criteria and the following formulae for the important contact parameters of: critical deformation (ω_C (also known as interference depth)), critical area of contact (A_c), and critical contact force (F_c):

$$\omega_C = \left(\frac{\pi C S_y}{2E'}\right)^2 R \tag{24}$$

$$A_C = \pi^3 \left(\frac{C S_y R}{2E'}\right)^2 \tag{25}$$

$$F_c = \frac{4}{3}\left(\frac{R}{E'}\right)^2 \left(\frac{C}{2}\pi S_y\right)^3 \tag{26}$$

Where R is the equivalent radius of curvature (determined differently for contact shapes) and is assumed as equal to the abrasive radius (because the interaction is assumed as between a sphere and a plane). S_y is the abrasive yield strength and E' is the equivalent elastic (Young's) modulus, which is found by:

$$\frac{1}{E'} = \frac{1-v_1^2}{E_1} + \frac{1-v_2^2}{E_2} \tag{27}$$

E_1 and E_2 are the Young's moduli of the workpiece and abrasive respectively. v_1 and v_2 are the Poisson's ratios of the workpiece and abrasive, respectively. C is the critical yield stress coefficient and is calculated by:

$$C = 1.295e^{0.736v} \tag{28}$$

Where v in this case, is the workpiece's Poisson's ratio. The critical velocity of abrasive (V_c), which is the velocity before the onset of plastic deformation, is found by:

$$V_c = \sqrt{\frac{4\omega_c F_c}{5m_{abr}}} \tag{29}$$

Where m_{abr} is the abrasive mass.

By noting the previously calculated critical values, the values of spherical deflection, contact area, and contact force (which allows predictions on values to be made) can be normalized. Normalized spherical deflection, contact area, and contact force are found by the following:

$$\omega^* = \frac{\omega}{\omega_c} \qquad A^* = \frac{A}{A_c} \qquad F^* = \frac{F}{F_c} \tag{30}$$

When dividing impinging velocity by critical velocity, normalized velocity is acquired. If normalized velocity is much less than 1, elastic conditions can be assumed [76]. For diamond only interaction (micro analysis) the normalized velocity at the maximum impinging velocity (of 31.4 m/s) was calculated as 0.028 and for the whole abrasive interaction (macro analysis), the normalized velocity was calculated as 0.102. These values are much less than 1, therefore elastic conditions were assumed, and the coefficient of restitution was approximated as having a value of 1. Jackson and Green [76], with their developed FEM model, found that normalized contact force simplifies to:

$$F^* = (\omega^*)^{3/2} \quad with \quad A^* = \omega^* \tag{31}$$

Force at a particular deformation was then inferred as:

$$F_{imp} = F_c \left(\frac{\omega(V)}{\omega_c}\right)^{3/2} \tag{32}$$

Deformation was then inferred by using the inferred normalized force equation, deformation equations, critical velocity equation and critical force equation:

$$\omega(V) = \left(\frac{5V^2 m_{abr}\omega_c^{3/2}}{4F_c}\right)^{2/5} \tag{33}$$

To find force at a certain impinging velocity, the derived deformation equation above was substituted into the inferred impinging force equation. It is also possible to substitute derived deformation into the widely used force model [74]:

$$F_{imp} = \frac{4}{3}E'\sqrt{R}[w(v)]^{3/2} \tag{34}$$

To find the area of contact it was noted that at elastic conditions, normalized contact area equals normalized deformation. This was then substituted into the normalized contact area equation. The radius of circular contact area, a can also be found.

$$A = A_C \omega(V), \qquad\qquad a = \sqrt{\frac{A}{\pi}} \tag{35}$$

Contact pressure/stress was found by (14) in the analytical section shown previously.

To calculate polishing time, the initial surface roughness R_{a1}, and desired surfaces roughness R_{a2}, were determined. Grain surface size required volume was found by assuming that each surface asperity on the workpiece is a sphere. This determines the volume of required removal from the polishing action:

$$V_{R_a} = \frac{2\pi}{3}(R_{a2}^3 - R_{a1}^3) \tag{36}$$

Indentation volume per impinging particle was found with:

$$V_{cut} = \frac{\pi}{6}(\omega(V)^2 + a^2)\omega(V) \tag{37}$$

Where $\omega(V)$ and a are described on the previous page. The number of hits required by the impinging particles to achieve the desired surface finish is found by dividing the difference in volume of grain size by the volume of each particle's impinging cut:

$$Hits = V_{R_a}/V_{cut} \tag{38}$$

The time for polishing was then be found by dividing the number of hits required by the number of impinging particles per second:

$$t = \frac{Hits}{particles\ per\ second} \tag{39}$$

3.3.2. Results

When analysing the combined abrasive media (entire media) impinging force, the values for various impinging velocities were found to increase logarithmically as velocity increased, increasing from 0.11 N at an impinging velocity of 6.28 m/s, to 0.761 N at an impinging velocity of 31.4 m/s. Figure 20 below shows this increase visually.

When conducting the micro-analysis, polishing forces (per diamond particle) exhibit the same behaviour (as expected), while forces grew from 0.098 mN at 6.28 m/s, to 0.675 mN at 31.4 m/s. Figure 20 below shows this increase visually.

Contact stresses between asperity and particle grew from 5.469 GPa to 10.411 GPa (as increasing velocity was increased from 6.28 m/s to 31.4 m/s). Polishing times (to polish from an initial surface roughness of 2.2 μm to a desired roughness of 0.1 μm), decreased exponentially from a high of 41.187 minutes at 6.28 m/s, to a low of 0.615 minutes at 31.4 m/s. See Figure 20 below for a visual representation of the decrease in polishing time.
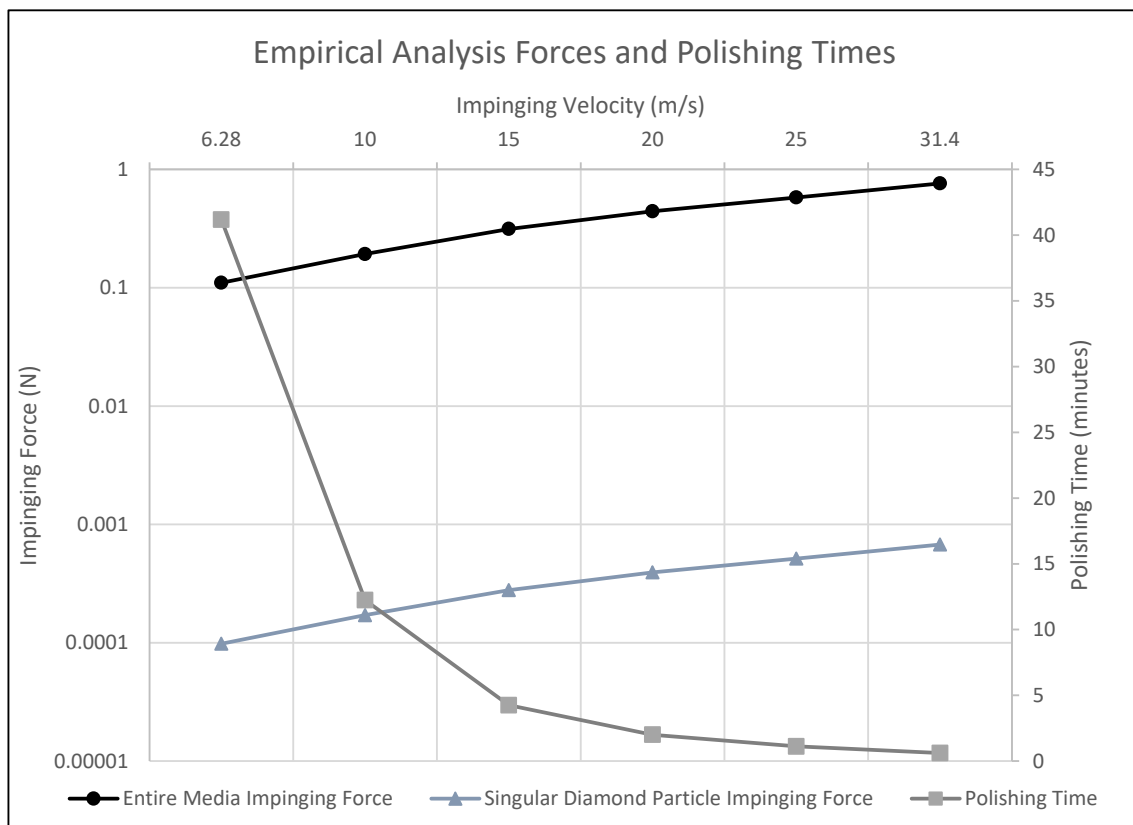
Figure 20 - Notable Results from the Empirical Analysis

3.4. Simulation of Material Removal on Workpiece Asperity

3.4.1. Methodology

The third and final method of modelling presented in this dissertation is that of simulation. Simulation based models are helpful in that a wide range of parameters can be accounted for and when using the correct tools, it allows for a simple manner of verifying other developed models [59]. What is important to note here is that the polishing process is random in nature, and abrasive particles often impinge upon the workpiece at different times, angles, and are of different size. If these random effects are great enough, the process parameters can interact with each other in an unexpected fashion, where the effects of the process can contrast what was predicted [59]. Simulation gives an additional insight into the process and aids in creating the most optimal process possible (especially as less desired variables e.g., temperature changes, are outputs that can be easily found because of simulation).

SolidWorks was used as the simulation engine for the process. A static simulation method was chosen, where SolidWorks makes use of the finite element method to identify process behaviour. The process is modelled by assuming that a single diamond particle impinges upon a single asperity of a Ti-6Al-4V workpiece. The asperity size was assumed as 2.2 μm in diameter while the contact area between workpiece and abrasive was increased according to the applied impinging force/velocity (which grows as shown in the previous two sections). Figure 21 (a) and (b) below, show how the asperity was modelled for different impinging velocities (where the force was applied at 45º, and the contact area was increased according to impinging velocity).
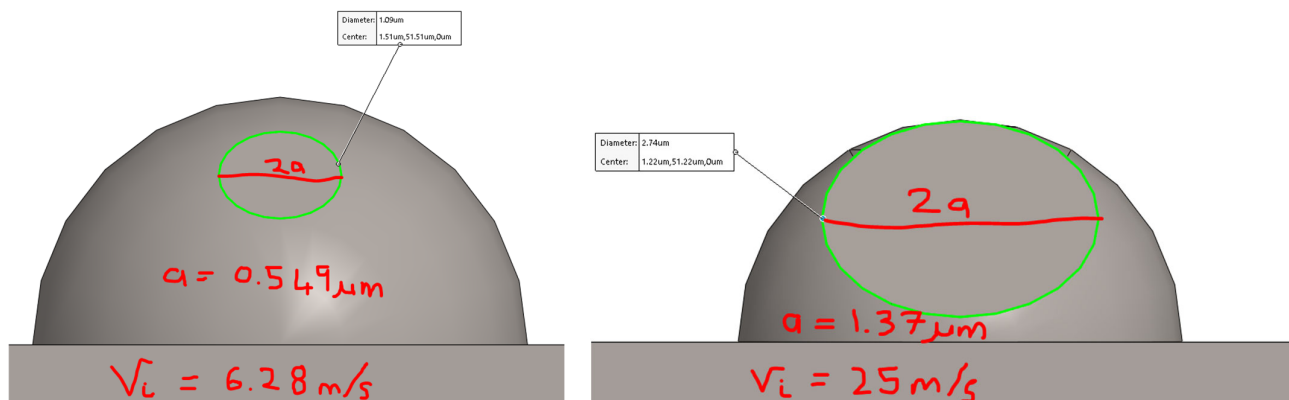
Figure 21 - (a) Contact area for an impinging velocity of 6.28 m/s, (b) Contact area for an impinging velocity of 25 m/s

Simulations were run to correspond to the same intervals as the analytical and empirical calculations sections (at 6.28 m/s, 10 m/s, 15 m/s, 20 m/s, 25 m/s, 31.4 m/s). It is important to note that in the results, the deformation scale has been increased to 10:1 (to appropriately visualise the deformation occurring in the micro simulation).

3.4.2. Results

The graph below shows the results acquired from the simulations (maximum contact stress and displacement for various impinging velocities). Figure 22 below shows how workpiece deformation and contact stresses increase while impinging velocity is increased (a similar trend to the previous methods is noted). It can also be seen that below approximately 15 m/s impinging velocity, the minimum theoretical contact stress (7.2 GPa) to induce ductile regime polishing conditions is not met (thus polishing velocity should be kept at over 15 m/s for efficient polishing). The results also show that brittle fracture will not occur as the maximum contact stresses are below the shear modulus of Ti-6Al-4V (45.2GPa). The results acquired for workpiece deformation and contact stresses were found to agree well with the previously calculated maximum contact stresses and maximum deformation from both the analytical and empirical solutions. As in the previous section, the linear trend of increasing deflection and contact stress is present. The presented simulations affirm the analytical and empirical analyses and thus provide another strong basis to move onto machine design with.
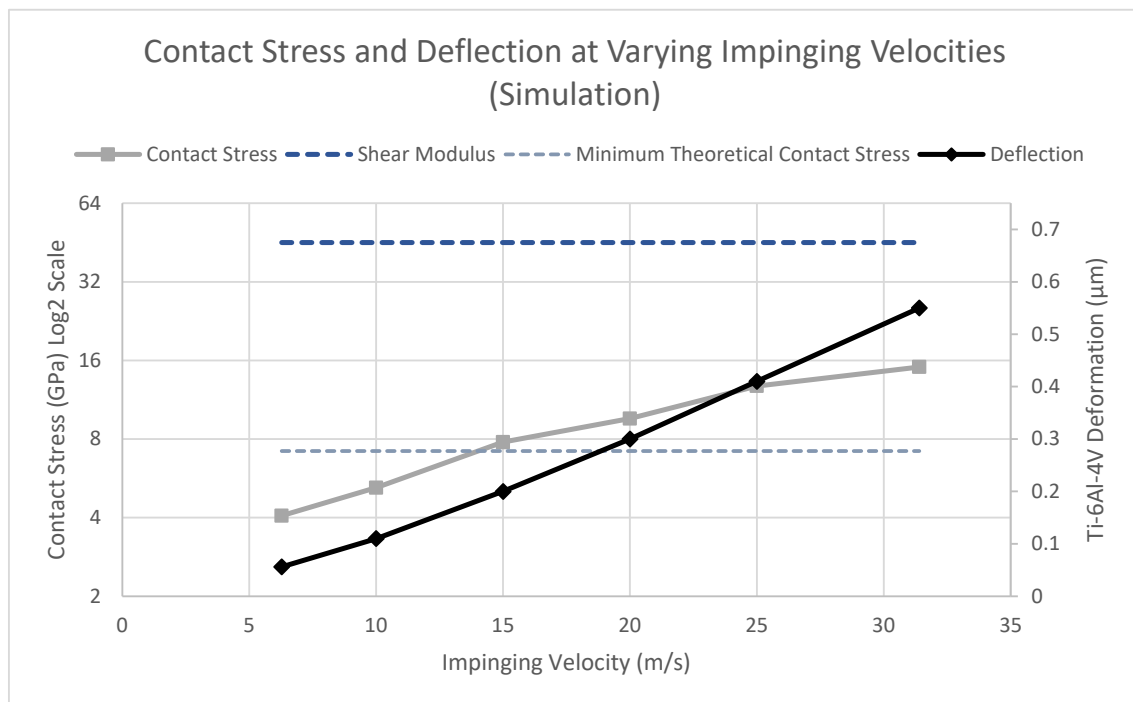
Figure 22 - Simulation Based Results (Summarised)

Figure 23 and Figure 24 on the following two pages show the simulation results acquired for deformation (displacement) and contact stresses, respectively. When comparing the displacement solutions, these align well with the empirical model (micro-model/singular impinging diamond model) and the contact stresses agree well with both the analytical and empirical methods for previously calculated contact stresses and maximum workpiece deformation.

$$V_{imp} = 6.28 \frac{m}{s} \quad F_{imp} = 0.0056N$$
$$\delta_{max} = 0.056\mu m \; \sigma_{cmax} = 4.07GPa$$

$$V_{imp} = 10 \frac{m}{s} \quad F_{imp} = 0.014N$$
$$\delta_{max} = 0.111\mu m \; \sigma_{cmax} = 5.06GPa$$

$$V_{imp} = 15 \frac{m}{s} \quad F_{imp} = 0.0320N$$
$$\delta_{max} = 0.2\mu m \; \sigma_{cmax} = 7.781GPa$$

$$V_{imp} = 20 \frac{m}{s} \quad F_{imp} = 0.056N$$
$$\delta_{max} = 0.301\mu m \; \sigma_{cmax} = 9.628GPa$$

$$V_{imp} = 25 \frac{m}{s} \quad F_{imp} = 0.0890N$$
$$\delta_{max} = 0.41\mu m, \sigma_{cmax} = 12.77GPa$$

$$V_{imp} = 31.4 \frac{m}{s} \quad F_{imp} = 0.1404N$$
$$\delta_{max} = 0.55\mu m \; \sigma_{cmax} = 15.09GPa$$
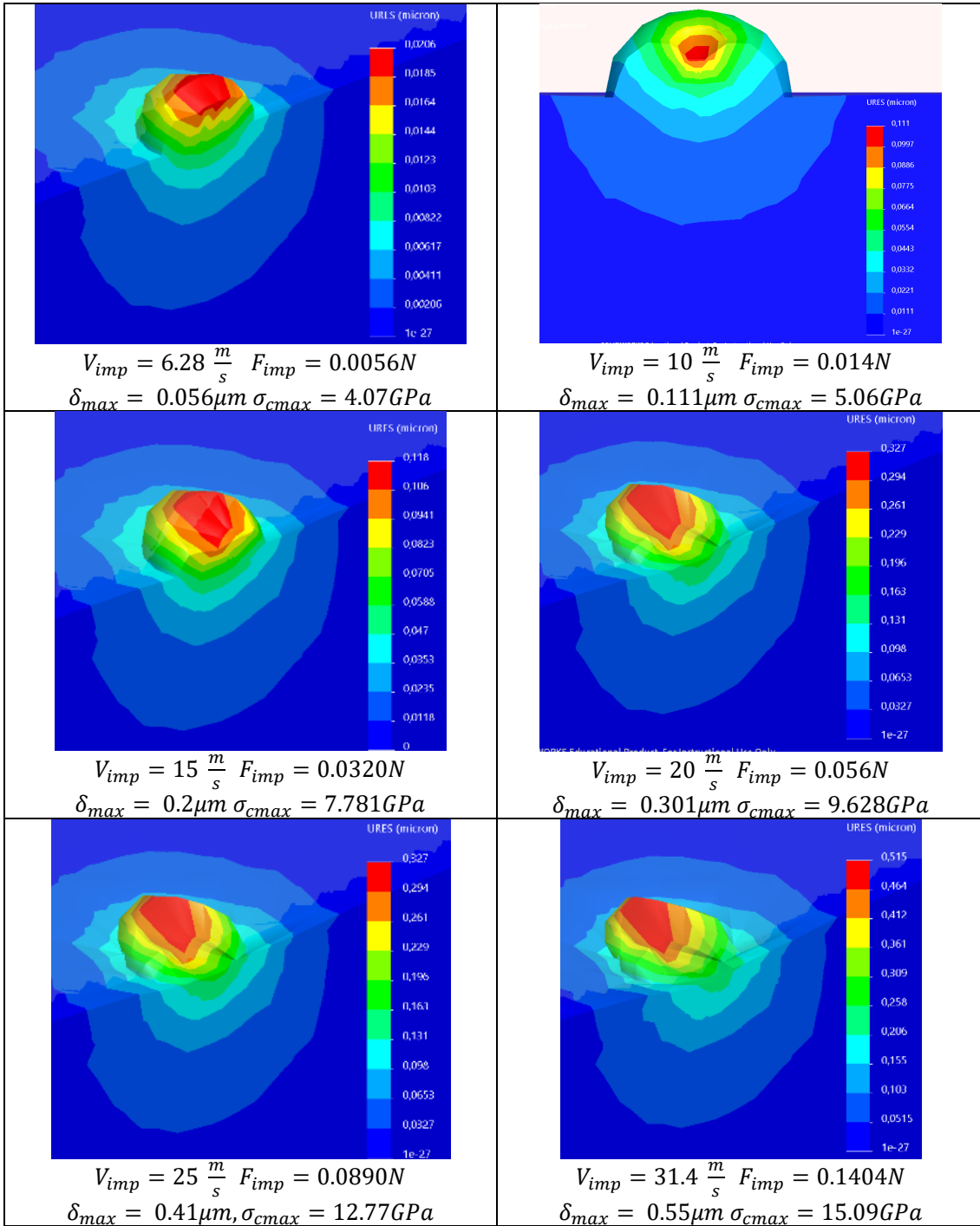
Figure 23 - Simulation Displacement Solutions

$V_{imp} = 6.28 \frac{m}{s}$ $F_{imp} = 0.0056N$ $\delta_{max} = 0.056\mu m$ $\sigma_{cmax} = 4.07GPa$	$V_{imp} = 10 \frac{m}{s}$ $F_{imp} = 0.014N$ $\delta_{max} = 0.111\mu m$ $\sigma_{cmax} = 5.06GPa$
$V_{imp} = 15 \frac{m}{s}$ $F_{imp} = 0.0320N$ $\delta_{max} = 0.2\mu m$ $\sigma_{cmax} = 7.781GPa$	$V_{imp} = 20 \frac{m}{s}$ $F_{imp} = 0.056N$ $\delta_{max} = 0.301\mu m$ $\sigma_{cmax} = 9.628GPa$
$V_{imp} = 25 \frac{m}{s}$ $F_{imp} = 0.0890N$ $\delta_{max} = 0.41\mu m, \sigma_{cmax} = 12.77GPa$	$V_{imp} = 31.4 \frac{m}{s}$ $F_{imp} = 0.1404N$ $\delta_{max} = 0.55\mu m$ $\sigma_{cmax} = 15.09GPa$
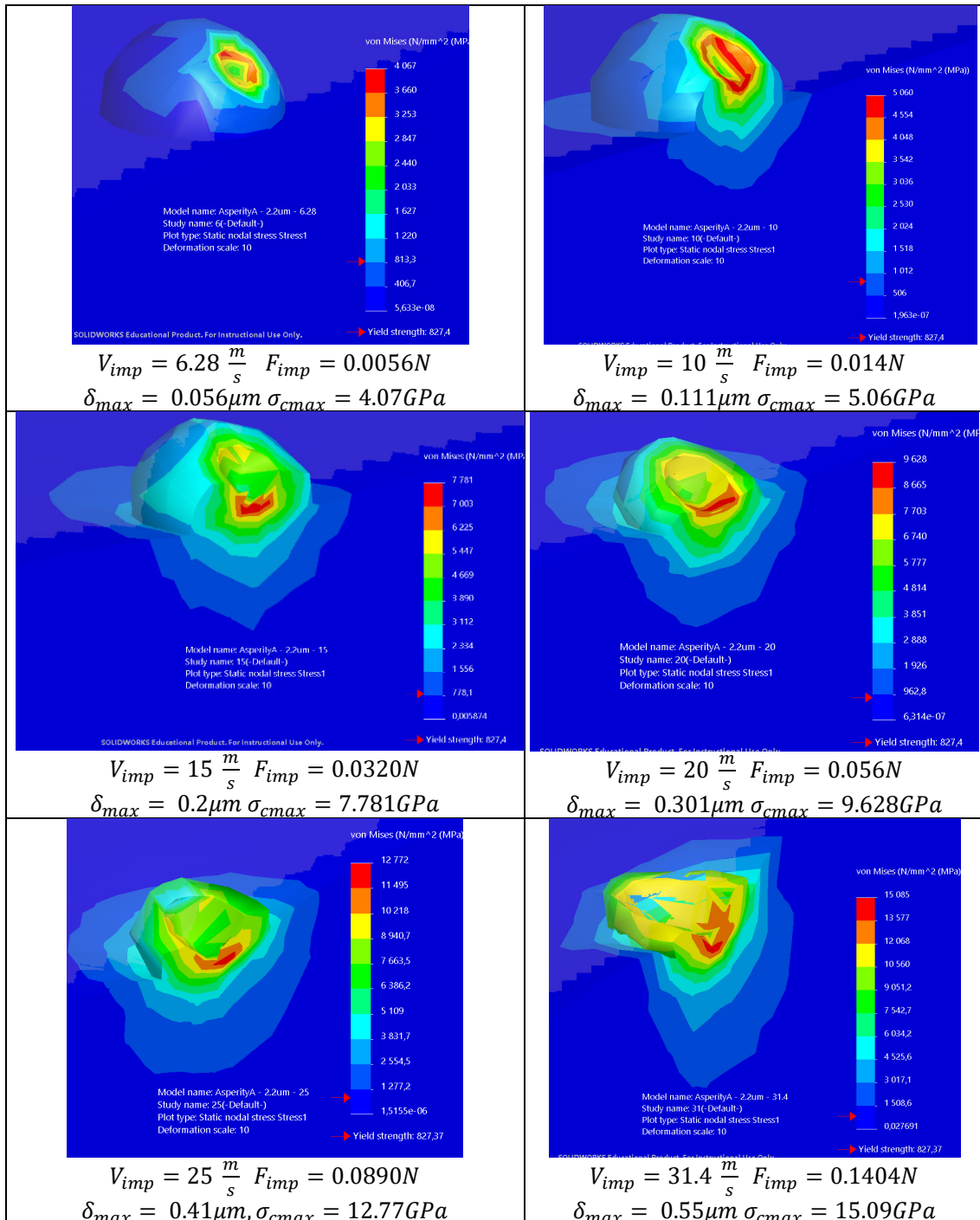
Figure 24 - Contact Stress Simulation Results

3.5. Conclusion/Comparison for Analytical, Empirical and Simulation based Results

Analysis of all displayed results proves to show that flexible abrasive assisted polishing is a viable finishing technique. The results in all cases show that material removal will occur for polishing conditions that can be implemented in machine design (polishing time, impinging velocity, and polishing angle). This conclusion is drawn due to the minimum theoretical contact stress being reached in all three analyses. Visual representation of the deformation of material in the simulation subsection helps to affirm the process hypothesis.

Ductile regime polishing conditions are maintained throughout as the maximum (shear modulus) contact stress is never passed even at a high impinging velocity. Deformation of workpiece is far below the critical depth of cut (proven in all three analyses) and contact forces match in both the empirical and analytical analysis (with the analytical analysis providing force input to the simulation-based model).

The results obtained in these analyses allow for the determination of a range of polishing parameters for machine design to obtain ductile regime polishing conditions.

Chapter 4 - Machine Design and Development

A major measurable output of this project/dissertation and critical to the success of the following stages of this project was that of designing and developing a machine capable of polishing SLS processed Ti-6Al-4V components. This intensive process involved many machine-element-design calculations, a large amount of 3D modelling, manufacturing components, ordering parts from a variety of different suppliers, designing a safe electrical and pneumatic network for the system, making sound engineering choices, and assembling the machine with correct tolerances, fitments, and sizing.

The component design was split up as follows:

- Abrasive output/discharge - involving the design of a system to take abrasives in and project them out at a high enough velocity to impart ductile regime polishing conditions upon a workpiece.
- Abrasive collection, hydration, and recycling – designing a sub-system to collect all used media, filter out the unusable media, rehydrate the dry abrasives, and then send the abrasives back to the output system
- Structural design and enclosure – designing a modular and adjustable frame to ensure all abrasives are contained and to make the machine ergonomically usable for the operator, as well as to absorb all machine forces and support accessories.
- Control design and placement – designing of electrical and pneumatic diagrams and implementing this into the assembly so that most of it is hidden and so that control can occur from a singular location (allowing ease of parameter adjustment by the operator).

4.1. Component Design and Subassemblies

4.1.1. Abrasive Output/Discharge

This subassembly was designed for the principle of taking in abrasive media and increasing the media's exit velocity, before shooting out and directing the media at a workpiece. Tolerances were of crucial importance in this subassembly and machine component calculations were required to make sound engineering decisions. Figure 25 on the following page shows the final design used in the machine for this sub-assembly and these labels are used for reference throughout this sub-chapter. The components acquired before design were: nylon impeller, impeller casing, support stand and drive motor. The system needed to be modified for a speed-up ratio and the designed/new components added to the system were: large pulley, small pulley, belt, motor support stand, (precision grinding) spindle, spindle housing and a media output nozzle.

The drive motor has a power rating of 372.9 W (0.5 hp) and a maximum output rotational speed of 1370 rpm. The Nylon 66 impeller (chosen for its high strength, low density, high durability, and low corrosivity) has a diameter of 120 mm. This meant that if the motor was connected to the impeller directly, the maximum output velocity would be: 8.61 m/s.

To achieve a velocity that allows for efficient polishing time and that meets the ductile regime polishing conditions, a higher output velocity was required. A pulley and belt system with a speed ratio of 4 was chosen. The speed ratio was chosen as the nylon impeller is only able to handle a rotational speed of 5000 rpm (heat and friction cause great damage to the fins and structure of the impeller above this limit). The speed-up ratio chosen allows for an output rotational speed of 5480 rpm (which corresponds to 34.432 m/s). 31.42 m/s was set as the maximum speed (corresponding to 5000 rpm) due to the restrictions stated above. A precision spindle (grinding spindle) was required to handle the high rotational speed and to transmit the motor's rotation to the output (impeller) with the correct tolerances and the critical restriction of concentricity (required to ensure the impeller does not have interference with the housing). Calculations regarding bearings, life, and sizing (which lead to spindle selection) are described in this chapter.

The media is inlet into the hole above the nylon impeller shown in Figure 25. The impeller is covered and sealed, but this has been omitted in the drawing to show details of the impeller. The media output (as labelled) is connected to either the heating nozzle (for thermoplastic cores) or to a simple metal guiding block (for gelatin cores). A secondary output nozzle was designed to provide a more refined stream of abrasives, but this created clogging and back-pressure due to the small output hole and was thus not further developed.
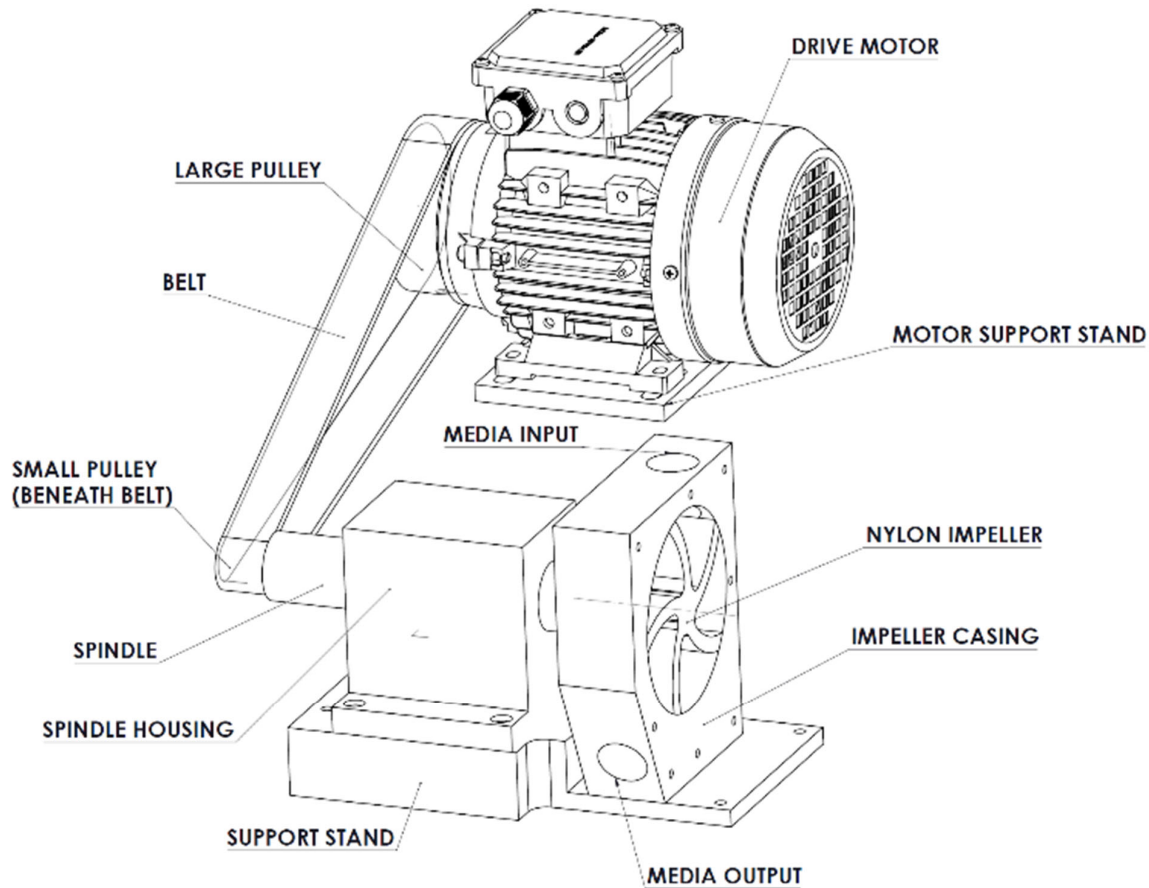
Figure 25 - Abrasive Discharge Assembly

4.1.2. Belt-Pulley System

A polyurethane flat belt was used to connect the driver pulley to the driven pulley. A slight angle (crown/camber) was created around the circumference of the pulleys to prevent belt slip. A v-belt or timing belt was not used as it was expected that impeller jamming would occur at high speed and with varying abrasive feeds (a desirable design feature was that the belt would slip off to prevent damage to the motor's spindle, the impeller and the high-precision grinding spindle).

Driver and driven pulley diameters were selected from the Misumi catalogue [77] (also noting that the maximum recommended flat pulley ratio is 4:1) as follows: 96 mm for driver pulley (D), 24 mm for driven pulley (d). The driver pulley was chosen at this size so that the face was not larger than the motor's (so that no interference would occur between the mounting and the pulley, and to minimize the torque required from the motor). The driven pulley was chosen as the smallest pulley possible to minimize mass (increase belt efficiency) and reduce heat. 24 mm was the smallest available pulley with a bore that could fit the precision spindle's pulley end inside (with enough thickness between the pulley and bore to handle the forces exerted upon it). The pulleys were fixed onto their respective shafts using set screws. The set screws

chosen were of size M5. The two figures below (Figure 26 and Figure 27) show more detailed drawings of the pulleys. These pulleys were manufactured out of aluminium (to minimize mass and thus improve efficiency).
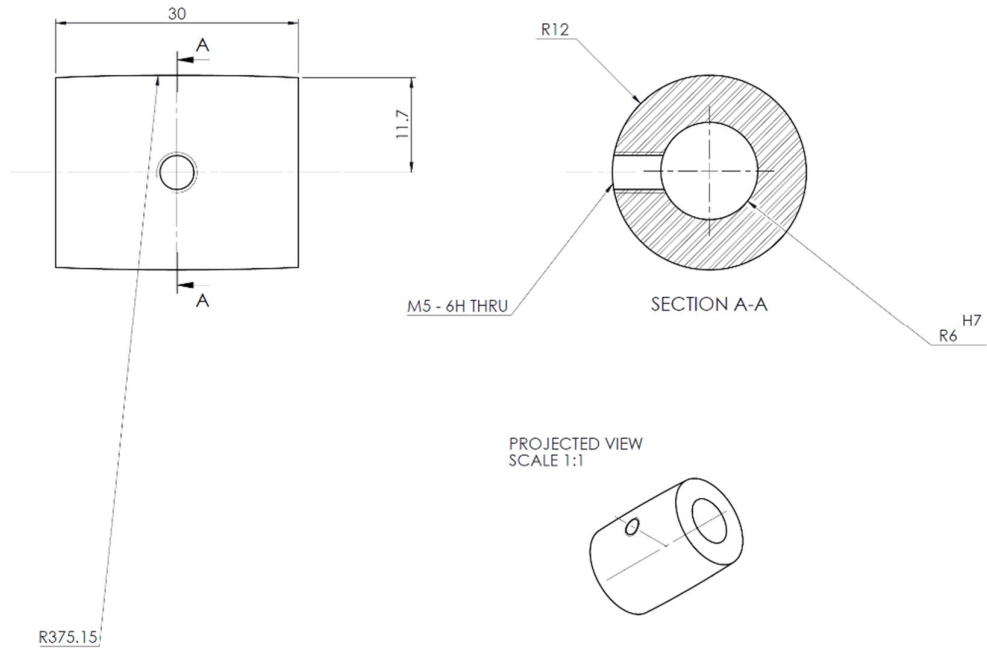
Figure 26 - Driven Pulley (small)
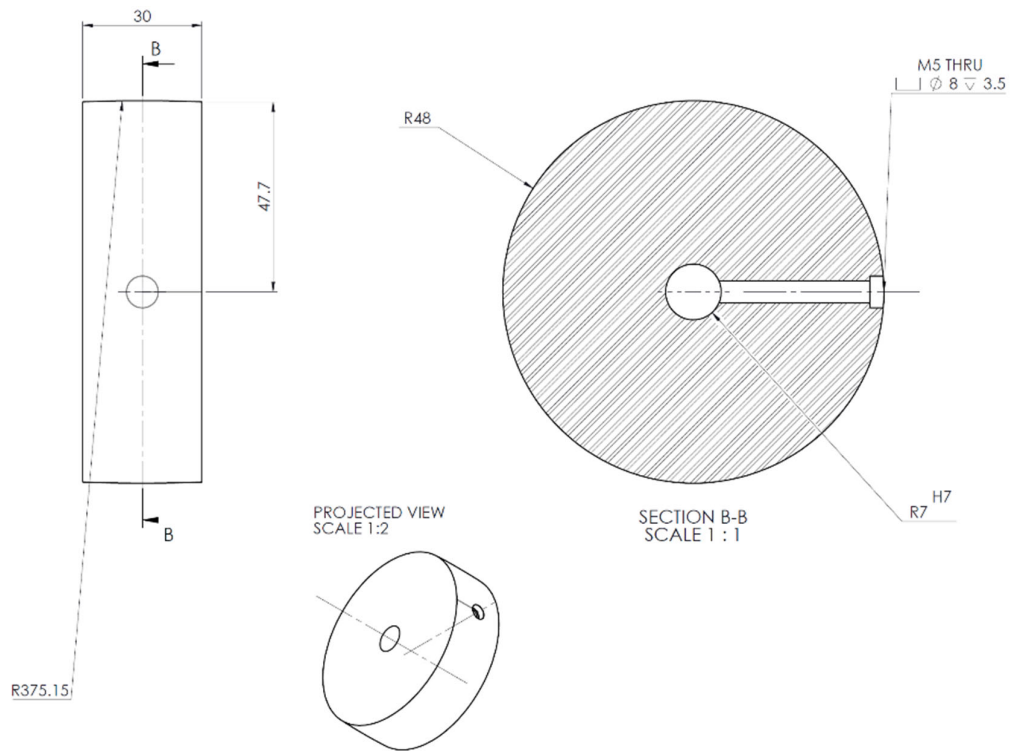
Figure 27 - Driver Pulley (large)

A simplified drawing of the spindle is shown below (where views of the bearings and interior workings are not displayed). An appropriate housing for the spindle needed to be designed to ensure that the inherited motor stand would allow for the adaption of fitting a spindle instead of a straight-motor output as well as to ensure concentricity and location. The designed spindle housing can be seen in Figure 28 below while the simplified spindle drawing can be seen in Figure 29. The spindle is secured into the housing by use of a set screw.
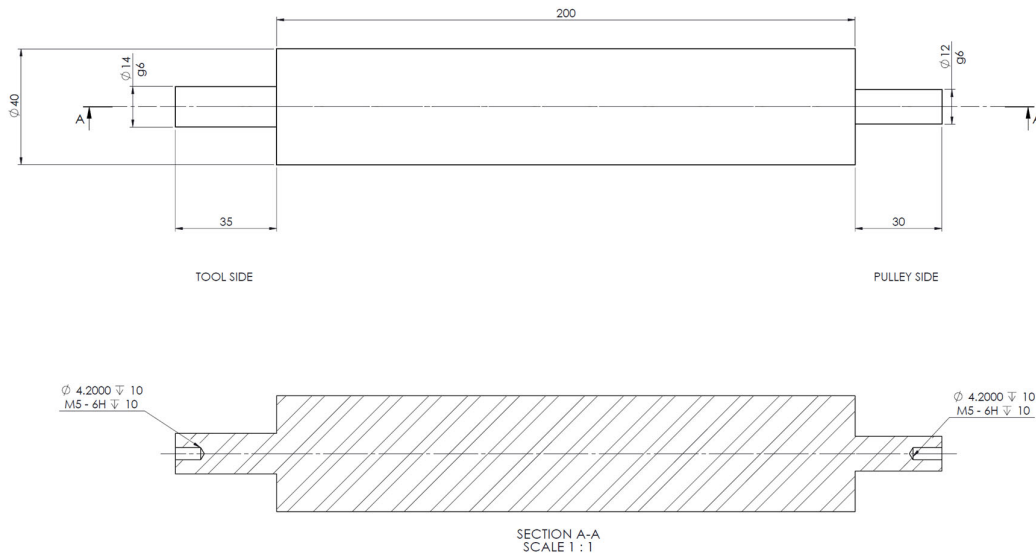
Figure 29 - Simplified Spindle Drawing (no bearings and internal features)
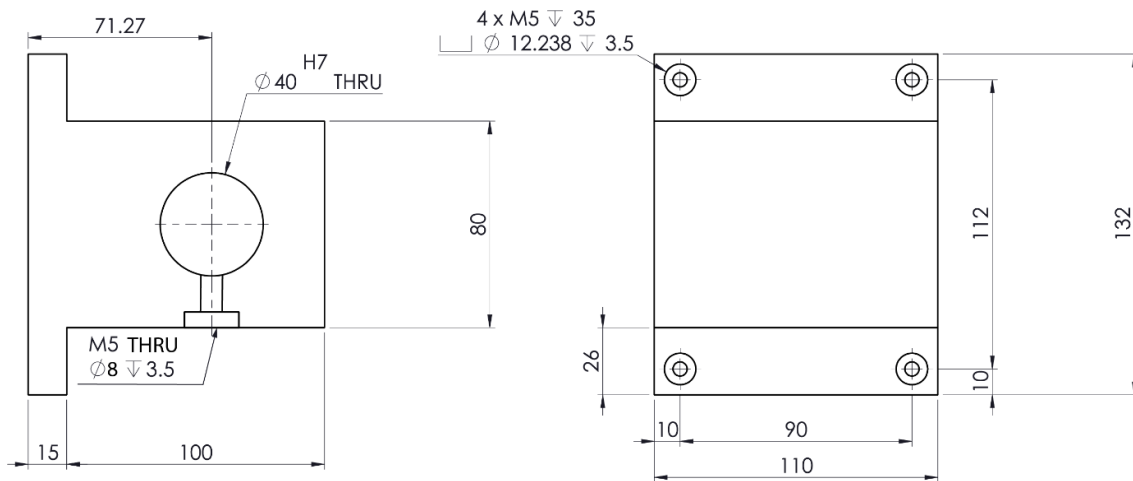
Figure 28 - Designed Spindle Housing

To design the pulley and belt dimensions as well as the spindle and housing dimensions, design calculations were required.

The outputs of belt calculations are belt width, pulley centre-to-centre distance and belt thickness. Juvinall and Marshek's [78] design textbook was used as the basis for design calculations.

The goal of this design was to optimize centre-to-centre distance (C_B). Centre-to-centre distance relates directly to contact arcs between the driver (α_2) and driven (α_1) pulleys as:

$$\alpha_1 = \pi - 2\,asin\left(\frac{D-d}{2C_B}\right) \tag{40}$$

$$\alpha_2 = \pi + 2\,asin\left(\frac{D-d}{2C_B}\right) \tag{41}$$

Wrap angle is calculated by:

$$\alpha_{belt} = 180^0 + \left(\frac{a_2 - 180^0}{2}\right) \tag{42}$$

The belt length can be found by:

$$L_B = [4C_B^2 - (D-d)^2]^{1/2} + \frac{1}{2}(D\alpha_2 + d\alpha_1) \tag{43}$$

Using optimization and space constraints in addition to the above equations, lead to the decision to use a centre-to-centre distance of 320 mm and an associated belt length of 832.55 mm. The belt width was chosen to be 25 mm due to the motor spindle's length (30 mm).

Shaft and bearing calculations were completed to select the appropriate precision spindle and to ensure that the spindle bearings could properly transmit the forces. Life calculations on the bearings were also completed to ensure sufficient longevity. These calculations also aided in selecting appropriate pulley sizes.

The driver pulley's maximum rotational speed is 1370 rpm and this translates to a tangential velocity of 6.886 m/s. The motor power is 372.85 W. The effective pull is calculated by:

$$F_u = \frac{P_{motor}}{v_{belt}} \tag{44}$$

54.143 N was the calculated value of effective pull. The belt friction coefficient was assumed at 0.2 as per the Misumi catalogue [79].

To find the low force on the belt:

$$P_2 = \frac{F_u}{e^{f\alpha_{belt}} - 1} \tag{45}$$

The high belt force is simply found by:

$$P_1 = P_2 + F_u \tag{46}$$

Horizontal and vertical components of force, were found by:

$$F_{RPH} = (P_1 + P_2) \cos\left(\frac{\Pi}{2} - \frac{\alpha_1}{2}\right) \tag{47}$$

$$F_{RPV} = (P_1 + P_2) \sin\left(\frac{\Pi}{2} - \frac{\alpha_1}{2}\right) \tag{48}$$

These were calculated to be 171.128 N and 6.091 N respectively. This was multiplied by a service factor of 2 (for single ply flat belts) to obtain service force. Multiplying the small pulley's radius by the resultant force (of the horizontal and vertical force components - $F_{RTOT} = 342.473\ N$), the torque present on the pulley was calculated as $T_{total} = 4.11\ Nm$. The smallest allowable shaft diameter was determined by first calculating the maximum allowable shaft torque. The shaft material is made of EN24(T), which has an ultimate tensile strength of 850 MPa and a Yield Strength (S_y) of 680 MPa. The maximum allowable torque was calculated by:

$$\tau_{max} = \frac{S_y}{2RF} \tag{49}$$

Where RF is the reserve factor was chosen as 3. The minimum allowable shaft diameter was calculated to be 5.696 mm:

$$d_{min} = \left(\frac{16T_{total}}{\pi\tau_{max}}\right)^{1/3} \tag{50}$$

OHL (overhung load) was calculated to compare to F_{RTOT} and was found to be 271.076 N (less than F_{RTOT}). Thus, the value of 342.473 N for F_{RTOT} was used for the bearing life calculations.

The appropriate bearing shaft size for the grinding spindle chosen was 22 mm. According to the SKF bearing catalogue, these bearings have a dynamic load rating of 14000 and a static load rating of 7250 [80].

Bearing life in hours was calculated by:

$$L_{10h} = \frac{10^6}{(60)(\omega)}\left(\frac{C_2}{F_{RTOT}}\right)^3 \tag{51}$$

Life was calculated to be 227711 hrs (assuming 8 hours of operation a day, this operation is equivalent to 77.98 years). Thus, the bearings of the selected spindle were found to be satisfactory.

4.1.3. Abrasive Collection, Media Hydration, and Media Recycling

After media has been output from the abrasive discharge system, it impinges upon the workpiece. The media must be filtered and collected so that it can be reused. A funnel type collection system made from sheet metal (easy to shape and cost effective) was designed and developed. The funnel which has sharp gradients to allow for the flow of abrasive media was named as the "hopper". Supports are attached on top of the hopper to allow for the connection of a filtering mesh top. The mesh top serves two purposes, it ensures that the workpiece can be rested on it without falling into the bin (or it will catch it if the operator drops it), and it filters the abrasives to ensure that media that has clumped together will not pass through. A mesh size of 6 mm was chosen (abrasive media is 2 mm on average and largest abrasives are 4 mm in diameter). The mesh is cleaned after every use to ensure that excess particles are not stuck to the mesh.

The abrasives fall through the hopper's chute into a bin. The bin has a guided gradient inside of it which allows abrasives to roll down to the flat, lower, inner portion of the bin. The stirrer motor is attached (with an appropriate stirring shaft and shaft end) and connected to electricity. The output of the MQH (minimum quantity hydration), a small nozzle, is also attached to the bin to allow for the input of mist. The stirrer motor is then turned on and the speed is set (approximately 60 rpm).

When initially hydrating the media (before polishing occurs), two different methods were used (of similar effectiveness). The media was run through the machine but bypassed the impeller (from bin to feed ejector, through hose, back through the hopper and into the bin again) and was hydrated by the MQH at a specified mist rate. The stirrer motor provides the mixing action and ensured that the media was constantly moving (even mixing occurs). The second method was to place all media in a bucket, place the stirrer motor and stirrer in the bucket and then manually hydrate (or use the MQH) to achieve the desired hydration level. Both methods were effective however, the manual method was easier to control and allowed for faster hydration. For both cases, the media was continually weighed to assess when the desired hydration level had been reached.

When polishing, the bin recycles the media back up to the impeller system from the bin. This was done by using a piping system. The media was sucked out from the bin by a SCHAMLZ SEC-400 feed ejector (a vacuum suction device). The feed ejector was secured to the feed pipe adaptor by a set screw. The feed pipe adaptor was welded to the bin. A hose was

connected to the other side of the feed ejector by means of a hose clamp. A clear flexible hose (Alfagomma 2660L) of 52 mm in diameter and able to deal with a minimum of 8 bar of pressure was chosen (as this was what was required by the feed ejector). The other side of the hose was connected to the input of the impeller housing (as seen in Figure 25) using a swage nipple and a hose clamp. The media was kept in constant motion to provide consistent feed rate to the discharge system. The same stirrer motor (Figure 34) was used to create this motion and the stirring speed was varied to vary the feed rate. See Figure 31 for stirrer assembly and Figure 30 for the designed recycling system.
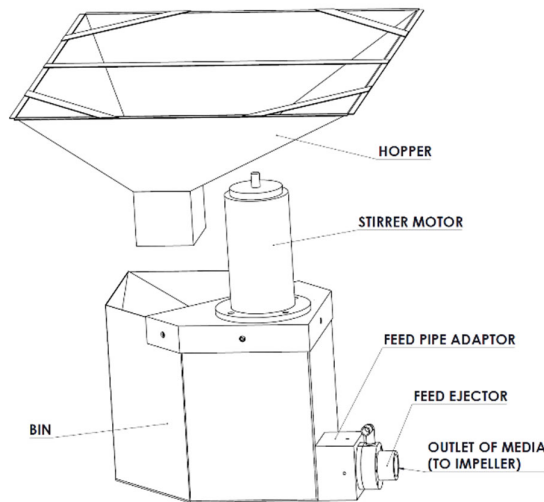
Figure 30 - Abrasive Collection and Recycling System (without mesh, hoses and MQH)
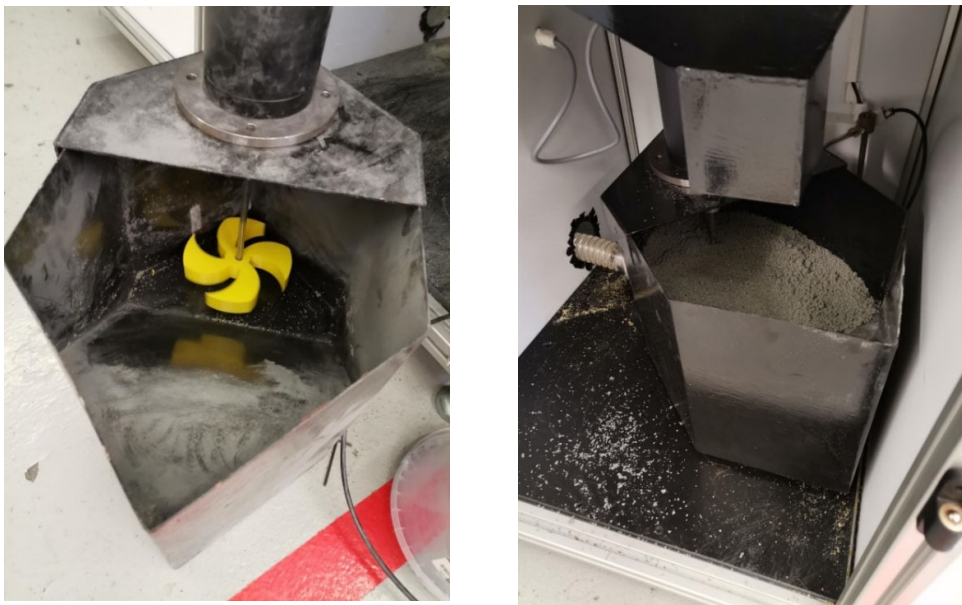
Figure 31 - (a) Empty bin with attached stirrer and stirrer motor (b) Installed subassembly and visible end of hopper as well as a bin full of abrasive media

The two figures below (Figure 32 and Figure 33) show the designs created for the collection system for the bin and hopper, respectively.
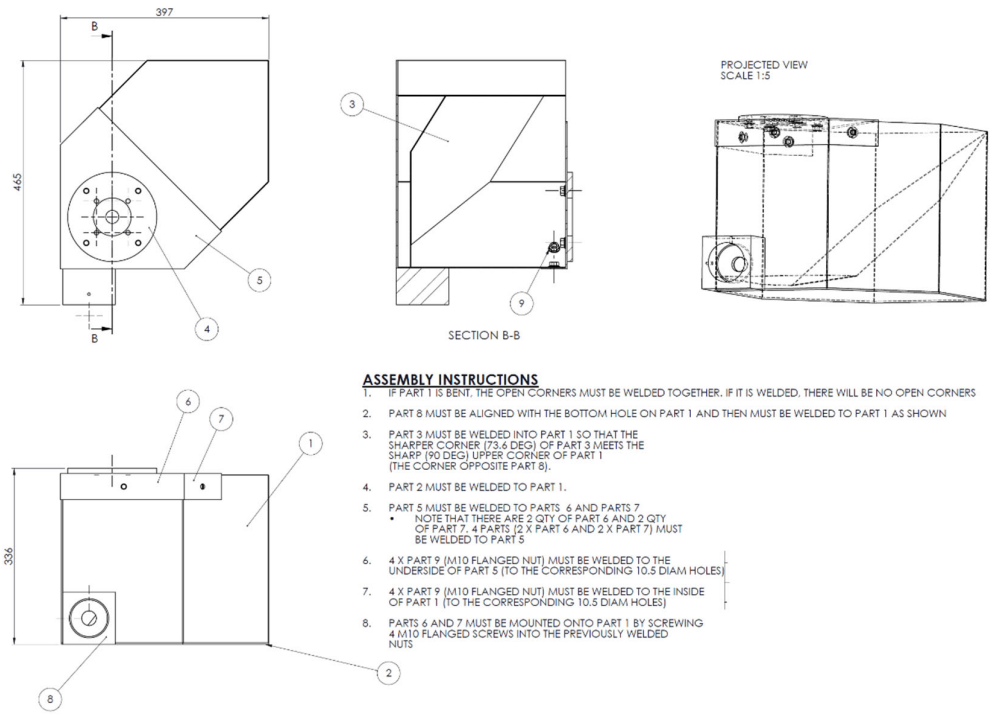
Figure 32 - Bin Assembly Drawing (9 parts required)
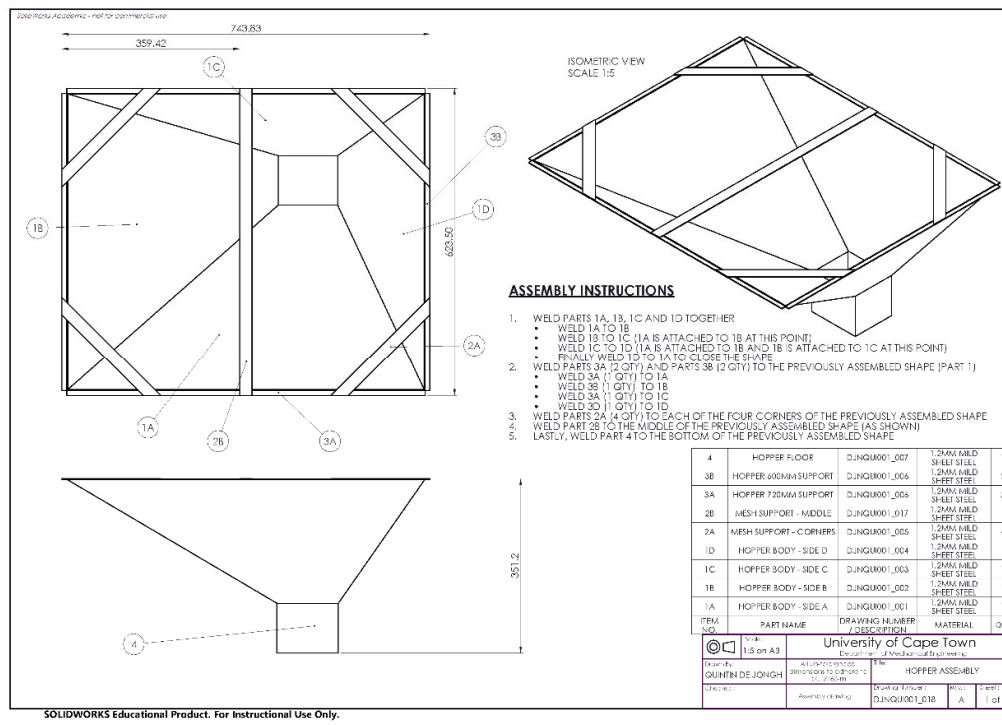
Figure 33 - Hopper Assembly Drawing (8 unique parts required)
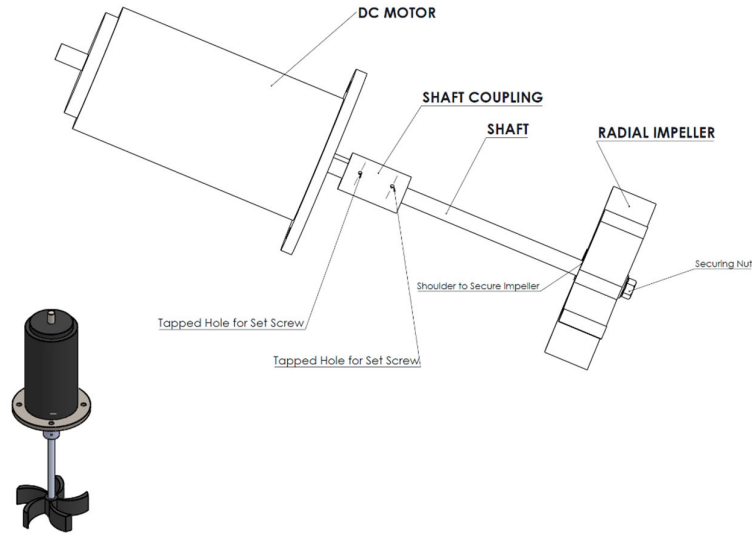
Figure 34 - Stirrer Motor and Stirrer Design

Calculations to determine/predict the rate of abrasive feed from the bin to the discharge system were required to ensure a constant recycling system of polishing (where abrasives do not need to be constantly refilled) and to ensure that the feed was not so high as to jam the impeller and clog the system. These calculations allowed for the required mass of abrasives to be determined.

These calculations also allowed for the determination of the required air pressure for the feed ejector (set at the FRL (filter-regulator-lubricator)) as well as the stirrer motor speed and the required hose (wall thickness and hose length).

Firstly, it was important to know the ratings and technical data of the feed ejector. This was found on the Schmalz website for the SEC-400 feed ejector [81] and is summarised below in Table 7.

Table 7 - Feed Ejector Parameters

Parameter	Value
Maximum Suction Rate (m^3/s)	0.00833
Air Consumption Suction (m^3/s)	0.0375
Pressure Range (bar)	2 to 6
Nozzle Size (mm)	40

The packing factor of abrasives to air was assumed as 0.3 (70% air suction, 30% media suction). The inlet diameter of the feed ejector is 75 mm and the outlet diameter is 52 mm. The polishing machine height from the feed ejector is 1.2 m (with a pipe length of 2.5 m). The abrasive discharge system has an inlet opening of 29.77 mm. Atmospheric pressure is assumed as 101.325 kPa (sea level pressure in Cape Town).

Abrasive radius is assumed as in previous sections (1 mm), while abrasive density is assumed as 680 kg/m^3 (density of gelatin). Abrasive mass was calculated to be 2.848 mg and the volume as 4.188 mm^3.
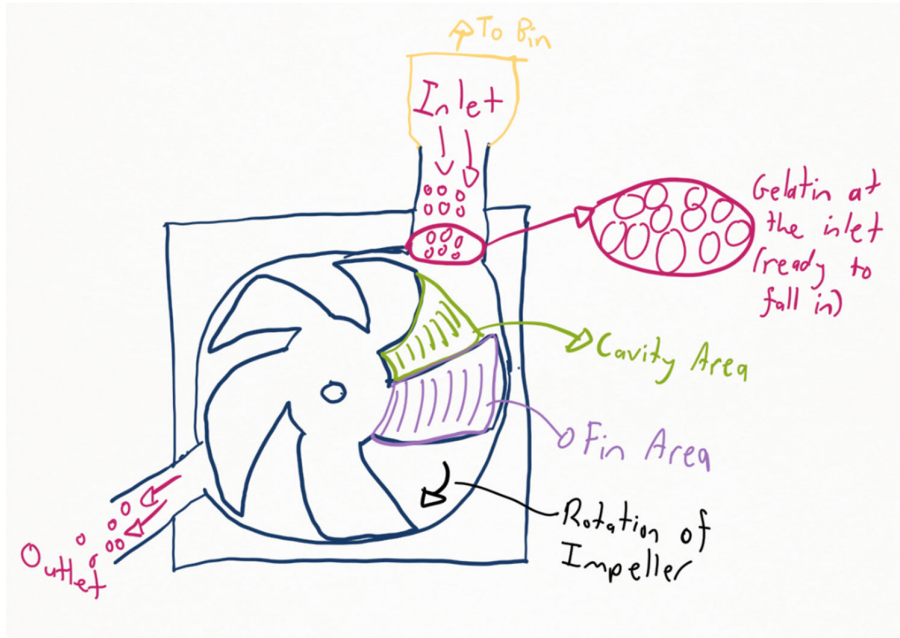
Figure 35 - Diagram of Abrasive Interaction at Impeller

To calculate the number of abrasives required per hour, the feed rate into the impeller was calculated. Figure 35 shows a diagram of abrasive inlet to the impeller.

As in Figure 35, the amount of gelatin in the cross section of the inlet fitting was determined initially. The cross section of this inlet is 29.77 mm. The largest amount of 2 mm abrasives that can fit inside of the inlet is 170. However, it was more realistic to take a packing factor of 0.5 as well as another factor for abrasives travelling up the pipe (as abrasives are not stacked on top of each other at the inlet). The secondary factor is assumed as 0.25. It was calculated that 21.25 abrasives (n_{abr}) were available for inlet to the impeller at any given time.

The impeller cavity opening times were then calculated (how much time is available for abrasive inlet). This varies for each impeller rotational speed. This is calculated by:

$$t_{opening} = \frac{d_{opening}}{V_{impeller}}$$

(52)

This output is the same as the time required for an impeller fin to travel the distance of the diameter opening. At the lowest velocity of 6.28 m/s, the opening time is 0.0047 s while at the highest velocity (31.4 m/s) it is 0.0009 s

The number of openings there are per second (for varying impeller velocities/rotational speeds) was calculated by:

$$n_{open/s} = \frac{1}{2t_{opening}}$$

(53)

Note the number of openings was divided by two as half of all rotations done by the impeller do not have cavity openings (the fin is going past the opening and thus will not allow abrasives in). For the low velocity level, 105.47 openings are available per second, while for the high velocity level, 527.38 openings are available per second.

By multiplying $n_{open/s}$ by the number of abrasives available for inlet, n_{abr}, the number of abrasives entering the impeller per second was found (2241 and 11207 for 6.2 8m/s and 31.4 m/s impeller velocities, respectively). Finally, this value was multiplied by the mass of a single particle (2.848 mg) to determine the required mass of abrasives per second (6.4 g/s for the low velocity and 31.9 g/s for the high velocity). Note that this translates to an impeller abrasive input requirement of 22.98 kg/hour for the low velocity and 114.92 kg/hour for the high velocity. However, it is important to note that the recycling system ensures that the required number of abrasives per time is lessened significantly.

Using the maximum pressure setting (6 bar), the feed ejector suction rate is 0.00833 m^3/s. Using Bernoulli's principle, abrasive outlet speed is calculated:

$$v_{feedout} = \sqrt{\frac{P_1 + 0.5\rho v_{feedin}^2 - P_2 - \rho g h_2}{0.5\rho}}$$

(54)

Where P_1 is 6 bar (maximum pressure setting), ρ is abrasive density, v_{feedin} is inlet suction speed (4.621 m/s), P_2 is atmospheric pressure g is gravitational acceleration and h_2 is the height of the abrasive outlet from the ground (1.2 m). The maximum abrasive outlet velocity was calculated to be 38.38 m/s while the minimum abrasive outlet velocity (at 2 bar) was found to be 16.76 m/s. The output diameter of the feed ejector (52 mm) shows that 523 abrasives could fit into the cross section of the output. With the same factors used, this shows that 65.375 abrasives are able to travel through the output per time period. At the low pressure, the abrasives take 0.1491 seconds to reach the impeller inlet, while at the high pressure they take 0.0651 seconds to reach the inlet. This result shows that less abrasives may enter the impeller than initially expected but if an initial build of abrasives in the pipe is created, the fill up rate should be sufficient to provide a constant flow of abrasives into the impeller.

Determining the travel time from the output the inlet of the feed ejector was necessary to determine the initial required abrasive mass for input to the bin. The low-pressure calculations show that abrasives take 0.1491 seconds to travel from feed ejector to impeller. The impeller

(shooting the abrasives at a low speed of 6.28 m/s) would require 0.0796 seconds to shoot the abrasive to the hopper funnel. If the hopper funnel takes 1 second (low estimate) to funnel the abrasive back to the bin, the total required abrasive recycling travel time is 1.2287 seconds.

If the pipe volume is at any time filled with 20% of its volume by abrasives (the rest by air), the mass of abrasives in the pipe is 2.883 kg. If a 5 minute back up of particles is required for the highest velocity (31.4 m/s), we would need an additional 9.5765 kg of abrasives in the bin. This means that for the highest conditions (which would be an overestimate), 12.46kg of abrasives are required. The bin volume is 0.0428 m^3 and this can fit approximately 30 kg of abrasives in it at any time.

The above calculations provided an estimate on initial abrasive amount requirements as well as pressure setting, impeller velocity and other general media recycling requirements. These estimates provided a starting point onto which experimental analysis was then performed to find the correct settings and exact process requirements for each condition.

In practice, finding the correct pressure settings for the required velocity required a large amount of testing as if the suction rate was too high, the impeller would clog. This would then require disassembly to unclog the impeller. The optimal pressure was found to be 4.5 bar for a high impeller velocity (31.4 m/s) and 6 bar for a low impeller velocity (6.28 m/s). It was also found that only 3 kg of abrasives was required to achieve a constant abrasive recycling system for 30 minutes and 5 kg of abrasives was needed for an hour (some abrasives needed to be collected or emptied out of the pipe due to the large scale of the system). It should also be noted that the feed ejector should not be fully covered by abrasives as air is required in the piping to ensure the piping does not get clogged. The ratio of media to air was found to be approximately 1:2 (1 part media for every 2 parts air). This was achieved using the stirrer motor spinning at a low rotational speed. A rotational speed of 45 rpm was used for the high impinging velocity while a rotational speed of 60 rpm was used for the low impinging velocity. Overall, the recycling system proved to be a success and allowed for efficient polishing.

Media hydration was determined by measuring the output rate of mist of the MQH (measuring how much water was collected in 1 hour at each setting). The results are summarised in Figure 36 below.

Figure showing "MQH Spray Rate vs. Setting" with Water Output per hour (ml) on the y-axis and Spray Rate (1/sprays per second) on the x-axis. Trendline equation: $y = 225.29e^{-2.106x}$
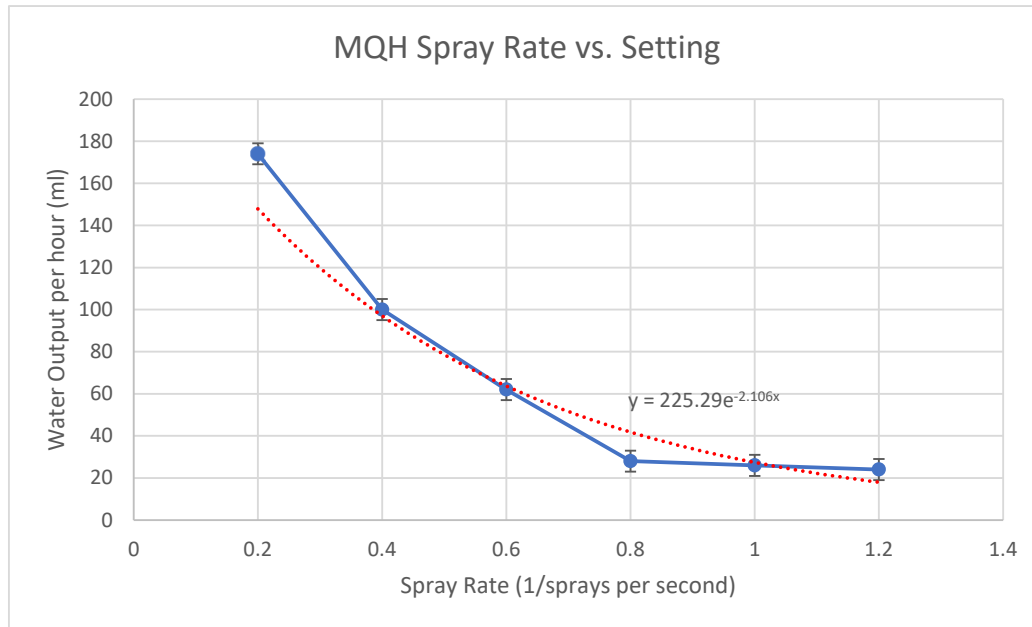
Figure 36 - MQH Misting Rate

At the highest measured setting of 5 sprays per second (0.2 seconds per spray), it would take approximately 35 minutes for 1 kg of abrasives to reach 10% hydration. When a faster rate of hydration for the media was required, a manual spray bottle (1 ml output per spray) was used, while the stirrer motor agitated the media. In cases when precise and completely even mixing was required (experimental purposes), the centrifugal mixer (described in the experimental preparation chapter) was used to achieve the uniformity of hydration. The drawback to this method was that the hydration took several hours to complete for a full volume of abrasive media (not suitable for large amounts of experiments or for industry).

The stirrer motor speed changes with voltage setting. This needed to be measured to control the motor properly and to optimize parameters. Higher stirrer motor speeds allow for more media agitation in the storage bin and thus a higher input rate to the feed ejector. At higher media hydrations, lower media input is required to the ejector (to ensure clogging does not occur). However, if stirrer motor speed is too low, sufficient mixing of sprayed water and media does not occur. A tachometer was used to measure the speed at various voltages and a completely linear relationship was found (as expected). See the graph (Figure 37 - Stirrer Motor Speed Chart on the following page).

Impeller and motor output measurements were also done for the abrasive discharge output. This was necessary so that the variable speed drive could be properly set up (as the measurement units are in Hz (frequency)). The results are shown in Table 8.
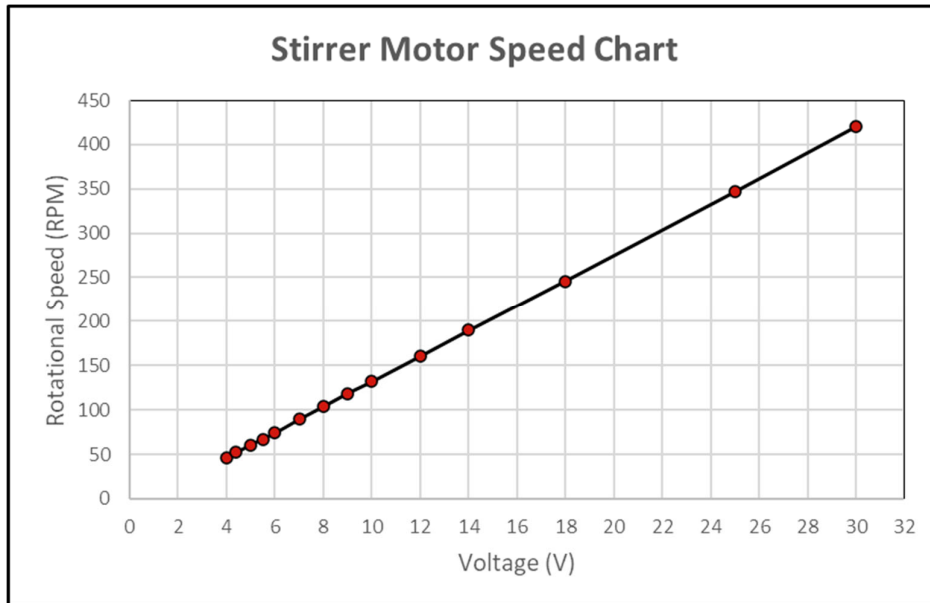
Figure 37 - Stirrer Motor Speed Chart

Table 8 - Spindle operation speeds

With Spindle			
Impeller Output (m/s)	RPM	Motor RPM	Hz Setting
5	796	199	3.32
6.28	999	250	4.17
10	1592	398	6.63
12.5	1989	497	8.28
15	2387	597	9.95
17.5	2785	696	11.6
20	3183	796	13.27
22.5	3581	895	14.92
25	3979	995	16.58
27.5	4377	1094	18.23
30	4775	1194	19.9
31.42	5000	1250	20.83

4.2. Structural design and enclosure

The frame allows for a large amount of modularity and flexibility of design. The initial design had an error in that the mounting height for the abrasive discharge system was too high and would have meant that the space for polishing was minimal (with interference occurring). More aluminium extrusions were ordered, and the height was calculated to allow for the greatest polishing space possible. Three different discharge heights were made to allow for changes in output design. The whole discharge system (and output of nozzle) can be moved back and forth on the extrusions to allow for longer or shorter nozzles as well as for more complex discharge systems.

An adjustable holding stand was made from aluminium extrusions (to hold workpieces). The stand can be moved up and down in the frame (the levelling foot is adjustable in height too and is used to transmit forces to the body to minimize vibrations). This design aids the user in that the workpiece does not need to be held by the operator while polishing (meaning the operator can focus on using the controls and ensuring smooth process operation). The design can be seen in the Figure 38 below.
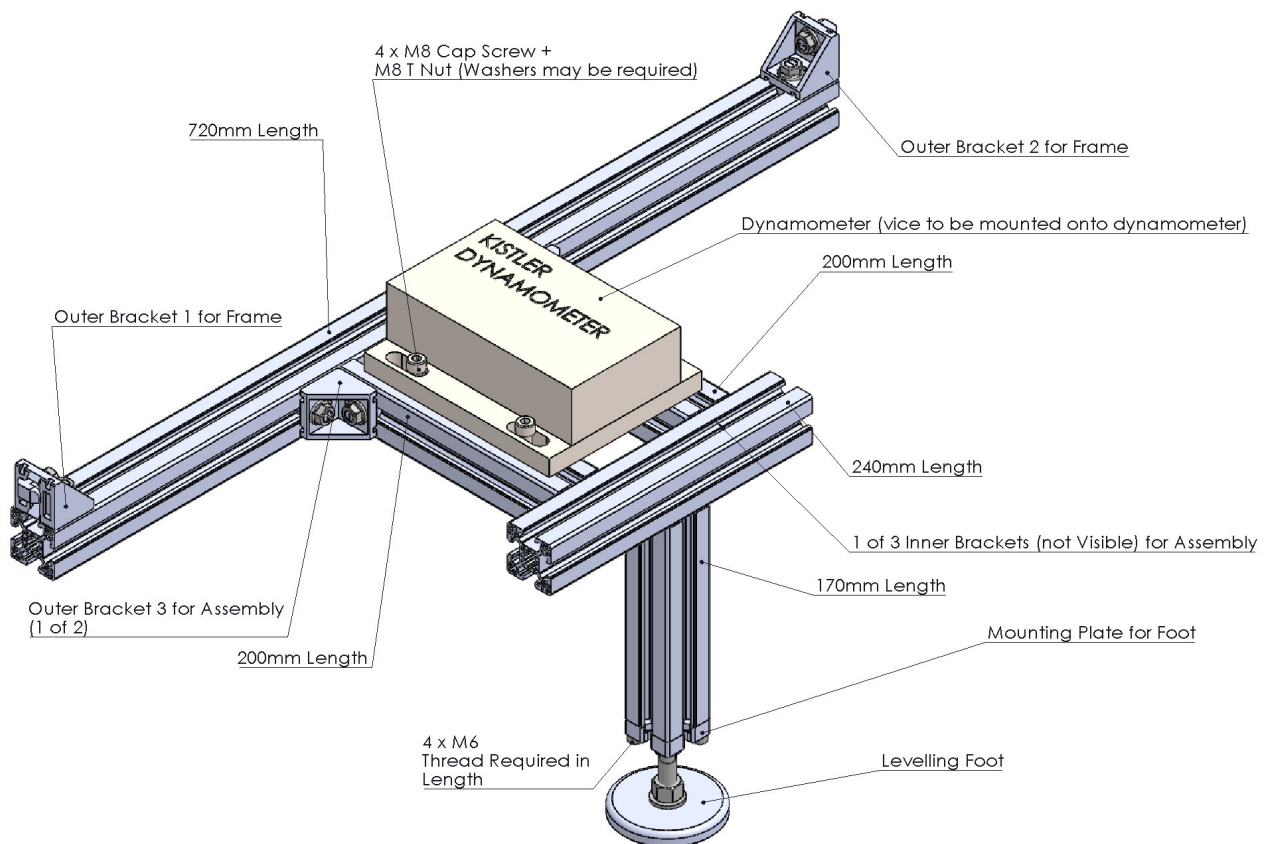
Figure 38 - Designed Aluminium Mounting Stand for Workpieces/Dynamometer

In addition to the holding stand, frame assemblies were made for the MQH (to mount it to the machine) as well as for the controls (the variable speed controller is fixed to the designed frame, while the MQH I/O control as well as the pressure I/O and the FRL are loosely fixed to the extrusions). Figure 39 shows the two designed mini assemblies.

MOUNTING FRAME FOR SPEED CONTROL AND ACCESSORIES

MINI-FRAME FOR MQL
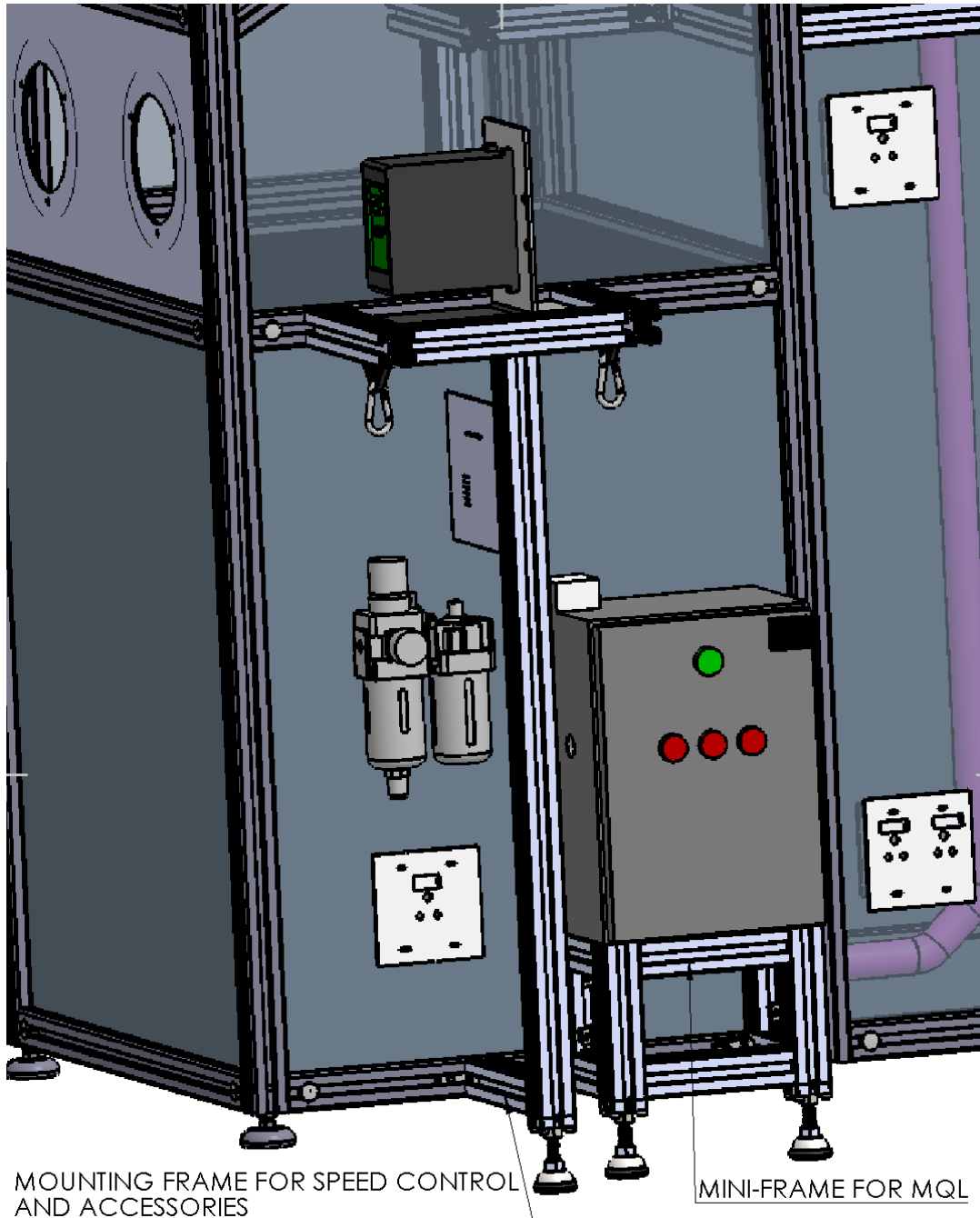
Figure 39 - External Frame Structures for the MQH and the Variable Speed Drive

4.3. Control design and placement

Figure 40 below shows all controls for the machine: variable speed drive to control AC induction motor (impeller speed), FRL to control pressure (feed ejector suction rate), MQH to control misting rate, DC Speed controller to control stirring speed, DB board to control all electrics (lights, motors, plug points and MQH), MQH I/O switch and Pressure I/O,
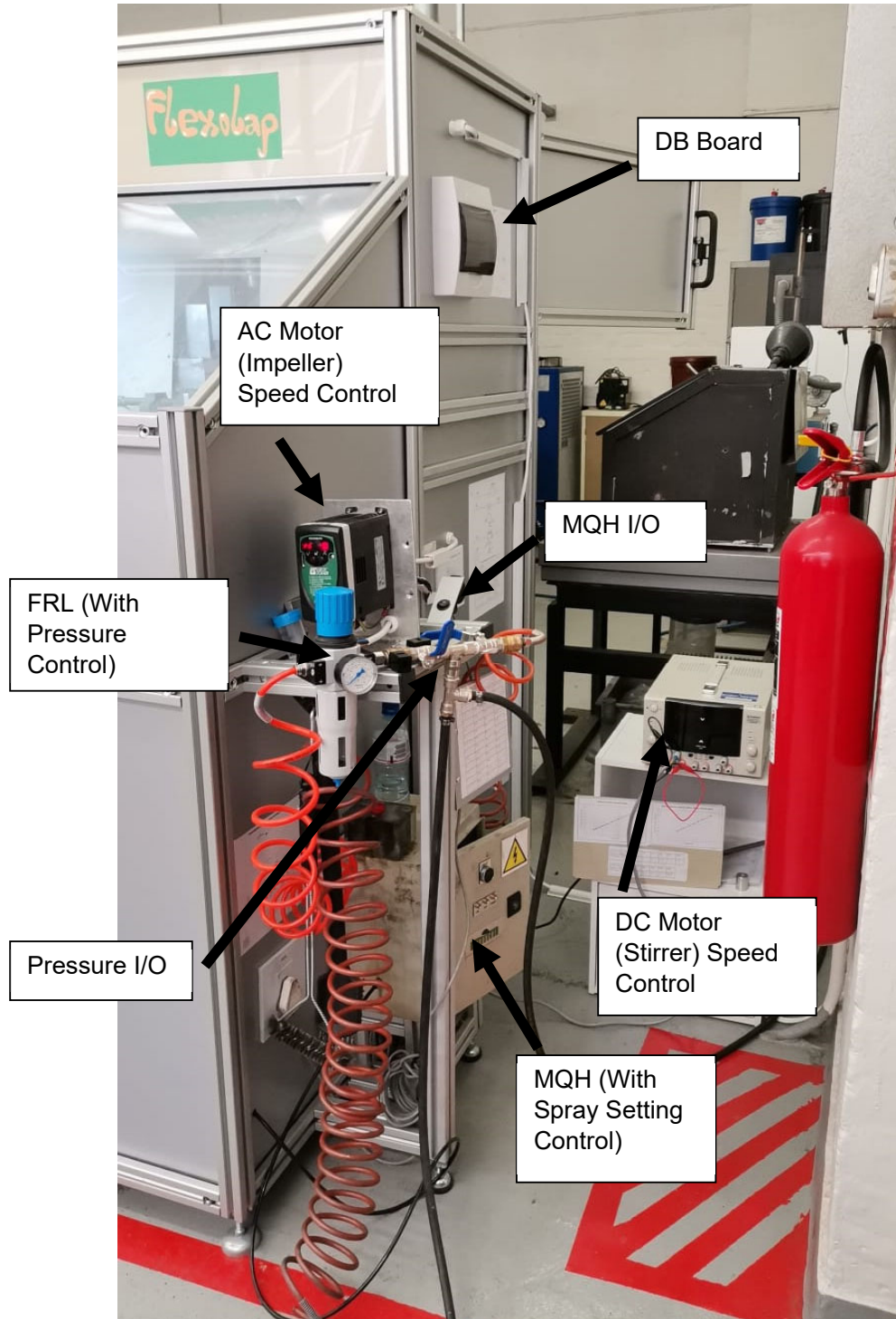
Figure 40 - Machine controls and placement

The control placement was designed in the manner shown previously so that all process parameters could be controlled in a single area without the user needing to move around the machine. This is important as a variety of happenings may occur in which the operator needs to access many controls at once. For example, the impeller may clog, or the belt may slip off and the process needs to be stopped immediately.

Combining this design with the previous subassembly that allows the workpiece to be fixed, and does not require the user to hold it, means that operation of the machine becomes relatively simple.

4.3.1. Electrics and Wiring

It was necessary to create a compliant and fully independent electrical system that allows for the system to be connected to the main power supply. This is required so that the machine can be presented to industry with a detailed design and a knowledge of how to maintain the electrical connections as well as to track how the wiring was done. The first step was to determine the required electrical components and their connections. All output components and their placements were known: DC stirrer motor, AC impeller motor, MQH system and machine lights. These are controlled by 30 V AC/DC power supply, Digidrive variable speed controller, MQH I/O switch and a simple light switch, respectively. The maximum amperage of each component was simply calculated using Ohm's law (V=IR) or it was looked up from the designer's ratings. An appropriate circuit breaker was then selected (three 10 A circuit breakers and one 20 A circuit breaker for the individual components and one 63 A mains circuit breaker for the entire system). The type of wire was then selected (10 A rated wire for components except for the AC drive which had 16 A rated wire and 30 A rated wire for the DB board and mains). With all this knowledge, the ladder (circuit) diagram could be created. This is presented on the following page in Figure 41.

The amounts and lengths of wires were cut and the required thickness and amounts of conduit (trunking) was purchased. Trunking was then installed along the internal and external of the frame (on the frame panels). Wiring was then completed on the plug points, lighting, and connections to components. The wire was then neatly tucked into the trunking, covered, and brought to the distribution board. The distribution board was wired with circuit breakers, labelled and then it's wiring was taken to the mains. This wiring was placed in half moon shaped external trunking (to prevent the operator from tripping over the trunking). Testing with a multi-meter then occurred to ensure no short circuits were present and then the electrical portion of this project was declared complete.
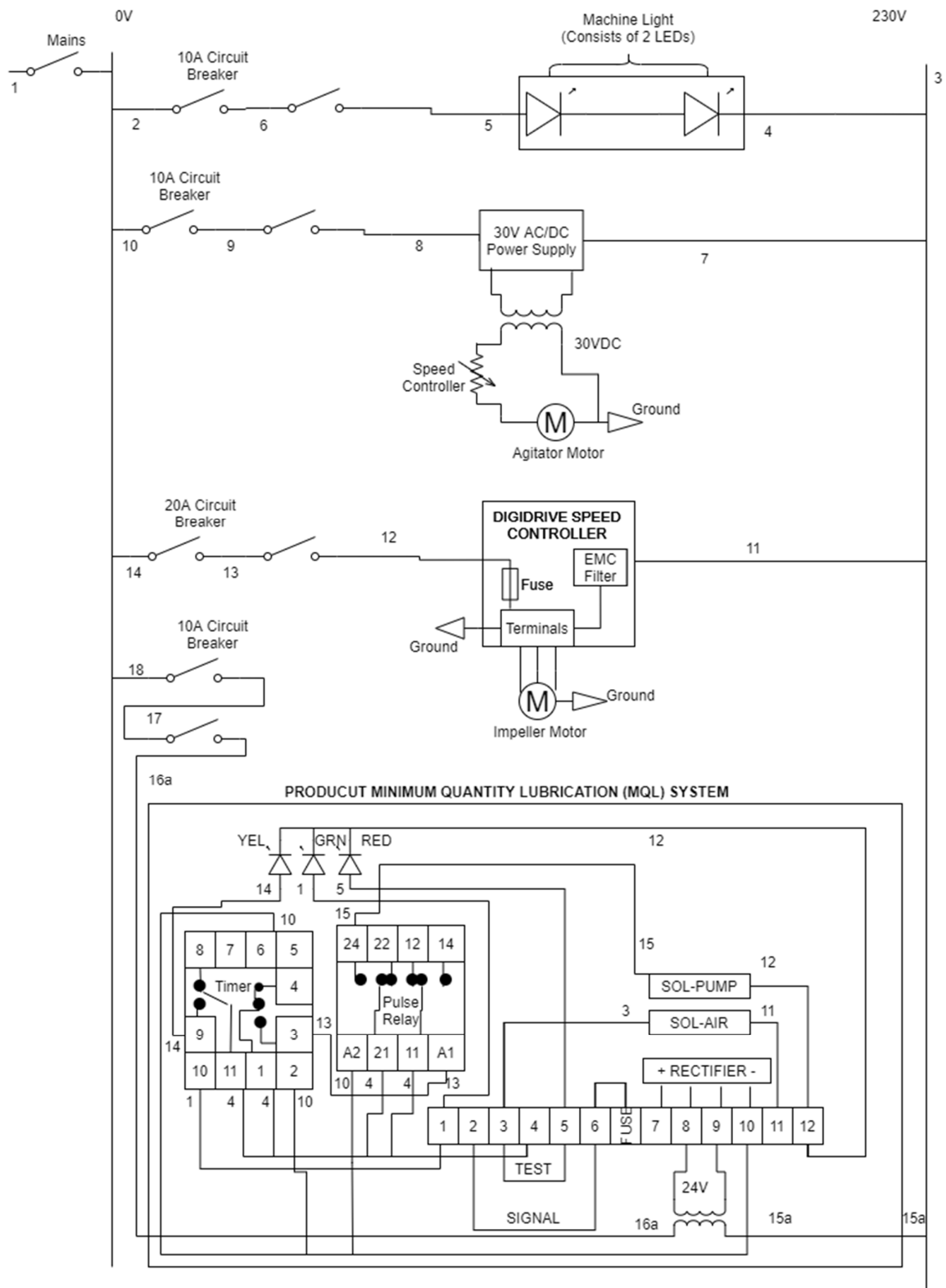
Figure 41 - Ladder/Circuit Diagram of the Designed Machine

4.3.2. Pneumatics

Although slightly less intricate than the electric system, the process of creating a pneumatic system is entirely necessary to understand the flow and allow for acquisition of correct parts as well as (most importantly) to simplify maintenance in the future (just as required for the electrical system). The design process for this system was very similar to the electrical system and the pneumatic diagram can be seen in Figure 42 below. The air compressor supplies air at a pressure of 10 bar, this then travels to a ball valve for the control of air for the entire lab which is turned on and further travels to two other ball valves that control the input of air to either the FRL (and subsequently the feed ejector) or for the MQH unit.
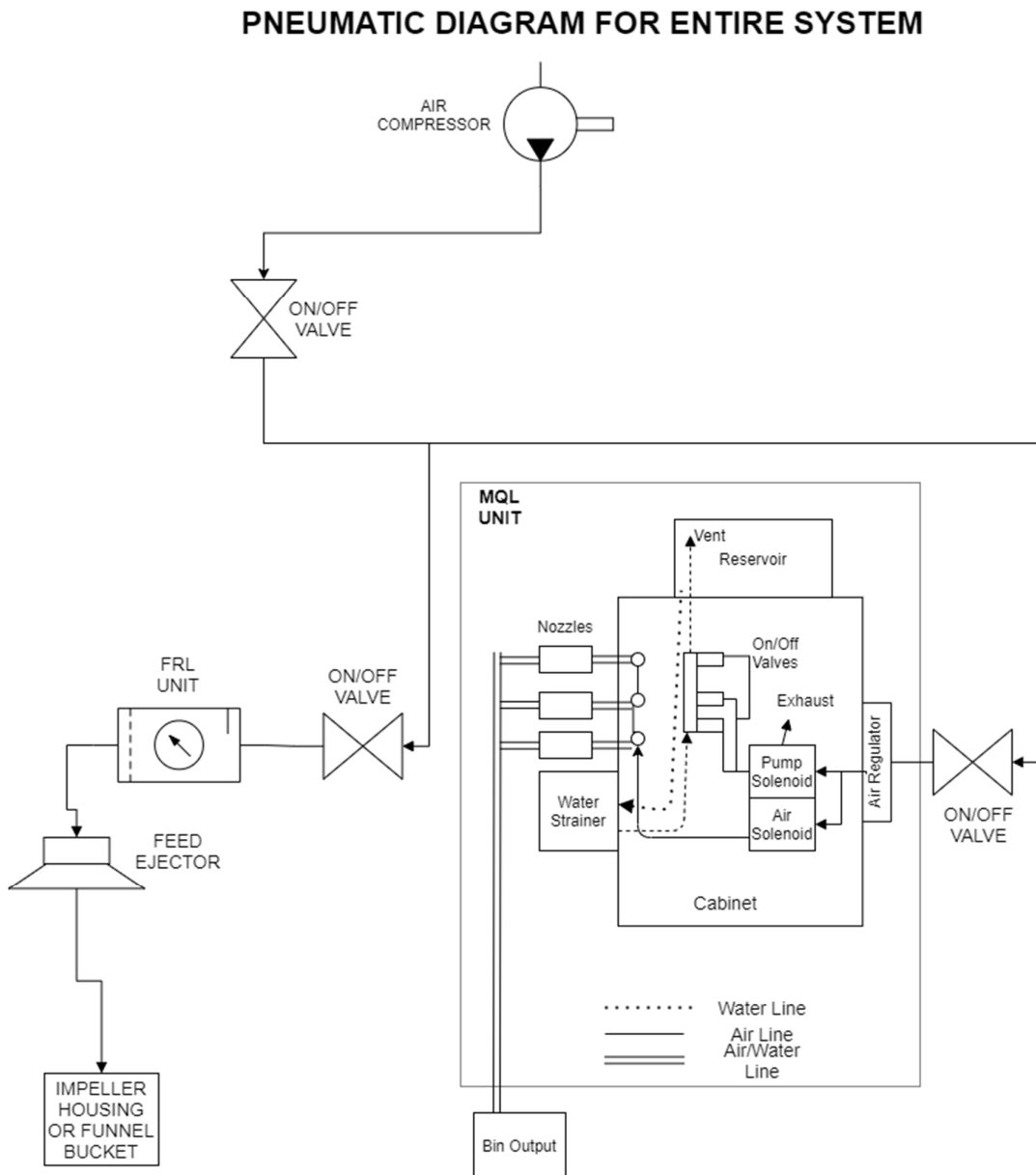
Figure 42 - Pneumatic Diagram for Designed Machine

4.4. Assembly

Much of the subassemblies described previously give a partial description of how assembly occurred. Thus, this sub-chapter will be presented as a summary rather than a detailed description.

Assembling the individual components and subassemblies in an elegant and professional manner that allowed for simple use and adjustability down the line was the driving factor for how the final assembly was made. The frame was sourced from Bosch-Rexroth and is made of aluminium 'V' extrusions that allow for modularity of design. I-Bond (high strength aluminium composite that sandwiches a polyethylene core) slots into the extrusions snugly, to seal the frame from external factors and keep the system closed. Note that some Perspex was also used (when transparency was required). The height of the abrasive output discharge system was set so that the nozzle outputs the media at 45 degrees. This can be adjusted as necessary by slotting a different stand into the frame. This subassembly was fixed onto the mounting plate and the mounting plate was bracketed onto the frame to ensure minimal vibration. The previously assembled hopper was installed into the frame with the cut mesh top (these are both slotted into the extrusions easily). The bin is placed under the hopper chute and the stirrer motor is attached and detached to the bin as required (if hydration is required to occur separately to the mixing process). The MQH unit, FRL unit, power box, and control box are all fixed to the frame. The figures on the following page show CAD models with descriptions of individual components. This design led to the actualization of the figure presented in Figure 45.

Figure 44 and Figure 43 show the final SolidWorks models of the machine. Figure 45 shows an image of the completed machine which was developed after conceptualization using the SolidWorks models below.

Figure 44 - Unlabelled Back View of Assembly
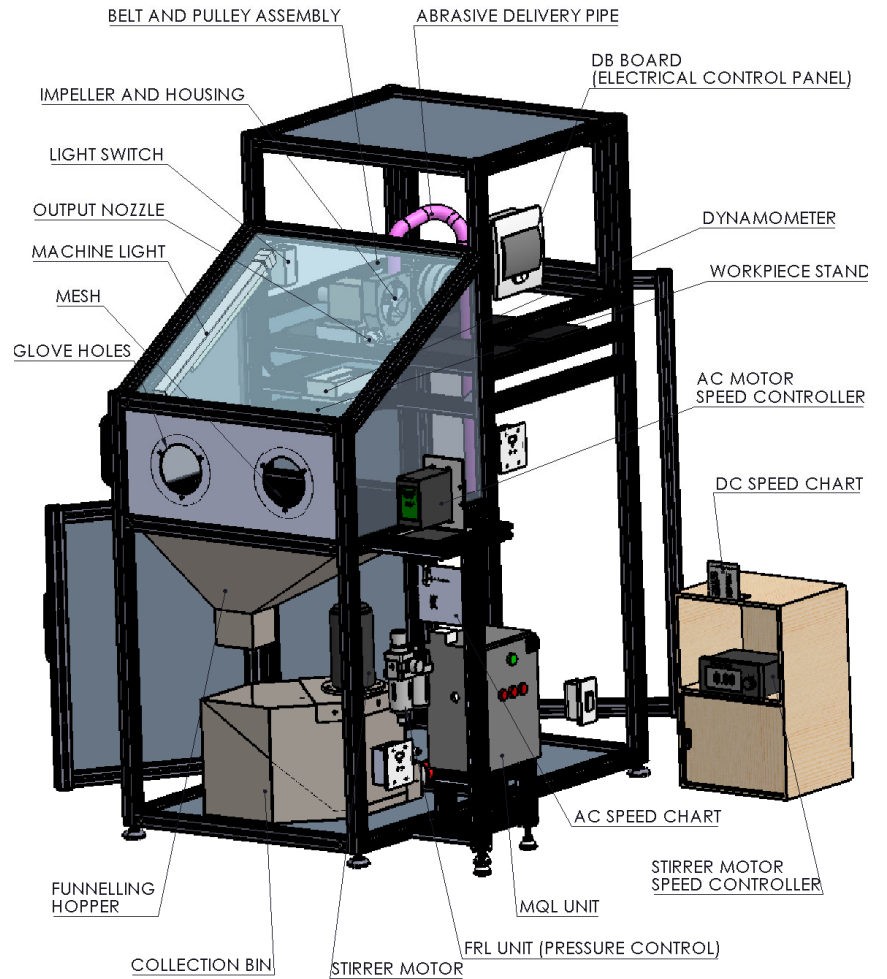
Figure 43 - Labelled Front View of Assembly

Figure 45 - Image of Finalised Machine

Chapter 5 – Abrasive Media Selection & Preparation

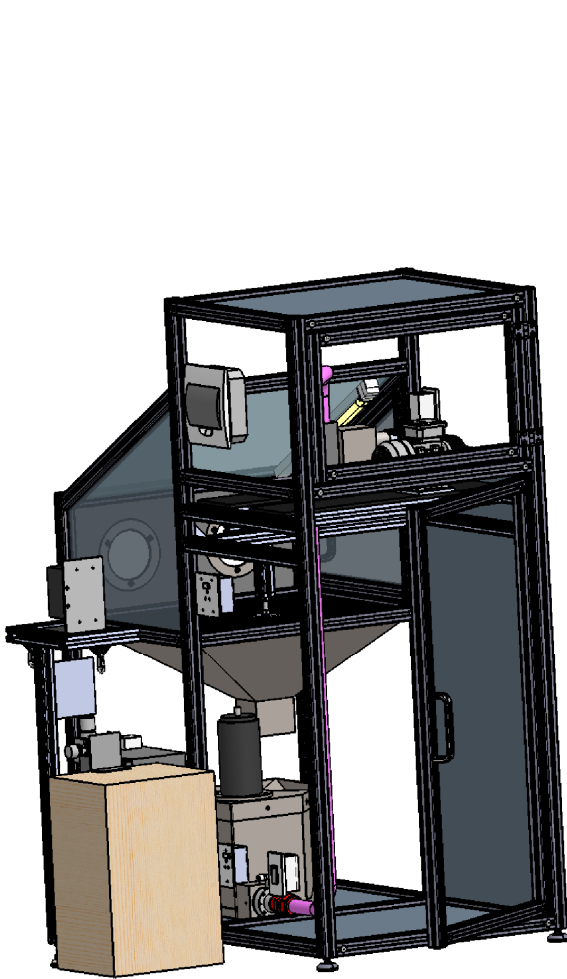This chapter provides the reasoning for abrasive selection and describes the experimentation done to prove that the selected abrasives would work as expected. Abrasive preparation for polishing is also briefly discussed.

As mentioned in the literature review, choosing the correct media combination is critical to achieving an efficient and optimal polishing process. Past research [1] [16] [6] [46] [48] has shown that using media with a large array of viscoelastic levels allows for a great choice of polishing conditions. The control of viscoelasticity has typically been by the method of heat addition (particularly with thermoplastic cores) or by water addition (particularly with bio-media cores). Due to previous research showing successful results with the use of multi-cone abrasive media (gelatin, SiC and diamond), its relatively low energy consumption compared to the heating of thermoplastics, the ease of acquisition (gelatin is easily bought in store) and its ability to absorb water (proven in multiple studies and as its main use is creating food jelly), the multi-cone media was chosen as the primary abrasive for this study.

However, as much of the previous research does not describe abrasive selection; confirmation and investigation into the abrasive's suitability was required. The results and methodology below are focussed mainly on experimental data acquisition.

Figure 46 on the following page shows a microscopic image (magnification of 50 X) of the acquired gelatin and its approximate size (1 mm in diameter). Upon inspection under the microscope, we see that the media shape varies a lot, with some pieces exhibiting a more spherical shape and others showing a longer and more cylindrical shape. The presence of grooves and the rough texture are positive indications that the SiC and diamond abrasives will adhere to the surface of the gelatin. The smaller than expected size is beneficial to the process in that more abrasives can enter the impeller at a single period.
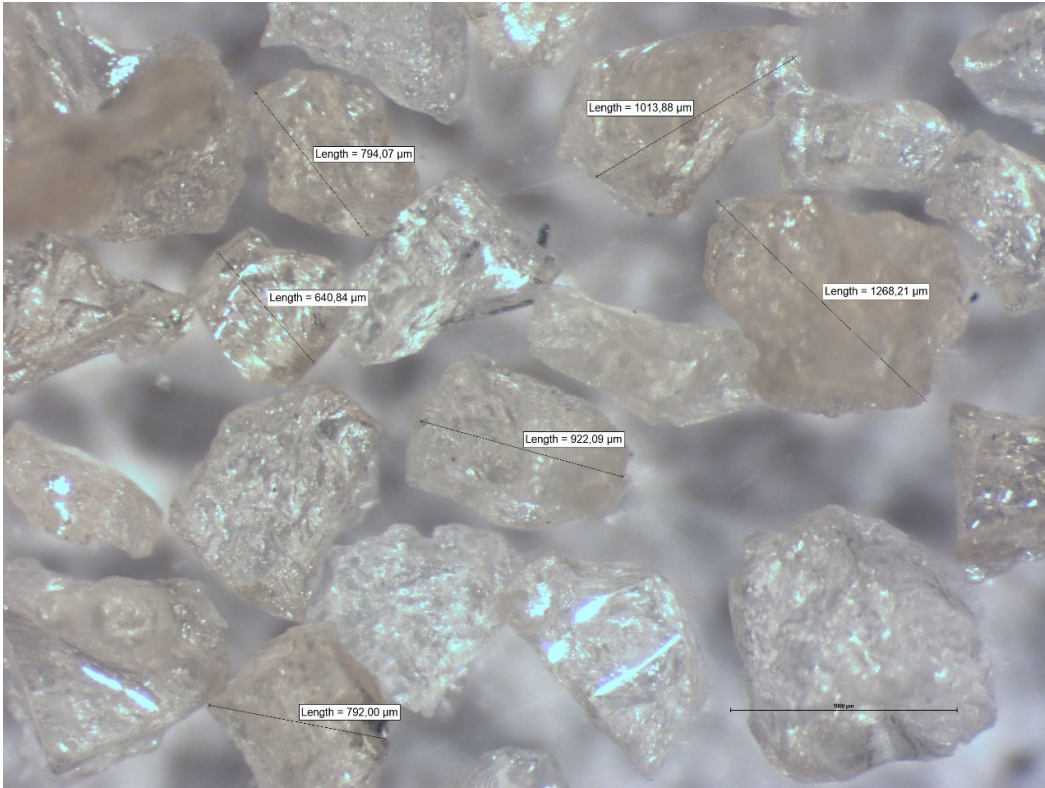
Figure 46 - Gelatin under Microscope

It was important to determine how quickly the media dehydrates (if too quick, the viscoelasticity cannot be adequately controlled over time) as well as to determine how well media can absorb water. An experiment was completed to determine the dehydration of gelatin over time. 500 g of gelatin and 250 g of water was placed in a container and mixed in a TurboMix planetary centrifugal mixer for 30 minutes to ensure uniform mixing. An abrasive was picked and put under a microscope for 45 minutes, with images being taken every 5 minutes (see Figure 47).

a. 0 minutes
b. 5 minutes
c. 10 minutes
d. 15 minutes
e. 20 minutes
f. 30 minutes
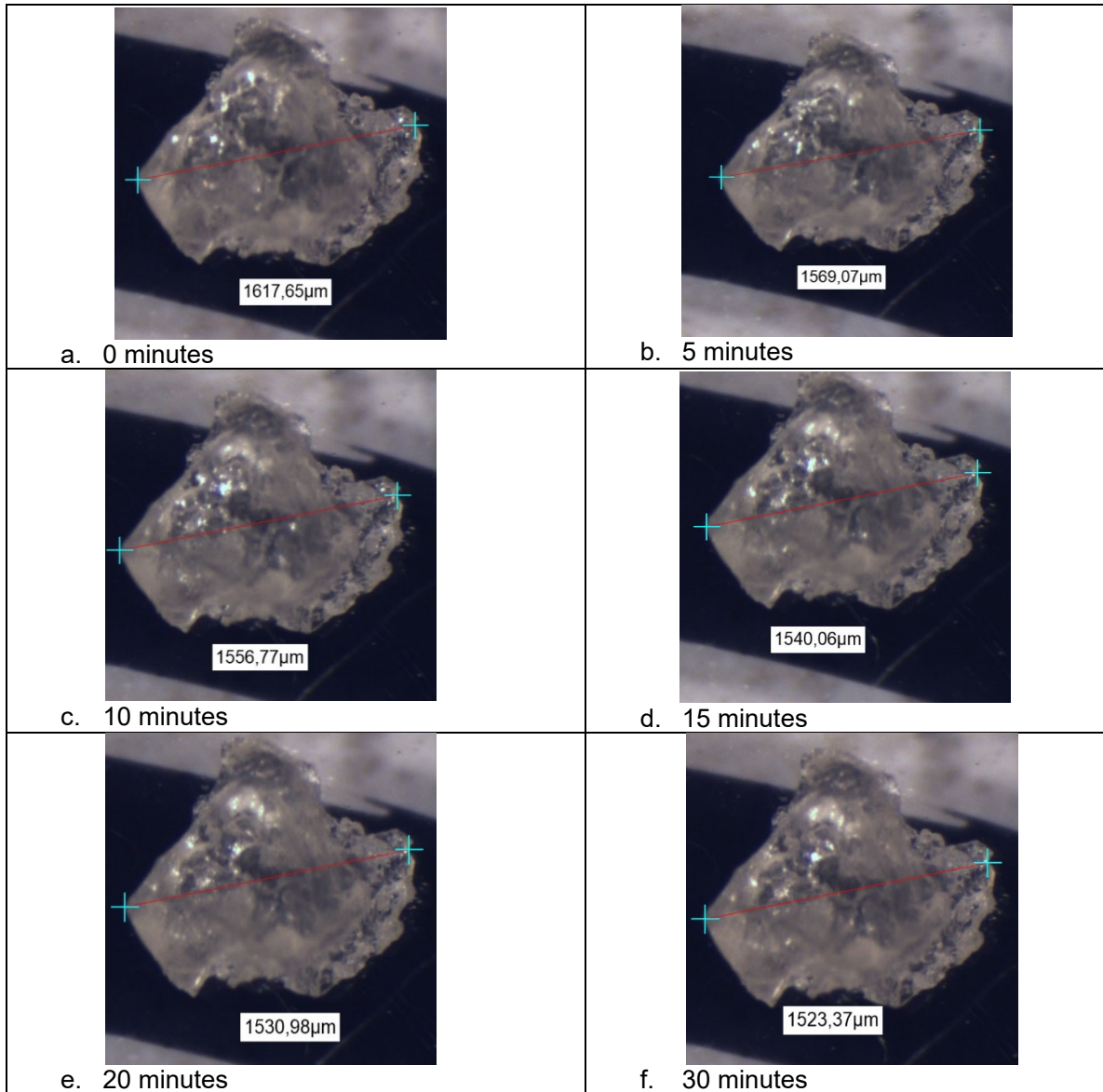
Figure 47 - Gelatin Dehydration Over 45 minutes

Measurements on the exact same point show the size reduction in the gelatin particle, with most dehydration occurring in the first 5 minutes. However, the diameter of media increased highly with respect to previously measured dry abrasives (1 mm dry diameter to 1.5 mm hydrated diameter). Media diameter decreased by approximately 0.1 mm over 45 minutes for all experiments, which is significantly less than the 0.5 mm growth in diameter from the dry condition. This experiment was repeated multiple times and very similar results were found, in that reduction in size was approximately 0.1 mm over 45 minutes after growing by approximately 0.5 mm from the dry condition. This experiment shows that the gelatin core is a suitable media for absorption and retention of water. It also means that the viscoelasticity of the media can be controlled by use of water rather than heat.

The next step in abrasive selection was coating the abrasives in diamond and silicon carbide. The fine diamond powder used was of varying mesh size (#1000, #3000 and #5000) and silicon carbide powder is of mesh size #3000.

The silicon carbide and diamond amounts were measured on an Ohaus Adventurer Precision Scale. 2.9% by weight of Silicon Carbide was added to the gelatin and 0.1% (up to 0.5% in experiments) by weight of diamond was added to the gelatin. A few sprays of silicon spray were used as the binding agent in the mixture, and this was then mixed in the PCM TurboMix. This method of creating abrasive media was followed as previous researchers had outlined (multi-cone with multi-powder) and so intermediate adhesion analysis was not completed. The silicon carbide had visibly changed the appearance of the gelatin particles, and the effect of the diamond was not noticeable by the naked eye. The results of this chapter in conjunction with the initial polishing and pre-experimental polishing results from Chapter 7 provided confidence to conclude that this media combination was suitable for its application.

Chapter 6 - Experimental Design, Set-Up, and Procedure

An important part of this dissertation is the design, set-up, and execution of experiments, with acquisition of measurable results an essential requirement (as this leads to the subsequent analysis of results, comparison to theoretical models and the development of further models). This chapter describes the experimental environment created, the design of experiments, selection of experimental variables and collection of data/measurement of results. Much of the abrasive preparation has been mentioned in the previous chapter and while it forms a crucial part of the experimental procedure, the detail will be limited in this chapter.

6.1. Workpiece Preparation

Workpiece preparation for polishing (including processing and correct placement and gripping) is critical to achieving experimental uniformity. The acquired Ti-6Al-4V components were produced by SLS and are comparatively rough (6 µm Ra value) and vary largely from surface to surface (up to 2 µm variance), as will be shown in the following chapter. To ensure that result comparison is fair and to reduce experimental time, surface grinding was performed on all the workpiece surfaces. This reduced the surface roughness to approximately 0.8 µm Ra value (with variance not greater than 0.15 µm). Once the surface was ground, profilometer readings (Ra, Rymax and Rz) were taken and the workpiece was cleaned in an ultrasonic cleaner to get rid of any impurities. It was then wrapped in a soft silk cloth until polishing occurred.
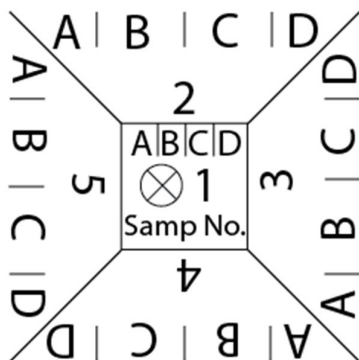
Figure 49 - Reference Sticker for Workpieces
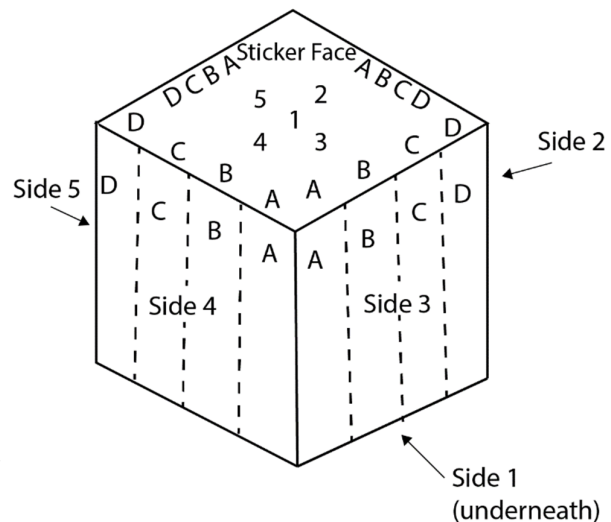
Figure 48 - 3D Drawing of References on Workpiece in Relation to Sticker

The workpiece cube needed to be referenceable and markings on the cube were not preferred (surface damage avoidance). Thus, a sticker was made with referencing for 5 sides and 4 subdivisions per side. The subdivisions are used for time increments while the sides are used for experimental set-ups (i.e. change in hydration level or change in impinging velocity). This sticker was stuck on one side of the cube and thus eliminated one side from being polished. The two figures on the previous page (Figure 48 and Figure 49) show the sticker and how the sticker is related to the 3D workpiece. An example of how the experiments were set up in relation to the referencing system is shown in Table 9 below (note that this is only for the first sample). Note that there were 3 layers of designed experiments: subdivisions (for each time, demarcated A, B, C or D), sides (for each experimental condition outside of time, demarcated 1, 2, 3, 4 or 5) and finally experiment number/set-up (27 sets starting with AS1, AS2 and AS3 and ending in ID1, ID2 and ID3).

Table 9 - Experimental Conditions Relating to the Referencing System for Sample 1

Experiment Number and Conditions	Division Number → Side Number ↓	A	B	C	D
AS1 31.4 m/s 10% Hydration 0.1% Diamond	1	2.5 mins	10 mins	25 mins	45 mins
AS2 15 m/s 10% Hydration 0.1% Diamond	2	2.5 mins	10 mins	25 mins	45 mins
AS3 6.28 m/s 10% Hydration 0.1% Diamond	3	2.5 mins	10 mins	25 mins	45 mins
BS1 31.4 m/s 10% Hydration 0.3% Diamond	4	2.5 mins	10 mins	25 mins	45 mins
BS2 15 m/s 10% Hydration 0.3% Diamond	5	2.5 mins	10 mins	25 mins	45 mins

The workpiece standoff distance and injection angle needed to remain constant in the experiments and the initial design of holding the workpiece by hand was not ideal for maintaining these conditions. A workpiece stand was thus developed (as shown by Figure 38 in the Design and Development chapter). The dynamometer allows for the attachment of a vice grip, and this holds the workpiece. The stand ensured a consistent stand-off distance was maintained however the requirement for a consistent injection angle was not achieved by this. This was solved by designing and subsequently printing a PLA workpiece stand that held the workpiece at an angle of 45º and fits into the vice grip (Figure 50). The 3D printed holder also has the added benefits of covering all other surfaces except for the one being polished (see Figure 51) and allows for portions of the workpiece to be covered (with more 3D printed bars). The bars can be used to allow for multiple time step experiments to occur on one surface as per the reference sticker.
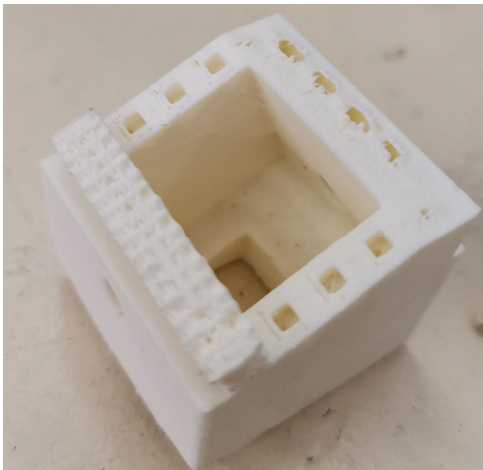
Figure 50 - 3D Printed PLA workpiece stand with single covering bar
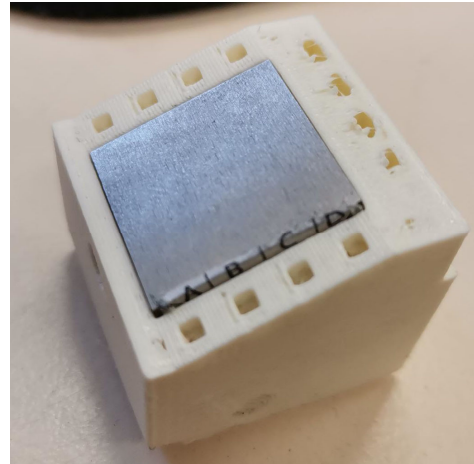
Figure 51 - 3D Printed Stand with workpiece inside

Below (Figure 52) is a sketch on the process of abrasive preparation for experiments.
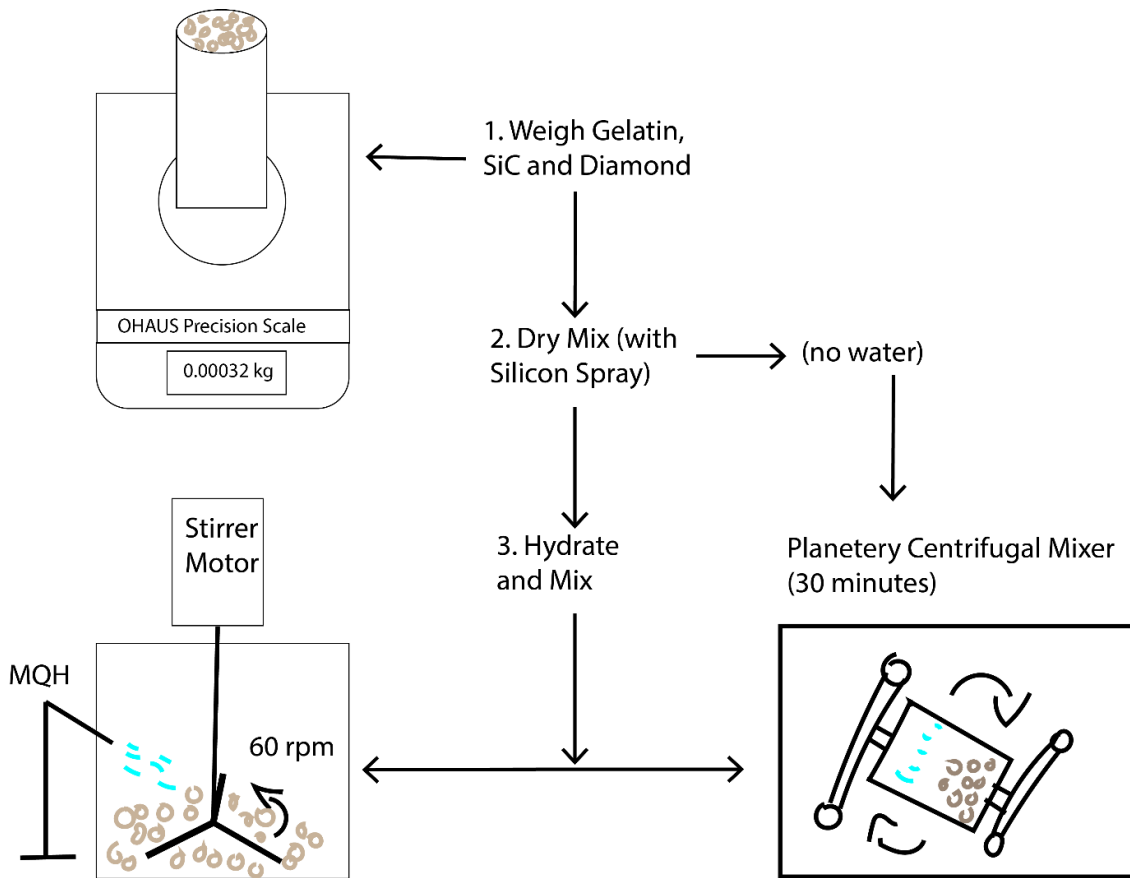
Figure 52 - Abrasive Preparation Sketch

6.2. Experimental Procedure

Following preparation of the abrasives, workpiece, and machine/environment (and knowing controllable input parameters and desirable outputs), it is important to develop a repeatable plan on how to implement the experiments. This involves initial data acquisition, workpiece preparation (namely surface grinding and cleaning), preparing the abrasive media and the machine, running the experiments, properly shutting the process down, final data acquisition and results analysis. The details of this are outlined in the flowchart shown in Figure 53 on the following page.
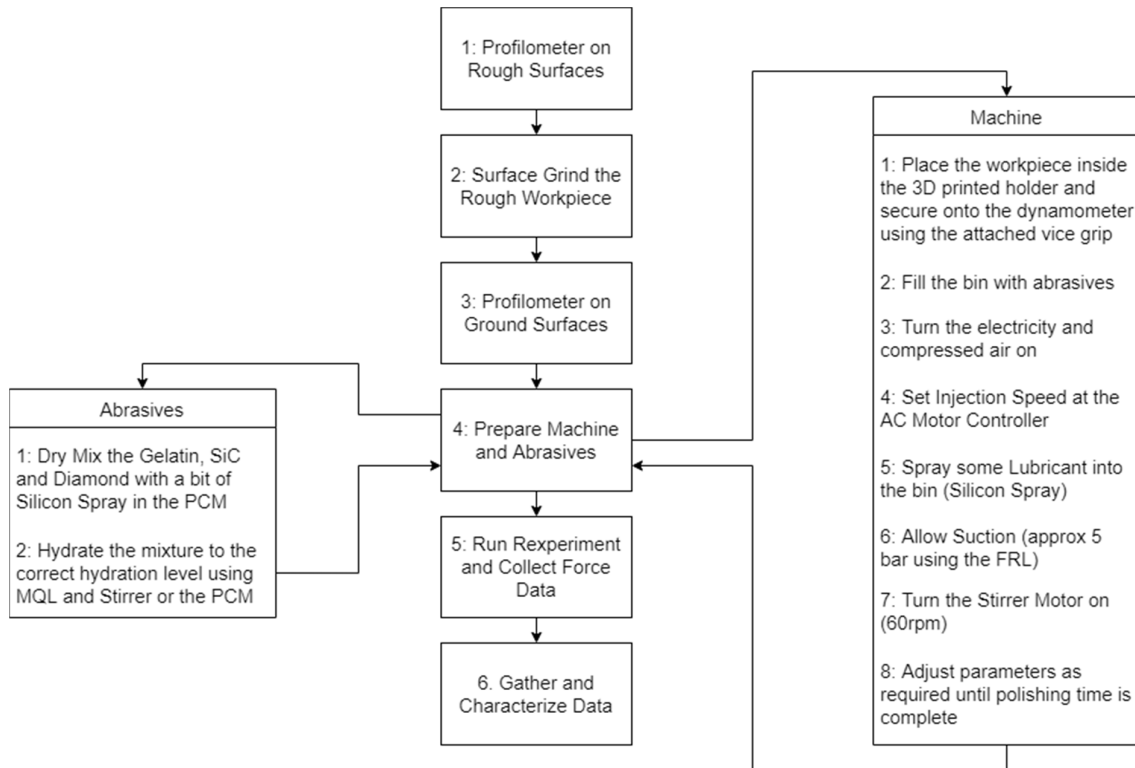
Figure 53 - Experimental Plan & Procedure

6.3. Experimental Variables

Greater amounts of experimental variables require a larger number of experiments to get a full set of results. The following parameters (see Table 10) were the parameters controllable by the machine (and had a direct implication on the polishing effect):

Table 10 - Parameters for experimental variables

Parameters (Details)	Units	Lower Limit to Upper Limit
Impinging velocity	m/s	6.28 – 31.4
Standoff distance	mm	20 – 750
Polishing Time	seconds	30 – 2700
Abrasive Water Content	%	10 – 50
Workpiece Inclination Angle	°	0 – 90
Diamond Mesh Size	#	1000 - 5000
Diamond Concentration	%	0.1 – 0.5

To reduce the required number of experiments, some parameters were kept constant as they have been proven by other researchers to be the optimal setting. These are:

- Standoff distance, which should be kept very low so that abrasives do not lose velocity and thus impart the maximum energy. This is kept at 20 mm as per other researchers [1] [4] [6].
- Workpiece Inclination Angle, which should allow for a balance between cutting forces and normal forces (allowing for the most optimal polishing [1] [24]). Angle is thus kept at 45 º.
- Diamond Mesh Size, which should be finer to allow more adherence and coverage onto the gelatin (#5000 diamond mesh was thus used).

With these three parameters constant, the following was decided for the varying parameters:

- Impinging velocity was limited by the impeller's lowest and highest speeds. To get a more accurate estimation of how velocity impacts polishing, a middle setting was included. Three velocity steps were thus present.
- Polishing time was given lower and upper limits as per previous researchers [1] [4]. Due to the impeller getting jammed at higher hydration levels, the time steps were reduced for abrasive hydration levels of 30% and 50%.
- Diamond concentration had not been varied by previous researchers increase in the concentration by 3 X and 5 X was chosen to see if this would have any effect on polishing results. Greater increases did not occur due to the limitations on budget and the difficultly in acquiring fine mesh diamond powder.

The independent variables studied in this experiment and their respective conditions are shown below:

- Polishing time (the duration of polishing experiment)
    - 60 seconds, 180 seconds, and 300 seconds for 30% and 50% hydrated media
    - 2.5 minutes, 10 minutes, 25 minutes, 45 minutes for 10% hydrated media
- Abrasive media hydration levels (the amount of water contained in the media as a function of its original mass)
    - 10%, 30%, 50%
- Media impinging velocity (the velocity that the abrasive media exits the nozzle and hits the workpiece)
    - 6.28 m/s, 15 m/s, 31.4 m/s

- Abrasive media diamond concentration (the ratio of diamond to other media constituents)
    - 0.1% diamond (97% gelatin - 2.9% SiC - 0.1% diamond), 0.3% diamond (97% gelatin - 2.7% SiC - 0.3% diamond), 0.5% diamond (97% gelatin - 2.5% SiC - 0.5% diamond)

For less hydrated media (at 10% hydration), 36 experiments are required (4 time steps, 1 hydration step, 3 velocity steps and 3 concentration steps). For more hydrated media (30% and 50%), 54 experiments are required (3 time steps, 2 hydration steps, 3 velocity steps and 3 concentration steps). This output a total of 90 required experiments to be run. As the time step experiments occur in the same experimental run, the number of overall experimental set-ups required was 27. Each experimental set-up and experimental run take approximately two hours, leading to a total experimental time of 54 hours.

6.4. Collection of Data

Desired outputs (dependant variables) had been decided on previously and were decided on due to outputs from the previous models/other researchers' outputs (force) and typical performance parameters of polishing (surface roughness and texture/topography). The measured outputs and their methods of measurement were:

- Surface roughness parameters – measured using a Taylor Hobson Surtronic 3P Profilometer
    - Ra
    - R_{ymax}
    - Rz
- Surface Texture, Quality and Topography – measured using a FEI Nova NanoSEM and MIRA Tescan 3
    - Qualitative measurement
- Live Signal Analysis
    - Force measurements – using a Kistler 9625 dynamometer
    - Sound Pressure Level – Using a GRAS 40PH AE Sensor/Microphone
    - Vibrational measurements – using a Kistler 8772A50 accelerometer
    - Imaging – using a FLIR C5 thermal video camera

Set up for the data acquisition tools are shown on the following page (Figure 54, Figure 55, Figure 56) and include: Kistler dynamometer, Kistler accelerometer, sensitive microphone (AE sensor) and FLIR thermal video camera.

More description on signal collection is described in the results section (preceding the display of force, AE sensor and accelerometer results) and the following chapter describes profilometer and microscope data collection in more detail too.

Figure 55 - FLIR C5 Camera Set-Up Inside the machine

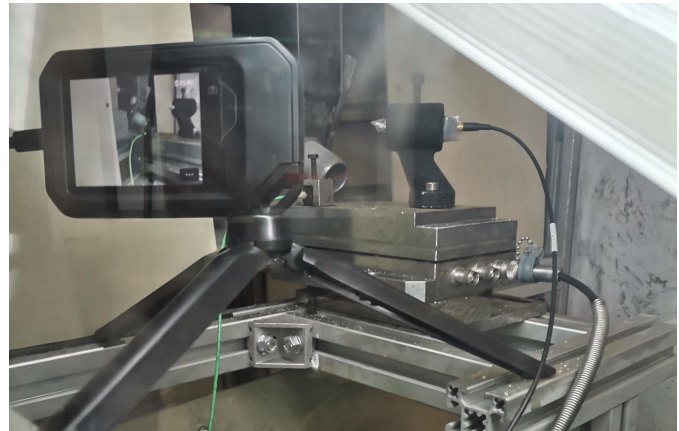Figure 56 - Dynamometer, Accelerometer and AE Sensor Set-Up
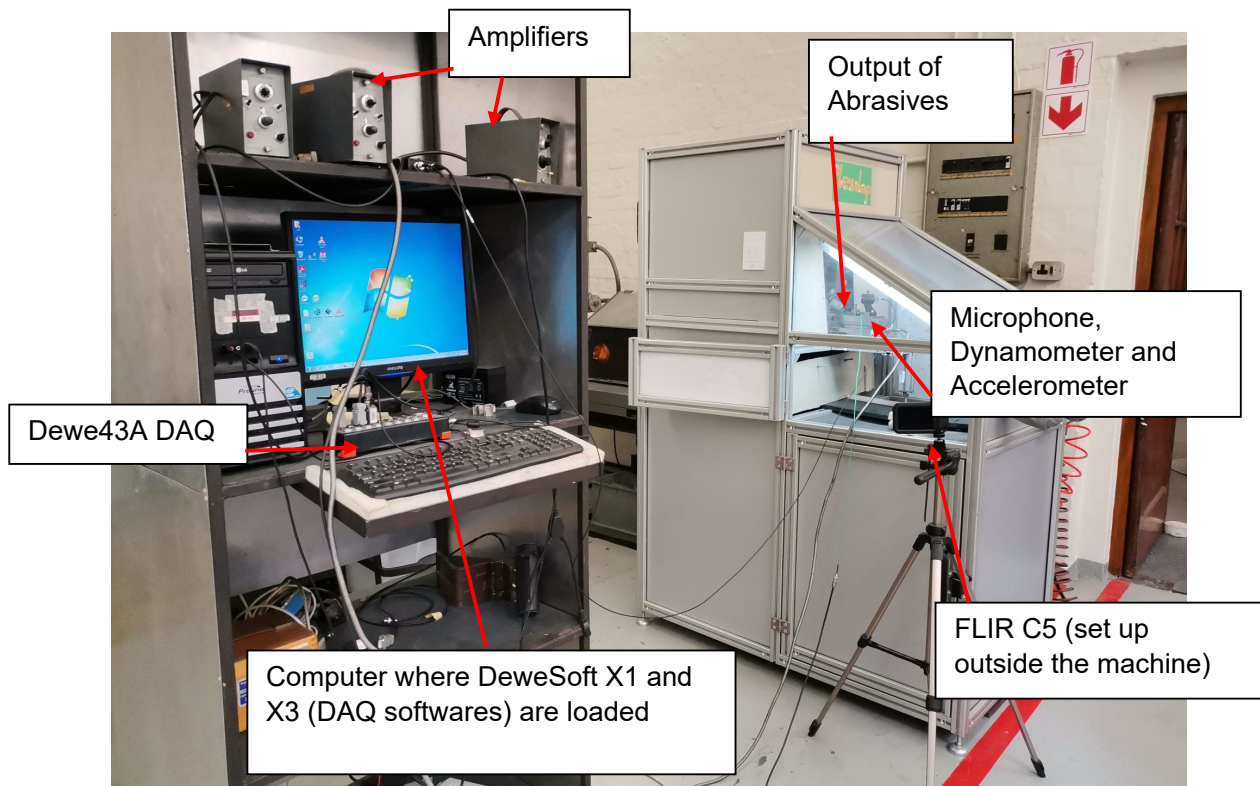
Figure 54 – Data Acquisition and Experimental Set Up for Acquisition of Force, Sound Pressure, Acceleration and Video Measurements

6.5. Design of Experiments

Excel worksheets were created to be able to reference the samples/experiments to the workpieces (as per the sticker in Figure 49) as well as to collect and store the data. Figure 57 below shows a portion of the designed experiments with stated independent variables as well as references to the workpiece samples, correlating to Table 9 as well.

AS1	4 Experiments			Sample 1		AS2	4 Experiments	
Impeller Velocity	31.4	m/s		Side 1		Impeller Velocity	15	m/s
Wetness	10	%				Wetness	10	%
Concentration	0.1	%				Concentration	0.1	%
1A	2.5	minutes				2A	2.5	minutes
1B	10	minutes				2B	10	minutes
1C	25	minutes				2C	25	minutes
1D	45	minutes				2D	45	minutes

BS1	4 Experiments			Sample 2		BS2	4 Experiments	
Impeller Velocity	31.4	m/s		Side 1		Impeller Velocity	15	m/s
Wetness	10	%				Wetness	10	%
Concentration	0.3	%				Concentration	0.3	%
1A	2.5	minutes				2A	2.5	minutes
1B	10	minutes				2B	10	minutes
1C	25	minutes				2C	25	minutes
1D	45	minutes				2D	45	minutes

Figure 57 - Sides and Samples for Some Experiments

Note that there are 27 experiment sets which are:

- AS1, AS2, AS3
- BS1, BS2, BS3
- CS1, CS2, CS3
- DB1, DB2, DB3
- EB1, EB2, EB3
- FC1, FC2, FC3
- GC1, GC2, GC3
- HD1, HD2, HD3
- ID1, ID2, ID3

Where each experiment set refers to a specific hydration, concentration, and impeller velocity (as well as a specific side of a workpiece sample).

Another excel worksheet was created to store the collected data and allow for analysis and graph creation. As can be seen in Figure 58 below, surface roughness data for each experiment was filed in (as well as pre-experimental roughness data and reminders for microscope images). This worksheet was used for experiment set E. More information regarding the analysis and graphing/comparison of results is presented in the results and discussion chapters.

Experiment Set E

Water Content	Constant	50%
Concentration	Constant	97-2.5-0.5
Impeller Velocity	Varying	6.28 - 31.4
Polishing Time	Varying	in, 3 min, 5 min

EB1	4 Experiments		Sample 4	Side 1						
Impeller Velocity	31.4	m/s	Ra @0	0.70125						
Wetness	50	%	Ry @0	5.95875						
Concentration	0.5	%								
			Ra	Surface Plots	Microscop	SEM		Rymax	Rt	Ra Before
1A	60	seconds	0.51	☐	☐	☐		3.3	2.26	0.75
1B	180	seconds	0.46	☐	☐	☐		3.06	2.81	0.74
1C	300	seconds	0.34	☐	☐	☐		4.03	2.78	0.65

EB2	4 Experiments		Sample 4	Side 3	NOTE					
Impeller Velocity	15	m/s	Ra @0	0.9						
Wetness	50	%	Ry @0	9.2						
Concentration	0.5	%								
			Ra	Surface Plots	Microscop	SEM		Rymax	Rt	Ra Before
2A	60	seconds	0.59	☐	☐	☐		5.2	4.52	1.05
2B	180	seconds	0.52	☐	☐	☐		3.63	3.03	0.88
2C	300	seconds	0.48	☐	☐	☐		3.79	2.64	0.85

EB3	4 Experiments		Sample 4	Side 4	NOTE					
Impeller Velocity	6.28	m/s	Ra @0	0.7125						
Wetness	50	%	Ry @0	8.065						
Concentration	0.5	%								
			Ra	Surface Plots	Microscop	SEM		Rymax	Rt	Ra Before
3A	60	seconds	0.54	☐	☐	☐		4.71	3	0.72
3B	180	seconds	0.41	☐	☐	☐		3.24	2.72	0.85
3C	300	seconds	0.41	☐	☐	☐		3.16	2.93	0.64

Figure 58 - Experiment Set E Worksheet

The following chapter presents results achieved before experiments were run. Verifications to the process design were thus made and functional operation was ensured. Material investigation and preliminary results analysis also occurred in this chapter.

Chapter 7 – Pre-Experimental and Initial Polishing Results

7.1. Description on SEM and Results Analysis

SEM images provide us with results of great significance. There are two notable SEM imaging techniques, that of backscattered electron (BSE) imaging and that of secondary electrons [82]. It is important to note that electron microscopy (EM) makes use of an electron beam for imaging due to the interaction between matter (surface) and electrons. There are many other forms of EM, such as TEM, which provide information on the inner structure of a sample.

BSE imaging electrons come from a wide region inside the volume of interaction (with this happening because of the elastic collisions between electrons and atoms). Larger atoms create higher signals, and the number of atoms reaching the detector is directly related to the atom's atomic number (Z). This makes BSE a helpful imaging technique for determining the atomic composition of the sample. BSE is often used for finding information on crystallography and topography of the sample as well.

Secondary electron imagery electrons come from the surface regions of the sample (or just below), and these occur due to the inelastic interaction between electron beam and sample/surface. Secondary electrons contain lower energy than BSE. Secondary electron imagery is most often used and is beneficial for the examination of surface topography (more so than BSE). Secondary electron imagery is the most common mode of SEM imagery. As stated by Goldstein et al. [83], the interpretation of topography is relatively simple when concerning secondary electron images (by noting the contrast, highlights and shading of the image). BSE imagery used for atomic composition uses atomic number contrast to determine percentage composition in a more quantitative but still similar manner.

The SEM used for acquisition of results is the FEI Nova NanoSEM (see Figure 61). Varying magnifications and SEM imaging types were used for the analysis of results but for the experimental results post-polishing, results were exclusively acquired with secondary electron imagery at 500 X magnification and 1500 X magnification.

To gather information regarding surface roughness parameters, a Taylor Hobson Surtronic 3P was used (see Figure 60). Information on Ra, $Rymax$ and Rz were gathered using the highest resolution possible at a cut-off of 2.5mm.

For other surface texture information, a Nikon Eclipse MA200 inverted metallurgical microscope was used (see Figure 59). Most information was using the highest magnification of 100 X.

Figure 61 - FEI Nova NanoSEM

Figure 60 - Taylor Hobson Profilometer

Figure 59 - Nikon Inverted Metallurgical Microscope

7.2. Pre-Polishing Results

7.2.1. As Acquired from SLS

a. 500x Magnification, Section 1

b. 5000x Magnification, Section 1

c. 500x Magnification, Section 2

d. 5000x Magnification, Section 2

e. 500x Magnification, Section 3
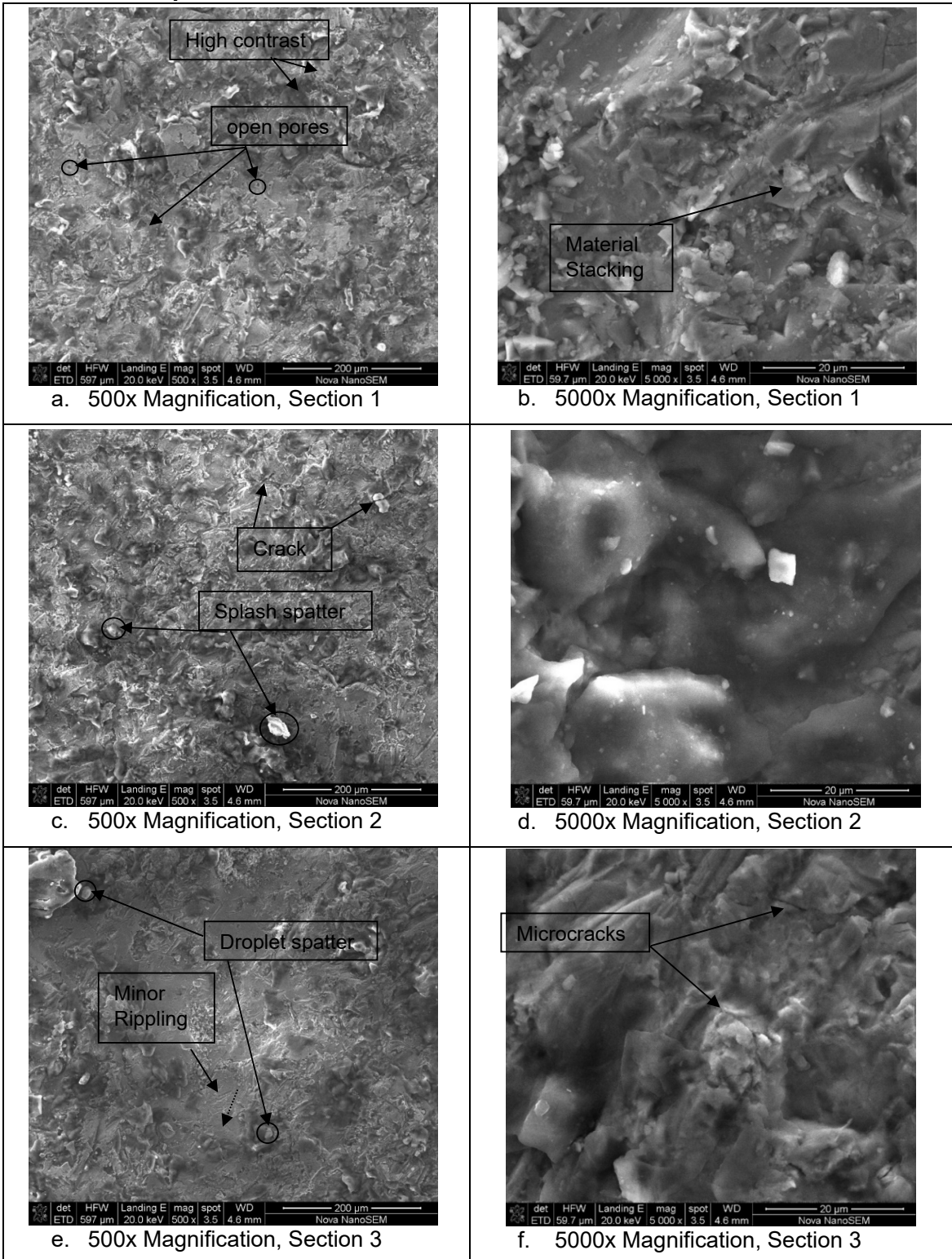
f. 5000x Magnification, Section 3

Figure 62 - Secondary Electron SEM Images of SLS Produced Ti-6Al-4V (no post processing)

The composition of the samples was confirmed through BSE and the results of this are shown in Table 12 and Table 13.

The secondary electron SEM images in Figure 62 on the previous page show that the sample surface is very rough (high levels of contrast are visible), where peaks and valleys vary significantly in height from the mean, and the surface texture is notably irregular. Many surface irregularities are noted on the surface due to manufacturing by SLS and these are labelled in Figure 62. Some examples of issues that lead to these irregularities are described in the following sentences. High scanning speeds often lead to microcracks between the melt pool and partially melted powder particles [84]. Rippled surfaces appear when surface tension due to motion of the laser causes a shear force while pores occur due to the entrapment of gaseous bubbles and when these pores are exposed to loading, they can also cause microcracks on the surface. Using the profilometer to acquire surface roughness parameters, the following results in Table 11 were acquired:

Table 11 - Ra Measurements on SLS Ti-6Al-4V Sample

	Experiment 1	Experiment 2	Experiment 3	Average
Ra (μm) μm	5.79 ± 0.01	6.42 ± 0.01	6.76 ± 0.01	6.32 ± 0.49
Rymax (μm)	18.85 ± 0.01	21.16 ± 0.01	19.72 ± 0.01	19.91 ± 1.16
Rz (μm)	17.35 ± 0.01	19.71 ± 0.01	16.55 ± 0.01	17.87 ± 1.58

Figure 63 below shows the surface plot for a sample (where sharp peaks and valleys are noted, verifying the SEM results).
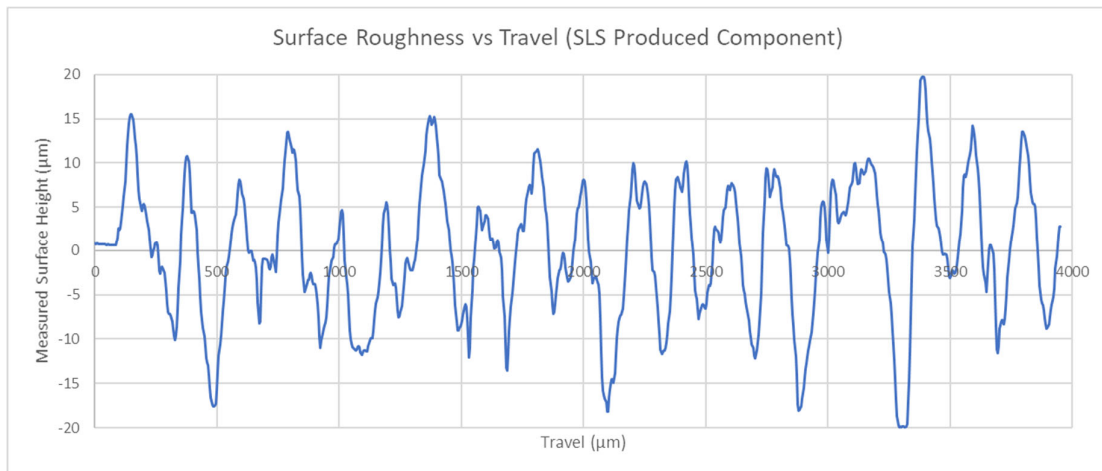

Figure 63 - Surface Plot of SLS Produced Component

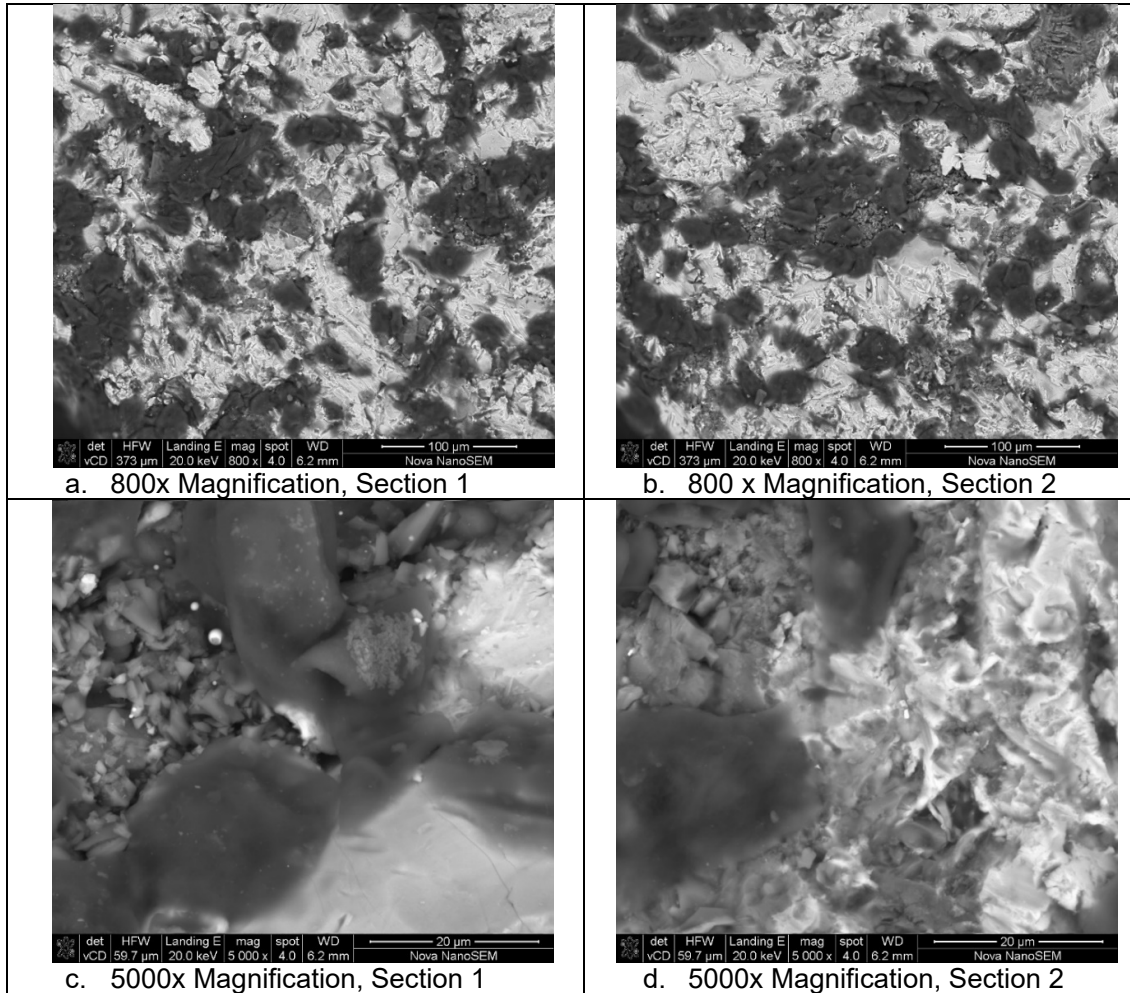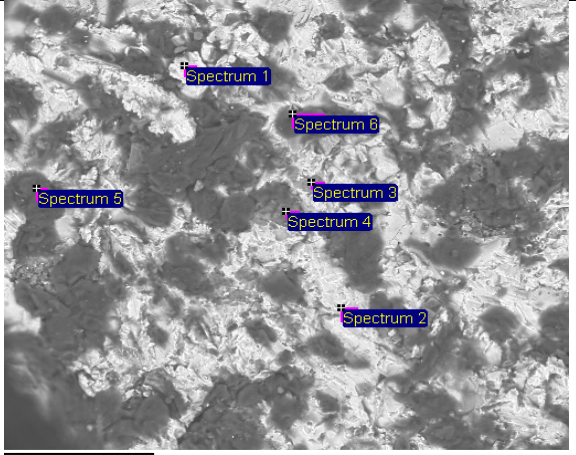| a. 800x Magnification, Section 1 | b. 800 x Magnification, Section 2 |
| c. 5000x Magnification, Section 1 | d. 5000x Magnification, Section 2 |

Figure 64 - BSE SEM images of SLS produced Ti-6Al-4V (no post processing or finishing)

Figure 64 above shows the BSE imagery used on the SLS Ti-6Al-4V sample (with an 800 X and 5000 X magnification on two respective sections). These images were used in the EDS analysis displayed in Table 12 and Table 13 on the following page. The EDS analysis was done to analyse the sample's atomic composition. The results are summarised in the table and show that the samples may have slightly higher values of aluminium than expected and slightly lower values of titanium and vanadium, however this confirmed that the acquired samples are titanium aluminium vanadium alloys with composition reasonably close to that of Ti-6Al-4V.

Table 12 - Lower Magnification EDS Analysis
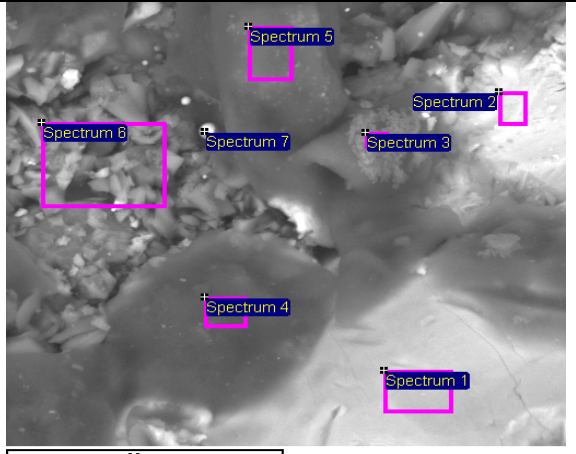
Spectrum	% Al	% Ti	%V
1	6.27	89.37	4.36
…			
6	9.85	90.15	0
Mean	7.80	89.415	2.32

EDS Image 1

Table 13 - Higher Magnification EDS Analysis

Spectrum	% Al	% Ti	%V
1	6.37	89.83	3.8
…			
6	39.3	56.61	4.09
Mean	20.56	77.01	2.43

EDS Image 2 (higher magnification)

7.2.2. Ground samples

Before polishing the samples, surface grinding was completed, and the results of the ground samples varied on each.

For each sample, surface roughness parameters were measured twice per division on each side of the sample (with most samples having 5 sides of available polishing, with 4 divisions per side, that relates to 40 measurements per sample). The referencing system used has been previously discussed and displayed. Figure 65 shows the roughness parameter results for one side. Note that these results were acquired using the profilometer mentioned previously and were measured prior to SEM/EBS imaging.

Sample 5	Ra Measurements (µm)									
	A		B		C		D			
	Ra1	Ra2	Ra1	Ra2	Ra1	Ra2	Ra1	Ra2	Average	Error
Side 1	0.63	0.62	0.62	0.8	0.45	0.58	0.66	0.5	0.61	±0.06
Side 2	0.66	0.69	0.74	0.72	0.7	0.77	1.14	0.99	0.80	±0.03
Side 3	1.03	0.92	0.89	0.92	1.35	1.51	1.26	1.08	1.12	±0.06
Side 4	0.75	0.62	0.66	0.7	0.71	0.65	0.59	0.66	0.67	±0.04
Side 5	1.14	0.94	1.08	0.92	0.91	1.31	0.87	1.34	1.06	±0.15
Sample 5	Rymax Measurements (µm)									
	A		B		C		D			
	Rymax1	Rymax2	Rymax1	Rymax2	Rymax1	Rymax2	Rymax1	Rymax2	Average	Error
Side 1	12.46	4.9	5.2	7.51	5.03	5.04	5.44	4.88	6.31	±1.31
Side 2	7.17	7.17	6.51	7.81	6.3	7.54	7.6	8	7.26	±0.37
Side 3	7.35	8.03	8.23	9.52	14	13.45	10.41	10.71	10.21	±0.35
Side 4	8.21	7.09	7.1	8.28	8.41	6.21	6.49	10.45	7.78	±1.06
Side 5	7.2	5.25	6.04	8.6	8.45	11.6	5.57	12.15	8.11	±1.78

Figure 65 - Measurement Results for a Sample (Sample 5)

Pre-acquisition of all the ground sample surface parameters allowed for an appropriate comparison to be made between polished surfaces and ground surfaces.

Ra values for all samples varied between an average low of 0.53 µm ± 0.04 µm and an average high of 1.14 µm ± 0.08 µm, with the average of all Ra values being 0.76 µm ± 0.05 µm. $Rymax$ values varied from an average low of 4.82 µm ± 0.17 µm to an average high of 11.24 µm ± 0.31 µm, with the average of all $Rymax$ values being 7.78 µm ± 0.22 µm.

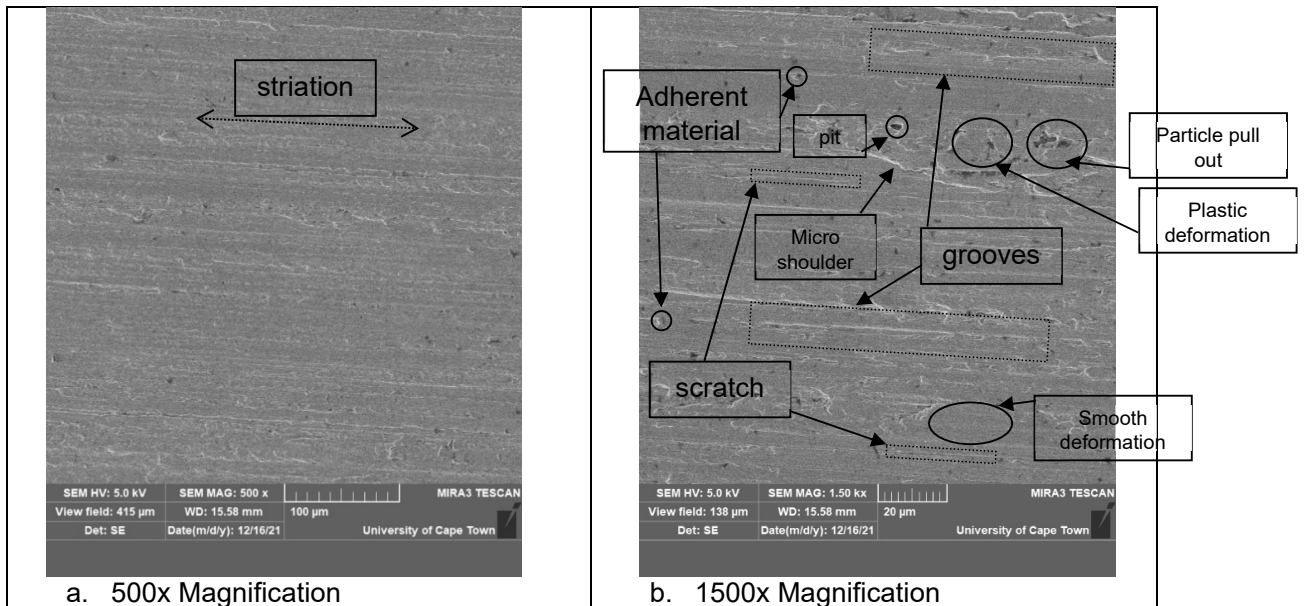a. 500x Magnification   b. 1500x Magnification

Figure 66 - Secondary Electron SEM Imagery of a Ground Sample (Sample 2 - Side 5, Section 1)

Figure 66 shows the SEM imagery (secondary electron) of a ground sample at two magnifications. The Ra value for this sample was an average value of 0.70 µm ± 0.07 µm and the $Rymax$ value had an average value of 6.85 µm ± 0.20 µm. The 1500 X magnification image allows for a good inspection of the surface of the ground sample. The presence of grooves and scratches is noted due to the extrusion of abrasive grains of the grinding wheel [85]. This leads to both brittle fracture/particle pull out, plastic deformation, and smooth deformation on the surface. Adherent material is clearly seen on the surface too (although sporadic in nature, meaning minimal adherent material is visible on this sample). Plastic pileups/deformation suggest that rubbing and ploughing occurred on the workpiece [86], while pit appearance is noted too (minimal pits are present on this sample). CVD grits lead to striations, and this can be seen in the 500 X image in Figure 66a. The purpose of polishing is to remove many of the undesirable effects of surface grinding and to create a lower overall surface roughness.

Note that profilometer results are used in conjunction with microscopy results to determine surface quality before and after polishing. Determining accurate quantitative surface roughness values from microscopy images is not possible, however the changes in visible

peaks and valleys as well as the presence of impurities and markings/surface defects, can be noted. In addition to the noticeable changes in texture, the microscopy images can be used in conjunction with the profilometer results to draw conclusions on surface quality and roughness changes.

7.3. Polishing Initial Results

To affirm the calculations, design and development, many initial tests were carried out on various samples to ensure that the polishing action was indeed occurring and that the machine could provide the required experimental conditions for meaningful results to be measured.

Figure 67 below shows the progress of polishing an aluminium plate. Firstly, the plate was sanded with an appropriate sandpaper of 200-grit, then 600-grit and finally, wet sanded with an 800-grit sandpaper. After this, a check on mirror finish was done by placing the plate by the output nozzle (Figure 67a). Half of the plate was masked with insulation tape so that comparisons could be drawn. The plate was then polished at a high velocity (31.4 m/s), a medium water content (20%) and with a diamond concentration of 0.3%. The plate was polished for 30 minutes, and the results can be seen in Figure 67b, where a mirror finish can clearly be observed in the polished section (where the output nozzle reflection can be observed). The improvement in surface texture is noticeable as well (a much lesser presence of scratch marks is observed) and the mirror finish indicates a lower surface roughness. Table 14 shows the notable improvement of surface parameters over time due to the polishing action.
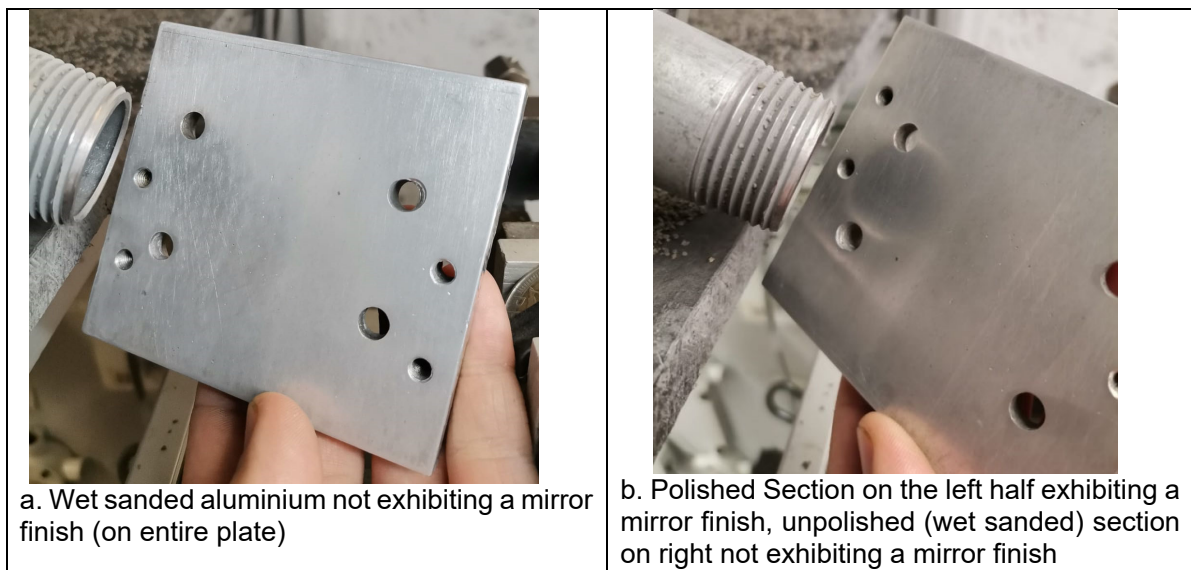

| a. Wet sanded aluminium not exhibiting a mirror finish (on entire plate) | b. Polished Section on the left half exhibiting a mirror finish, unpolished (wet sanded) section on right not exhibiting a mirror finish |

Figure 67 - Results of Polishing an Aluminium Plate

Table 14 - Aluminium Plate Measured Surface Parameters (averages of 3 readings)

Unpolished (wet sanded with 800 grit)			Polished		
Ra - µm	Ry - µm	Rz - µm	Ra - µm	Ry - µm	Rz - µm
0.38 ± 0.03	4.02 ± 0.12	4.54 ± 0.35	0.16 ± 0.02	1.65 ± 0.15	0.98 ± 0.13

Figure 68 shows the polishing results of a typical 5 Rand coin (which has an aluminium-bronze core and a copper-nickel ring). Note that the coin was cleaned before and after polishing with de-ionized water, a degreasing solution and with acetone. The noticeable removal of scratch marks and the removal of much of the texture is observed. Table 15 shows that the coin's surface roughness reaches a measured value of less than 0.10µm (over an average of 3 readings on the flat portion of the coin where the South African emblem is present).
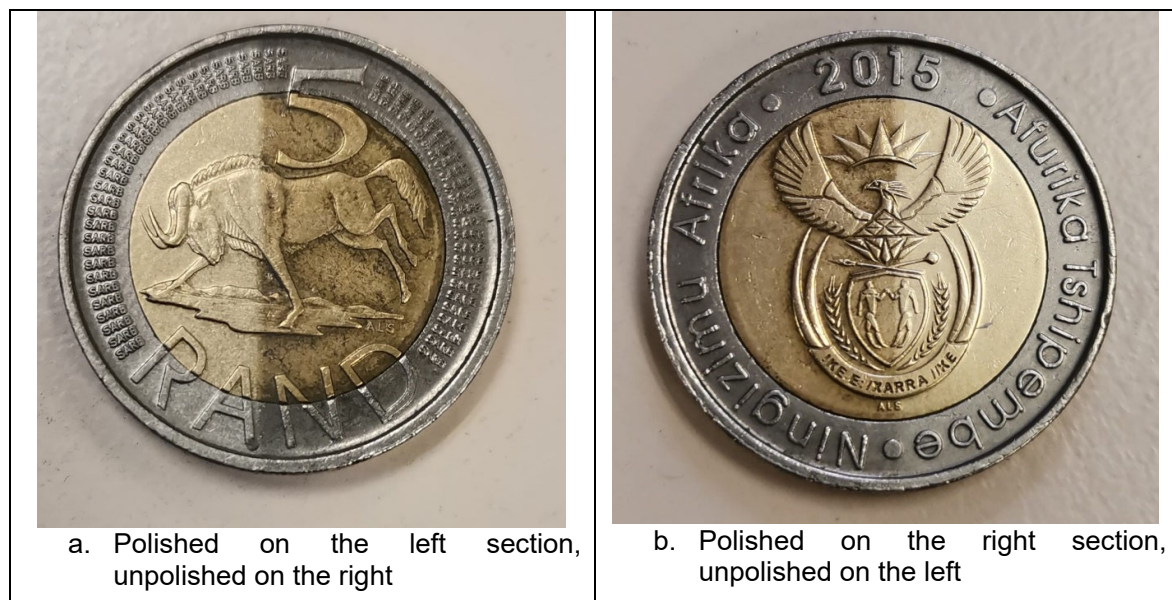

a. Polished on the left section, unpolished on the right	b. Polished on the right section, unpolished on the left

Figure 68 - Results of Polishing a 5 Rand Coin

Table 15 - R5 Coin Measured Surface Parameters

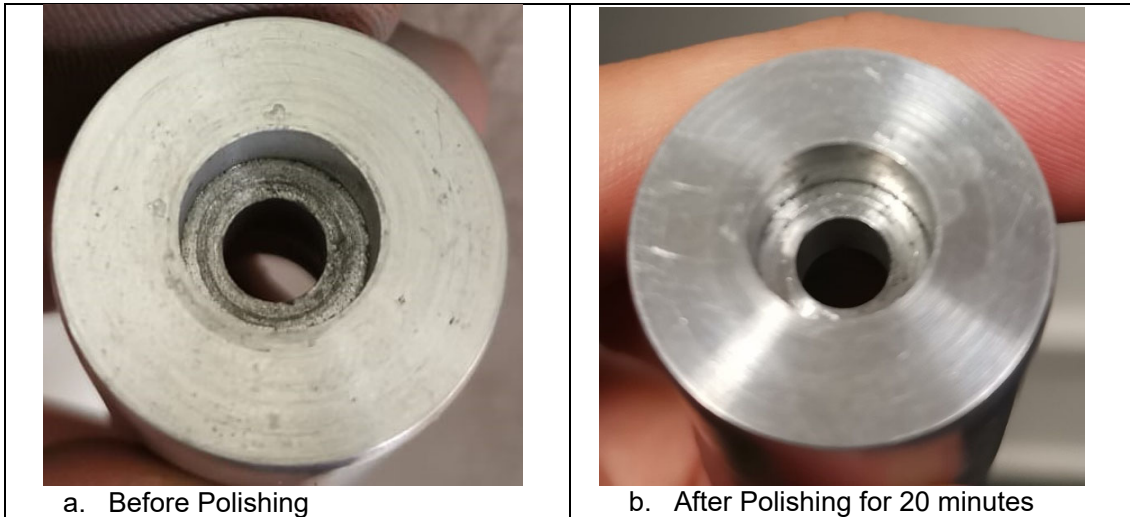| Unpolished (cleaned)			Polished		
Ra - µm	Ry - µm	Rz - µm	Ra - µm	Ry - µm	Rz - µm
0.34 ± 0.02	2.00 ± 0.13	1.52 ± 0.08	0.08 ± 0.01	1.07 ± 0.10	0.98 ± 0.04

| a. Before Polishing | b. After Polishing for 20 minutes |

Figure 69 - Results of Polishing a Small Pulley

Table 16 - Small Pulley Measured Surface Parameters

Unpolished			Polished		
Ra - µm	Ry - µm	Rz - µm	Ra - µm	Ry - µm	Rz - µm
0.55 ± 0.03	3.68 ± 0.13	2.24 ± 0.17	0.25 ± 0.02	1.71 ± 0.08	1.37 ± 0.12

Figure 69 shows a small aluminium pulley (used in the machine) where 20 minutes of polishing shows a vast improvement to surface texture and roughness overall which is observed both quantitively by surface roughness and qualitatively by the vast increase in reflectivity of the surface. Table 16 shows the improvement in surface roughness where all three values of measured surface roughness decrease by a large amount.

All the above results (although less relevant to scientific outputs) are essential and undoubtedly valuable to proving the developed machine's capabilities. The chapter following this is of more relevance to quantifiable scientific outputs and proves to show fulfilment of the objectives stated earlier in this dissertation.

Chapter 8 – Experimental Results

Figure 70 below demonstrates how the gathered and interpreted results are displayed (and in which respective order) as well as how the results are interlinked and connect one section to another.
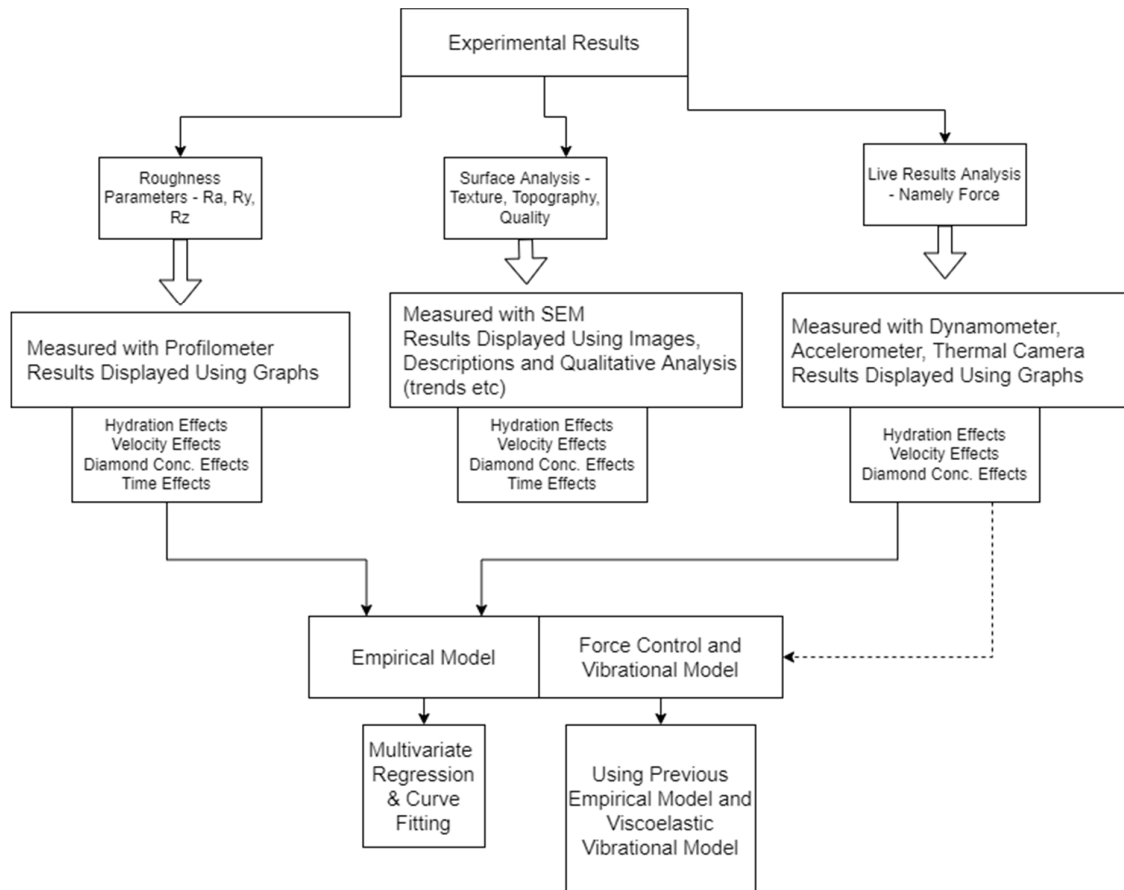

Figure 70 - Flowchart of Results Presentation and Connection

Each variable provides a different set of results. For example, polishing time influences both the surface roughness parameters and surface texture of the workpiece; analysis of this meant that readings needed to occur at a fixed hydration level, diamond concentration and impeller speed (as only one variable can change for a one-dimensional analysis). The same logic applies for hydration levels (a fixed time, velocity, and concentration were required), concentration (fixed time, velocity, and hydration were required) and velocity (fixed time, hydration, and concentration were required).

The derived empirical model and developed mass-spring damper model is displayed in a separate chapter (the following chapter) to highlight the differences and due to the occurrence of results happening at vastly different stages of the investigation.

8.1. Surface Roughness Parameters

Using measured values and created graphs, collected data concerning surface roughness is presented in this subchapter. Trends and influencing factors are easily notable from the presented data and, as with other chapters, the results presented here aid in future design of the polishing process as well as optimization of parameters (and thus selection of parameters for desired output). The results presented below are divided into the influence of polishing time, hydration level, impinging velocity and diamond concentration. Many of the results were drawn from the polishing time influence and the hydrational, diamond concentration and velocity influence were inferred from this. Thus, results for $Rymax$ are only presented for polishing time and the influence of other parameters is described concurrently in this section.

8.1.1. Polishing Time Influence

As stated in nearly all literature regarding Flexolap polishing, time is one of the most important process parameters (time measures productivity in industry), and the reduction of it (while still maintaining adequate surface quality) is the most desirable aspect in industry [4] [16] [46] [50]. All figures and associated graphs of surface roughness change over time for varying impinging velocities show similar results to the of the predictive models presented previously. Surface roughness shows a sharp decrease in the initial stages of polishing before reaching a perceived surface roughness limit and overal surface roughness does not decrease from here. Higher impinging velocities show a much lower limit, implying that greater material removal and hence a greater polishing action occurs at higher impinging velocities. Razali [1], in a similar fashion, showed that polishing velocity has a great impact on final roughness limit as well as the polishing time to achieve the desired surface roughness (Figure 6 shows these results well). Maximum peak height (from peak to valley) shows a very similar trend to that of surface roughness (these parameters are related closely in the polishing process and this was expected).
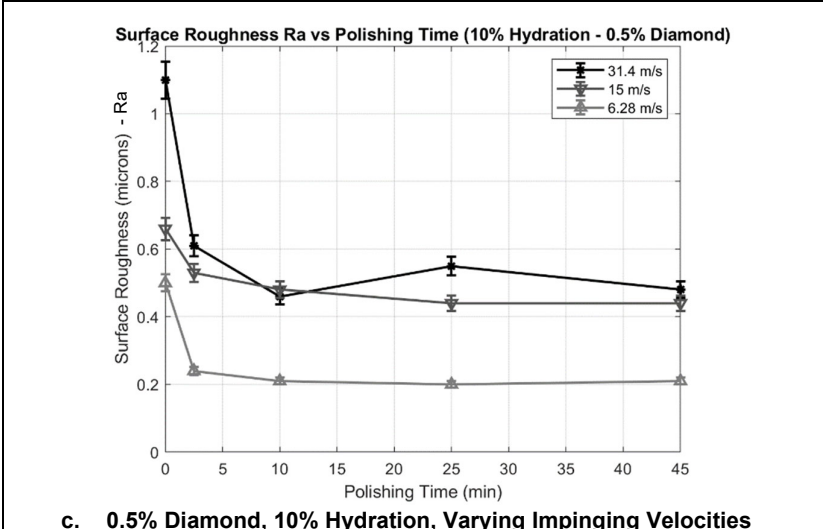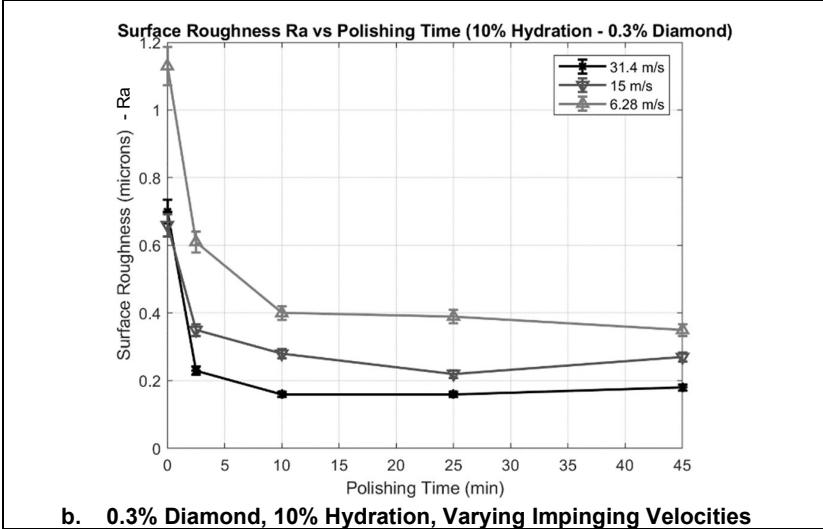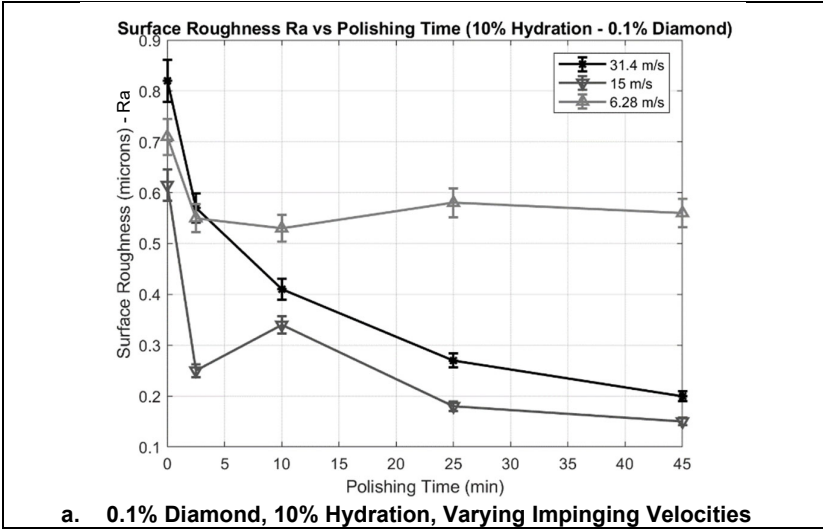
a. 0.1% Diamond, 10% Hydration, Varying Impinging Velocities

b. 0.3% Diamond, 10% Hydration, Varying Impinging Velocities

c. 0.5% Diamond, 10% Hydration, Varying Impinging Velocities

Figure 71 - 10% Hydration Ra Changes Over Time

Figure 71 shows that the greatest decreases from initial surface roughness occur for the highest impinging velocity (31.4 m/s) and least so for the lowest impinging velocity (6.28 m/s). Figure 71c shows a low surface roughness reached for the low impinging velocity, but this is due to the comparatively low initial surface roughness (approximately 0.5 µm) while the high impinging velocity shows a higher final surface roughness, but a much larger initial decrease in surface roughness (an approximate change of 0.5 µm). The first 10 minutes of polishing prove to be most vital in the sense that surface roughness (Ra) sees the greatest decrease in value over this period with minimal changes to Ra occurring after this period. The large decrease in Ra over this period implies that the greatest material removal occurs in this 10-minute range. Nearly identical trends can be seen for peak height $Rymax$ decrease over time (see Figure 72) with all previously described analysis for Ra holding true for $Rymax$. The intrinsic link between these parameters in polishing imply that the measured trends will be the same, however affirmation of these expectation is important in analysis.
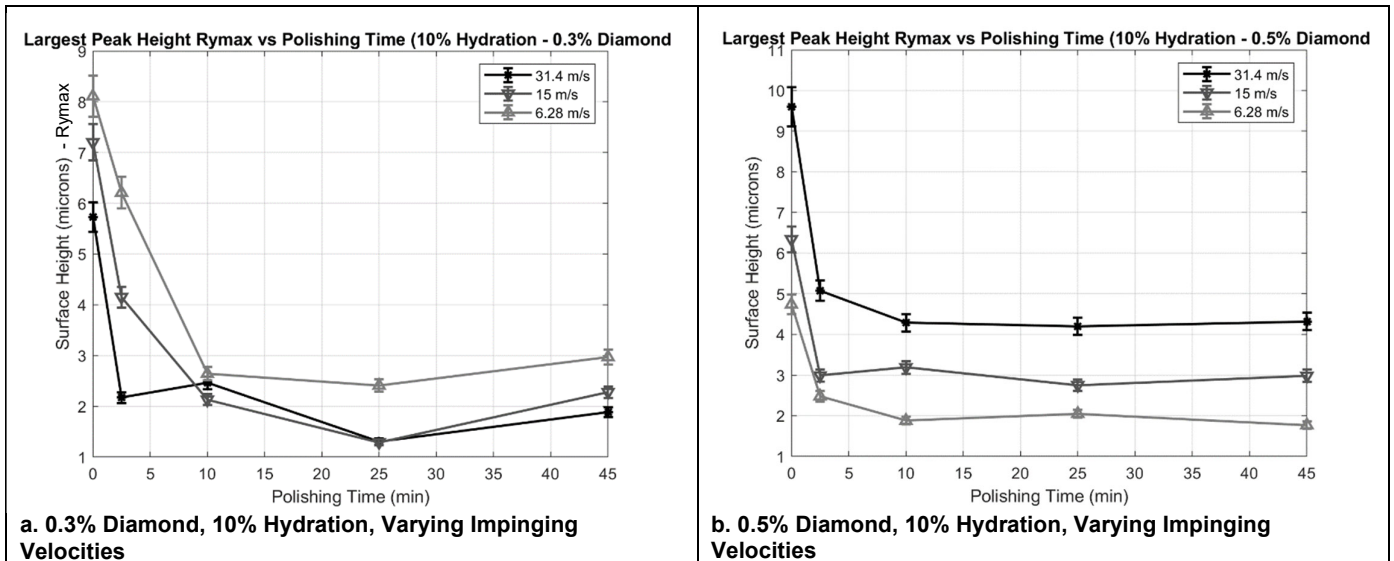

a. 0.3% Diamond, 10% Hydration, Varying Impinging Velocities

b. 0.5% Diamond, 10% Hydration, Varying Impinging Velocities

Figure 72 - 10% Hydration Rymax Changes Over Time

a.   0.1% Diamond, 30% Hydration, Varying Impinging Velocities

b.   0.3% Diamond, 30% Hydration, Varying Impinging Velocities

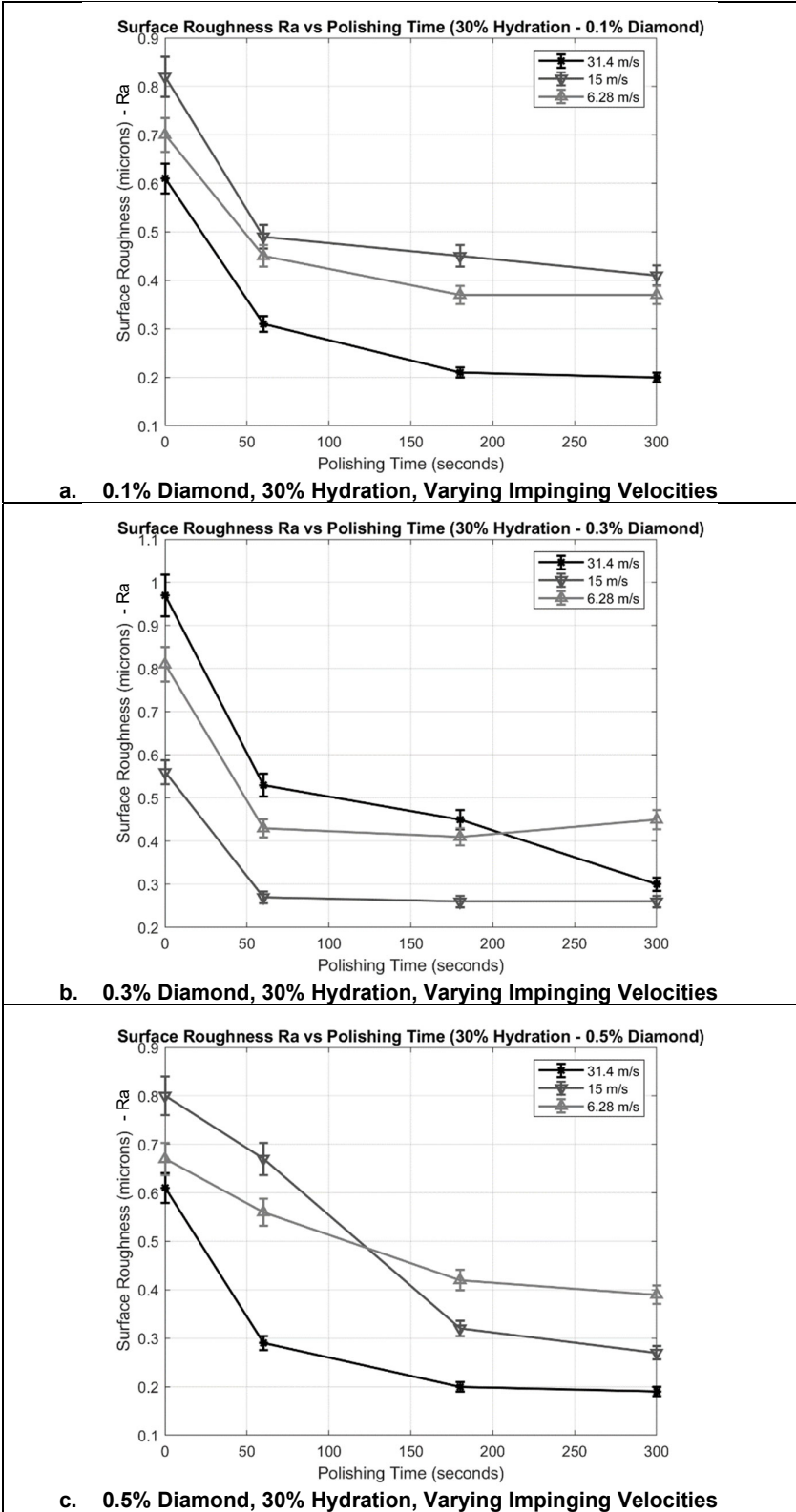**c.   0.5% Diamond, 30% Hydration, Varying Impinging Velocities**

Figure 73 - 30% Hydration Ra Changes Over Time

For the increased hydration level (30%) results shown in Figure 73, the experimental polishing time is lower than at the lower hydrational level (10%). However, a fast initial decrease in surface roughness is still noted (with most limits being reached in the first 150 seconds). It is again noted that higher polishing velocities show a much greater initial surface roughness decline, and particularly with higher hydration which shows a tendency to a lower convergence of final surface roughness. Investigations into hydration of media have shown that higher elasticity media (lower water content) leads to greater work hardening in the substrate of workpiece materials as well as a deeper local polishing effect [6]. The deeper localised polishing action leads to greater initial polishing rates but the work hardening effect of low hydrated media (which saturates hardness values quickly) means that material removal becomes more difficult for the polishing action to achieve and thus surface roughness convergence values are higher [6]. Higher hydrated media exhibits more extensive polishing action (thus the more gradual decrease in Ra) but a lower rate of work hardening and thus a lower saturation value of Ra. Lower velocities show a much more gradual decline and a higher limit overall (as expected). Investigations into impinging velocities have shown that stronger abrasive action on the workpiece surface occurs at higher velocities [6]. The change in $Rymax$ over time (see Figure 74) for all conditions of diamond concentration is again quite similar to that of Ra, aiding in verification of the intrinsic link between the two outputs.
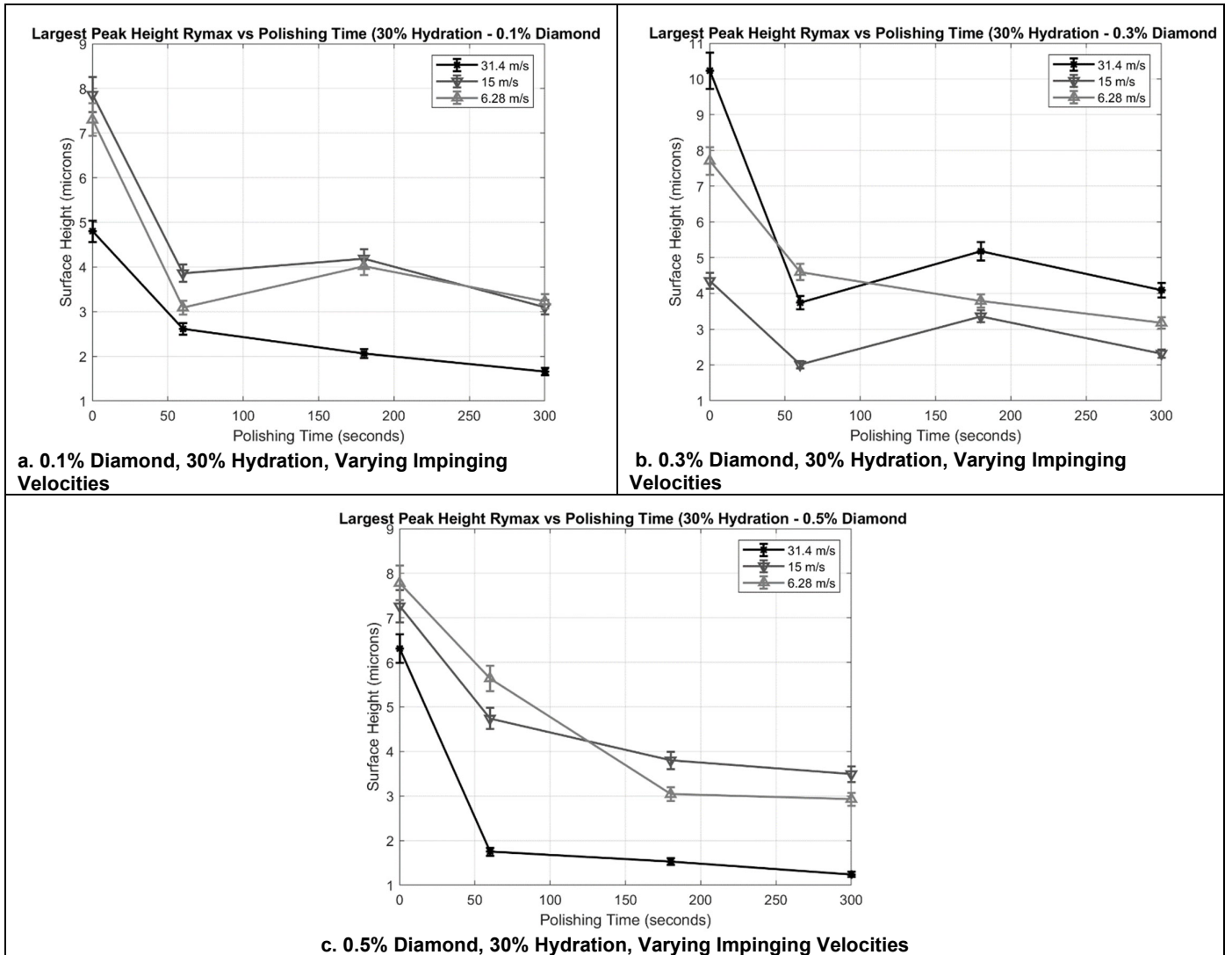
a. 0.1% Diamond, 30% Hydration, Varying Impinging Velocities

b. 0.3% Diamond, 30% Hydration, Varying Impinging Velocities

c. 0.5% Diamond, 30% Hydration, Varying Impinging Velocities

Figure 74 - 30% Hydration Rymax Changes Over Time

a. **0.1% Diamond, 50% Hydration, Varying Impinging Velocities**

b. **0.3% Diamond, 50% Hydration, Varying Impinging Velocities**

c. **0.5% Diamond, 50% Hydration, Varying Impinging Velocities**
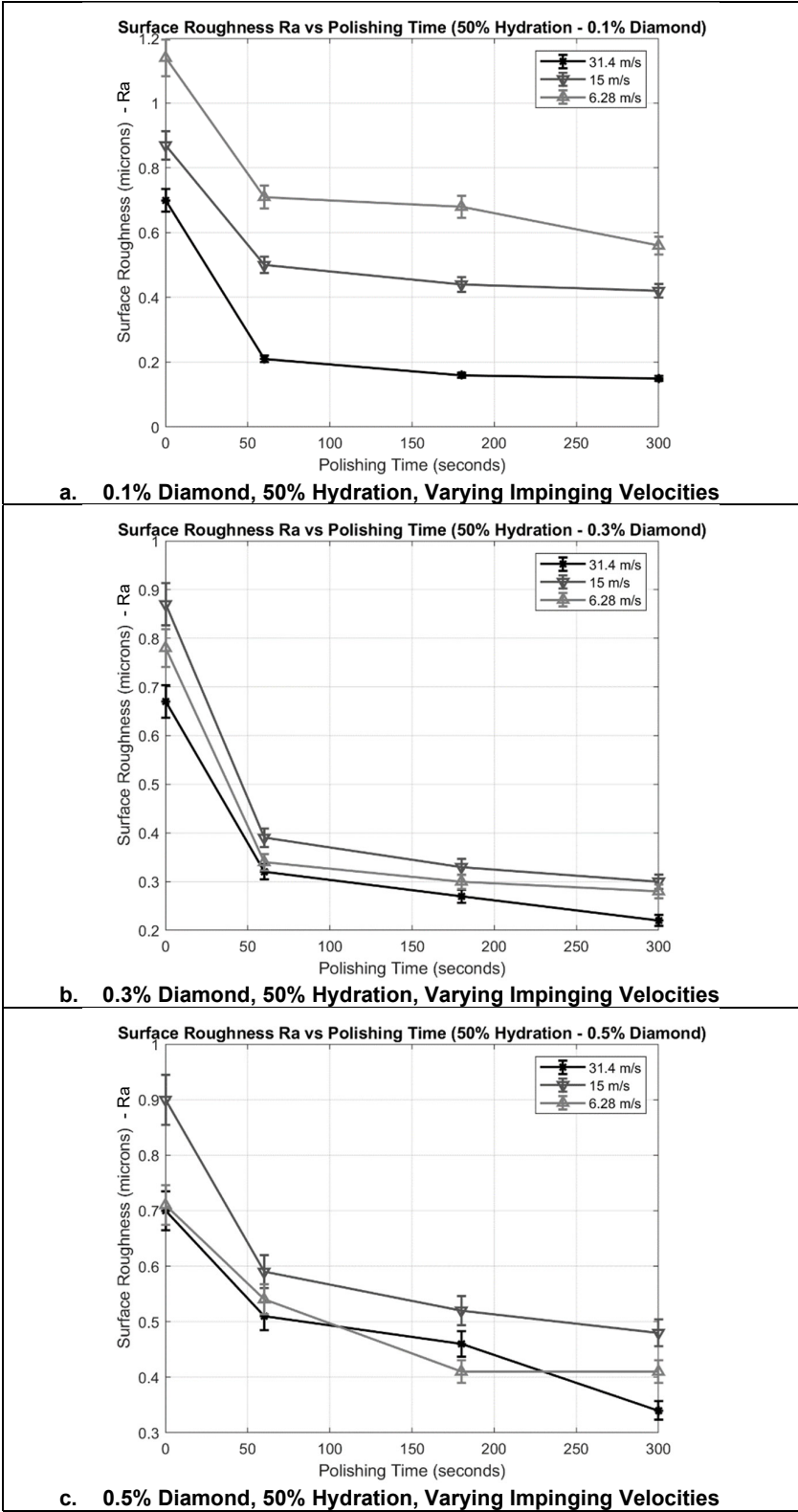
Figure 75 - 50% Hydration Ra Changes Over Time

For the 50% hydrational results shown in Figure 75, the highest impinging velocity shows the greatest overall decrease as well as the lowest overall limit, however, the lower impinging velocities prove to be much more effective than at lower hydrational levels and have greater overall changes in Ra from initial to final roughness. Similar trends are noted to the previous results in Figure 73 with sharp initial decreases present in Ra and limits being reached reasonably fast. $Rymax$ graph trends (see Figure 76) are somewhat different and do not relate as well to Ra as the previous two results do. The same trend in initial sharp decrease is noted though. $Rymax$ results prove less about the change in surface than Ra but the results give an indication of how well polishing action has occurred and verify the results achieved for overall surface roughness. The trends in Ra and $Rymax$ should be similar in blast polishing analysis and prove that as overall roughness decreases, so does maximum peak height.

a. 0.1% Diamond, 50% Hydration, Varying Impinging Velocities

b. 0.3% Diamond, 50% Hydration, Varying Impinging Velocities

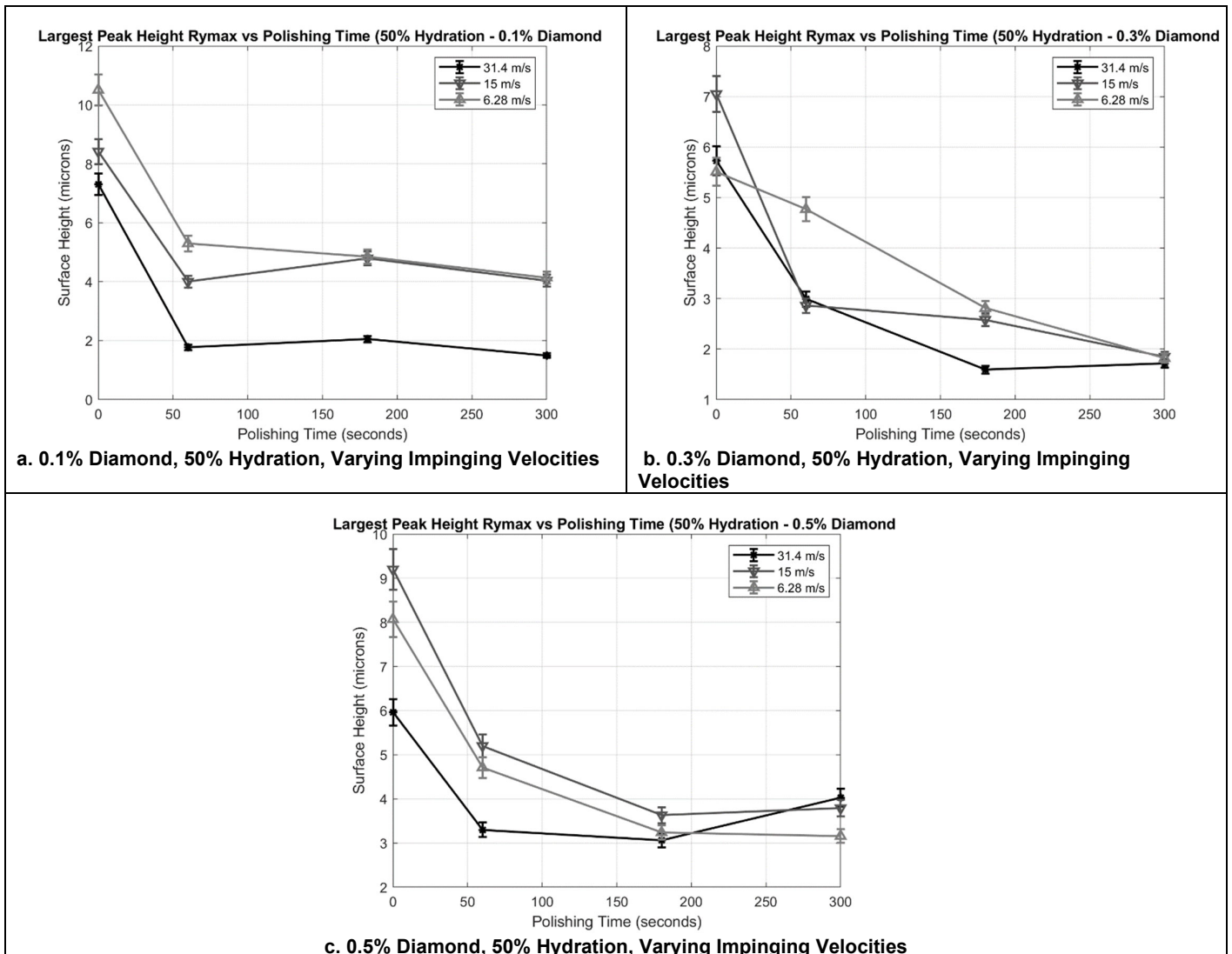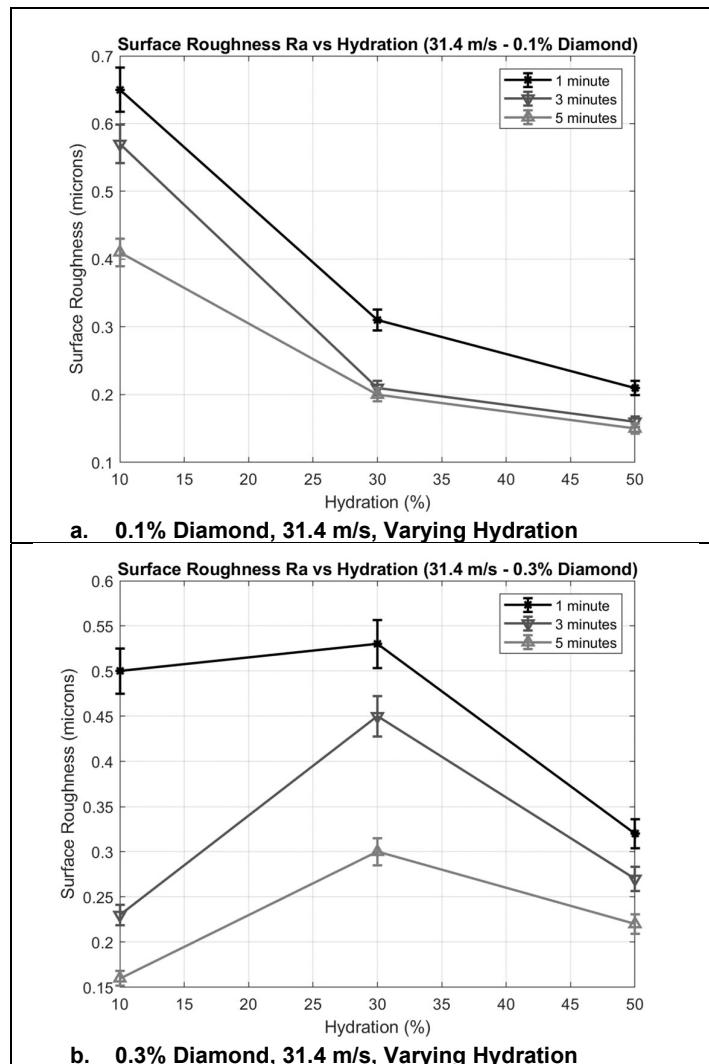c. 0.5% Diamond, 50% Hydration, Varying Impinging Velocities

Figure 76 - 50% Hydration Rymax Changes Over Time

8.1.2. Hydration Influence

For the study of influence of hydration on polishing parameters, the graph x-axis was changed to that of hydration while surface roughness was kept as the y-axis variable. An easy to note trend is that higher polishing times always result in a lower surface roughness. An interesting to note trend in this section is that higher hydration does not directly imply lower surface roughness (especially after short polishing times of 5 minutes and less). As mentioned previously, investigations into polishing have shown that greater substrate work hardening occurs at higher elasticities (lower water content) and lower water content medias create a more local polishing action, leading to the higher surface roughness convergence and greater initial rate of material removal (the opposite effect of lower surface roughness convergence and lower initial rate of removal is expected in higher hydrated media). The results in this section are analysed to see if the expected trends are notable under a large variety of polishing conditions.
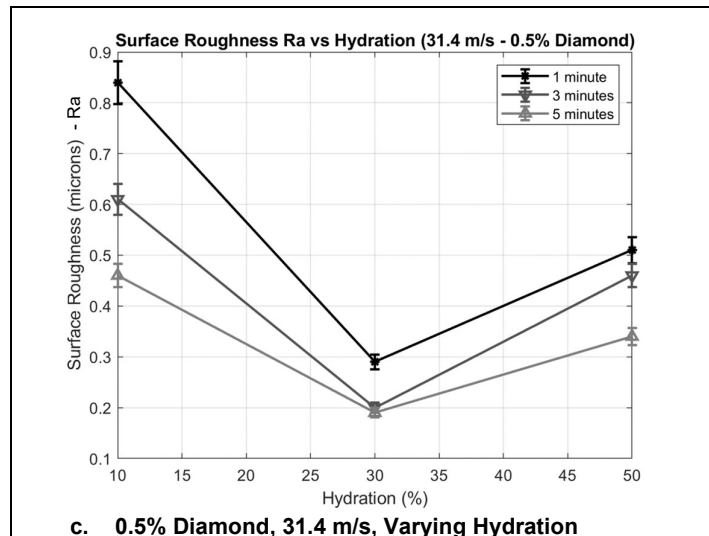

a.   0.1% Diamond, 31.4 m/s, Varying Hydration

b.   0.3% Diamond, 31.4 m/s, Varying Hydration

c. 0.5% Diamond, 31.4 m/s, Varying Hydration

Figure 77 - 31.4 m/s Ra Changes Over Hydration

Figure 77 does not display a direct correlation between hydration and surface roughness over increases in diamond concentration and this may be due to the shorter polishing time durations (where surface roughness convergence is expected to take comparatively longer for higher hydrated media). However, it should be noted that the incurrence of an inflection point at 30% hydration (where surface roughness trends invert) becomes prevalent throughout the display of hydration results. The results in Figure 78 show the same occurrence of an inflection point at 30% hydration and do not display a consistent trend over diamond level increases. The vibrational model displayed later in this dissertation suggests some reason as to why an inflection point is occurring at 30%. Contact stresses, forces and deformations of the 30% media upon impact (for all values of impinging velocity) are much greater than that of the 50% hydrated media (approximately double) but these parameters are also much lower than that of the 10% hydrated media (approximately one third less). This suggests that the 30% hydration mark for media is the point at which surface roughness trends on Ti-6Al-4V change due to shear stress contact limits being crossed.
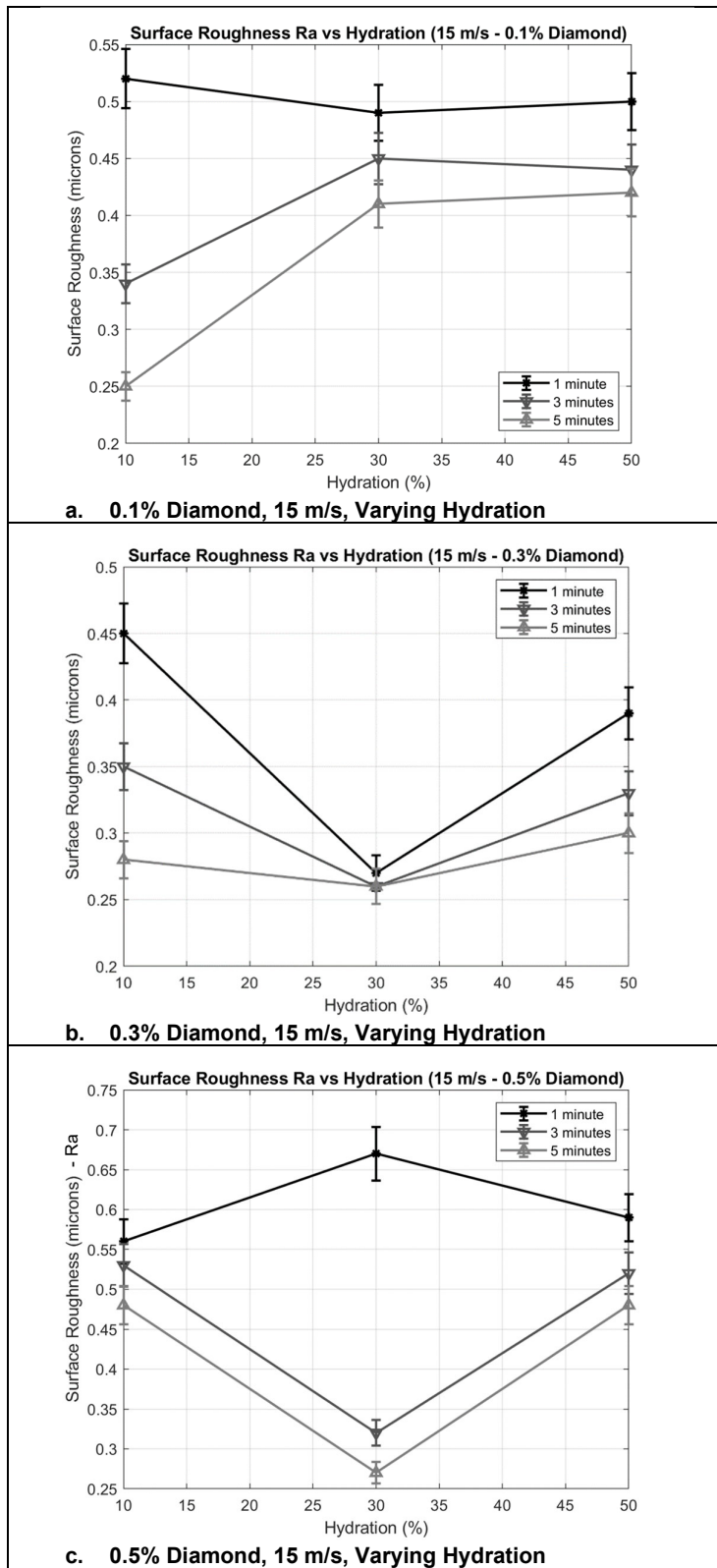
a. 0.1% Diamond, 15 m/s, Varying Hydration

b. 0.3% Diamond, 15 m/s, Varying Hydration

c. 0.5% Diamond, 15 m/s, Varying Hydration

Figure 78 - 15 m/s Ra Changes Over Hydration

Figure 79 suggests the same observations as previously stated for Figure 77 and Figure 78, with no trends apparent in the changing of hydrational levels. A lack of observable trends in the results may be in part due to the short observational times, which mean that the convergence value of Ra is not reached. Comparing the 10% hydration results to the 30% and 50% results is also difficult as Ra measurements for 10% were taken at different times to that of the 30% and 50%, meaning that Ra values needed to be inferred for direct comparison. Again, the inflection point at 30% is noted.


a. 0.1% Diamond, 6.28 m/s, Varying Hydration

b. 0.3% Diamond, 6.28 m/s, Varying Hydration
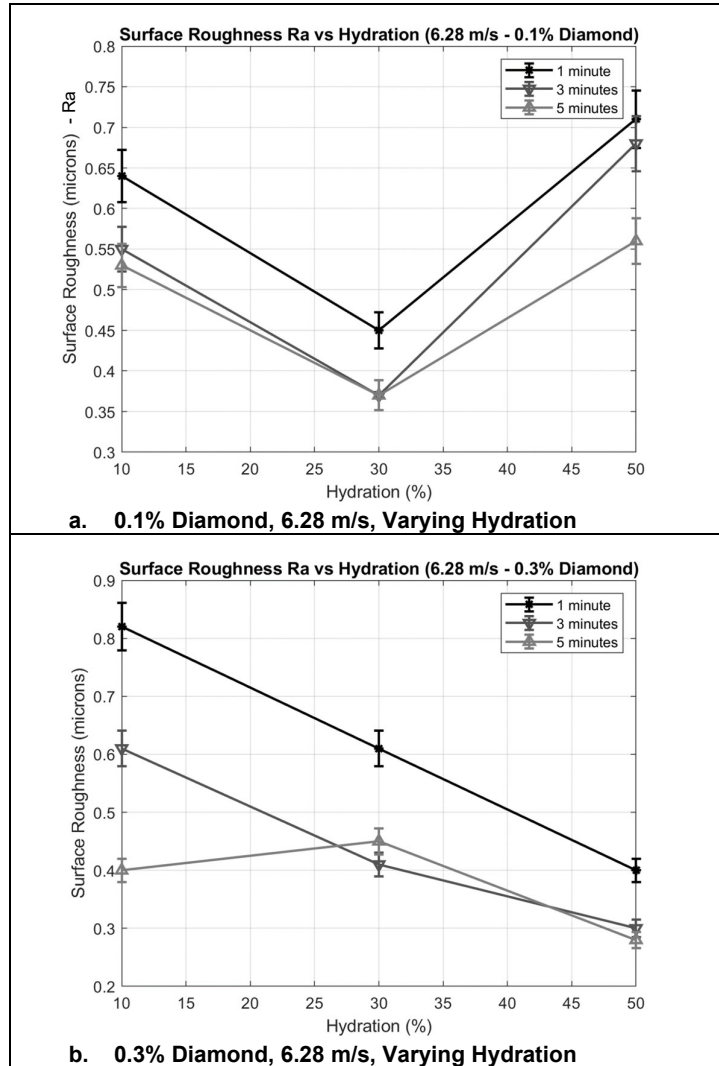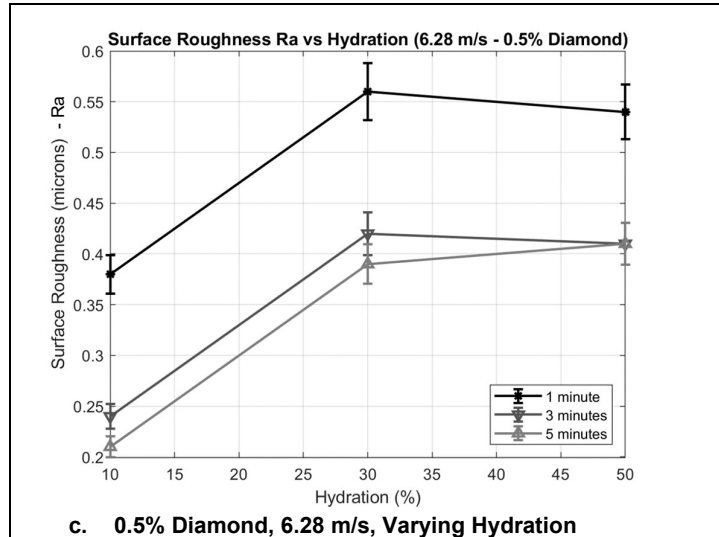
Figure 79 - 6.28 m/s Ra Changes Over Hydration

8.1.3. Impinging Velocity Influence

For the most part, the effect of impinging velocity is highly noticeable, with greater impinging velocities resulting in larger material removal rates (particularly over the first ten minutes of polishing) and a lower overall surface roughness (finer surface). Although some results may not be adequately described below due to different starting surface roughness, higher impinging velocities almost certainly lead to much greater overall reductions in surface roughness. These observations agree with the previous statement in this dissertation: "Investigations into impinging velocities have shown that stronger abrasive action on the workpiece surface occurs at higher velocities [6]."
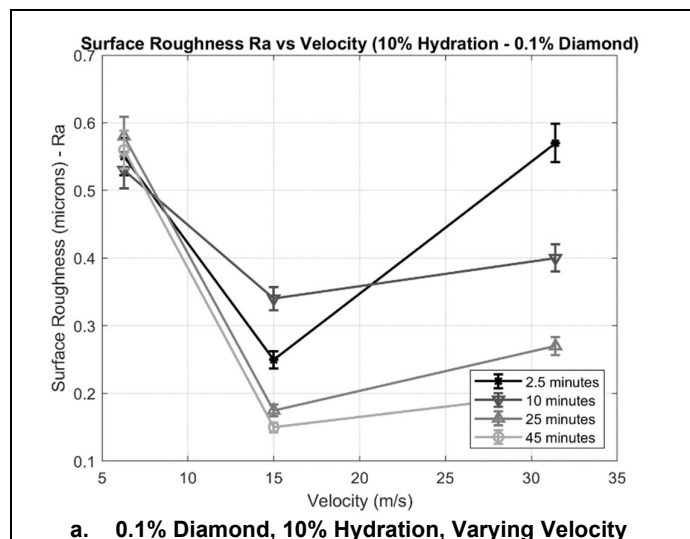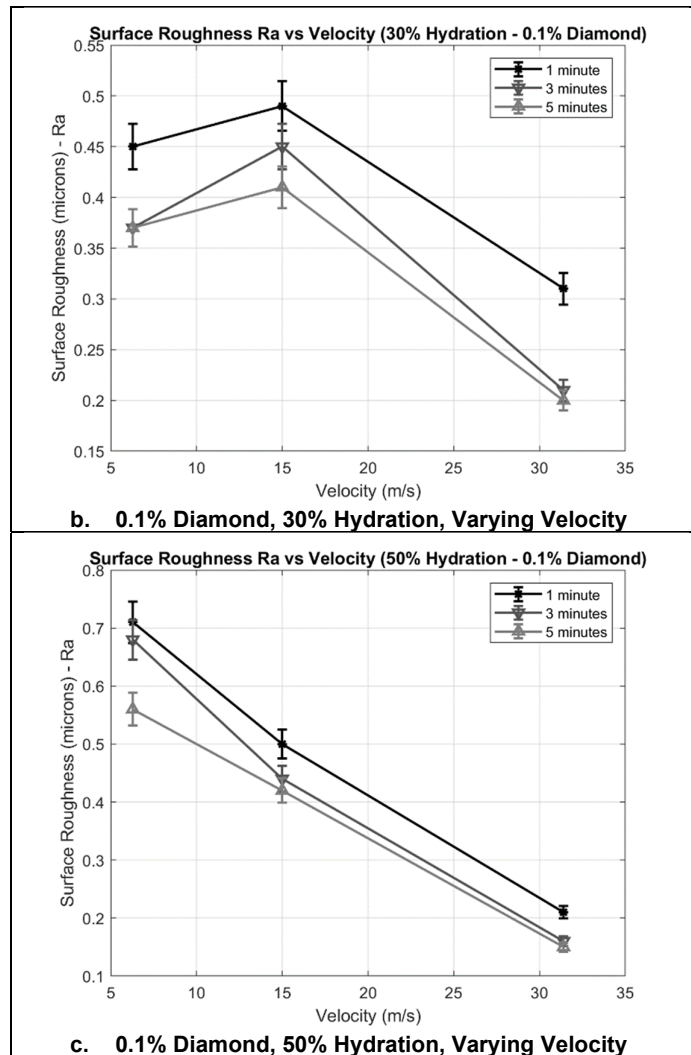
Figure 80 - 0.1% Diamond Ra Changes Over Velocity

Figure 80 shows that higher impinging velocities lead to lower surface roughness and that higher hydrational levels tend to aid in achieving even lower values of Ra. *Figure 81* displays a similar trend with the notable outlier of *Figure 81*b which can be attributed to the much lower initial surface roughness of the 6.28 m/s sample (see *Figure 73*b).
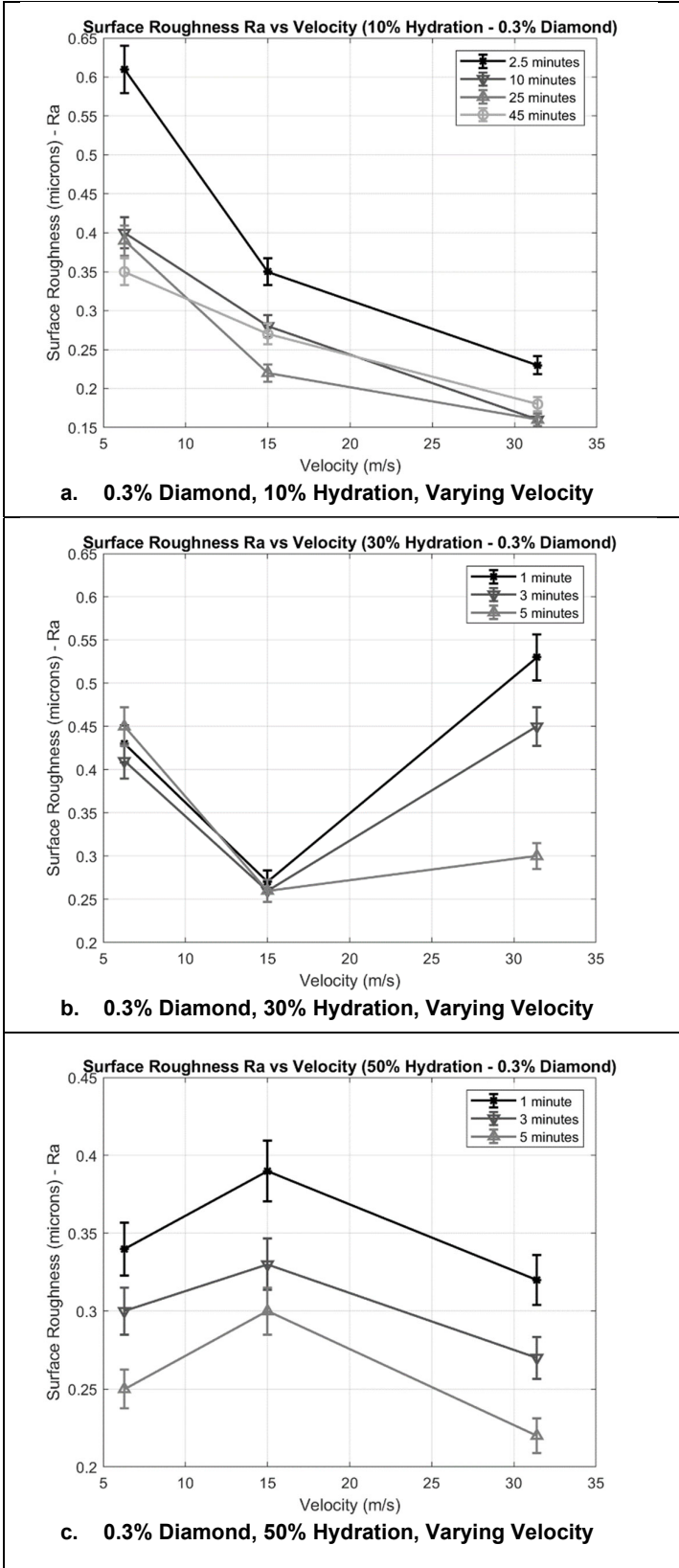
a. 0.3% Diamond, 10% Hydration, Varying Velocity

b. 0.3% Diamond, 30% Hydration, Varying Velocity

c. 0.3% Diamond, 50% Hydration, Varying Velocity
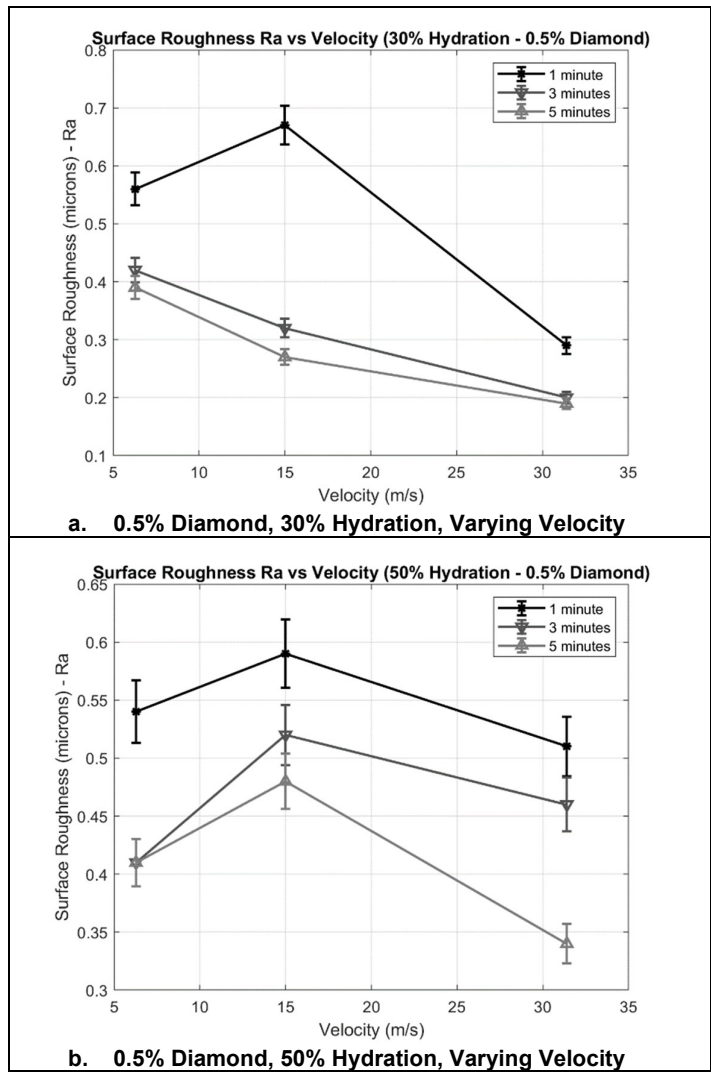
Figure 81 - 0.3% Diamond Ra Changes Over Velocity

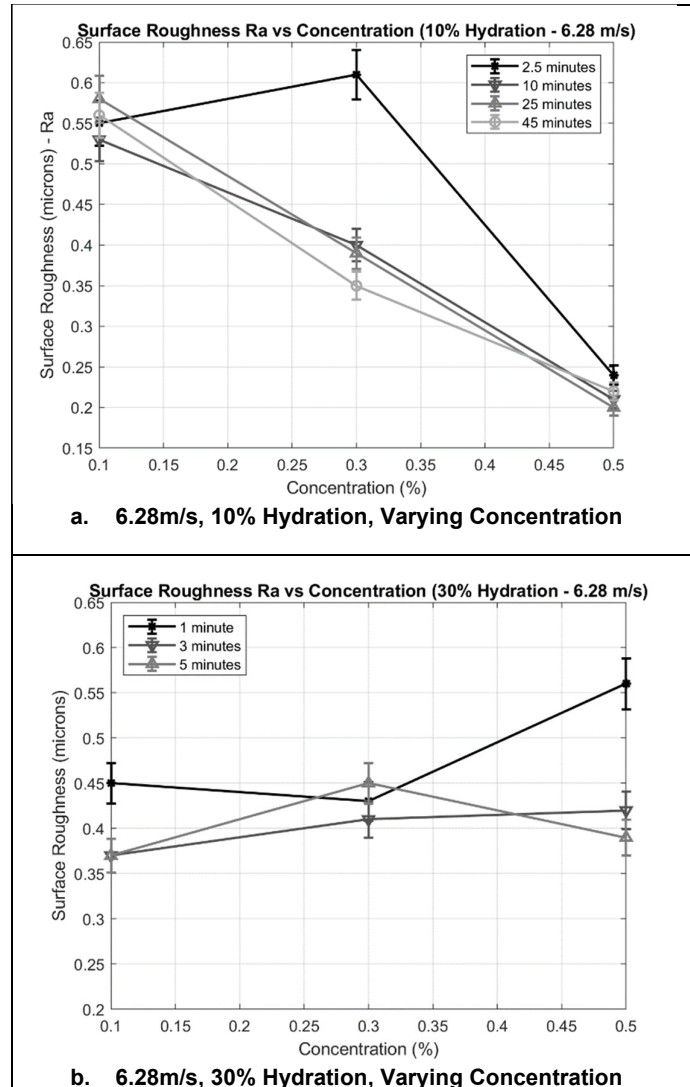*Figure 82 - 0.5% Diamond Ra Changes Over Velocity*

Figure 82 aids in the confirmation that higher impinging velocities lead to lower values of Ra.

8.1.4. Diamond Concentration Influence

Diamond concentration results show interesting trends in relation to impinging velocity and time. At lower impinging velocities, higher diamond concentrations lead to lower surface roughness while at higher impinging velocities, higher diamond concentrations lead to a higher surface roughness. It is postulated that at higher impinging velocities and higher diamond concentrations, too many micro-interactions between diamond abrasive and workpiece asperity are occurring due to large media deformations (thus many particles are forced into the surface to create a rougher surface). A nonaligned hitting angle may be occurring (i.e., the 45-degree polishing angle is no longer maintained for all diamond particles) and thus asperities may be pushed up rather than folded over. At lower impinging velocities, the deformation is much less and the greater diamond content may be leading to a larger contact

of abrasives with the workpiece, allowing for more contacts to occur with causing misaligned contact between the workpiece and media particles.

Figure 83 below shows that at 6.28 m/s (a low impinging velocity) surface roughness may decrease with increased diamond concentrations while an increase in hydration may change this (due to larger deformation and possible misaligned hitting).
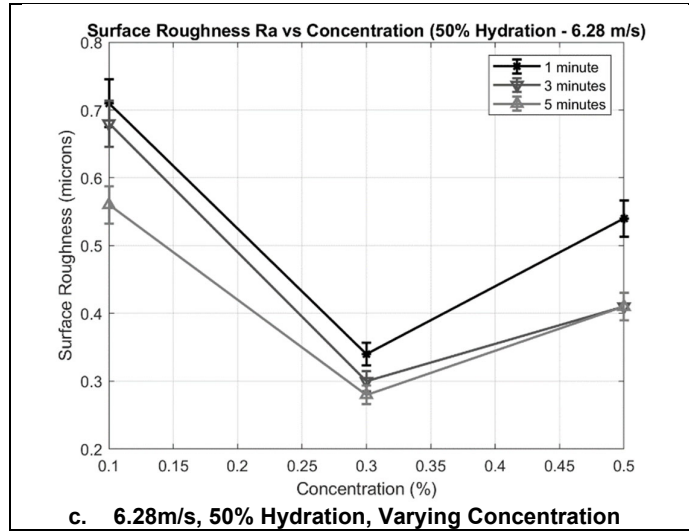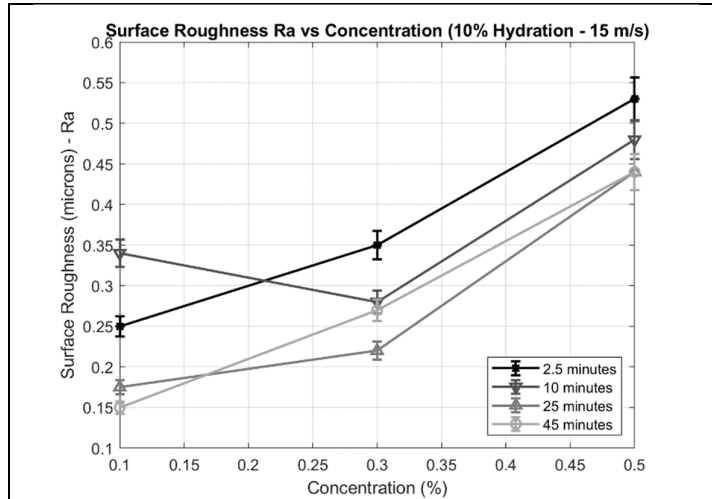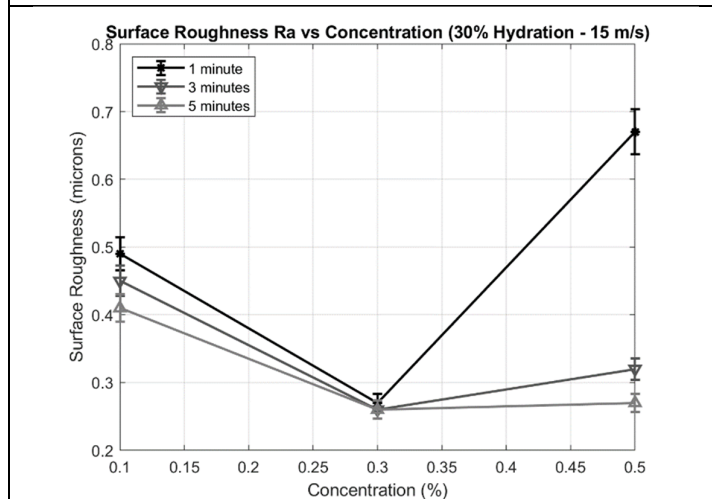

a.   6.28m/s, 10% Hydration, Varying Concentration

b.   6.28m/s, 30% Hydration, Varying Concentration

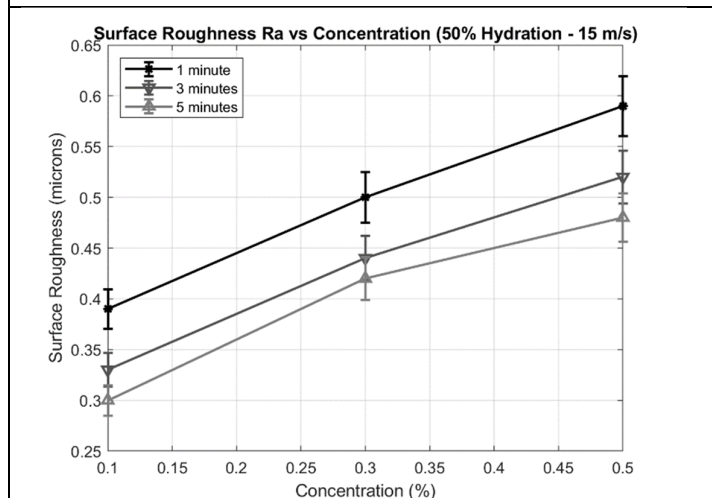*Figure 83 - 6.28 m/s Ra Changes (varying concentration)*

Figure 84 and Figure 85 both imply that higher diamond concentrations at higher conditions of impinging velocity (15 m/s and 31.4 m/s) result in greater surface roughness overall with the exception of Figure 85b where the starting roughness of the 0.5% diamond concentration sample was lower than that of the 0.3% sample.

Figure 84 - 15 m/s Ra changes (varying concentration)

a.   31.4m/s, 10% Hydration, Varying Concentration

b.   31.4m/s, 30% Hydration, Varying Concentration

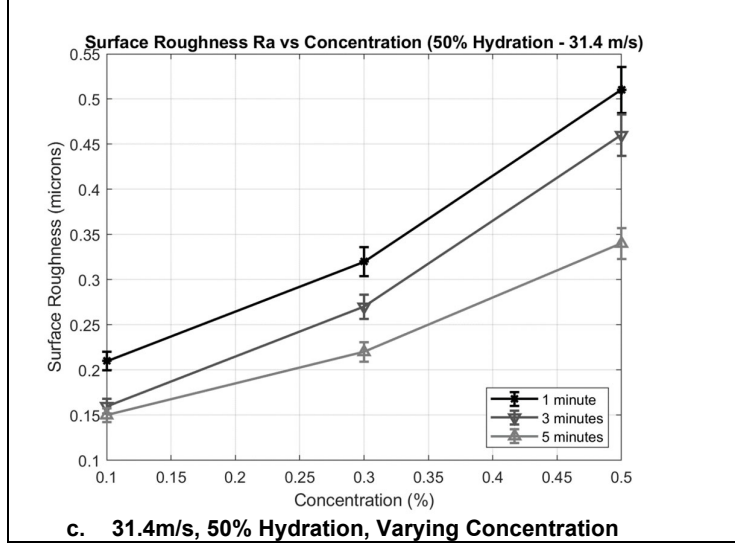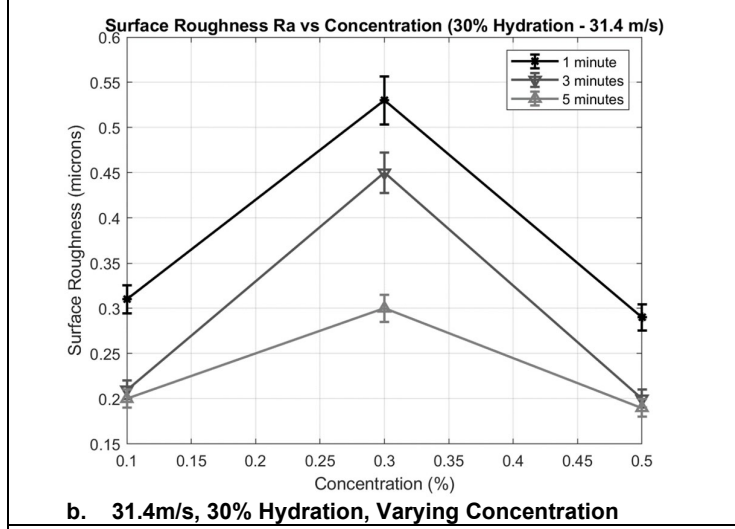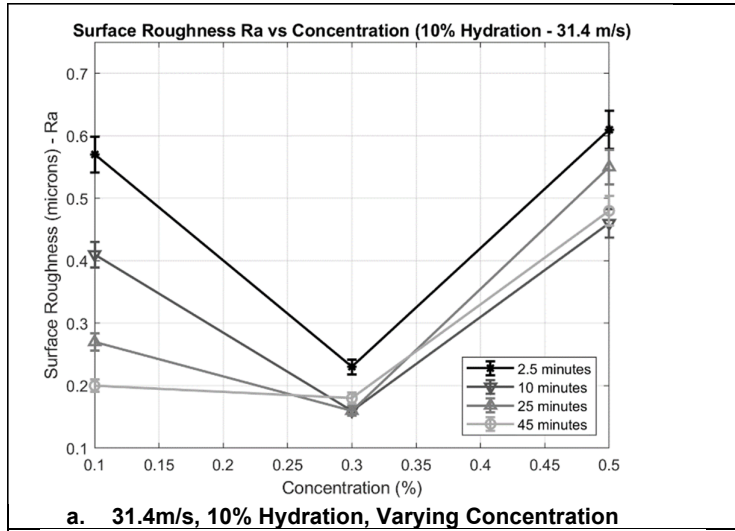**c.   31.4m/s, 50% Hydration, Varying Concentration**

Figure 85 - 31.4 m/s Ra changes (varying concentration)

8.2. Surface Analysis – Texture, Topography, Quality

SEM images are used to present the results of polishing factors on the surface of Ti-6Al-4V samples (under the experimental conditions stipulated in the previous chapter). All images are presented at 1500 X magnification.

Surface improvement in this context is defined as a less rough surface (heights between peaks and valleys has lessened) as well as a lesser appearance of surface imperfections (notably surface scratches, porosity/pits, micro shoulders, groove height and adherent material) as well as a reduction in brittle failure from grinding (with a preference for smooth deformation caused by ductile regime polishing) and finally a more uniform texture overall. The form should be flatter for an improvement to have taken place.

Figure 86 is a labelled SEM image of an unpolished but surface ground workpiece. In direct comparison to the unfinished sample (see Figure 62 for references), the surface texture has greatly improved but the presence of peaks (asperities) and valleys are certainly present throughout. The form is not entirely flat, and many micro shoulders are present in addition to some observable pits and adherent material. Grooves and striations (striations are more visible on 500 X images) are present too. Brittle fracture and plastic deformation have occurred on this surface due to rubbing and ploughing of the workpiece from the grinding wheel abrasives. Minor scratches are also present on the surface from the grinding action. Directionality of grind is apparent too (i.e. the surface lay appears horizontal initially).
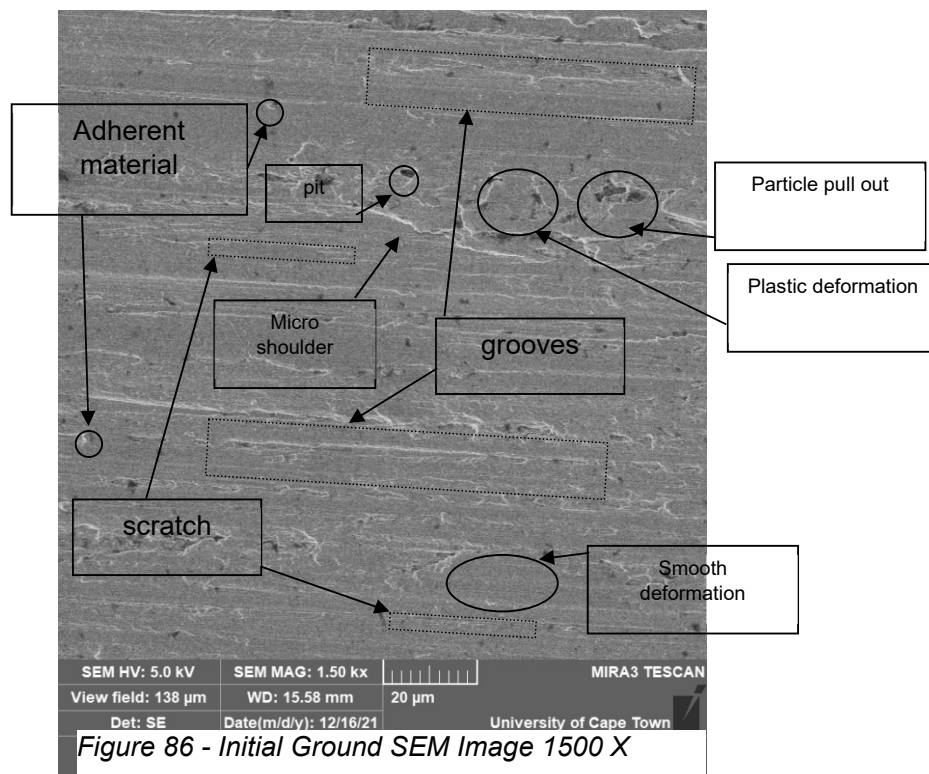

Figure 86 - Initial Ground SEM Image 1500 X

Table 17 - Key to Labelling of SEM Image Results
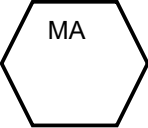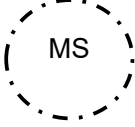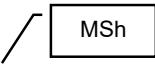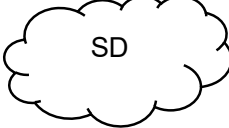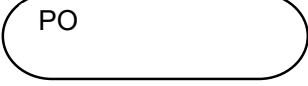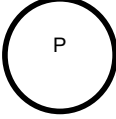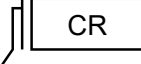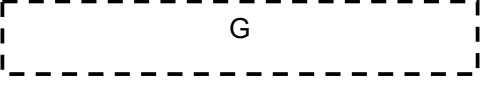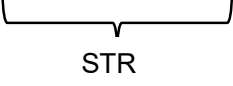
Material Adherence	MA
Micro Scratches	MS
Micro Shoulder	MSh
Plastic Deformation	PD
Smooth Deformation	SD
Particle Pull Out	PO
Pit	P
Crack	CR
Groove	G
Striation	STR

Table 17 provides a key to the labelling of features found on the SEM images to follow. A description of these features (and why/how they occur) has been provided previously throughout various sections. Note that two of the first figures have been provided with captions to allow for a description of how results are to be presented.

8.2.1. Polishing Time Influence

The results in this sub-chapter are displayed in order of increasing time intervals to display the effects of polishing time on surface features. As the higher hydration media could not be used for longer than 5 minutes per experiment, many of the displayed results below are at the condition of 10% hydration (where polishing occurred for 45 minutes). However, higher hydrated media did show workpiece surface texture improvement after between 3 and 5 minutes. Results that display this clearly are included and analysed in the following pages.

Figure 87 shows the change of surface over 45 minutes for conditions of 0.1% diamond concentration, 10% hydration and 31.4 m/s impinging velocity. A clear improvement in surface quality is noted over time with surface inclusions, pores and imperfections decreasing in quantity and a flatter form becoming more apparent. The presence of adherent material at 2.5 minutes is noted throughout the surface and the quantity and size of the adhered material decreases heavily with time, with no visible adherent material at the 45-minute mark. At this low hydration, the presence of micro-scratches over the scan area increases significantly as noted in Figure 87. The height of micro shoulders decreases over time and less particle pull out is present on the surface (with more smooth deformation present over time). This set of results implies that high polishing time and high impinging velocity aids in creating a smoother surface with a lesser quantity of adherent material and undesired grinding features e.g. deep grooves and large micro shoulders.

a. 2.5 minutes | b. 10 minutes

c. 25 minutes   d. 45 minutes

0.1% Diamond Concentration, 10% Water, 31.4 m/s impinging velocity, 1500x magnification
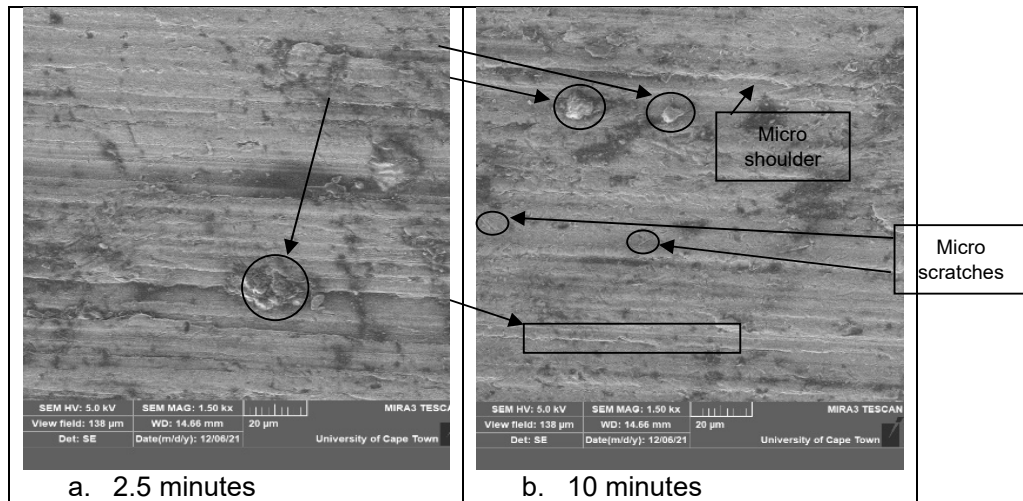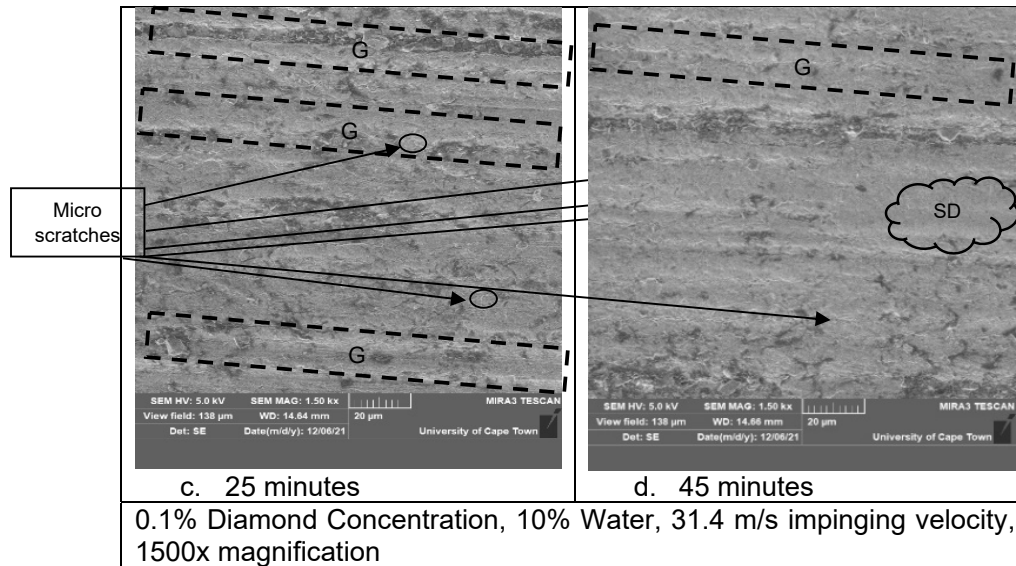
Figure 87 - 0.1%D, 10%H, 31.4 m/s, 1500 X SEM Images

Although results are presented over the course of a much shorter time interval (300 seconds instead of 45 minutes), improvements can be seen when a media hydration of 50% has been utilized. The initial surface had a large presence of micro-scratches over its area and this has been greatly reduced over time. The size and number of pits have also decreased. However, over this short period, the height/depths of grooves have not decreased significantly and micro shoulders are still present. Smooth deformation is also present in the 300 second image, while the 60 second image which does not exhibit signs of surface deformation due to polishing.

a. 60 seconds   b. 180 seconds   c. 300 seconds

0.1% Diamond Concentration, 50% Water, 31.4 m/s impinging velocity, 1500 X magnification
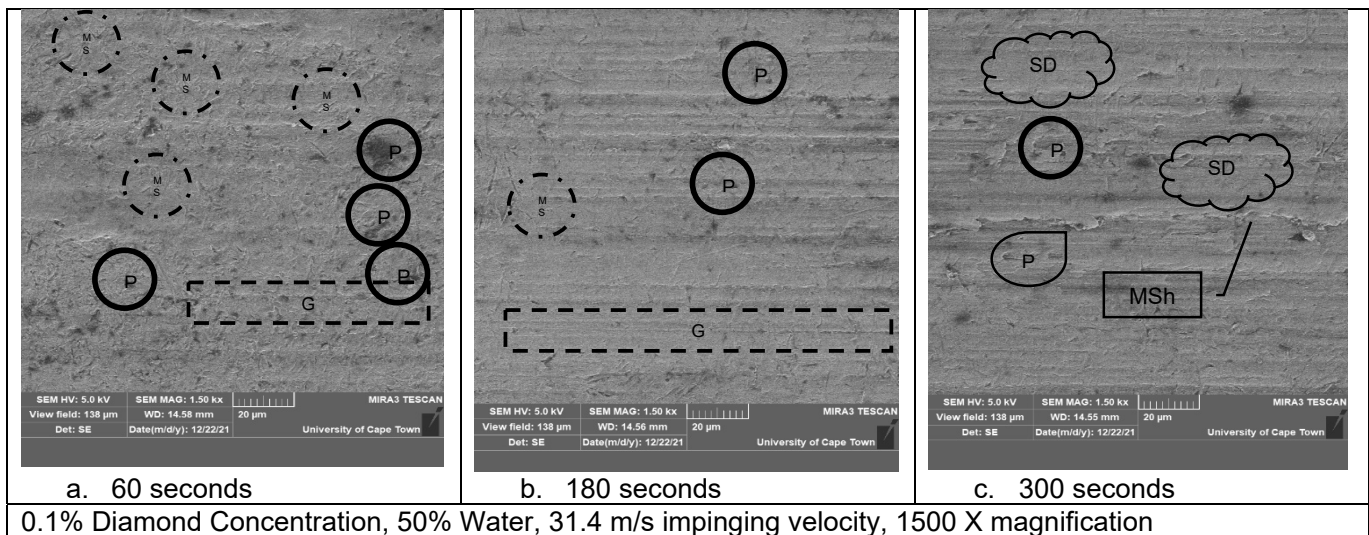
Figure 88 - 0.1%D, 50%H, 31.4 m/s, 1500 X SEM Images

Figure 89 shows results for increased diamond concentration (0.3%) at low hydration (10%) and high impinging velocity (31.4 m/s). The flattening in form overall is apparent, with asperity peaks and valleys much closer together at the 45-minute mark than at the 2.5 minute mark. An important note is that impurities, material adherence and pits have decreased greatly in

quantity and size over time, with no material adherence visible in the 45 minute image. The overall texture appears to be more uniform over time with a lesser overall roughness (contrast has decreased). The disappearance of undesired grinding features over time is noted (particularly that of exaggerated grooves). The presence of micro surface scratches due to the polishing media abrasives increases heavily over time. It is noted that there is a greater presence of scratch marks for the 0.3% diamond concentration results than for the 0.1% diamond concentration results. Surface lay appears to remain horizontal over time. Micro shoulder height decreases significantly over time, and these appear to be flattening toward the mean roughness height. The presence and height/depth of grinding grooves decreases over time.

a. 2.5 minutes   b. 10 minutes

c. 25 minutes   d. 45 minutes

0.3% Diamond Concentration, 10% Water, 31.4 m/s impinging velocity, 1500 X magnification

Figure 89 - 0.3%D, 10%H, 31.4 m/s, 1500 X SEM Images

a. 60 seconds   b. 180 seconds   c. 300 seconds

0.3% Diamond Concentration, 30% Water, 31.4 m/s impinging velocity, 1500 X magnification
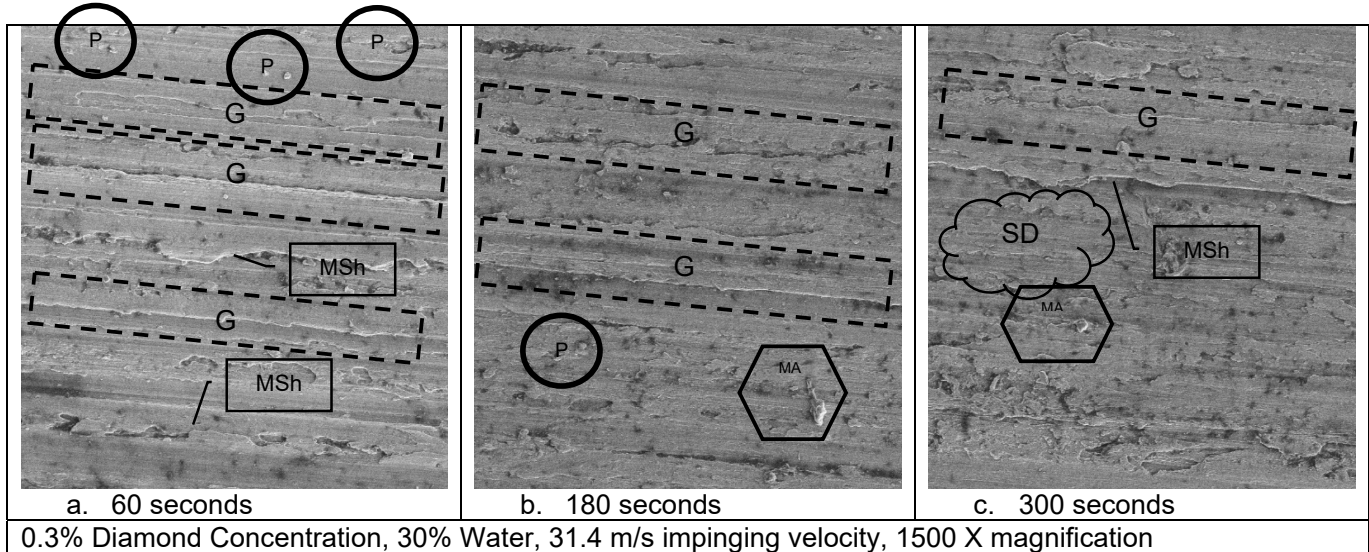
Figure 90 - 0.3%D, 30%H, 31.4 m/s, 1500 X SEM Images

Figure 90 results are under similar conditions to those of Figure 89 with similar polishing conditions (with the only change being that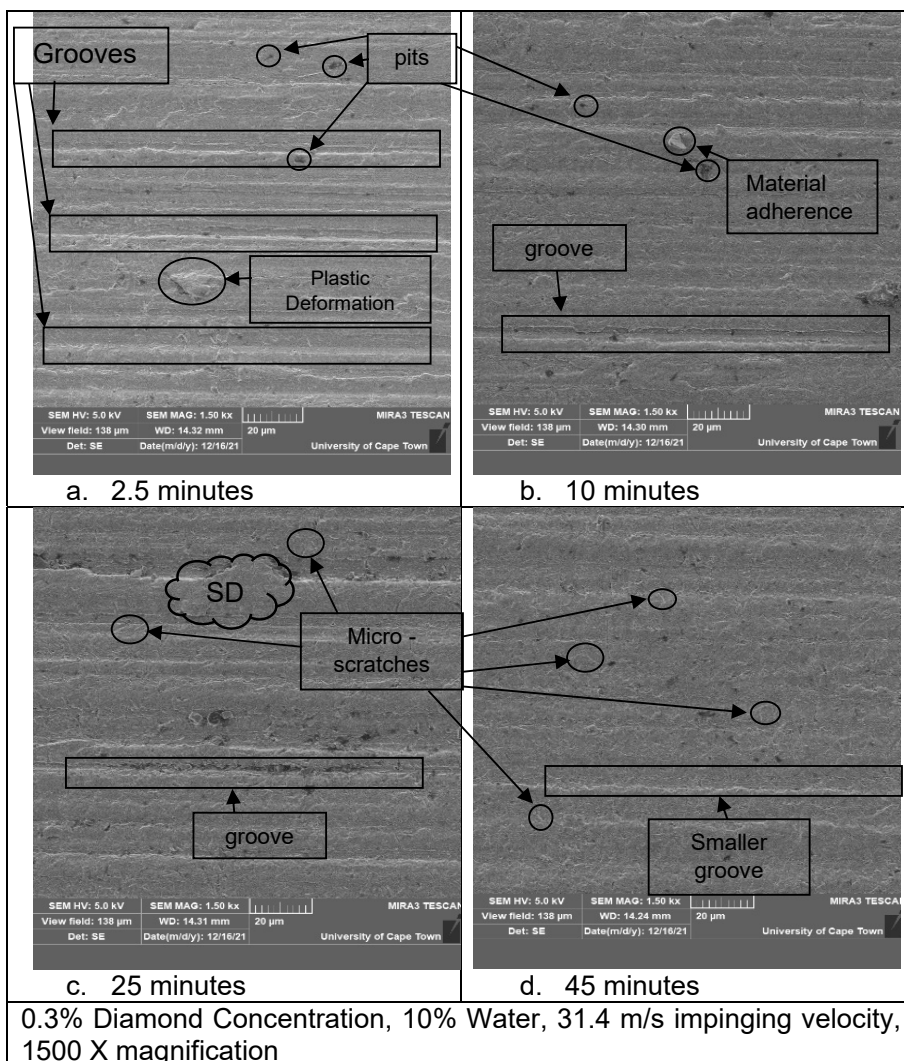 of increased hydration – from 10% to 30% and the much lower time interval). It is noted that micro scratches do not develop over time. In the previous results in Figure 89, scratches begun to appear at 2.5 minutes. Form has flattened, and roughness height has decreased significantly after 300 seconds. The texture also appears much smoother and more uniform. Over time the presence and height/depth of grooves decreases significantly, and this suggests that over a longer period of time, grooves may begin to disappear due to the polishing action. Micro-shoulders are still present at the 300 second mark. As previously, pit size decreases in size and quantity over time.

Figure 91 displays similar results to Figure 89 in terms of surface change over time. Adherent material is not present at all on the surface of the 45-minute image, while micro-scratches due to polishing abrasives have increased. Smooth deformation presence increases over time (implying that ductile regime polishing has indeed occurred). Groove heights/depths become much smaller over time and micro-shoulders look to have been eliminated. The unwanted surface features from grinding (notably particle pull out in this case) have been removed and the surface texture appears more uniform over time. Heights of valleys and peaks have decreased in time, implying a lower overall surface roughness.

a. 2.5 minutes	b. 10 minutes
c. 25 minutes	d. 45 minutes

0.5% Diamond Concentration, 10% Water, 31.4 m/s impinging velocity, 1500 X magnification
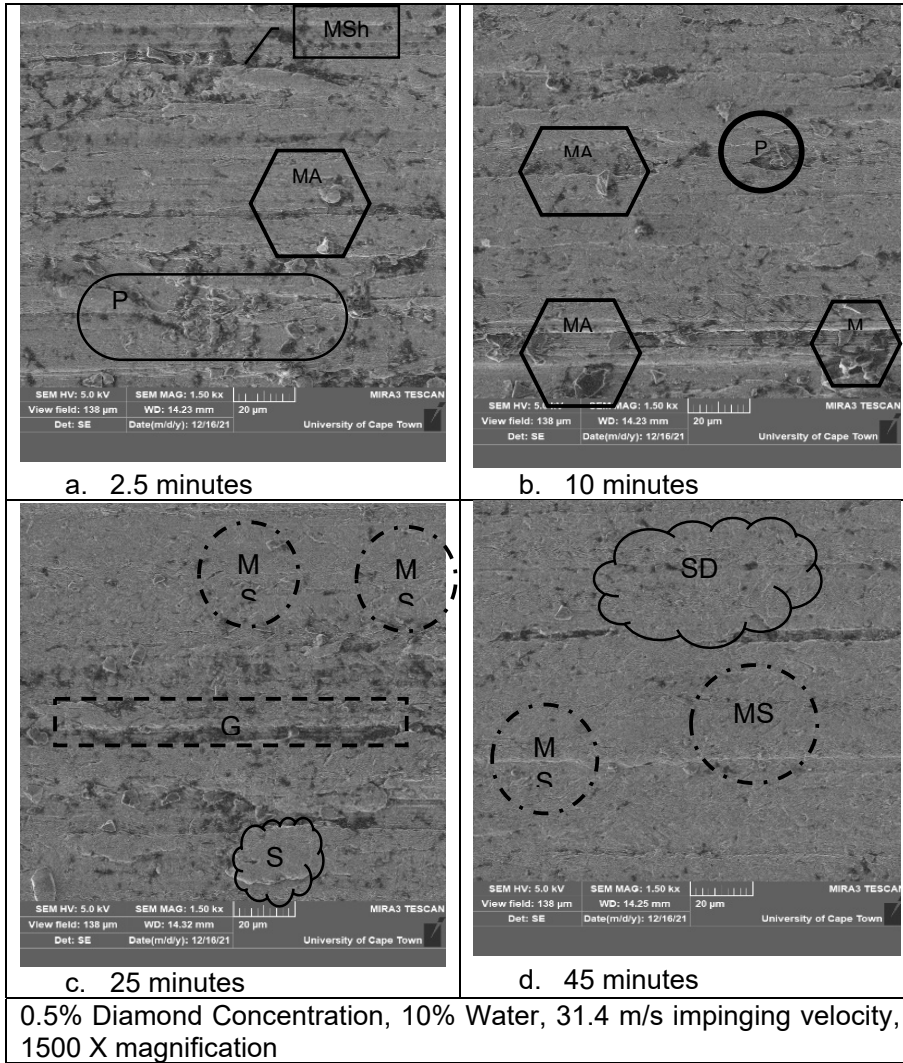
Figure 91 - 0.5%D, 10%H, 31.4 m/s, 1500 X SEM Images

Figure 92 shows a great improvement in surface roughness and form as well as uniformity of surface texture and removal of imperfections, lessening the depth of pores. The height/depth of grooves is decreased significantly over time and material adherence once again seems to be removed over time. However, at the low hydrational level, the presence of scratch marks due to abrasive (mostly dry) polishing increases significantly with time. At this lower velocity, removal of impurities and decreasing the height of grooves, micro shoulders and minimizing pit size and appearance appears to take a longer time (as expected due to the lower kinetic energy and removal force).

a. 2.5 minutes	b. 10 minutes
c. 25 minutes	d. 45 minutes

0.1% Diamond Concentration, 10% Water, 15 m/s impinging velocity, 1500 X magnification
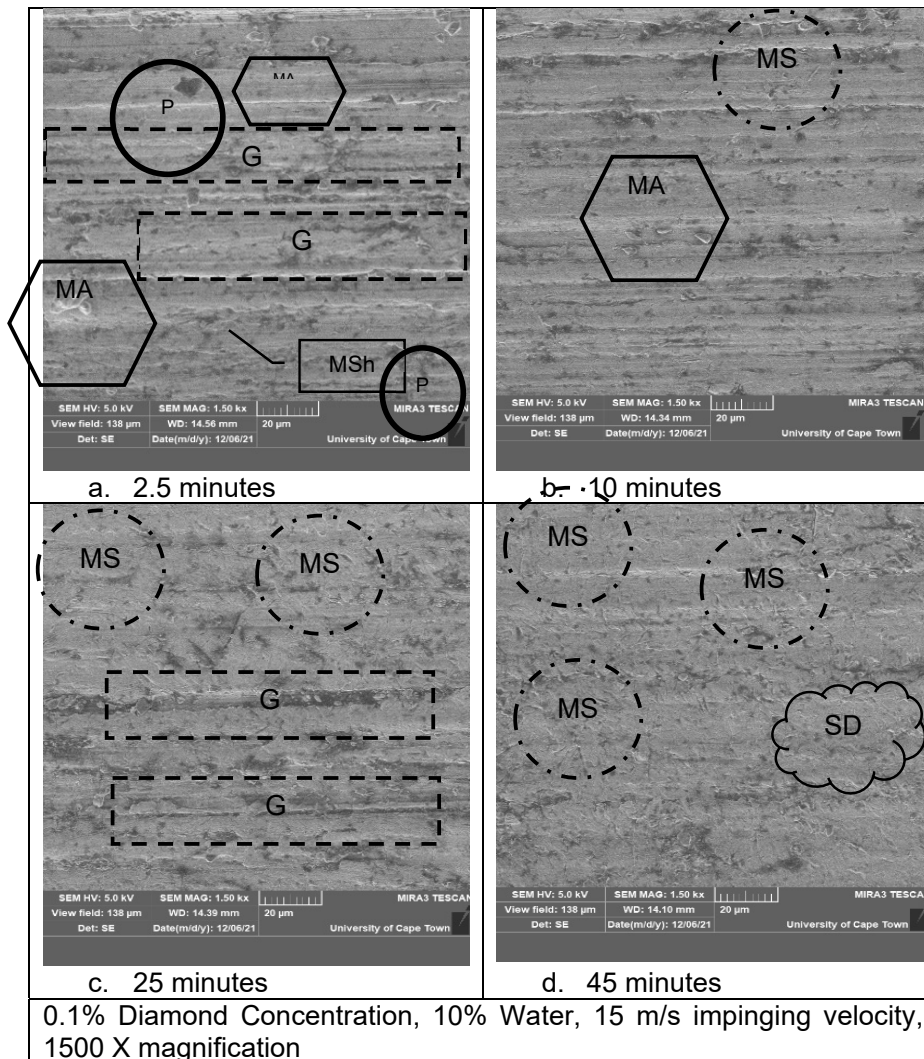
Figure 92 - 0.1%D, 10%H, 15 m/s, 1500x SEM Images

Results for 0.5% diamond concentration at 10% hydration and 15 m/s impinging velocity over 45 minutes are shown in Figure 93. As previously, micro-scratches increase over time when media hydration is low, while adhered material is removed, and smooth deformation and plastic deformation takes over that of brittle failure and particle pull out. Grooves tend to decrease in height/depth while the surface texture appears more uniform over time. Providing sufficient polishing time, even at this lower velocity, appears to allow desired polishing effects to occur.

a. 2.5 minutes	b. 10 minutes
c. 25 minutes	d. 45 minutes

0.5% Diamond Concentration, 10% Water, 15 m/s impinging velocity, 1500 X magnification
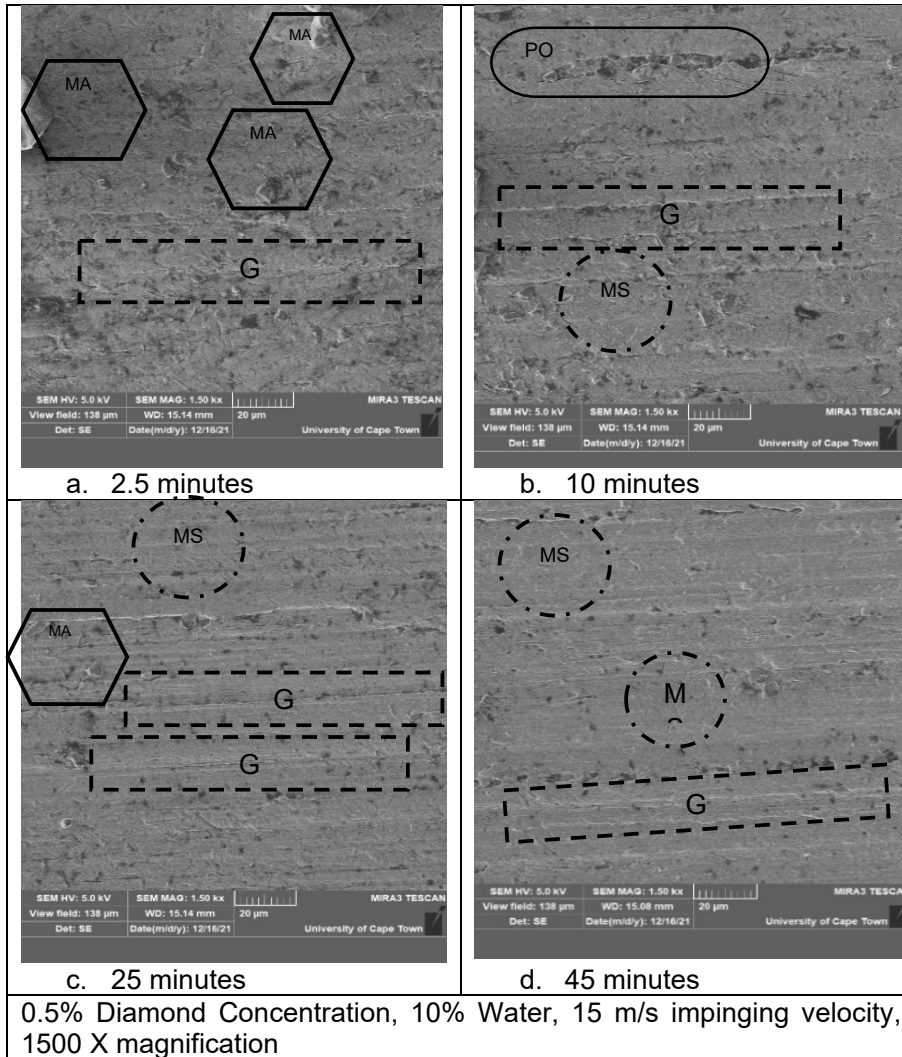
Figure 93 - 0.5%D, 10%H, 15 m/s, 1500 X SEM Images

| a. 60 seconds | b. 180 seconds | c. 300 seconds |

0.5% Diamond Concentration, 30% Water, 15 m/s impinging velocity, 1500x magnification
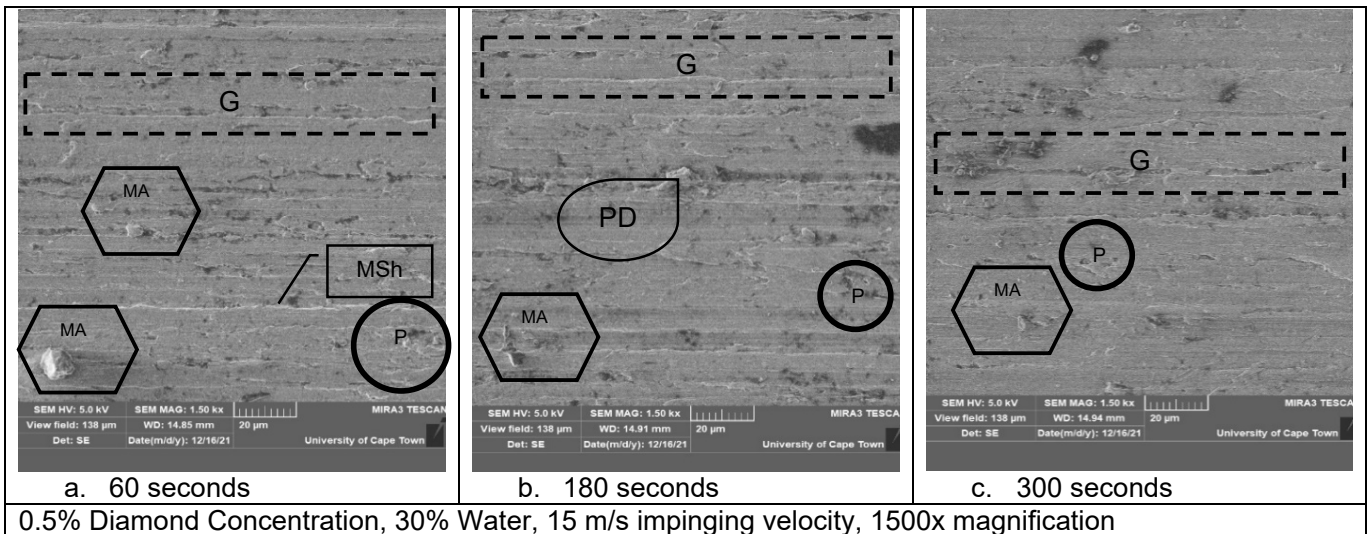
Figure 94 - 0.5%D, 30%H, 15 m/s, 1500 X SEM Images

Figure 94 shows results for a 0.5% diamond concentration at a 30% water content at a lower impinging velocity of 15 m/s. Note that adhered material is not fully removed after the 300 seconds of polishing, but the adhered material has significantly reduced in size. Micro-shoulders have reduced significantly in size and the overall texture appears more uniform. Pit size has certainly decreased over time and gap heights/depths become smaller over time too. It is important to note that micro scratches are not present on the surface of any of the images (due to the hydrational effects of polishing). To completely remove adhered material and remove pit presence/minimize size, a larger polishing time would be required but even the short 300 seconds shows that polishing time is an important parameter in the Flexolap polishing process.

Figure 95 shows a low velocity (6.28 m/s), low diamond concentration (0.1%) and low hydration (10%) set of results. At this low velocity, the appearance of micro-scratches does not appear, however surface texture is not noticeably changed with only small improvements. This includes a slightly lesser presence and size of material adherence with slightly smaller heights/depths in surface grooves. Micro-shoulders have not been eliminated though.

a. 2.5 minutes   b. 10 minutes   c. 25 minutes   d. 45 minutes

0.1% Diamond Concentration, 10% Water, 6.28 m/s impinging velocity, 1500 X magnification
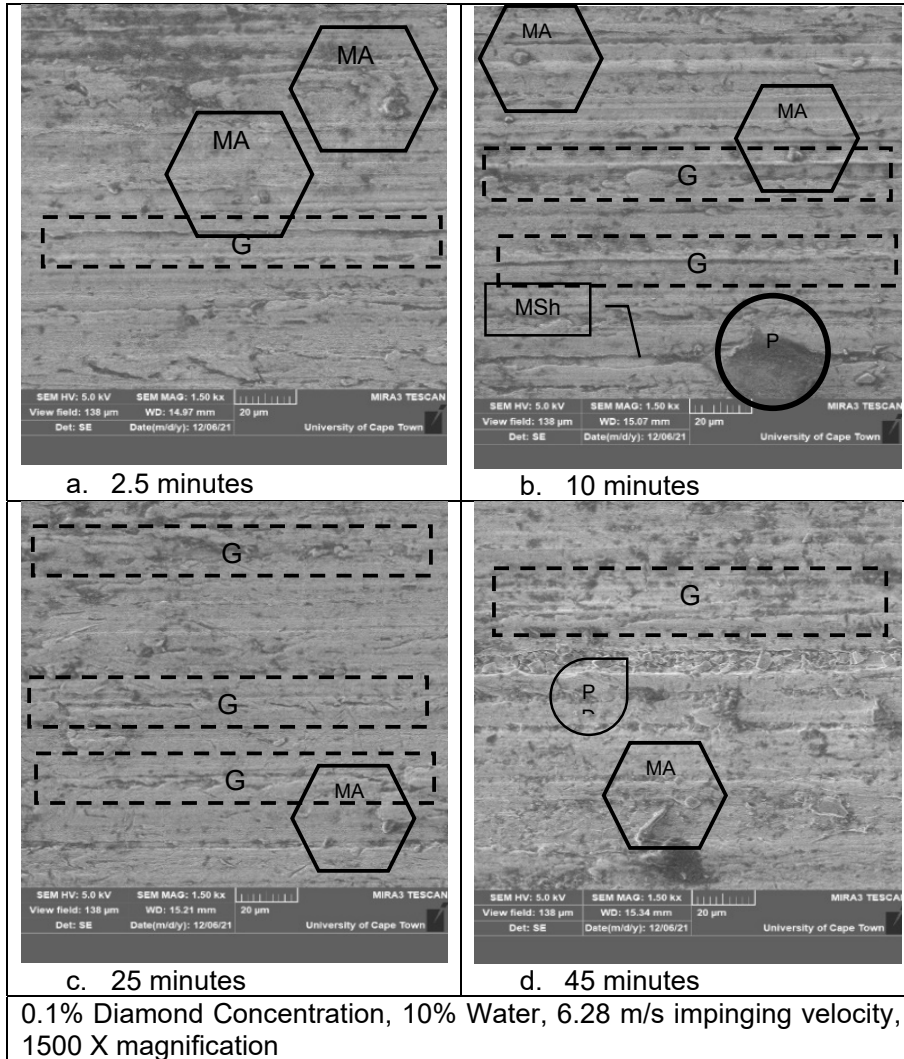
Figure 95 - 0.1%D, 10%H, 6.28 m/s, 1500 X SEM Images

a. 60 seconds   b. 180 seconds   c. 300 seconds

0.1% Diamond Concentration, 30% Water, 6.28 m/s impinging velocity, 1500 X magnification
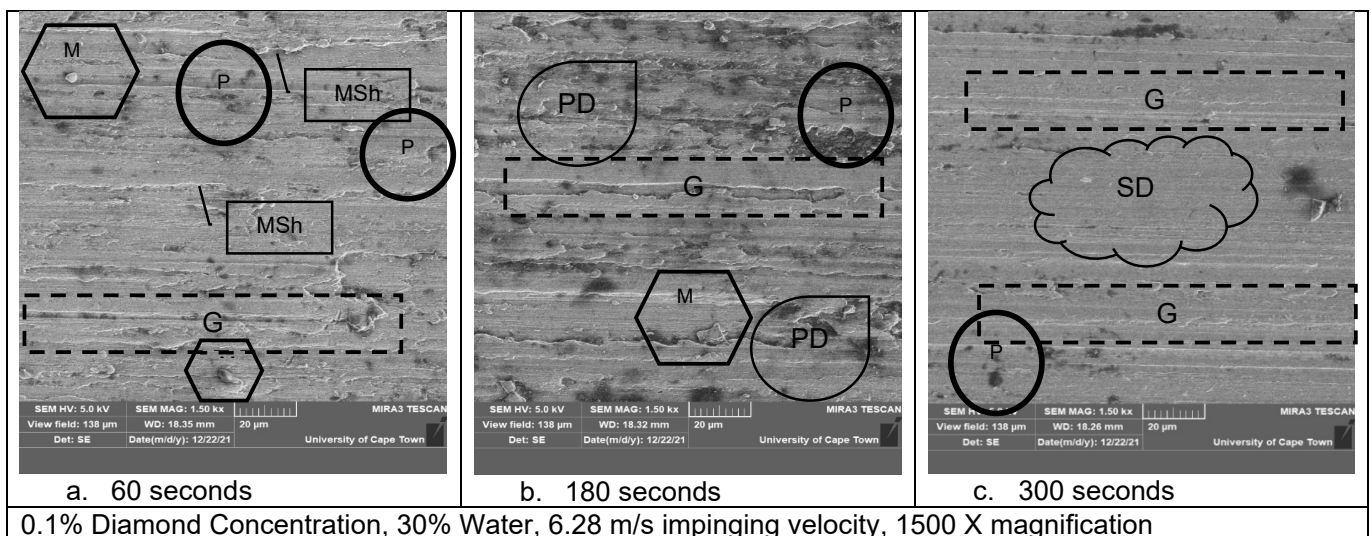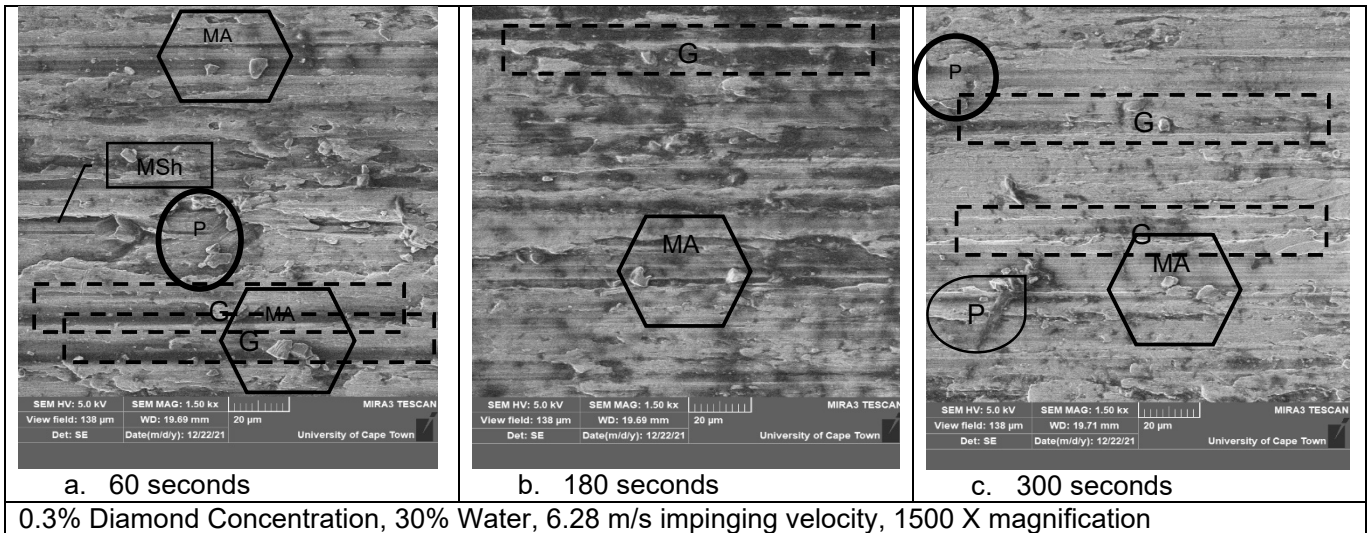
Figure 96 - 0.1%D, 30%H, 6.28 m/s, 1500 X SEM Images

In contrast to the previous set of results shown in Figure 95, an improvement in surface uniformity as well as a lessening in roughness over time is shown in Figure 96. This occurs at lower polishing times (of 300 seconds) and proves that hydration may aid in polishing at low velocities (particularly due to the increase in kinetic energy, which allows ductile regime polishing conditions to occur at lower polishing velocities). Notably, smooth deformation appears after 300 seconds, pit quantity and depth have decreased and micro-shoulders are no longer visible in the 300 second image. Material adherence is also significantly decreased over time and gap height/depths have decreased over time.

The results shown in Figure 97 (for 0.3% diamond concentration, 30% hydration and 6.28 m/s impinging velocity) show similarities to the previous low velocity, higher hydration results. Material adherence quantity is decreased over time and particle pull out is notably decreased over time but none of the features have been eliminated over this short period of time.

a. 60 seconds	b. 180 seconds	c. 300 seconds
0.3% Diamond Concentration, 30% Water, 6.28 m/s impinging velocity, 1500 X magnification

Figure 97 - 0.3%D, 30%H, 6.28 m/s, 1500 X SEM Images

8.2.2. Hydration Influence

The following result shown in Figure 98 (comparing 30% to 50% at a high impinging velocity and low time) show a significant improvement in surface texture at higher hydration, with a flatter form and lower roughness heights for the higher hydrated results and the slight disappearance of horizontal lay at higher hydration. The micro scratches shown in the 50% image are due to the grinding wheel and as is shown in Figure 88, these are eliminated over time. Micro grooves appear to decrease in height/depth over hydration.

a. 30% Hydration	b. 50% Hydration
Impinging Velocity = 31.4 m/s, Diamond Concentration = 0.1%, Time = 1 minute, 1500 X Magnification	
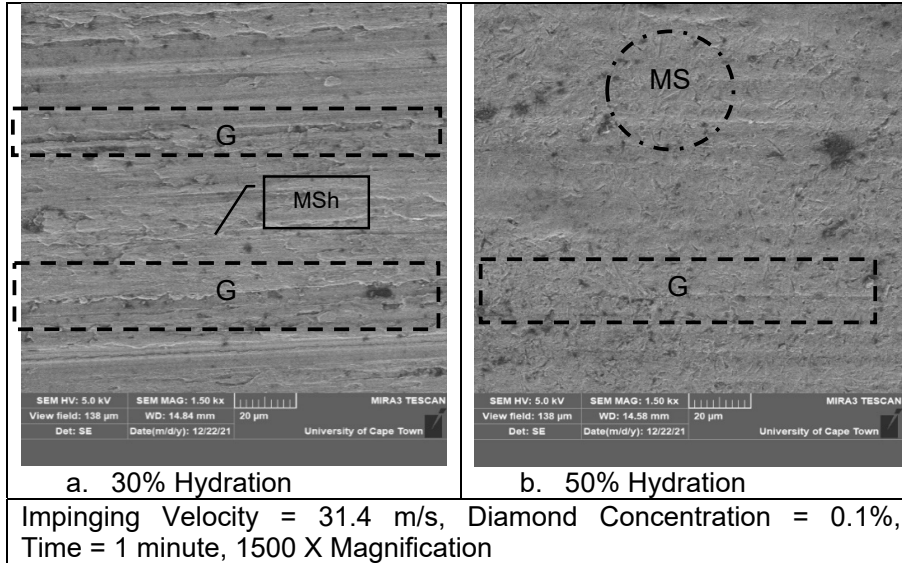
Figure 98 - 0.1%D, 1 minute, 31.4 m/s, 1500 X SEM Images

Figure 99 shows results at 3 minutes for a high impinging velocity at low diamond concentration. Again, higher hydrated media appears to produce a better-quality surface with a more uniform texture. Presence of scratch marks appear to reduce over hydrational increases for all hydrational results displayed. Particle pull out due to grinding has been eliminated at the higher hydrated results but has not been eliminated at the 10% hydration image. The higher hydrated media does not appear to display a presence of micro-shoulders while groove height/depth has decreased over hydrational increases.

| a. 10% Hydration | b. 30% Hydration | c. 50% Hydration |

Impinging Velocity = 31.4 m/s, Diamond Concentration = 0.1%, Time = 3 minutes, 1500 X Magnification

Figure 99 - 0.1%D, 3 minutes, 31.4 m/s, 1500 X SEM Images

At the higher time frame (5 minutes), higher hydration results in Figure 100 show surface improvement that seems to be much greater than that of the lower hydration results. Uniformity is much improved while micro-shoulder presence is decreased (although height is not decreased) and pits and material adherence appear much lower in presence and size at the higher hydration. Grooves are not notably different in size and presence between the two hydrations though.

| a. 10% Hydration | b. 50% Hydration |

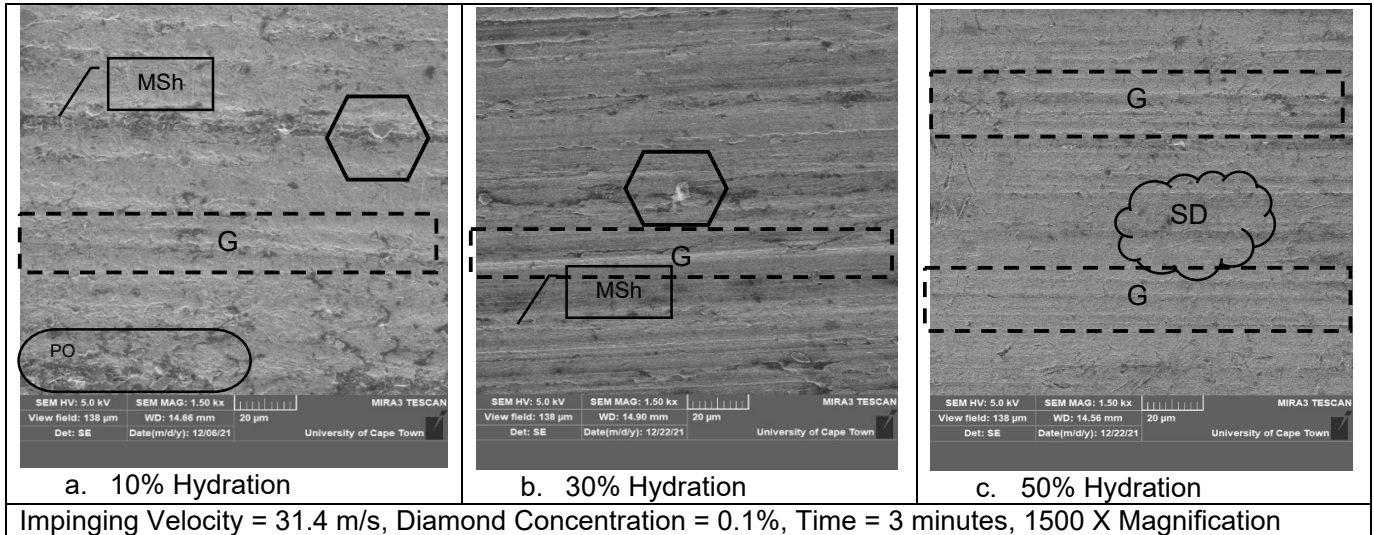Impinging Velocity = 31.4 m/s, Diamond Concentration = 0.1%, Time = 5 minutes, 1500 X Mag
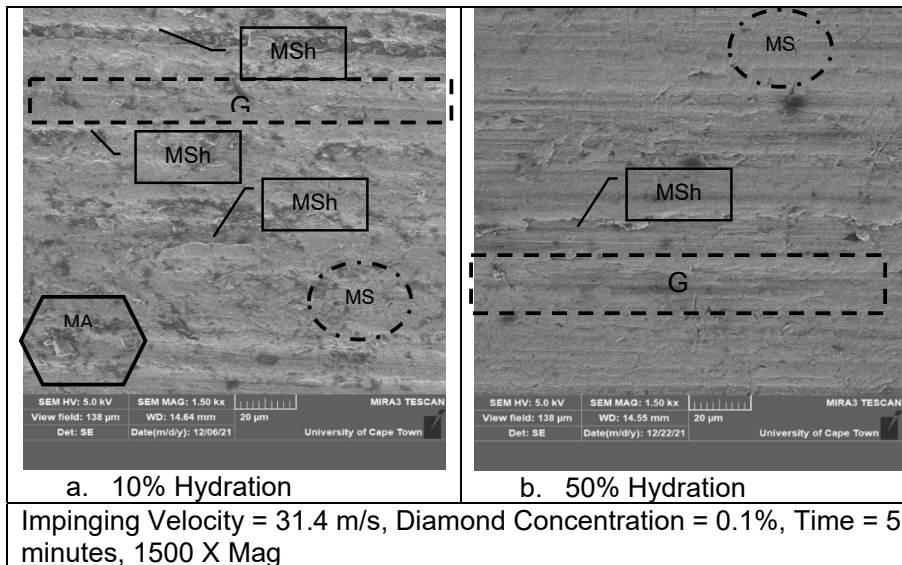
Figure 100 - 0.1%D, 5 minutes, 31.4 m/s, 1500 X SEM Images

Figure 101 shows results for a high diamond concentration (0.5%) at 3 minutes and an impinging velocity of 31.4 m/s. Plastic deformation and particle pull out (from surface grinding) is still present at the lower hydration and material adherence is larger in size at the lower hydration than at the higher hydration of 50%. The high hydrational image shows smooth deformation and no presence of plastic deformation. The 30% hydration image

shows a large presence of micro shoulders and pits and texture does not appear better than that of the 10% hydrational image.
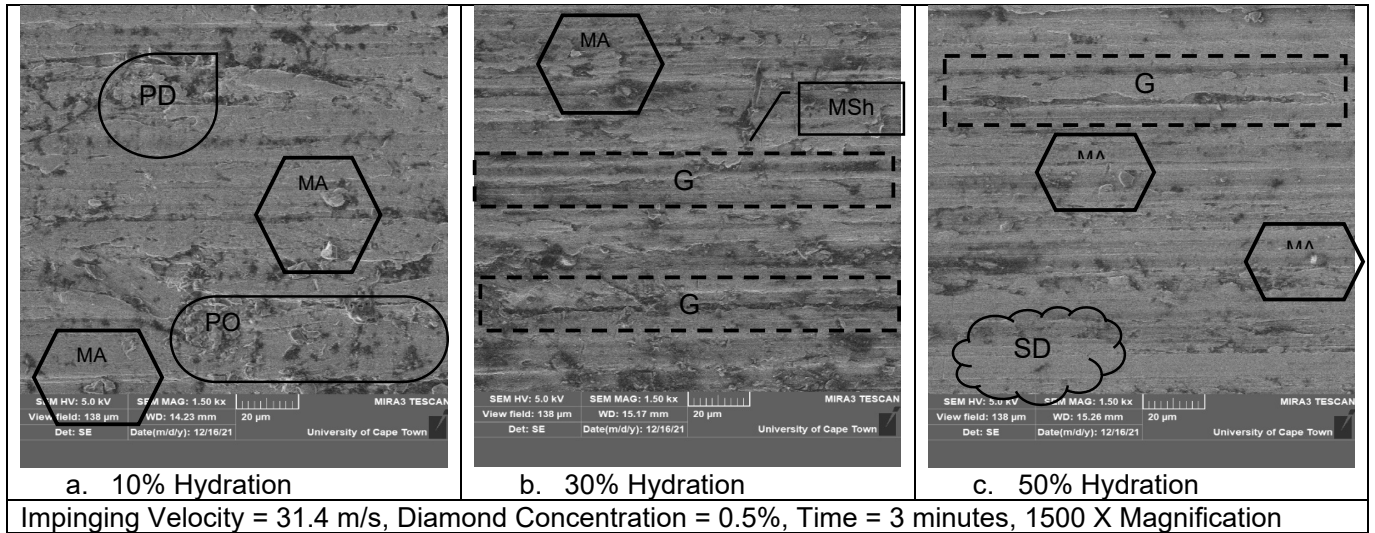
a. 10% Hydration	b. 30% Hydration	c. 50% Hydration

Impinging Velocity = 31.4 m/s, Diamond Concentration = 0.5%, Time = 3 minutes, 1500 X Magnification

Figure 101 - 0.5%D, 3 minutes, 31.4 m/s, 1500 X SEM Images

For the following low impinging velocity (6.28 m/s) results shown in Figure 102, the 50% hydrational image shows a much better overall texture and quality than the 10% hydrational image. Pit size and presence has decreased over hydration and adhered material is less apparent in both quantity and size at the higher hydrational image. Smooth deformation is also apparent in the 50% image and grooves are significantly less tall/deep than the 10% image.

a. 10% Hydration	b. 50% Hydration
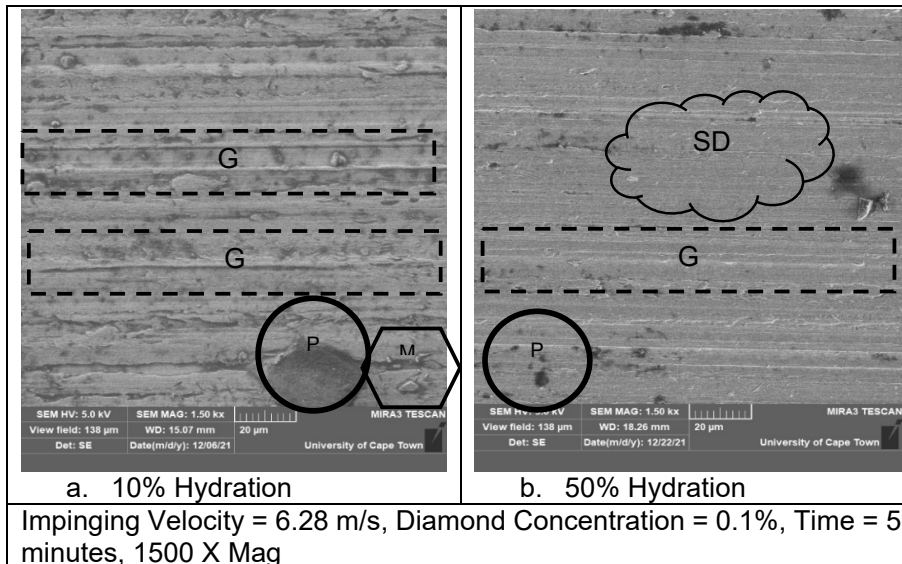
Impinging Velocity = 6.28 m/s, Diamond Concentration = 0.1%, Time = 5 minutes, 1500 X Mag

Figure 102 - 0.1%D, 5 minutes, 6.28 m/s, 1500 X SEM Images

8.2.3. Impinging Velocity Influence

As in the previous sub-chapter (surface parameter results) and the previous sections, the influence of impinging velocity is as follows: higher impinging velocity results in greater surface removal and a faster polishing action. Particularly for lower time periods, the higher impinging velocities generally show better surface improvements (although as time increases, the differences are less noticeable).
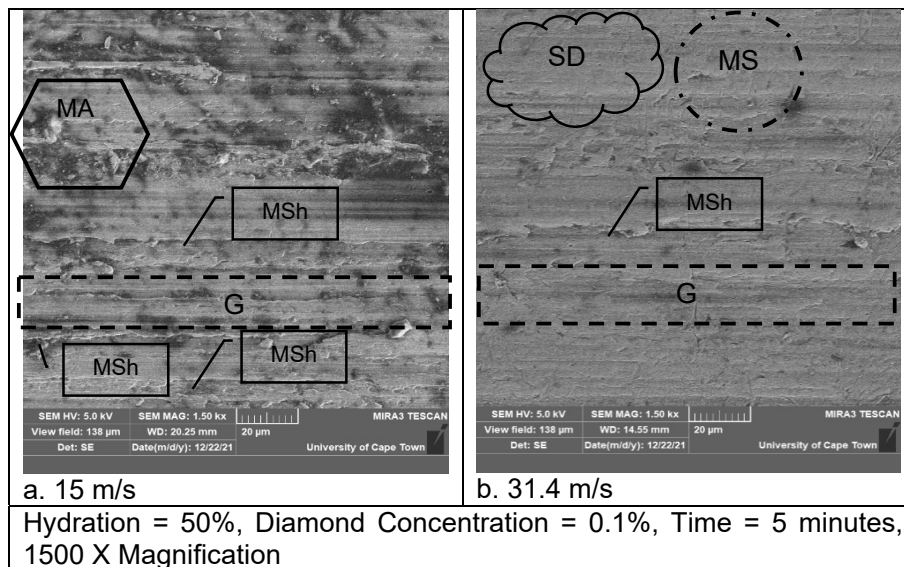

a. 15 m/s	b. 31.4 m/s
Hydration = 50%, Diamond Concentration = 0.1%, Time = 5 minutes, 1500 X Magnification	

Figure 103 - 0.1%D, 5 minutes, 50%H, 1500 X SEM Images

The images in Figure 103 show that the higher impinging velocity produces a much-improved surface compared to the lower impinging velocity. The texture appears more uniform at the higher impinging velocity and roughness heights have certainly decreased. Adhered material, presence of particle pull out due to grinding and micro-shoulders are all visible in the 15 m/s image and these are not apparent in the 31.4 m/s image. Plastic deformation and large pits are also apparent in the 15 m/s image while the 31.4 m/s image shows a much lesser presence of pits and deformation appear smooth. A greater presence of micro scratches is noted in the 31.4 m/s image.

Figure 104 shows that better surface texture is still achieved at the high impinging velocity, but that lower impinging velocity textures have still significantly increased in terms of roughness and uniformity. Micro scratches appear greater in presence over impinging velocity (also attributed to the low hydration of the media) however adherent material is not apparent in the 15 m/s and 31.4 m/s images and the height/depths of grooves has significantly decreased. Smooth deformation is apparent in the higher impinging velocity images (15 m/s and 31.4 m/s images) while undesired surface features from grinding are still apparent in the 6.28 m/s image.

| a. 6.28 m/s | b. 15 m/s | c. 31.4 m/s |

Hydration = 10%, Diamond Concentration = 0.3%, Time = 45 minutes, 1500 X Magnification
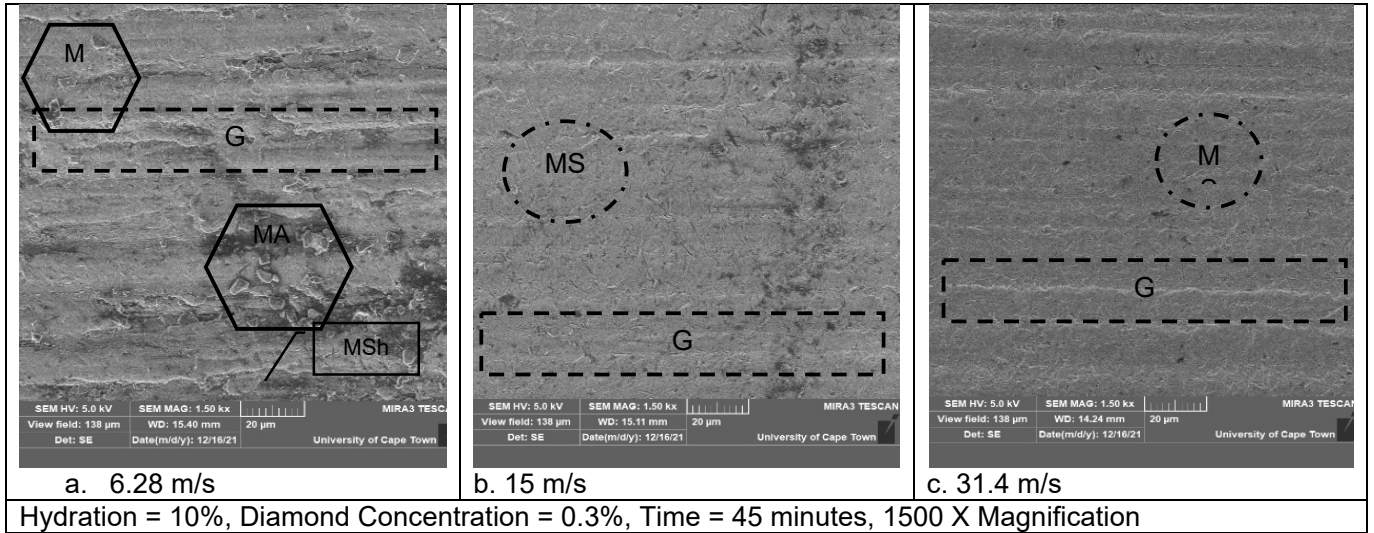
Figure 104 - 0.3%D, 45 minutes, 10%H, 1500X SEM Images

Figure 105 shows a very similar set of results to that of the other low hydration, high time results. Surface texture at higher impinging velocities appears flatter, scratches are still present and slight disappearance of horizontal lay is apparent. The results for lower impinging velocity in this case are much improved compared to the previous results (likely due to good initial texture). Pits, adhered material and micro shoulders are present in all images in the figure.

| a. 6.28 m/s | b. 15 m/s | c. 31.4 m/s |
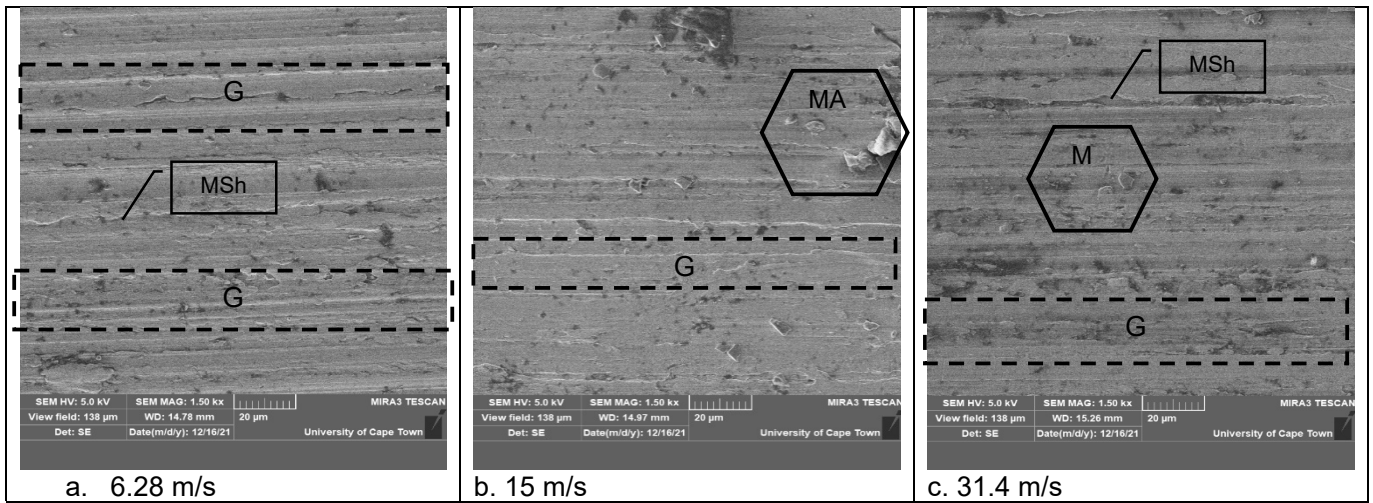
Hydration = 50%, Diamond Concentration = 0.5%, Time = 3 minutes, 1500 X Magnification

Figure 105 - 0.5%D, 3minutes, 50%H, 1500 X SEM Images

8.2.3. Diamond Concentration Influence

Diamond concentration influence on surface roughness appears varied and while there seems to be an effect on surface parameters, it does not seem to be as significant of a process parameter as impinging velocity, hydration or polishing time.

Figure 106 shows results for a low hydration (10%) at 31.4 m/s impinging velocity and 45 minutes polishing time. Micro scratches appear to increase as diamond concentration increases while the presence of micro cracks also appear greater at higher hydrations. Material adherence and pit quantity as well as micro shoulders appear greater at lower diamond concentrations (0.1% in particular). Figure 107 results display the same trends in micro scratch presence over diamond concentration as well as a higher presence of cracks. Material adherence also appears lower at 0.1% diamond concentration.

a. 0.1%   b. 0.3%   c. 0.5%

Hydration = 10%, Impinging Velocity 31.4 m/s, Time = 45 minutes, 1500 X Magnification
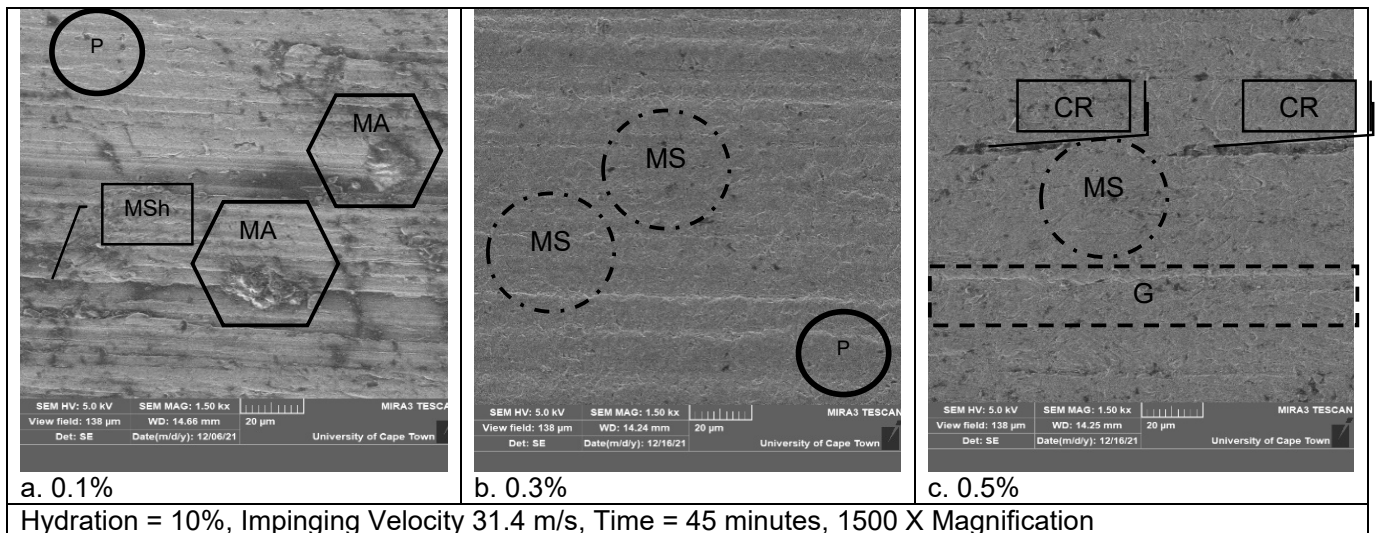
Figure 106 - 31.4 m/s, 45 minutes, 10%H, 1500 X SEM Images

a. 0.1%   b. 0.3%   c. 0.5%

Hydration = 30%, Impinging Velocity 31.4 m/s, Time = 5 minutes, 1500 X Magnification
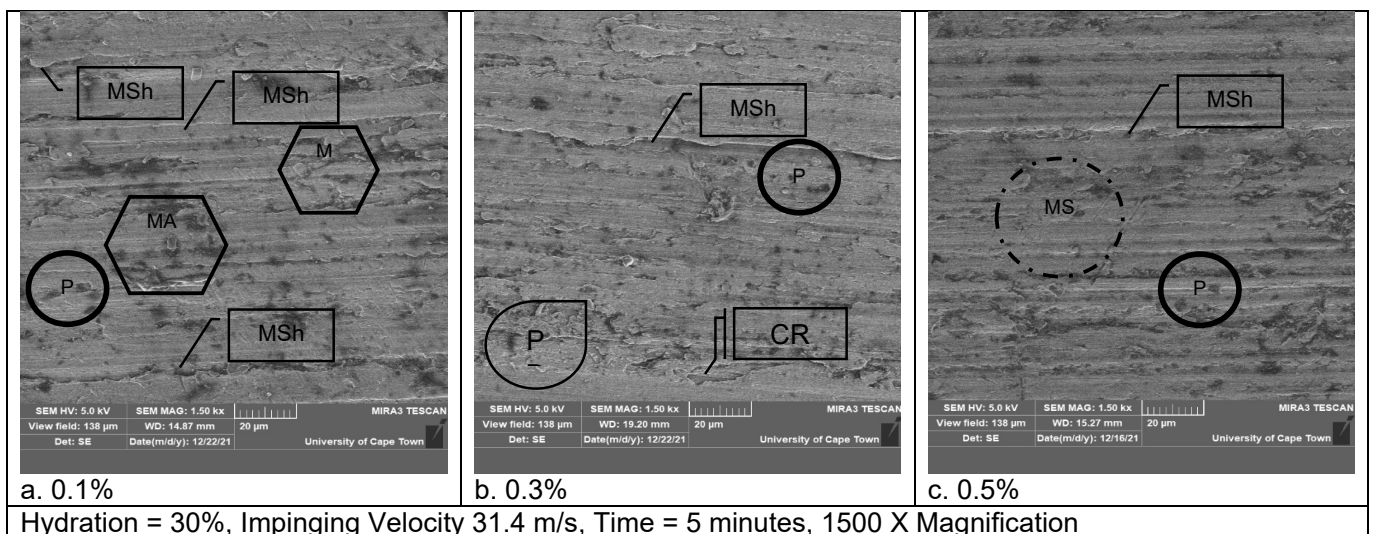
Figure 107 - 31.4 m/s, 5 minutes, 30%H, 1500 X SEM Images

a. 0.1%	b. 0.3%	c. 0.5%

Hydration = 10%, Impinging Velocity 15 m/s, Time = 25 minutes, 1500 X Magnification
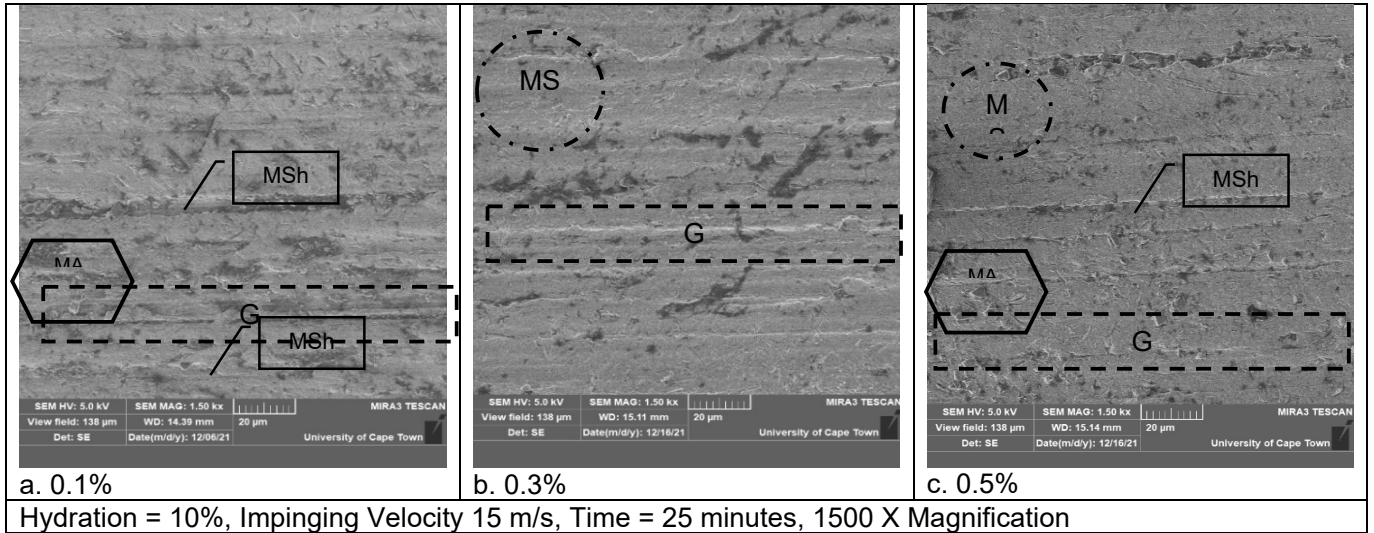
Figure 108 - 15 m/s, 25 minutes, 10%H, 1500 X SEM Images

Figure 108 again shows the increase in micro scratches over diamond concentration while at the lower impinging velocity, material adherence presence is not significantly different. Micro shoulders are apparent at all three sets of diamond concentration.

Figure 109 again shows larger micro scratches at higher diamond concentrations with a larger presence of cracks. However, for this low impinging velocity, overall surface texture and presence of undesirable grinding features has not improved.

a. 0.1%	b. 0.3%	c. 0.5%

Hydration = 30%, Impinging Velocity 6.28 m/s, Time = 5 minutes, 1500 X Magnification
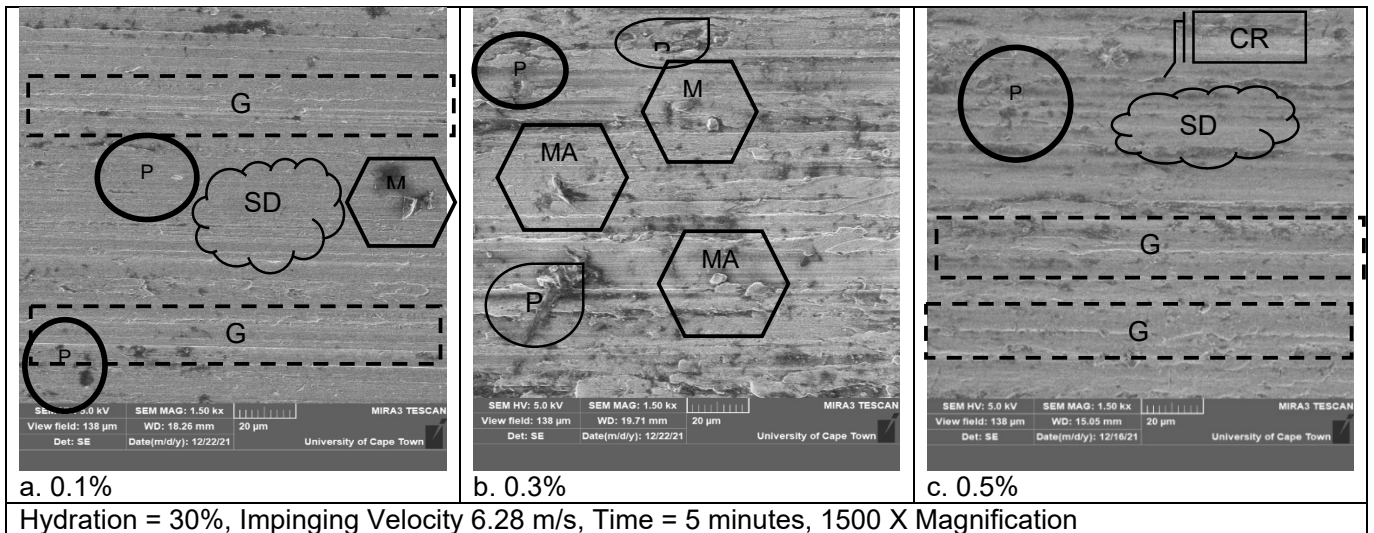
Figure 109 - 6.28 m/s, 5 minutes, 30%H, 1500 X SEM Images

Diamond concentration results imply that higher concentrations lead to a greater presence of micro scratches and micro cracks but also aid in removing impurities, pits and adhered material as well as lessening micro shoulder and groove height.

8.3. Live Analysis Results – Namely Force

As stated previously, all results were measured using a Dewe 43A DAQ and the appropriate DeweSoft DAQ software (DewesoftX1). Figure 110 below shows the selected set-up of the data acquisition software – where viewing screens for Force, Force Fast Fourier Transform (FFT), Sound Pressure Level, Acceleration and Video Images were chosen for viewing.
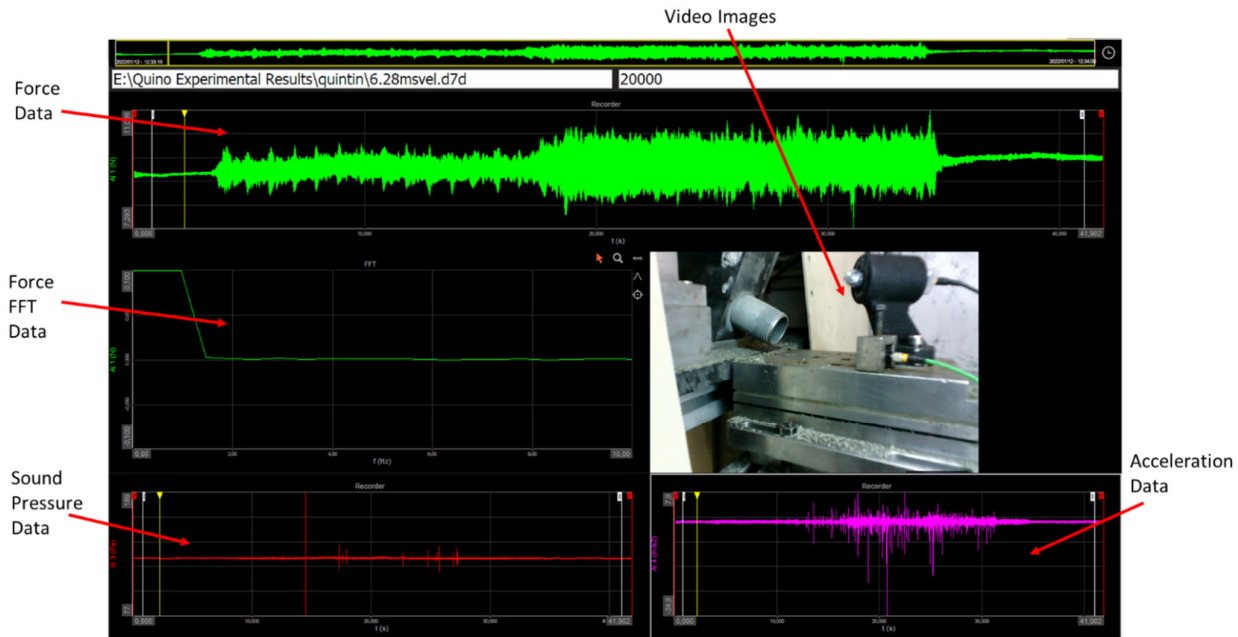
Figure 110 - DeweSoft Set-Up

Figure 111 shows the method of measuring force data (where the change in force between peak and valley indicates polishing force). 5 random measurements over the entire range of polishing occurred and these forces were then averaged to acquire the final force values (Table 18 shows an example of this).

Table 18 - Force Measurement Example

Velocity (m/s)	6.28
Hydration (%)	10
Concentration (%)	0.3

Force Reading No	1	2	3	4	5	AVG
Force Reading - N (±0.001 N)	2.069	1.573	1.787	2.031	1.271	1.7462

Figure 111 - Force Measurement Technique

8.3.1. 0.1% Diamond Concentration Results

Figure 113 and Figure 112 showed the measured force results for a 0.1% diamond condition over multiple impinging velocities and hydrations. T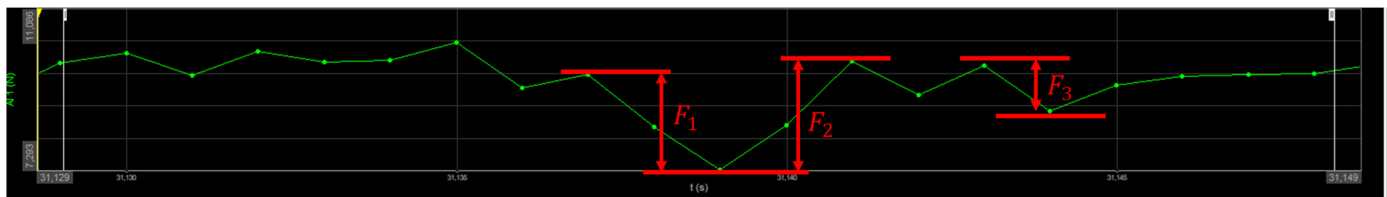wo obvious trends become apparent when analysing the force data. Firstly, impinging force decreases significantly with an increase in hydration. Secondly (and to be expected), an increase in impinging velocity shows an increase in impinging force. It should also be noted that an increase in hydration results in an increase in kinetic energy (due to mass increasing). Thus, this comparison would be even more disparate when comparing kinetic energy i.e., abrasives with more hydration would display even less force at the fairer comparison of equal kinetic energy.

Figure 112 - 0.1% Diamond Force Hydration Graph
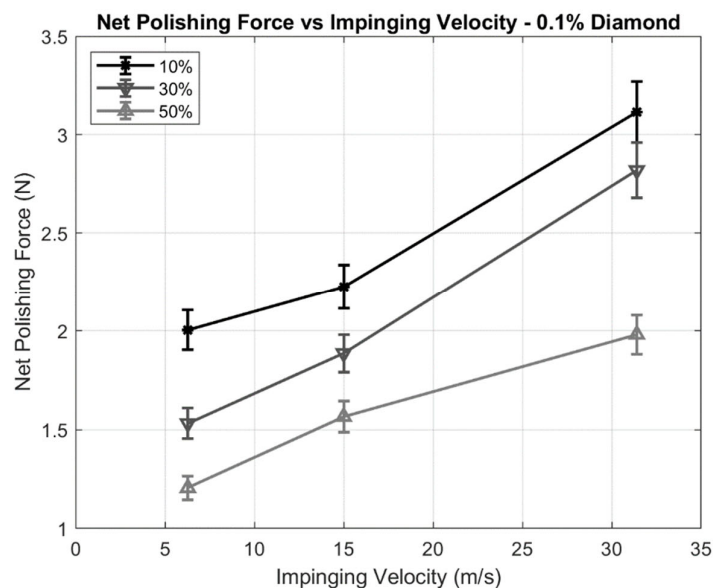
Figure 113 - 0.1% Diamond Force Velocity Graph

8.3.2. 0.3% Diamond Concentration Results

The measured results shown in Figure 114 and Figure 115 for a diamond concentration of 0.3% are very similar to that of 0.1% shown on the previous page, affirming the previously determined trends and statements. However, this shows that diamond concentration may not have an effect on overall polishing force (due to its minimal mass contribution and the expectation that diamond interacts on the micro-level and not the macro-level).

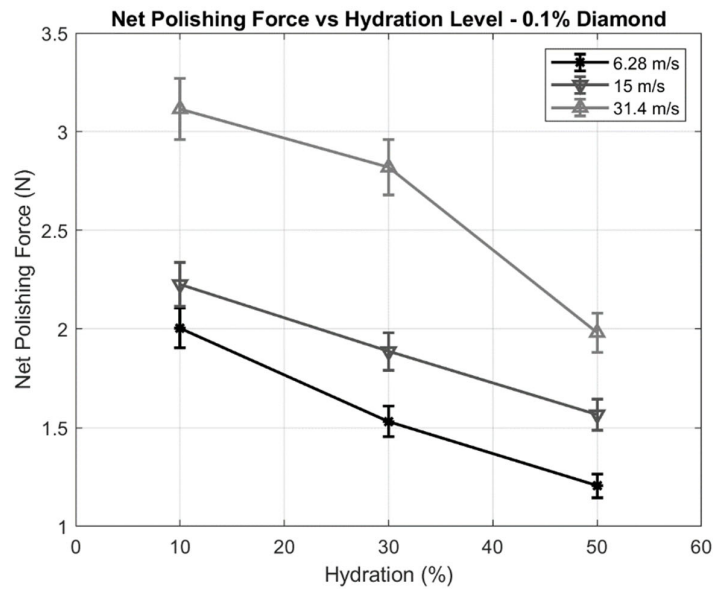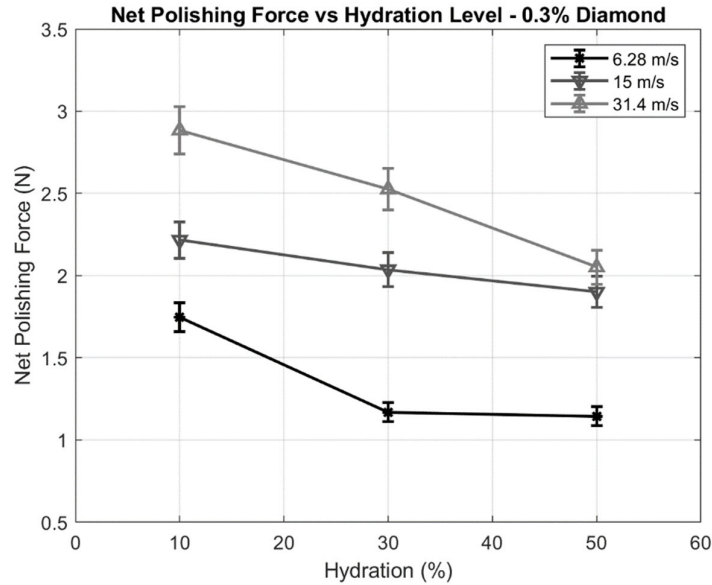*Figure 115 - 0.3% Diamond Force Hydration Graph*
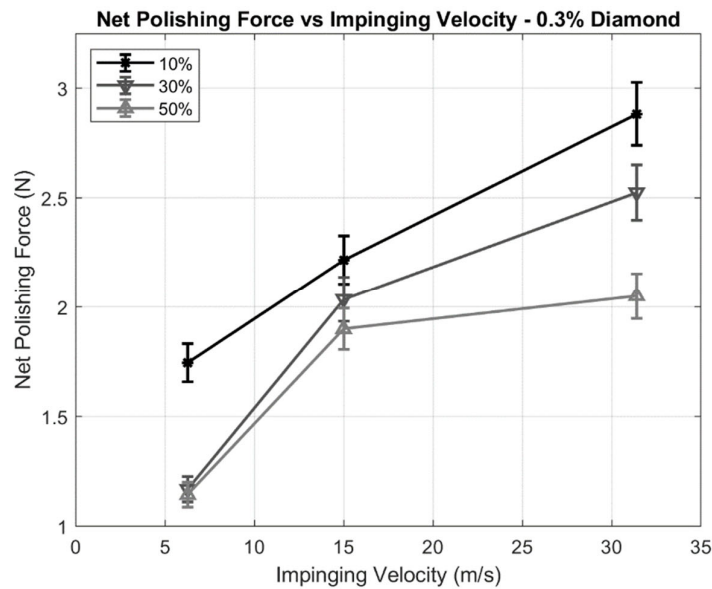
Figure 114 - 0.3% Diamond Force Velocity Graph

8.3.3. 0.5% Diamond Concentration Results

Once again, this set of results shown in Figure 116 and Figure 117 help to affirm what was previously stated; force increases with an increase in impinging velocity/kinetic energy and decreases with an increase in abrasive hydration. Again, the results prove to be very similar and so it is once again believed that diamond concentration is not related to overall polishing force.
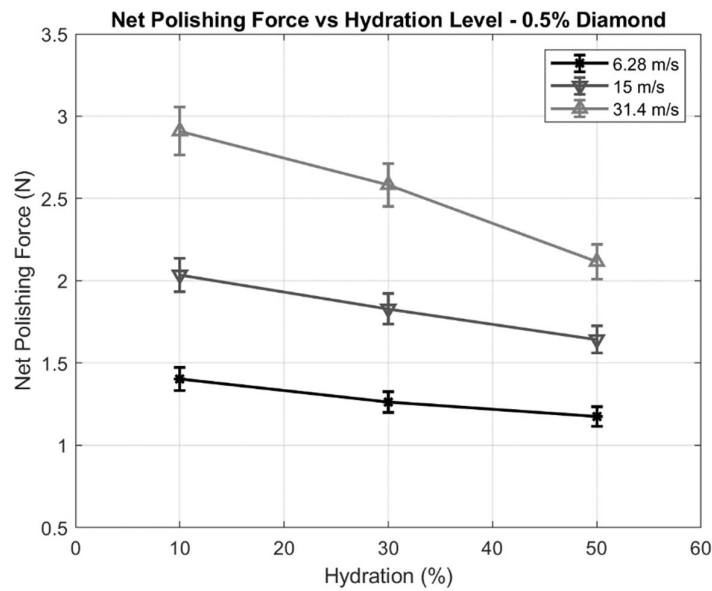
Figure 116 - 0.5% Diamond Force Hydration Graph
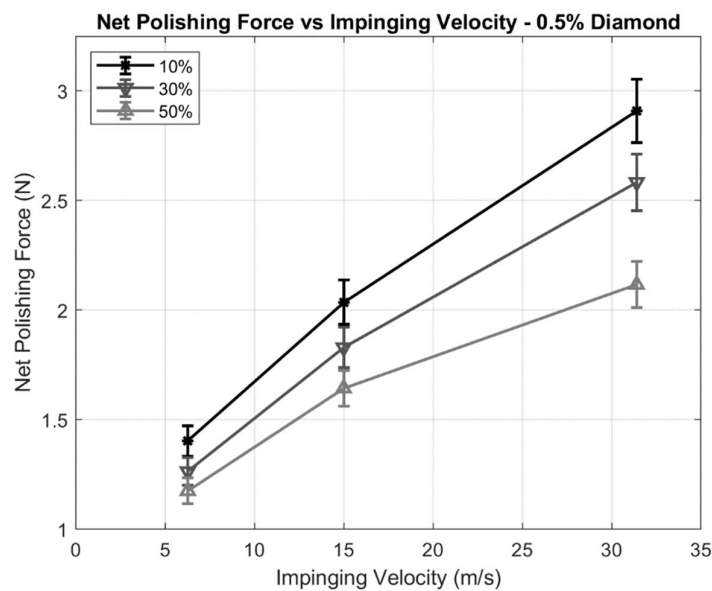
Figure 117 - 0.5% Diamond Force Velocity Graph

8.3.4. Averaged Results

Using the average of all acquired force results, the previously noted trends are fully maintained and this allows us to work with empirical data with the elimination of diamond concentration as a contributing factor to overall polishing force. The averaged results are displayed in Figure 118 and Figure 119.
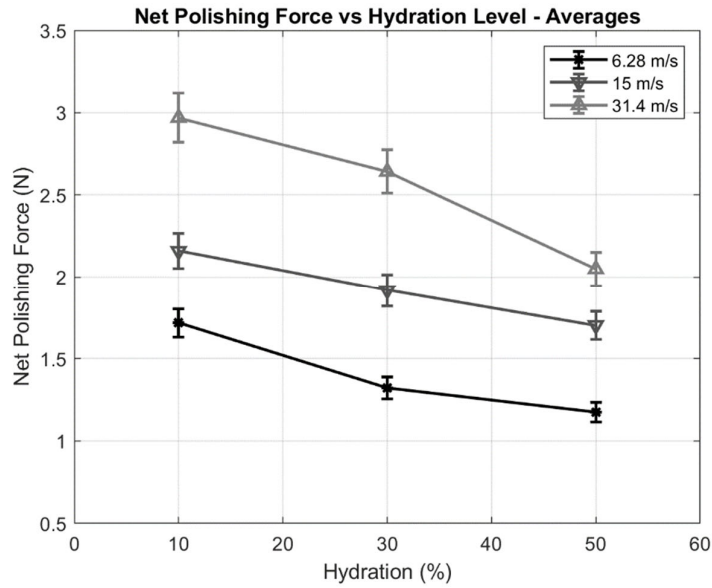
Figure 118 - Net Polishing Forces Hydration Graph
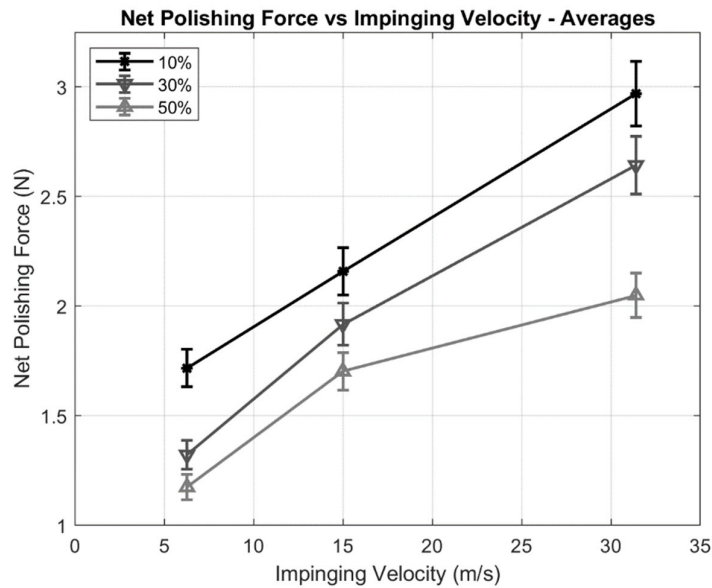
Figure 119 - Net Polishing Forces Velocity Graph

8.3.5. Empirical Equations

Using multivariate linear regression, the following relation for the correlation of velocity, hydration, and water content to output force is acquired:

$$F = 1.7160 - 0.01056H_\% - 0.6921D_\% + 0.04622v_{imp} \tag{55}$$

With an R Square value of 0.7951 and a multiple R value of: 0.8917.

If diamond concentration is neglected as an input factor, an equation is acquired in the form of:

$$F = 1.5084 - 0.01056H_\% + 0.04622v_{imp} \tag{56}$$

With an R Square value of 0.7580 and a multiple R value of: 0.8707.

These outputs are helpful in the development of further models as well as for comparison to previously developed force models.

8.3.6. Acceleration and Sound Pressure Level Results

Although not primary outputs, the same process was followed for the measurement of acceleration and sound pressure level (the experiments were carried out at the same time), and the following two figures shown in Figure 120 and Figure 121 were produced for the averages of all measured values. The results are not used elsewhere in this report but there are interesting trends present in both the below figures. Measured acceleration tends to be higher at greater impinging velocities but lower at higher media hydration levels (this could be due to the greater deformation and contact time that more hydrated abrasives have with the workpiece). Sound pressure level is once again higher at higher impinging velocities (although this could be due to the greater pitch the belt and motor produce at higher velocities). Higher hydration level shows a weak relationship to the sound pressure level, with a slight decrease in sound pressure level as hydration is increased.

Figure 120 - Measured Change in Sound Pressure Level vs Hydration

Figure 121 - Measured Acceleration vs Hydration
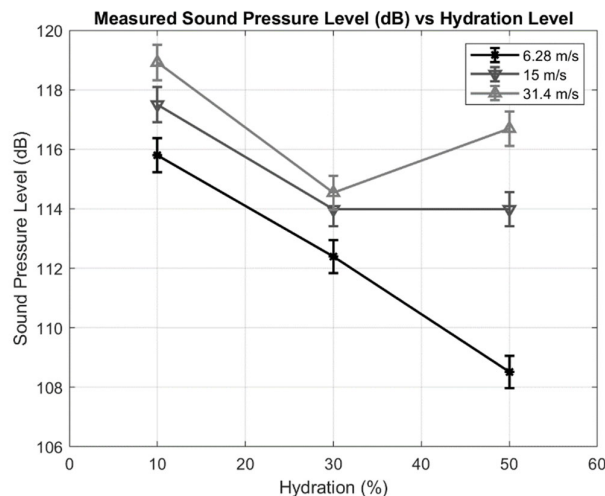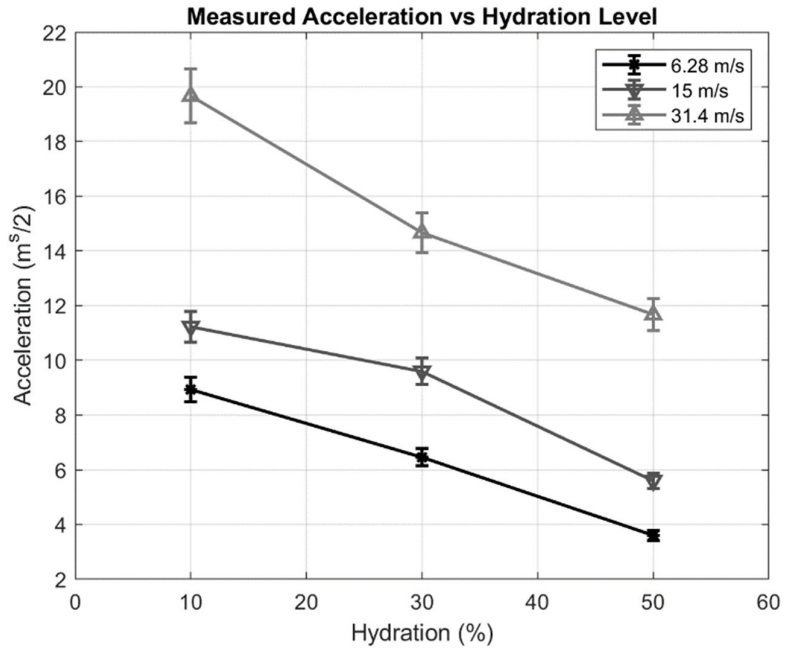
8.4. Consolidated Table of Findings

Table 19 shows the consolidated findings from the gathered experimental results, with a focus on similarities between the findings, noticeable trends and summarising the results. This summary allows for a comparison of results to easily be seen, noting that polishing time, hydration, and impact velocity results for both surface roughness and force have significant outputs (which are discussed in this consolidated table).

Table 19 - Consolidated Experimental Results Table

Hypothesis	Findings in Literature	Findings from Experiments
1. Greater polishing time leads to lower surface roughness and improved texture.	Polishing time shows a reduction in surface roughness up to a saturation point, after which, minimal reductions in surface roughness occur [1] [24]	Experimental results affirm the findings in literature and show that a saturation point is reached after a certain polishing time. It was also found that in some conditions (low hydration) polishing time can cause excess surface scratches to appear. However, surface texture appears more uniform and improved over time for conditions of medium to high hydration.
2. Higher hydration leads to a lower surface roughness while lower hydration leads to a higher surface roughness.	Higher hydration shows a lower overall saturation point for surface roughness than lower hydration. However higher hydration levels result in the saturation point taking longer to reach [1] [6]	Results of experiments agree with those of previous researchers in literature, showing that higher hydrations take longer to reach saturation point. However higher hydrations show lower saturation points.
3. Hydration level does not have a significant impact on surface texture.	N/A	Higher hydration levels show no presence of surface scratches while polishing while low levels and dry show a great presence of scratches (which increases over time). Hydration does show a significant impact on texture.
4. Higher hydration levels imply lower values of impact force while lower hydration levels imply higher values of impact force.	The literature agrees with the formulated hypothesis [1] [6]	Measured experimental values also agree with that of the formulated hypothesis.
5. Higher diamond concentrations result in greater and faster reductions of surface roughness and texture.	N/A	Higher diamond concentration at higher impinging velocities shows greater surface roughness than lower diamond concentration while higher diamond concentration at lower impinging velocities shows lower (finer) surface roughness than lower diamond concentration. The presence of micro scratches and micro cracks is higher at higher diamond concentrations but the reduction of grinding surface features is

		reduced quicker at higher diamond concentrations.
6. Higher impact velocities result in a desired surface roughness being achieved quicker.	Higher kinetic energies result in a more rapid surface roughness decline as well as a lower saturation point but this is limited to the extent that higher velocities may cause damage if the imparted stress is too high. [1] [25]	If the impact velocity is greater than that required to cause ductile regime polishing conditions, effective polishing will occur, but higher velocities tend to show a faster rate of polishing and a larger difference in initial and final surface roughness. Maximum contact stress was never reached.
7. Accelerometer and sound pressure level readings are not correlated to polishing.	N/A	Acceleration and sound pressure level measurements show a similar trend to that of force and may provide another means of process control.

Chapter 9 – Vibrational Model & Results

Using the acquired/measured results from derivation (the empirically developed force model based on critical values and Hertzian contact mechanics) and experimentation (the multivariate linear regressed force model based on hydration and velocity), another model was developed to show how the hydration level of abrasive media affects the contact between abrasive and workpiece (by modelling the hydration as a damping factor). The result outputs (all as a variation of kinetic energy and hydration) of this model are impact force, contact time, damping ratio, damping coefficient, contact displacement and finally contact stress as a percentage of dry contact stress.

In this model, results are compared over kinetic energies rather than velocities (which helps provide more information regarding force changes and associated contact parameters). To compare results to previous experimental results from other researchers (notably Fukumoto et al. [6]), an abrasive radius of 0.5 mm was assumed. This changes the abrasive mass to 0.35605 mg for dry impact. It should also be noted that from experimental results (Figure 122), actual acquired abrasive grain diameter was closer to 1 mm on average (this varies largely based on the source and type of viscoelastic core).
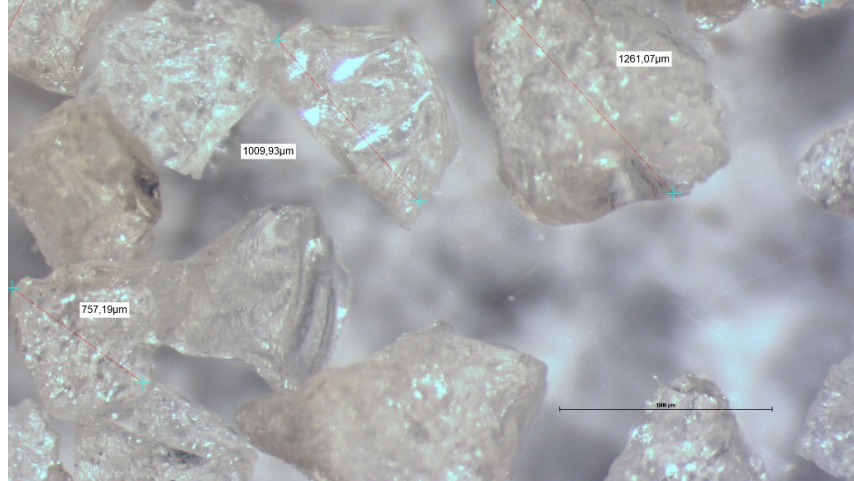

Figure 122 - Zoomed Microscopic Gelatin Image

The range of impact velocities for dry impact was developed at the intervals of 6.28 m/s, 15 m/s, 31.4 m/s, 45 m/s and 60 m/s. This corresponds to kinetic energies of 0.070 mJ, 0.049 mJ, 0.175 mJ, 0.3605 mJ and 0.6409 mJ.

To keep kinetic energy constant over the intervals, the following velocities in Table 20 were related to increasing hydrational levels of abrasives:

Table 20 – Velocity (in m/s) at Varying Hydration Levels (for constant Kinetic Energy)

10% Hydration				
5.9877	14.3019	29.9387	42.9058	57.2078
30% Hydration				
5.2516	12.5436	26.2580	37.6309	50.1745
50% Hydration				
4.8890	11.6775	24.4449	35.0325	46.7099

The following material properties in Table 21 were used as inputs to the model [46]:

Table 21 - Abrasive Properties for Vibrational Model

	Gelatin	SiC	Diamond	Water
Constituency (%)	47, 67, 87 or 97	2.9	0.1	0, 10, 30 or 50
Density	680	3020	3500	997
Diameter	1 mm	2.5 µm	2.5 µm	N/A
Elastic Modulus	43.2 kPa	330 GPa	1100 GPa	N/A
Poisson's Ratio	680	3020	3500	0.5

Workpiece properties used are: 113 GPa for the elastic modulus of Ti-6Al-4V, and 0.342 for the Poisson ratio of Ti-6Al-4V [46].

A critical varying material property for this analysis is that of elastic modulus, which changes as hydration levels are increased. Elastic modulus is a measure of material stiffness. Fukumoto et al. [6] in their study of multi-cone media hydration, found the static elastic modulus to change from 43.2 kPa to 7.8 kPa to 0.78 kPa to 0.52 kPa, for hydration levels of 0%, 10%, 30% and 50%, respectively. Gelatin, diamond, and silicon carbide elastic modulus remain the same over hydration levels so the only stiffness that is able to change is that of water. The elastic modulus of the abrasive compound was calculated by:

$$E_{abr} = (\frac{\%_{water}}{E_{water}} + \frac{\%_{gelatin}}{E_{gelatin}} + \frac{\%_{SiC}}{E_{SiC}} + \frac{\%_{diamond}}{E_{diamond}})^{-1} \qquad (57)$$

Using the change determined by Fukumoto et al. [6], the effective static elastic modulus contribution of water to the system is 0.9 kPa. This leads to a change in elastic modulus over hydration levels as seen in Figure 123 below.
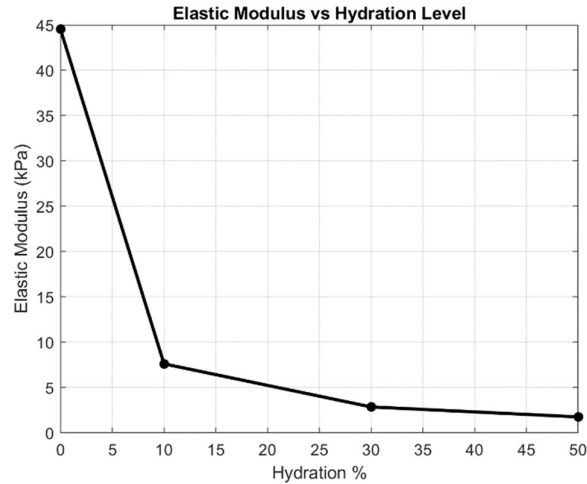
Figure 123 - Elastic Modulus as a function of Hydration Level

The variation of density as hydration is increased is important as well. This is found similarly to the equation for combined Elastic modulus

$$\text{E}_{\text{abr}} = (\frac{\%_{\text{water}}}{\text{E}_{\text{water}}} + \frac{\%_{\text{gelatin}}}{\text{E}_{\text{gelatin}}} + \frac{\%_{\text{SiC}}}{\text{E}_{\text{SiC}}} + \frac{\%_{\text{diamond}}}{\text{E}_{\text{diamond}}})^{-1} \tag{58}$$

9.1. Modified Empirical Models

9.1.1 Experimental Model

The measured force results in the previous chapter are related to abrasive hydration, diamond concentration, and impinging velocity. The effect of concentration is minimal and thus it was excluded from the analysis and a modified multivariate linear regression equation was found, as:

$$F_{imp} = 1.6876 - 0.01796H_\% + 0.066759V_{imp} \tag{59}$$

These were acquired from experimental results (by averaging force results over diamond concentrations). The averaged force results are as in Table 22:

Table 22 - Averaged Force Results over Diamond Concentrations

	6.28 m/s	15 m/s	31.4 m/s
10%	1.822 N	2.463 N	3.744 N
30%	1.597 N	1.990 N	3.318 N
50%	1.467 N	1.650 N	2.757 N

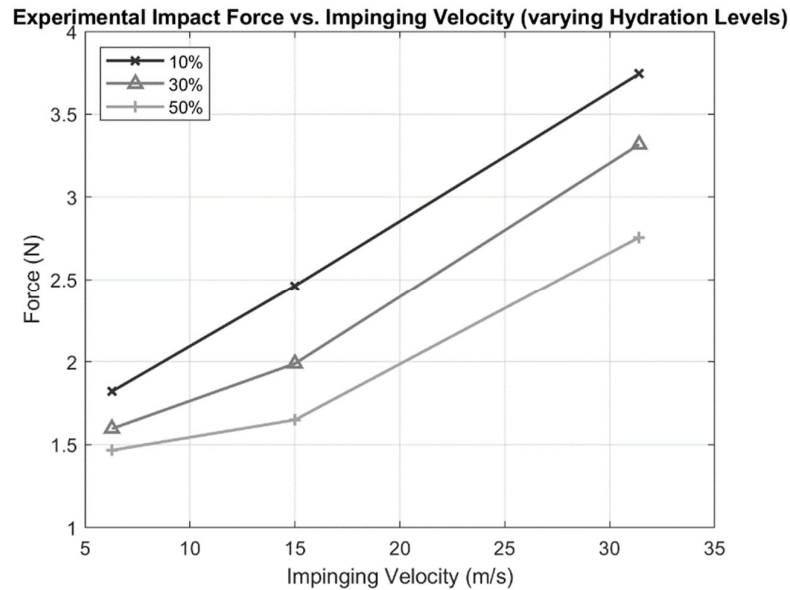This is visually represented by Figure 124 below.

Figure 124 - Visual Representation of Averaged Force Results over
Diamond Concentrations

From the above it is quite easy to see that higher hydration levels result in lower forces while higher impinging velocities result in higher forces. These results are important as they provide a basis on which to develop the model as well as to compare results to.

9.1.2. Theoretical Empirical-Analytical Model

Similarly, to the model presented in Chapter 3 – Empirical Modelling, the notion of critical values was used to calculate output force. However, for the variation of the model in this chapter, it is done over a range of hydrational values, rather than for just dry contact. The force outputs of this model are used as inputs to the vibrational model to follow and allow for the calculation of contact time, damping ratio, damping coefficient and contact stress.

Due to the same methodology being used as in Chapter 3 (but over a larger set of iterations), the equations and methodology are not presented here. The additions that are described are the mass differences at each hydration level, density increases, radius increases and the exact values of elastic modulus increases.

Initial mass is known and thus subsequent hydrational level mass increases by:

$$m_{abr} = (1 + H\%)\rho_{abr}V_{abr} \tag{60}$$

Where:

$$V_{abr} = \frac{4}{3}\pi R_{abr}^3 \tag{61}$$

Abrasive radius increased can be calculated after knowing the mass increases, as:

$$R_{abr} = r = \sqrt[3]{\frac{3m_{abr}}{4\rho\pi}} \tag{62}$$

Elastic modulus and density increases have been mentioned previously.

All results for abrasive properties at different hydrational levels are shown below in Table 23.

Table 23 - Abrasive constituent properties at varying hydration levels

Hydration (%)	Mass (mg)	Density (kg/m^3)	Radius (mm)	Elastic Modulus (kPa)
0%	$m_0 = 0.356\ mg$	$\rho_0 = 680\ kg/m^3$	$R_0 = 0.500$ mm	$E_0 = 43.2$ kPa
10%	$m_{10} = 0.392\ mg$	$\rho_{10} = 702\ kg/m^3$	$R_{10} = 0.512$ mm	$E_{10} = 7.61$ kPa
30%	$m_{30} = 0.509\ mg$	$\rho_{30} = 752\ kg/m^3$	$R_{30} = 0.545$ mm	$E_{30} = 2.87$ kPa
50%	$m_{50} = 0.588\ mg$	$\rho_{50} = 809\ kg/m^3$	$R_{50} = 0.558$ mm	$E_{50} = 1.765$ kPa

After completing the iterations of force calculation, the following results for impinging force at varying kinetic energies are found (see Figure 125):
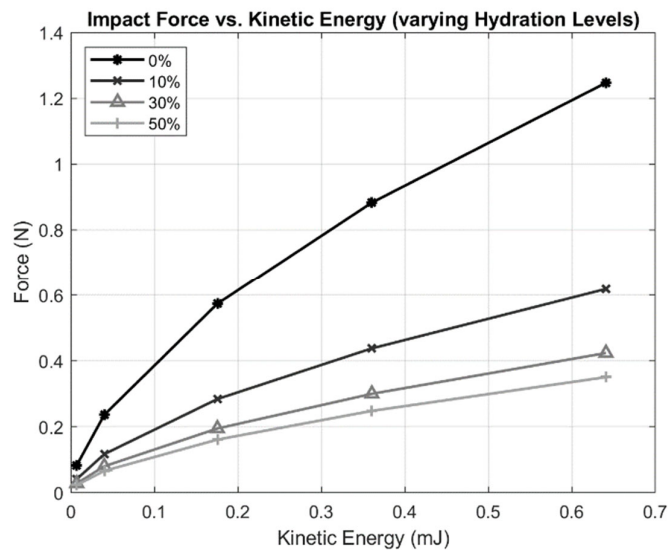
Figure 125 - Force results from critical value method (for varying kinetic energies over a range of hydration levels)

The force values found agree well with that of Fukumoto et al. [6], showing sharp decreases in impinging forces as hydration is increased.

With forces over varying kinetic energies and hydrational levels shown, the next required value is that of contact time, which provides a necessary input towards the vibrational model.

Contact time, similarly, to that of Kuppuswamy et al. [4], is found by using the conservation of momentum. Impact force is applied over a certain time for an abrasive mass m_{abr} and an abrasive impinging velocity v_{imp}. Contact time was thus calculated:

$$t_{contact} = \frac{m_1 v_1}{F_{imp}} \tag{63}$$

As with impinging velocity, the calculations for contact time, were developed for all iterations of kinetic energy and hydration level. The results for contact time are shown below in Figure 126). Results show logarithmic decay of contact time over kinetic energy increases, while contact time increases incrementally (in a somewhat linear fashion) as hydration level is increased. Again, these results agree well with those presented by Fukumoto et al. [6]. The verification of these results imply that the modelling is accurate and is a good basis for further modelling to occur.
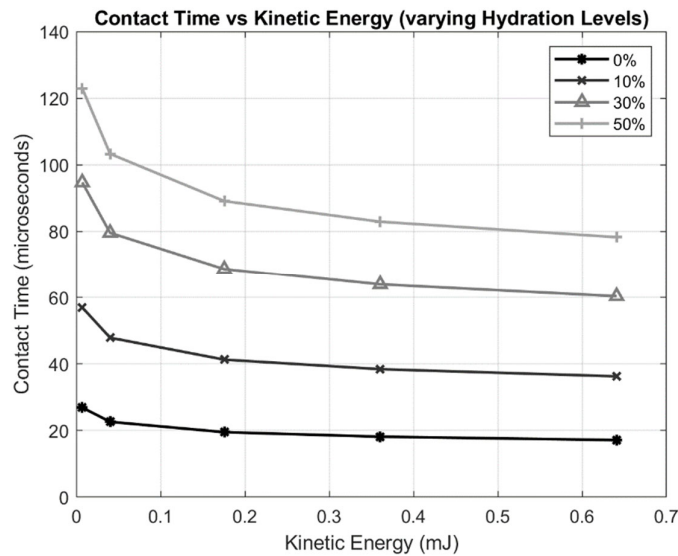

Figure 126 - Contact Time for Varying Kinetic Energies over Hydrational Levels

9.2. Vibrational Model Methodology

The use of a spring-dashpot model allows for the control of system conditions by changing the applicable system parameters. A large variety of polishing effects can be achieved with minimal changes to process design. This model was developed to determine the role of hydration in contact dampening.

Figure 127 below shows the models used at further analysis, with m representing abrasive mass, c representing damping coefficient (due to hydration) and k representing combined abrasive stiffness. x represents abrasive deformation while the fixed ground in the model is assumed as the SLM Ti-6Al-4V workpiece. As in the Kelvin-Voigt model, a damped free vibration is chosen as the basis of modelling (representing creep well) The more complex standard linear solid model was not chosen as stress relaxation is not a factor to consider when only a half of an oscillation is modelled). When dry contact was modelled, the dashpot was disregarded, and the contact was simply modelled as a spring attached to the workpiece and abrasive. Figure 128 shows a key for the diagrams.
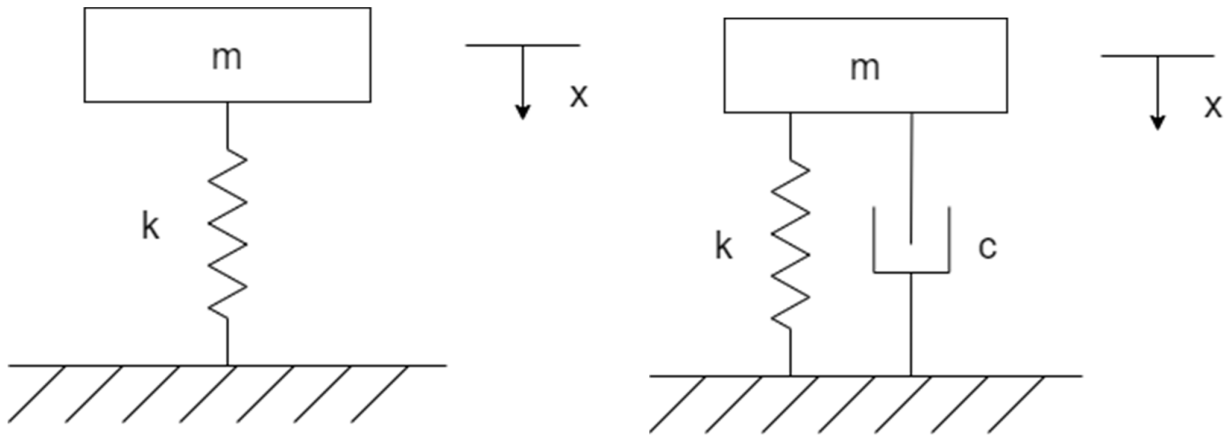
Figure 127 - a: Dry contact model - b: Hydrated contact model

Figure 128 - Vibrational Model Key

Using Hooke's law and the basis of viscoelastic modelling, the assumption that abrasive elastic modulus is equivalent to the spring stiffness of the system was made:

$$k_{abr} = E_{abr} \tag{64}$$

Following this, a force balance on the system was required, which is shown in Figure 129.
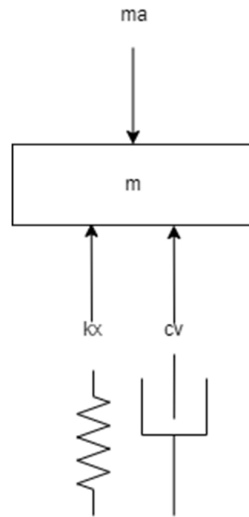
Figure 129 - Force Balance

This is represented by the equation of motion:

$$m\ddot{x} + c\dot{x} + kx = 0 \tag{65}$$

Which simplifies to:

$$\ddot{x} + 2\zeta\omega_n\dot{x} + \omega_n^2 x = 0 \tag{66}$$

Where:

$$\omega_n = \sqrt{\frac{k}{m}} = \sqrt{\frac{E}{m}} \tag{67}$$

$$\zeta = \frac{c}{2m\omega_n} \tag{68}$$

It should be noted that the changes in Elastic modulus and combined abrasive mass due to hydrational increase affect the natural frequency, meaning that the value needs to be calculated for each hydrational level. The same is relevant for damping ratio.

Damped frequency is described as the period of contact in this case and is shown by:

$$\omega_d = \omega_n \sqrt{1 - \zeta^2}$$

(69)
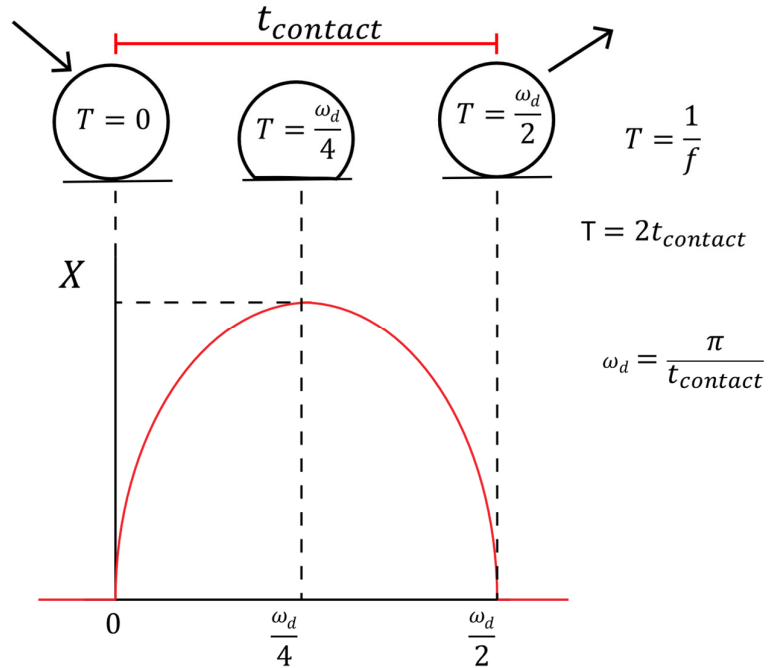
Figure 130 - Description of Period of Contact

As per the diagram developed and presented above (Figure 130), damped frequency was also determined as:

$$\omega_d = \frac{\pi}{t_{contact}}$$

(70)

Because the contact times for each hydration level were known, determining contact period as well as frequency ratio (from the ratio of damped frequency to the ratio of natural frequency) was possible.

Damping ratio was then be found by the following (a rearrangement on the damped frequency formula):

$$\zeta = \sqrt{1 - \left(\frac{\omega_d}{\omega_n}\right)^2}$$

(71)

With damping ratio known, damping coefficient was calculated by:

$$c = 2m\omega_n\zeta$$

(72)

Following the force balance diagram, the following for the displacement solution for a damped free vibration was found:

$$x(t) = A_1 \sin(\omega_d t)\, e^{-\zeta \omega_n t} + A_2 \cos(\omega_d t)\, e^{-\zeta \omega_n t} \qquad (73)$$

However, x(0) = 0, therefore $A_2 = 0$. Also note that x(t) is equal to the displacement $\delta(t)$. A_1 was calculated to be:

$$A_1 = \frac{\dot{x}_o}{\omega_d} \qquad (74)$$

Using geometrical constraints for the contact between a sphere and a plane, contact area as a function of deformation was derived as:

$$A = \pi(2\delta R - \delta^2) \qquad (75)$$

Finally, contact stress was determined to be:

$$\sigma = \frac{1.5 F_c}{\pi(2\delta R - \delta^2)} \qquad (76)$$

For the dry contact between abrasive and workpiece, damping is not present, and thus damped frequency was eliminated (leaving natural frequency as the period of contact) and the displacement solution simply becomes:

$$x = \frac{\dot{x}_o}{\omega_n} sin(\omega_n t) \qquad (77)$$

The maximum displacement occurs at $sin 90° = 1$, maximum deformation was thus be found by:

$$x = \frac{\dot{x}_o}{\omega_n} \qquad (78)$$

This solution is easily substituted back into the derived contact stress equation.

For the hydrated solutions (at 10%, 30% and 50%), the coefficient A_1 was initially found after determining natural and damped frequencies. By then plotting the graph or by finding the derivative of position and setting velocity equal to zero, the maximum displacement of the abrasive was determined. The contact stresses for each iteration of hydration level and associated kinetic energy were then determined.

9.3. Vibrational Model Results

The three major outputs of the vibrational model are of damping ratio, damping coefficient and unitless contact stress (as a function of dry contact).

The results calculated for damping ratio (see Figure 131) show that at low kinetic energies, the effect of damping is close to critical ($\zeta = 1$). The trend of logarithmic decrease in damping ratio becomes apparent as kinetic energy was increased, thereby making the system more underdamped. Lower damping ratios mean longer stabilization times and higher amounts of oscillations before equilibrium is reached (therefore greater displacements are present). These results align well with previous research with higher hydrational levels most certainly resulting in greater displacements and contact times [4] [6] [46] [48].
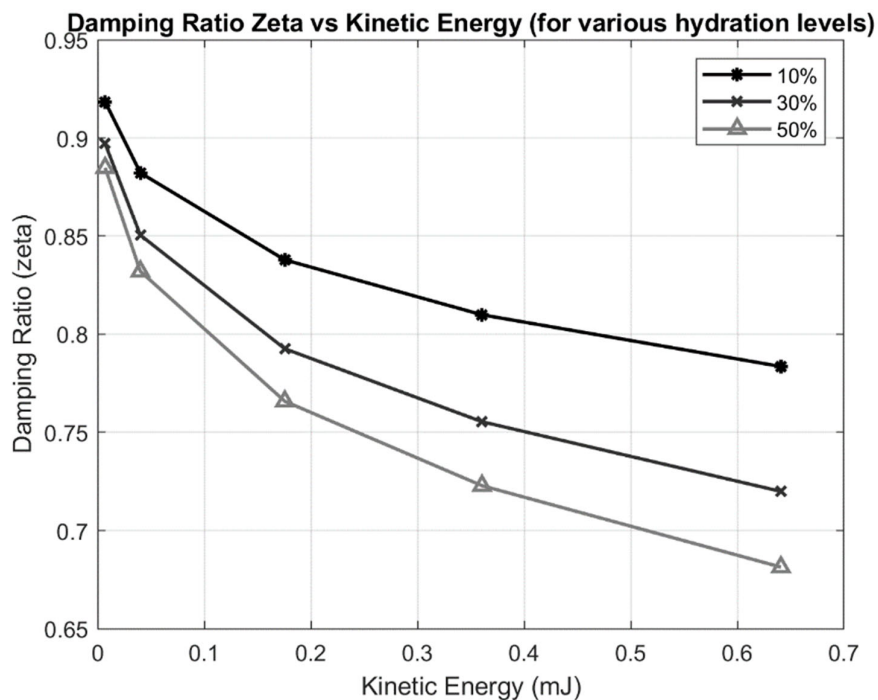
Figure 131 - Damping Ratio Results

Damping coefficient is relative to damping ratio and quite relevant to the system (mass plays a large role in the calculation of the coefficient). Thus, it can vary in case to case, but damping coefficient results (see Figure 132) show a similar trend to damping ratio, except that the steps between lower hydration and higher hydration are more dramatic.
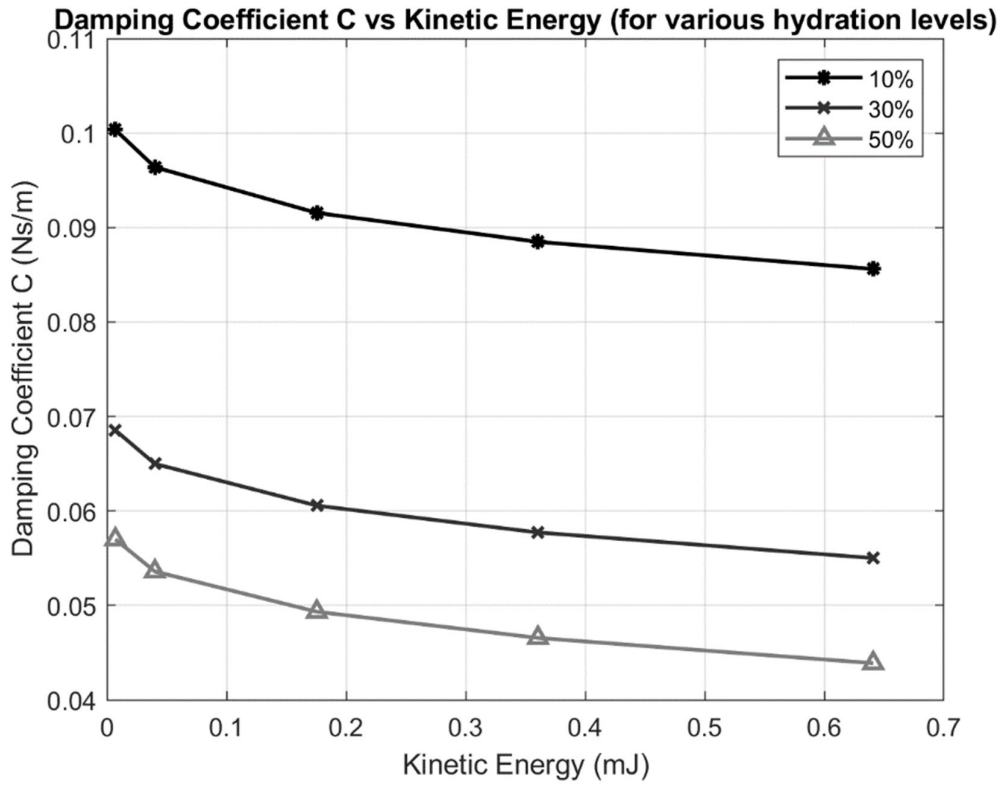

Figure 132 - Results of damping Coefficient

Another acquirable intermediatory result that was found from the vibrational analysis was maximum abrasive deformation (which serves as the input for contact stress calculation) See Figure 133 for results. As kinetic energy is increased, abrasive deformation increases logarithmically with sharp initial gradients, while deformation increases substantially as a function of hydration after the 10% hydration level. 30% and 50% hydration levels show nearly 1.7x and 2.3x increases, respectively (from the dry deformation values). The great increase in deformation is due to the large decreases in stiffness, again matching the results shown by Fukumoto et al. [6].
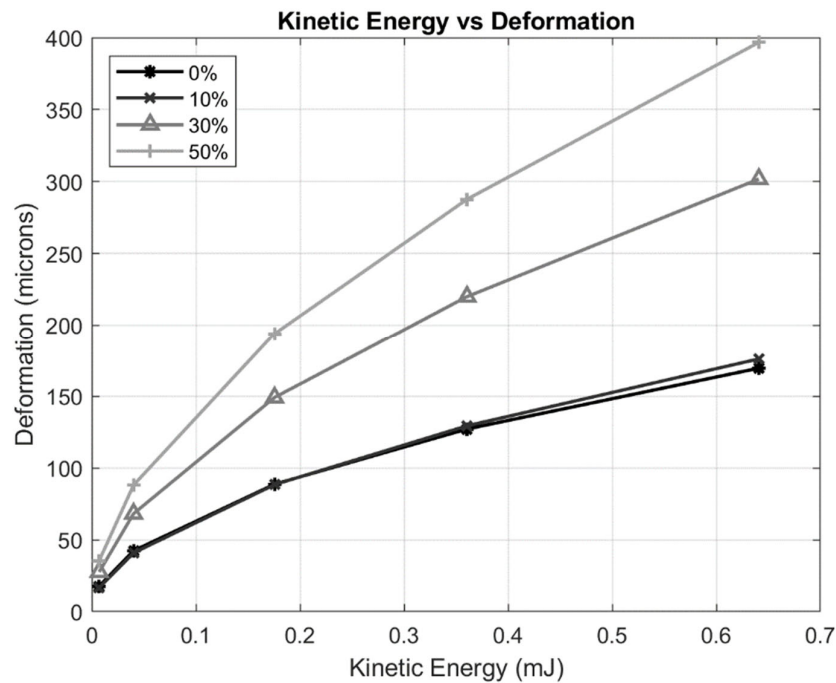
Figure 133 - Kinetic Energy vs Deformation

The final desirable result of this analysis was that of contact stress (which is of notable interest when studying material removal mechanisms). The results displayed below in Figure 134 are shown as a unitless percentage of dry contact stress to adequately describe the effect of hydration and kinetic energy on contact stress. The selection was also chosen due to the different deformations experienced by the workpiece and by the abrasive (the workpiece will have lesser deformation as it is harder and thus will experience greater contact stresses). Another reason for displaying unitless contact stresses is that this model cannot account for the micro interactions between Silicon Carbide/Diamond and the workpiece.

Interestingly, contact stress stays somewhat constant over the range of kinetic energy, particularly for higher hydration levels. Hydration levels play a large role on contact stress,

Figure 134 - Contact Stress Results for Vibrational Model

with 50% hydration approximately 18% of the dry contact stress and 40% hydration approximately 25% of the contact stress. The results show that the damping effect of hydrating media is greatly important to ensure minimal surface damage effects occur.

Kinetic Energy vs Contact Stress
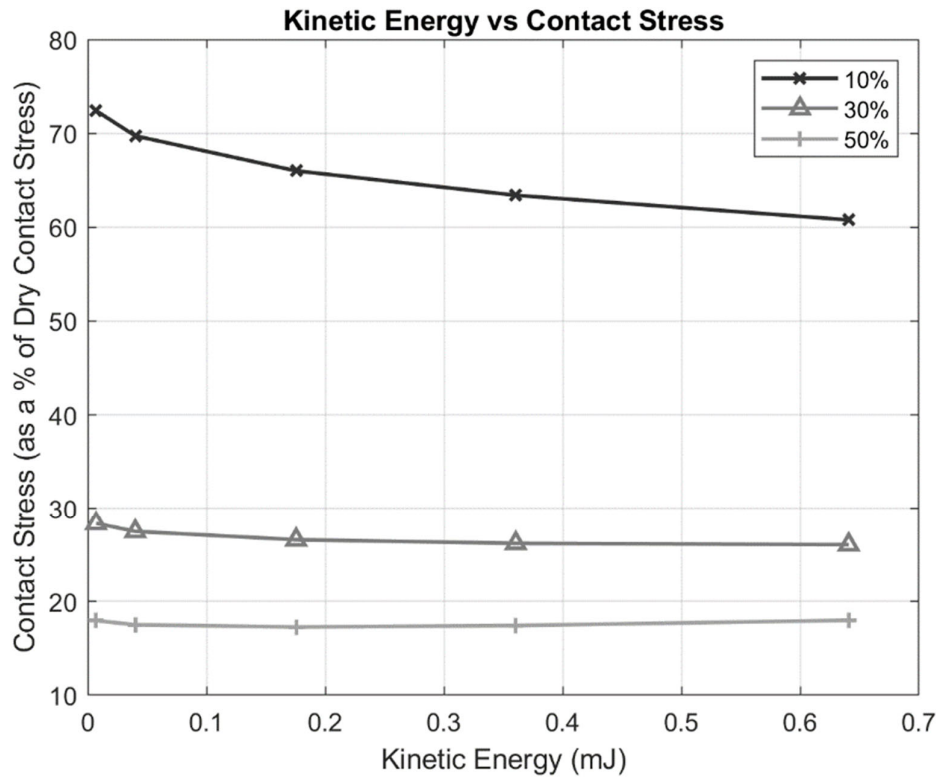
Chapter 10 – Discussion

Throughout the presentation of results in this dissertation, some discussion has taken place. This chapter serves to relate the findings of the study as well as to state limitations of the findings and provide explanations for results, both expected and unexpected/inconclusive.

10.1. Modelling of the Flexolap Polishing Process

Multiple (four) models of the Flexolap polishing process have been provided throughout this dissertation. All models are intrinsically linked to one another and provide some insight to the Flexolap polishing process.

The two initial force control models have different purposes and applications but relate to one another in terms of process development as well as model output confirmation. The analytical model, which is based on the notion of momentum, provides a basis on which to look at the macro-interaction between the entire multi-cone abrasive and SLM Ti-6Al-4V component during polishing. This model is useful in that core scientific principles (momentum and Hertzian contact mechanics) are used (along with minimal parameter inputs) to determine a wide range of desirable process outputs (notably force, polishing time, and contact stress) that can aid in control of wide array of process behaviours. The results of this process showed that ductile regime polishing action occur for all designed parameters and the prediction of force and polishing time agree with plenty of previous literature and research [1] [4] [16]. However, this model is limited in the sense that contact time or coefficient of restitution must be estimated.

The empirical model on the other hand focuses more on the micro-interaction between singular diamond abrasives and asperities of the SLM Ti-6Al-4V component. The basis of the model is from von-Mises yield criteria, the change from elastic to plastic behaviour as well as fundamental Hertzian mechanics and FEM developed models. This model provides a means of predicting process behaviour (force, contact stress and polishing time) without the need for assumption of contact time. This model can also be extended to provide a means of calculating macro-interaction data. Again, this model proved similar in nature to the analytical model, showing similar trends in force increase (logarithmic) and that ductile regime conditions occur at all designed conditions (only just occurring at the lowest impinging velocity though). The limitation of this model is that it has not been studied with other materials (different abrasives or workpiece materials). As this model agrees with the previous model, it also agrees with previous research findings.

The simulation model (a sub-model of the analytical model which could be extended to any of the models) was designed to provide affirmation of the previous model results (FEM is the basis of SolidWorks simulation). The model provided similar results but showed that sufficient

contact stress to cause ductile polishing conditions might only occur at polishing velocities of 15 m/s and greater. Previous results show that ductile regime polishing conditions occur at all impinging velocities. This model also confirmed (as in the previous two models) that workpiece deformation is far below the critical depth of cut. Not much research has been done on polishing contact stress and deformation and thus agreements with other researchers cannot be confirmed or unaffirmed (a limitation in a sense but a benefit in another). Note that this model is flexible in that it can be extended to any force model (as force, contact area and impinging angle are the only required inputs).

All the above models prove useful but fail to incorporate the important variable of media hydration (which acts as a damper). The ability to control viscoelasticity is critically beneficial to the polishing process and thus this model is of great interest to research in the blasting processes. Elastic modulus of material as hydration is increased is based on gathered empirical data (the dynamic elastic modulus of water is estimated from empirical data) while forces are estimated using the previously developed empirical force model (also compared to the gathered force data/empirical equation for additional confirmation on design). Contact time is estimated using momentum and compared to Hertzian contact time for accuracy. Using a spring-dashpot type model (based on Kelvin-Voigt), estimations on damping ratio/coefficient as well as deformation and unitless contact stress, were made. The damping coefficients provide insightful parameters to feed back to the force models and can thus help create a dynamic control for the polishing process. Research into viscoelasticity in literature is generally focussed on FEM developed contact models and thus this research is unique and provides another strong basis of modelling. No significant apparent limitations are present besides a need for more input data as well as application of the model.

Noting the areas on which to further develop research and to improve upon what has already been developed is beneficial to all those interested in the study. The developed spring-dashpot model can be improved by acquiring accurate empirical contact time data (with the use of high-speed cameras), which would then allow for determination of abrasive deformation and furthermore, elastic modulus of media could be inferred. Acquiring experimental force and surface roughness measurements for higher impinging velocities (over 40 m/s) would also aid in verification of the model and provide more empirical data on which to further develop the models.

10.2. Machine Design and Development

Machine design and development was split into multiple sections, some of which required in depth engineering calculations while others required more engineering intuitiveness and thoughtful design.

The abrasive output/discharge system required a belt and pulley system so that higher impinging velocities could be reached. A precision spindle was required to ensure concentricity. Calculations found that the smallest spindle shaft diameter was much greater than the minimum diameter and that the internal bearings would last for over 70 years before replacements are required. Design attempts toward a nozzle producing a more direct jet of abrasives were done, however when implemented in practice, the nozzle proved to require additional design (the abrasives collided with the wall of the nozzle instead of being directed straight out). However, this nozzle provides a prototype upon which further development could be attempted.

Abrasive media collection and recycling proved to be effective upon optimization of the suction system (using the feed ejector). Finding the correct pressure for suction and providing lubrication for the feed ejector and abrasives proved to be the solution to providing proper recycling of media. Calculations predicted more than enough abrasives media could be supplied to the impeller than required and pressure was thus decreased. Hopper and bin calculations showed that the welds were more than strong enough to fit into the aluminium slots as well as to hold a heavy stirrer motor.

The modular design of the frame allowed for different output heights to be chosen as well as for the fitting of longer or shorter nozzles. The aluminium extrusions also allow for many additional designs to be easily incorporated into the frame. This is evident in the addition of the workpiece stand/dynamometer holder, which allows the operator to polish 'hands-free'. This workpiece stand is typical of many experimental set-ups and was a necessary requirement to ensure consistency of experimental conditions.

Control design and placement was done after electrical design and pneumatic design. Both the electrical and pneumatic design were done using relevant engineering diagrams and implemented in a manner that they are minimally visible to the operator. All controls were placed in one sector of the machine and allow for the control of individual process parameters at a time.

A complete SolidWorks model of the developed machine is available incorporating everything from the glove holes to the workpiece stand and light switches. This is to be updated as changes are made to the machine as it allows for effective and traceable redesign, a tactic used by many in industry and research.

10.3. Abrasive Media

Testing the effectiveness of gelatin hydration (by hydrating the media and inspecting it as it dehydrated) gave confidence that the media would work as expected. The pre-experimental

polishing results that showed great improvement in surface roughness as well as texture allowed us to conclude that the gelatin-SiC-diamond media combination was effective at imparting polishing action/material removal to a workpiece. More detailed investigation into this abrasive compound may be particularly beneficial to the further study of the Flexolap polishing process.

10.4. Experimental Design and Results

The effects of multiple independent variables on various polishing outputs – notably surface roughness, maximum peak-to-peak height, surface texture, quality, and topography as well as impacting force, were investigated. Polishing time proved as expected in nearly all investigations, with surface roughness and peak-to-peak height generally showing a sharp initial decrease before converging to a limit. Polishing time seems to show a similar effect on texture/quality with longer times leading to the disappearance of previous lay and the overall flattening of form (much of the improvement occurs in the initial stages). Polishing time is not a factor in force measurements. Longer polishing time aids in decreasing the presence and size of adhered material, pits, particle pile up and brittle failure from grinding processes. When dry polishing conditions occur, higher polishing time leads to a larger presence of micro-scratches on the surface.

Media hydration in this study show varied results on surface roughness and maximum peak-to-peak height and this is because hydrational experiments were done over short time periods. The literature noted trends in initial surface roughness decline (gradient) of higher hydrated media being lower than that of lower hydrated medias do hold true though and higher hydrated media appears to take longer to reach surface roughness convergence from Flexolap polishing. Lower hydrated medias cause more surface scratching (particularly over longer times) while this occurrence is not apparent in higher hydrated medias, which also have a more uniform texture. Higher hydrated media appear to remove particle pull out and pits even over a short polishing time. Higher hydrated media tends to only cause smooth deformation on the surface of the workpiece and is more effective at removing undesirable effects from the surface grinding operation. When measuring impact force, higher hydrated medias provide less impact force than lower hydrated medias. This aligns well with the vibrational model developed.

For the largest part, impinging velocity shows results that were fully expected. Higher forces are measured at higher velocities and surface roughness/maximum peak-to-peak height generally decreased much faster than that measured at lower velocities. Desired surface textures are achieved faster with higher impinging velocities as well. Higher impinging velocities tend to cause more micro scratches (particularly at lower hydrational levels).Size of

material adherence and pits decrease faster at higher impinging velocities and the removal of particle pull out and deep grooves also occurs quicker at higher impinging velocities. The highest impinging velocity in this study is 31.4 m/s, which is only half of the highest impinging velocities of other researchers and so unexpected polishing changes may occur at higher impinging velocities (possibly surface damage or a limitation to the polishing effectiveness).

The effect of diamond concentration on polishing parameters is interesting with some unexpected results coming to surface. Higher diamond concentrations display larger surface roughness than lower diamond concentration when impinging velocity is higher while higher diamond concentration show lower surface roughness when impinging velocity is low. This could be due to the fact that at low impinging velocities, small deformations occur and thus more diamond particles are in contact with workpiece asperities. However, at higher impinging velocities, it may be that a large amount of diamond particles are forced onto the workpiece surface which create unaligned polishing action (where diamond particles no longer hit the workpiece at the designed polishing angle), thus causing a rougher surface.

All the above results aid greatly in either affirming previous researchers results or in providing data to parameters that had not been studied previously. These experimental results are also helpful in providing a large set of data on which to affirm or create empirical models.

This discussion has presented an interpretation and comparison of results while also highlighting any limitations present and showing how the research adds value to the field and to previous studies.

Chapter 11 - Conclusions

The conclusion of this dissertation serves to provide a summary of important results and how they relate to the research aims/questions as well as to highlight the contribution of this study to existing literature and research. Limitations on the overall study are provided as well.

The initial analytical polishing model showed polishing forces to increase from 0.0056 N for the lowest available impinging velocity (6.28 m/s) to 0.1403 N for the highest available impinging velocity (31.4 m/s). This increase was calculated to be exponential and matches with the exponential decrease in polishing time over the same velocity conditions (from 91.46 minutes to 0.25 minutes). Critical depth of cut was determined to be 2.53 mm for SLM Ti-6Al-4V and calculated deformations were below this by a factor of 10000. The analytical method showed the contact stresses increased logarithmically and were always greater than the theoretical shear to induce slip (7.2 GPa for SLM Ti-6Al-4V), for all impinging velocities.

The empirical polishing model showed forces to increase from 0.11 N at the low impinging velocity to 0.761 N at the high impinging velocity. For the micro interaction between diamond and Ti-6Al-4V asperity, the forces grew from 0.098 mN to 0.675 mN. Polishing time showed a similar exponential decrease (from 41.187 required minutes to 0.615 required minutes). Contact stresses grew from 5.469 GPa to 10.411 GPa for this model. The above two models are limited in that assumptions are made and if conditions reach out these assumptions, results may not prove prosperous.

The simulation model made use of the analytical model force results and areas as inputs and found contact stress to only be sufficient for ductile regime polishing to occur at impinging velocities of 15 m/s and greater. Workpiece deformation results were still much less than anything which could cause damage. Note that brittle failure was not calculated to occur using any of the above methodologies (brittle failure would occur at the shear modulus of Ti-6Al-4V, which is 45.2 GPa).

The vibrational model provides multiple important results. Firstly, the decrease in elastic modulus of the abrasive media (from 45 kPa to 0.52 kPa for hydration levels of 0% and 50% respectively) show the great influence that water has on the polishing process. Using the empirical model, forces were estimated to decrease as hydration was increased (and grow logarithmically over hydrational levels). The sharpest decrease is from 0% to 10% hydrational levels. These results agree well with the measured empirical force data. Contact time is also shown to increase from 20 μs to about 90 μs as hydration is increased from 0% to 50%. Damping ratio proves to decrease as hydration is increased and low kinetic energies show damping ratios close to critical. Damping coefficient decreases dramatically from 10% to 30%

(from about 0.09 Ns/m to about 0.06 Ns/m) and the change from 30% to 50% is much less (0.06 Ns/m to 0.05 Ns/m). Higher hydrated abrasive shows a much greater deformation (as expected) and thus a much lower contact stress. Unitless contact stress decreases from around 70% of the maximum at 10% hydration to 18% of the maximum at 50% hydration.

Abrasive selection was successful and the minimal dehydration of gelatin over time shows the applicability of the designed compound to its Flexolap polishing purpose. The initial polishing results (where a coin was polished to 0.075 μm in roughness and an aluminium plate was mirror finished to a roughness of 0.16 μm) aided in proving the effectiveness of the abrasive media compound and allowed for the conclusion that it is again applicable for the purpose. As is true for the following section, more study into adhesiveness of SiC and diamond to the viscoelastic core may aid in understanding the process better.

The machine design and development proved successful and its modularity and simplicity of use aids in presenting a machine ready for implementation to industry.

More in-depth detail to experimental results is shown in the discussion chapter and thus the mention of results in this chapter is limited to those most important and relevant. Greater polishing times and higher velocities generally allow for the achievement of surface finishes below 0.2 μm for Ti-6Al-4V components. All polishing surface roughness and maximum peak-to-peak plots over time show a great drop in roughness to a saturated value over the first 10 minutes. Higher hydrated media shows a low saturation value, but a greater time required to reach the saturated value (when compared to lower hydrated media). Hydration influence is particularly relevant when concerning surface texture and quality. Lower hydrated media tends to scratch the surface more and provides a much less uniform finish overall. Higher hydrated media also has a lesser force measurement. Higher impinging velocities decrease surface roughness at a much greater rate than that of lower impinging velocities (as expected) and tend to achieve more improved surface finishes more quickly. Higher impinging velocities also measure higher on impact force.

This following is a recommendation and summary on optimal conditions: polishing at higher impinging velocities (for this case, the maximum of 31.4 m/s) and at a medium-high hydration (30%) with sufficient time (greater than 25 minutes) should produce the most optimal polishing conditions for the Flexolap polishing of SLM produced Ti-6Al-4V components. As previous researchers have also stated, polishing at an angle of 45º, with a low stand-off distance (20 mm) will provide optimal polishing conditions. Diamond concentration should be made lower at high impinging velocities and high hydrational levels while it should be made higher at low impinging velocities.

Design and development of a Flexolap polishing machine was completed along with associated abrasive media development, model creations and experimental completion. This dissertation and its associated studies proved to be a success and the author hopes that further research will be completed by other students who are interested in the topic.

Chapter 12 – Recommendations

Following on from the previously presented discussions and conclusions, it is important to state recommendations to both further this research as well as to better it. These recommendations also serve to provide guidance to following students and to suggest paths upon which one can follow along their research journey.

Regarding machine design and development:

- Greater research into nozzle shape/size will help create a more controlled and focussed abrasive media shooting jet.
- Developing a singular electronic control system for abrasive output, pneumatic control, stirrer motor control and for other components may lead to greater industrial reach and an even easier to use process.

Regarding abrasive media:

- Diamond concentration does not seem to significantly affect the polishing process and output parameters, thus using a lower concentration of 0.1% will save resources.
- Using a thermoplastic abrasive core where viscoelasticity is controlled via a heat-controlled nozzle, may be a cheaper and more recyclable method of polishing.
- Using agar-agar will provide a vegan and more sustainable option than gelatin (with similar properties), especially if processed in house i.e., acquire seaweed, cryogenically grind it, and then use it as the viscoelastic abrasive core.

Regarding modelling:

- Furthering model development to other workpiece materials will provide plenty of further research opportunities.
- Incorporating the models into dynamic simulations will provide even more insight into the process.
- Incorporating the model into live analysis will allow for the development of an intelligent system that allows for process parameters to be controlled by the operator and thus allows for even greater industry interest.

The above recommendations and suggestions hope to aid other researchers and students in the further development of advanced manufacturing and to create a South African advanced manufacturing industry that is both competitive and successful (without the reliance on foreign processes).

References

[1] M. Razali, "Influence of surface modification by blast polishing method on the cutting performance of carbide tool," Toyohashi University of Technology, Toyohashi, 2016.

[2] J. Kozak, T. Zakrzewski, M. Witt and M. Debowska-Wasak, "Selected Problems of Additive Manufacturing Using SLS/SLM Processes," *Transactions on Aerosapce research,* vol. 1, no. 262, pp. 24-44, 2021.

[3] Y. Harada, Y. Ishida, D. Miura, S. Watanabe, H. Aoki, T. Miyasaka and A. Shinya, "Mechanical Properties of Selective Laser Sintering," *Materials,* vol. 13, no. 22, pp. 1 - 18, 2020.

[4] R. Kuppuswamy, S. Ozbayraktar and H. Saridikmen, "Aero-lap polishing of poly crystalline diamond inserts using Multicon media," *Journal of Manufacturing Processes,* vol. 14, no. 2, pp. 167-173, 2012.

[5] Y. Jhong, C. Chao, W. Hung and J. Du, "Effects of Various Polishing Techniques on the Surface Characteristics of the Ti-6Al-4V Alloy and on Bacterial Adhesion," *Coatings,* vol. 10, no. 1057, pp. 1-23, 2020.

[6] M. Fukumoto, K. Takai, M. Nizar, N. Arimatsu and M. Uemura, "Study on polishing mechanism of cemented carbide by blast polishing, 3rd Report: Influnece of water content in polsihing media on polishing mechanism," *Journal of the Japan Society for Abrasive Technology,* vol. 60, no. 5, pp. 261-266, 2016.

[7] R. Motsie, "An Overview of South Africa's Titanium Mineral Concentrate Industry," The Director: Mineral Economics, Pretoria, 2008.

[8] R. Hausmann and B. Klinger, "South Africa's export predicament*," *Economics of Transition,* vol. 16, no. 4, pp. 609-637, 2008.

[9] J. Fedderke and W. Simbanegavi, "South African Manufacturing Industry Structure and its Implications for Competition Policy," *Journal of Development Perspectives,* vol. 4, no. 1, pp. 134-189, 2008.

[10] G. Williams, S. Cunningham and D. De Beer, "Advanced Manufacturing and Jobs in South Africa: An Examination of Perceptions and Trends," in *International Conference on Manufacturing-Led Growth for Employment and Equality*, Johannesburg, 2014.

[11] J. Nicholson, "Titanium Alloys for Dental Implants: A Review," *Prosthesis,* vol. 2, pp. 100-116, 2020.

[12] C. Zhong, J. Liu, T. Zhao, T. Schopphoven, J. Fu, A. Gasser and J. Schleifenbaum, "Laser Metal Deposition of Ti6Al4V - A Brief Review," *Applied Sciences,* vol. 10, no. 764, pp. 1-12, 2020.

[13] J. Mountford, "Titanium-Properties, Advantages and Applications SOlving the Corrosion Problems in Marine Service," NACE International, Houston, TX, USA, 2002.

[14] K. Yamashita, K. Kitajima, K. Hamada and G. Kuratani, "Mirror polishing and Deburring Technology by AERO LAP," *J. Japan Soc. Abras. Technol.,* vol. 52, no. 2, pp. 66 - 69, 2008.

[15] K. Yamashita, "Deburring and Edge Finishing by Mirror-shot Polishing 'Aero Lap'," *Mach. Technol.,* vol. 58, no. 13, pp. 34 - 36, 2010.

[16] K. Kitajima and K. Yamashita, "Blast polishing by utilizing of multi-corn media," *J. Japan Soc. Abras. technol.,* vol. 50, no. 9, pp. 505 - 508, 2006.

[17] H. Sakaeju, "Mirror-shot polishing technique," *Mach. Technol.,* vol. 54, no. 10, pp. 29 - 31, 2006.

[18] H. Huang, Z. Gong, X. Chen and L. Zhou, "Robotic grinding and polishing for turbine-vane overhaul," *Journal of Materials Processing Technology,* vol. 127, no. 2, pp. 140-145, 2002.

[19] S. Lee, Z. Ahmadi, J. Pegeus, M. Majouri-Samani and N. Shamsaei, "Laser polishing for improving fatigue performance of additive manufactured Ti-6Al-4V parts," *Optics and Laser Technology,* vol. 134, pp. 1-12, 2021.

[20] K. Kitajima and A. Yamamoto, "Latest Trends in Deburring Technology," *International Journal of Automation Tehcnology,* vol. 4, no. 1, pp. 4-8, 2010.

[21] J. S. Assocation, *Edge quality and its grades for material removal parts,* JIS B0721, 2004.

[22] S. Kalpakjian and S. Schmid, Manufacturing Engineering and Technology, New Jersey, USA: Prentice Hall (Pearson), 2009.

[23] K. Minaki, K. Kitajimi, K. Minaki, M. Izawa and K. Tosha, "Study on improvement of surface texture of stainless steel by utilizing dry blasting," *Key Engineering Materials,* vol. 50, no. 8, pp. 477-482, 2006.

[24] K. Takai, M. Nizar, M. Uemura and M. Fukumoto, "Polishing mechanism of cemented carbide using blast polishing process, 1st report: Effects of injection speed and polishing time on surface roughness," *Journal of the Japan Society for Abrasive Technology,* vol. 57, no. 4, pp. 253-258, 2013.

[25] K. Takai, M. Nizar, M. Uemura and M. Fukumoto, "Study on the polishing mechanism of cemented carbide using blast polishing process, 2nd report: Effect of kinetic energy and injection angle on surface condition of cemented carbide," *Journal of the Japan Society for Abrasive Technology,* vol. 58, no. 6, pp. 386-391, 2014.

[26] M. Nizar, N. Arimatsu, H. T. K. Kawamistu and M. Fukumoto, "Study on optimal surface property of WC-Co cutting tool for aluminium alloy cutting," in *IOP Conference Series: Materials Science and Engineering 114 012024*, Vancouver, Canada, 2016.

[27] J.-P. Cheon and Y.-S. Pyoun, "Evaluation Tool Life and Cutting Characteristics of carbide Hob TiAlN Coating Surface Polishing Using Aero Lap Polishing Technology and Multi-con," *Journal of the Korean Society of Manufacturing Technology Engineers,* vol. 21, no. 5, pp. 848-854, 2012.

[28] A. Kubota, S. Motoyama and M. Touga, "Surface smoothing of a polycrystalline diamond using an iron-plate-H2O2 chemical reaction," *Diamond and Related Materials,* vol. 69, pp. 96-101, 2016.

[29] J. Watanabe, M. Touge and T. Sakamoto, "Ultraviolet-irradiated pecision polishing of diamond and its related materials," *Diam. Relat. Mater.,* vol. 39, no. 2013, pp. 14-19, 2013.

[30] R. Ramesham and M.F. Rose, "Polishing of polycrystalline diamond by hot nickel surface," *Thin Solid Films,* vol. 320, pp. 223-227, 1998.

[31] A. Zaitsev, G. Kosaca, B. Richarz, V. Raiko, R. Job, T. Fries and W. Fahrner, "Thermo-chemical polishing of CVD diamond films," *Diam. Relat. Mater. ,* vol. 7, pp. 1108-1117, 1998.

[32] Y. Chen, L. Zhang and J. Arsecularatne, "Polishing of polycrystalline diamond by the tecnique of fynamic friction. Part 2: material removal mechanism," *International Journal of Machine Tools & Manufacture,* vol. 47, pp. 1615-1624, 2007.

[33] M. Carvalhao and A. Dionisio, "Evaluation of mechanical soft-abrasive blasting and chemical cleaning methods on alkyd-paint graffiti made on calcareous stone," *Journal of Cultural Heritage,* vol. 16, pp. 579-590, 2015.

[34] D. Hansel, "Abrasive blasting systems," *Metal Finishing,* vol. 98, no. 6, pp. 26-28, 30-32, 34-42, 2000.

[35] Okamoto, "Mirror Finishing Technology for Improvement of Mold Releasbaility," MReport, 9 May 2020. [Online]. Available: https://www.mreport.co.th/en/experts/technology/015-Mirror-Finishing-Technology-for-Mold-Releasability-Okamoto-Aero-Lap. [Accessed 24 November 2021].

[36] D. Draganovska, G. Izarikova, A. Guzanova and J. Brezinova, "General Regression Model for Prediciting Surface Topography after Abrasive Blasting," *metals,* vol. 8, no. 11, pp. 1-21, 2018.

[37] J. Brezinova, A. guzanova and D. Dragonovska, Abrasive Blast Cleaning and Its Application, Pfaffikon, Switzerland: Trans Tech Publications, 2015; p 107.

[38] T. Klusner, F. Zielbauer, S. Marsoner, M. Deller, M. Morstein and C. Mitterer, "Influence of surface topography on early stages on steel galling of coated WC-Co hard metals," *Int. Journal of Refractory metals and Hard Materials,* vol. 57, pp. 24-30, 2016.

[39] B. Podgornik, S. Hogmark and O. Sandberg, "Influence of surface roughness and coating type on the galling properties of coated forming steel," *Surf. Coat. Technol.,* vol. 184, pp. 338-348, 2004.

[40] J. Greenwood and J. Tripp, "The Elastic Contact of Rough Spheres," *Journal of Applied Mechanics,* vol. 34, no. 1, pp. 153-159, 1967.

[41] J. Greenwood and J. Williamson, "Contact of Nominally Flat Surfaces," *Proceedings of the Royal Society (London),* vol. A295, pp. 300-319, 1966.

[42] W. Chang, I. Etsion and D. Bogy, "An Elastic-Plastic Model for the Contact of Rough Surfaces," *Journal of Tribology,* vol. 109, pp. 257-263, 1987.

[43] L. Kogut and I. Etsion, "Elastic-Plastic Contact Analysis of a Sphere and a Rigid Flat," *Journal of Applied Mechanics,* vol. 69, pp. 657-662, 2002.

[44] T. Stolarski, Tribology in Machine Design, London: Butterworth-Heinemann, 1999.

[45] G. Naghieh, H. Rahnejat and Z. Jin, "Contact Mechanics of viscoelastic layered surfaces," in *Transactions on Engineering Sciences, vol 14.*, Bradford, United Kingdom, 1997.

[46] Q. de Jongh, M. Titus and R. Kuppuswamy, "A Force Controlled Polihsing Process Design, Analysis and Simulation Targeted at Selective Laser Sintered Aero-Engine Components," in *International Conference on Competitive Manufacturing*, Stellenbosch, South Africa, 2020.

[47] Y. Zhao, D. Maietta and L. Chang, "An asperity microcontact model incorporating the transition from elastic deformation to fully plastic flow," *Journal of Tribology,* vol. 122, no. 1, pp. 86-93, 2000.

[48] M. Achtsnick, P. Geelhoed, A. Hoogstrate and B. Karpuschewski, "Modelling and evaluation of the micro abrasive blasting process," *WEAR,* vol. 259, pp. 84-94, 2005.

[49] D. Marshall, B. Lawn and A. Evans, "Elastic/Plastic indentation damage in ceramics: the lateral crack system," *J. Am. Ceram. Soc.,* vol. 65, no. 11, pp. 561-566, 1982.

[50] B. Karpuschewski, A. M. Hoogstrate and M. Achtsnick, "Simulation and Improvement of the Micro Abrasive Blasting Process," *CIRP Annals,* vol. 53, no. 1, pp. 251-254, 2004.

[51] A. Hoogstrate, B. Karpuschewski, C. van Luttervelt and H. Kals, "Modelling of High Velocity Loose Abrasive Processes," *Annals of the CIRP,* vol. 51, no. 1, pp. 263-266, 2002.

[52] B. Karpuschewski, A. Hoogstrate and M. Achtsnick, "Influence of the Nozzle Shape on Surface Quality and Efficiecny During Micro-Abrasive-Air-Jetting (pgs 263 - 271)," ICMEN, Kassandra, Greece, 2002.

[53] N. Feldmann and F. H. B. Bause, "B1.4 - Determining fractional Zener model parameters from low frequency DMA measurement," in *AMA Conferences 2017*, Nurnberg, Germany, 2017.

[54] H. Schiessel, R. Metzler, A. Blumen and T. Nonnenmacher, "Generalized viscoleastic models: theri fractional equations with solutions," *J. Phys. A: Math Ge.,* vol. 28, pp. 6567-6584, 1995.

[55] M. Bulicek and J. Malek, "ON KELVIN-VOIGT MODEL AND ITS GENERALIZATIONS," *Evolution Equations and control Theory,* vol. 1, no. 1, pp. 17-42, 2012.

[56] A. Assie, M. Eltaher and F. Mahmoud, "Modelling of viscoelastic contact-impact problems," *Applied Mathematical Modelling,* vol. 34, no. 1, pp. 2336-2352, 2010.

[57] S. Kucharski, T. Klimczak, A. Polijaniuk and K. J, "Finite-elements model for the ccontact of rough surfaces," *Wear,* vol. 177, no. 1, pp. 1-13, 1994.

[58] V. Yasterbov, J. Durand, H. Proudhon and G. Cailletaud, "Rough surface contact analysis by means of the Finite Element Method and of a new reduced model," *C.R. Mecanique,* vol. 339, pp. 473-490, 2011.

[59] G. Maliaris, C. Gakias, M. Malikoutsakis and G. Savaidis, "A FEM-Based 2D Model for Simulation and Qualitative Assessment of Shot-Peening Processes," *Materials,* vol. 14, no. 2784, pp. 1-14, 2021.

[60] A. W. Hashmi, H. S. Mali and A. Meena, "A critical review of modeling and simulation techniques for loose abrasive based machining processes," in *materialstoday: proceedings*, 2021.

[61] N. Dallinger and J. Hubler, "Simulation of bottle conveyors - Opportunities of the Discrete Element Method (DEM)," in *Conference: 3. International Symposium Plastic-Slide-Chain an Tribology in Conveyor Systems*, Chemnitz, 2017.

[62] D. Hansel, "Abrasive Blasting Systems," Clemco Industries Corp, Burlingame, California, USA, 1997.

[63] A. Amar and P. Tandon, "Investigation of gelatin enabled abrasive water slurry jet machining (AWJSM)," *CIRP Journal of Manufacturing Science and Technology,* vol. 33, pp. 1-14, 2021.

[64] Blastrite, "Blasting abrasives," Blasrite, 2019. [Online]. Available: https://www.blastrite.co.za/products/blasting-abrasives.html. [Accessed 01 08 2022].

[65] S. Schwarz, B. Hartmann, J. Sauer, R. Burgkart, S. Sudhop, D. Rixen and H. Clausen-Schaumann, "Contactless Vibrational Analysis of Transparent Hydrogel Structures Using Laser-Doppler Vibrometry," *Experimental Mechanics,* vol. 60, p. 1067–1078 , 2020.

[66] M. Donachie, Titanium: A Technical guide, 2nd edition, ASM International, 2000.

[67] V. André, R. Henriques, P. Paulo, D. Campos, C. Alberto, A. Cairo and J. Carlos, "Production of Titanium Alloys for Advanced Aerospace Systems by Powder Metallurgy," *Mater. res.,* vol. 8, no. 4, pp. 443-446, 2005.

[68] N. M. Dhansay, "Fracture Mechanics Based Fatigue and Fracture Toughness Evaluation of SLM Ti-6Al-4V," University of Cape Town, Cape Town, South Africa, 2015.

[69] P. Mercelis and J. Kruth, "Residual stresses in selective laser sintering and selective laser melting"," *Rapid Prototyp. J.,* vol. 5, no. 12, pp. 254-256, 2006.

[70] M. Benedetti, M. Cazzoli, V. Fontanari and M. Leoni, "Fatigue limit of Ti6Al4V alloy produced by Selective Laser Sintering," in *21st European Conference on Fracture*, Catania, 2016.

[71] E. Atzeni, S. Genna, E. Menna, G. Rubino, A. Salmi and F. Trovalusci, "Surface Finishing of Additive Manufactured Ti-6Al-4V Alloy: A Comparison between Abrasive Fluidized Bed and Laser Finishing," *Materials,* vol. 14, no. 5366, pp. 1-14, 2021.

[72] L. Lizzul, M. Sorgato, R. Bertolini, A. Ghiotti and S. Bruschi, "Surface finish of additively manufactured Ti6Al4V workpieces after ball end milling," in *18th CIRP Conference on Modeling of Machining Operations*, Ljubljana, Slovenia, 2021.

[73] S. Bagehorn, T. Meterns, D. Greitemeier, L. Carton and A. Schoberth, "Surface finishing of additive manufactured Ti-6Al-4V - a comparison of electrochemical and mechanical treatments," in *6th European Conference for Aerospace Sciences*, Munich, Germany, 2015.

[74] R. L. Jackson, H. Ghaednia, H. Lee and A. Rostami, "Contact Mechanics," in *Tribology for Scientists and Engineers*, New York, Springer Science+Business Media, 2013, pp. 93-132.

[75] T. Bifano, T. Dow and R. Scattergood, "Ductile-Regime Grinding: A New Technology for Machining Brittle Materials," *ASME Journal of Engineering for Industry,* vol. 113, no. 2, pp. 184-189, 1991.

[76] R. Jackson, I. Chusoipin and I. Green, "A Finite Element Study of theResidual Stress and Deformationin Hemispherical Contacts," *Journal of Tribology,* vol. 127, no. 1, pp. 484-493, 2005.

[77] MISUMI, "Flat Belt Pulleys & Idlers," MISUMI, [Online]. Available: https://us.misumi-ec.com/vona2/mech/M1100000000/M1102000000/M1102020000/. [Accessed 15 February 2022].

[78] R. C. Juvinall and K. M. Marshek, Machine Component Design (Fifth Edition), Singapore: John Wiley and Sons, 2012.

[79] Misumi, "Belt Specifications," 2012. [Online]. Available: https://us.misumi-ec.com/pdf/fa/2012/p1_1097.pdf. [Accessed 19 April 2022].

[80] SKF, "62/22," SKF, 2022. [Online]. Available: https://www.skf.com/africa/en/products/rolling-bearings/ball-bearings/deep-groove-ball-bearings/productid-62%2F22. [Accessed 19 April 2022].

[81] Schmalz, "SEC-400," Schmalz, 2022. [Online]. Available: https://www.schmalz.com/en/vacuum-technology-for-automation/vacuum-components/special-grippers/feed-ejectors/feed-ejectors-sec-306349/10.02.01.00080. [Accessed 17 February 2022].

[82] Thermo Fisher Scientific Phenom-World BV, "Different types of SEM Imaging - BSE and Secondary Electron Imaging," AZO Materials, 4 August 2017. [Online]. Available: https://www.azom.com/article.aspx?ArticleID=14309. [Accessed 25 January 2022].

[83] J. I. Goldstein, D. E. Newbury, J. R. Michael, N. W. Ritchie, J. H. J. Soctt and D. C. Joy, "Scanning Electron Microscopy and X-ray analysis," in *SEM Image Interpretation*, New York, Springer, 2018, pp. 111-121.

[84] S. Pal, G. Lojena, R. Hudak, V. Rajtukova, T. Brajlih, V. Kokol and I. Drstvenšek, "As-fabricated surface morphologies of Ti-6Al-4V samples fabricated by different laser processing parameters in selective laser melting," *Additive Manufacturing,* vol. 33, no. 101147, 2020.

[85] X. Ke, W. Wu, C. Wang, Y. Yu, B. Zhong, Z. Wang, T. Wang, J. Fu and J. Guo, "Material Removal and Surface Integrity Analysis of Ti6Al4V Alloy after Polishing by Flexible Tools wih Different Rigidity," *materials,* vol. 15, no. 1642, pp. 1-15, 2022.

[86] X. Shen, X. Song, X. Wang and F. Sun, "Grinding characteristics of CVD diamond grits in single grit grinding of SiC ceramics," *The Internation Journal of Advanced Manufacturing Technology,* vol. 114, pp. 2783-2797, 2021.

[87] G. Maliaris, C. Gakias, M. Malikoutsakis and G. Savaidis, "A FEM-Based 2D Model for Simulation and Qualitative Assessment of Shot-Peening Processes," *Materials,* vol. 14, no. 2784, pp. 1-14, 2021.

Appendix - Additional Design Information

List of Figures for Appendix

Additional information pertaining to design and development of the polishing machine is presented here (additional images to aid in visualising the development as well as drawings to aid in the understanding of component design).

An attempt at designing a nozzle for more directed output was attempted. This involved creating a lofted cut inside a two-piece output adaptor (which has a rectangular output when attached together). Flats were created on the adaptor to allow for tightening of the thread into the impeller housing with a spanner. The nozzle was implemented into the design; however, it caused a backlog of abrasive particles to become stuck in the nozzle and created minimal abrasive output. This happened because different output velocities made the output path longer or shorter (and changed the angle of output slightly). This meant that the abrasive would bounce off the lofted cut and around the internal body instead of being directed straight out. The two following drawings of the bottom and top of the nozzle illustrate the design process.
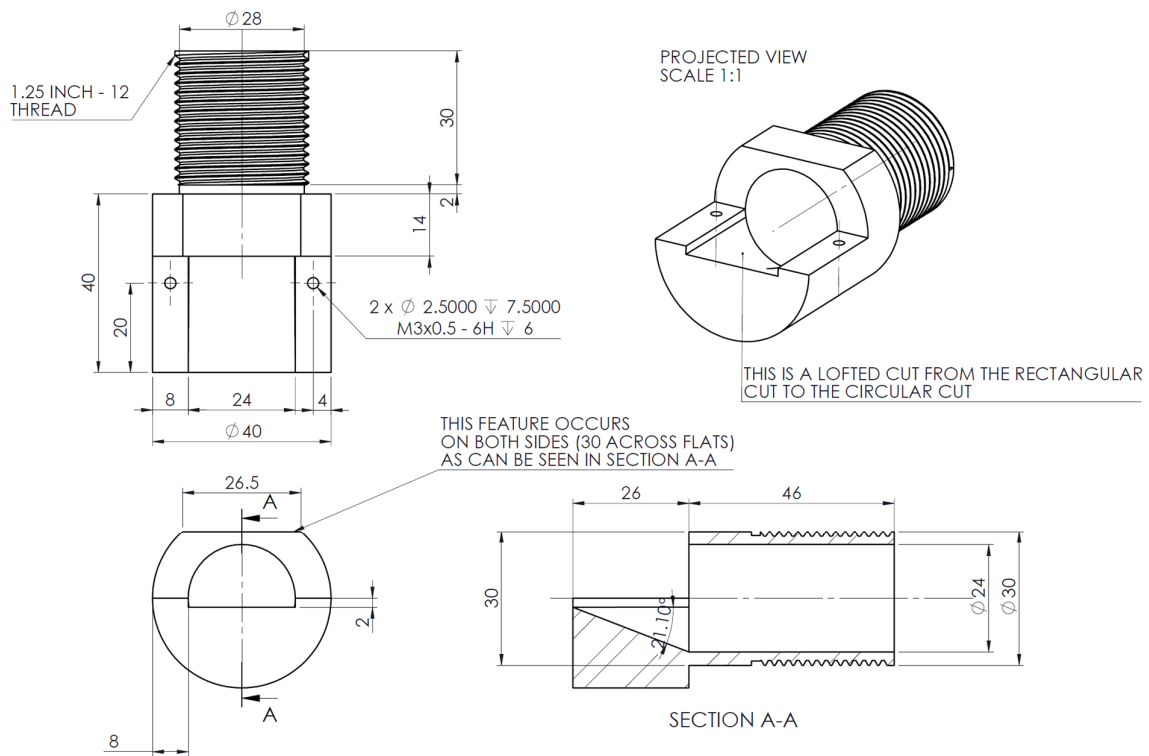
Figure A1 - Bottom of Nozzle Output

21.10°

LOFTED CUT
AS IN CRO001

SECTION E-E

2 X
Ø 3.50 THRU
Ø 6.50 ⊽ 7

R12

R20

8   24   2

PROJECTED VIEW
SCALE 2:1

Scale: 2:1 on A4	University of Cape Town Department of Mechanical Engineering			
Drawn By: QUINTIN DE JONGH	All un-toleranced dimensions to adhere to ISO 2768-m	Title: TOP ADAPTOR CRO		
Checked :	Material : Plain Carbon Steel	Drawing Number : CRO002	Rev. : A	Sheet : 1 of 1
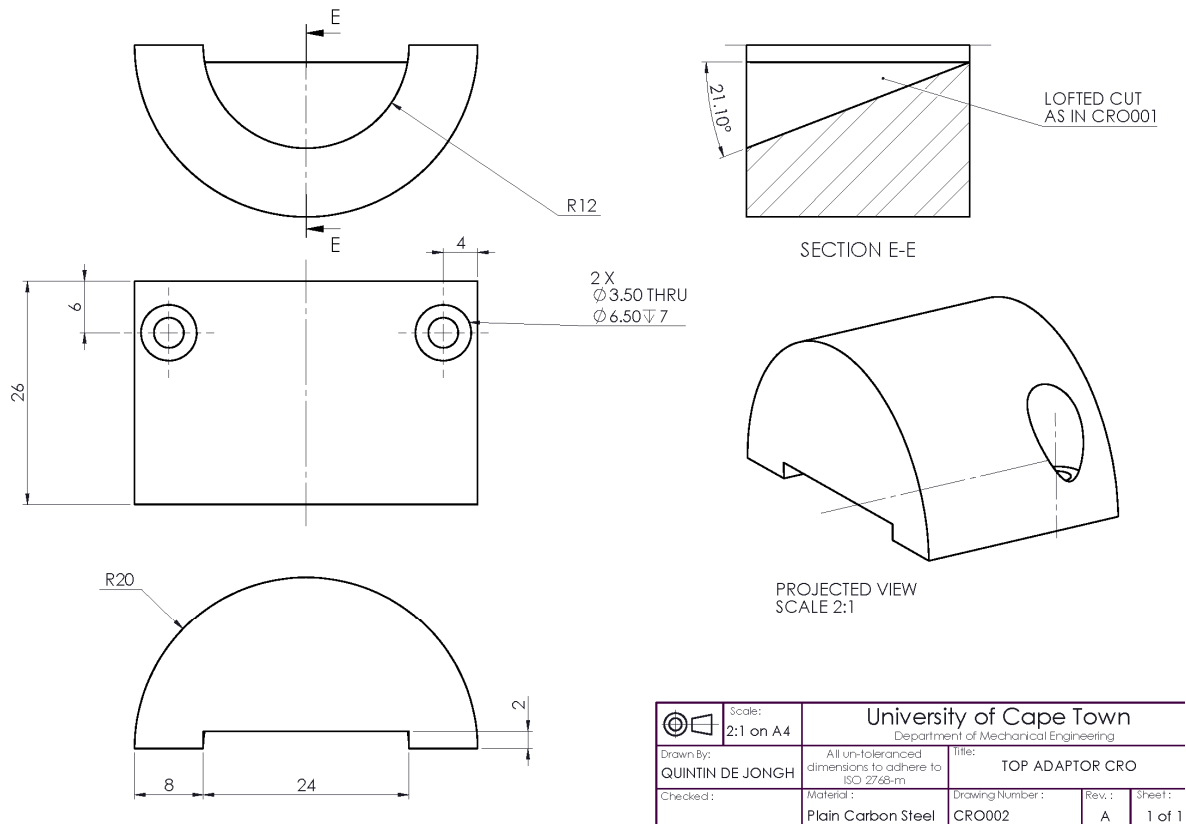
Figure A2 - Top of Nozzle Output

The figure below shows the impeller and flat pulley attached to either side of the precision grinding spindle (this forms a subassembly of the abrasive discharge system).

Figure A3 - Impeller Spindle Assembly

The two images below show the physical development and implementation of the designed subassembly. It should also be noted that a belt tensioning base plate was acquired to allow for proper tensioning and locating of the belt and pulleys relative to each other.

Figure A5 - Partially Assembled Abrasive Discharge System

Figure A4 - Fully Assembled Abrasive Discharge System

The figure below shows the blackening of the bin and hopper (to prevent oxidation) which form part of the abrasive recycling system).

Figure A6 - Blackened Bin and Hopper

The figure below shows the clear hose used for abrasive transport as well as all hose connectors and the feed ejector.

Figure A7 - Hose System

The figure below shows the design of the abrasive stirrer, consisting of a DC motor, a shaft coupling (with set screws), a sized shaft and a secured radial impeller (which was 3D printed).
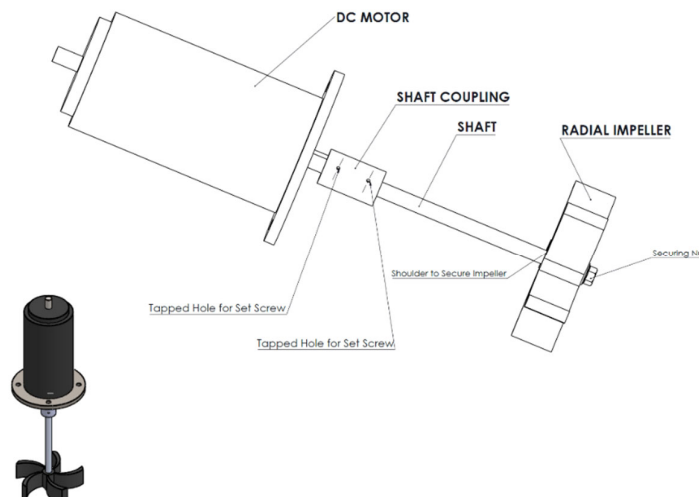
Figure A8 - Stirrer Assembly

The figures below show some images of the parts used in the system. The 6mm mesh is shown as well as the DC stirrer motor, the 3D printing process for the impeller and the feed ejector fitting into the designed and developed housing.

Figure A10 - 6mm Mesh

Figure A9 - DC Motor
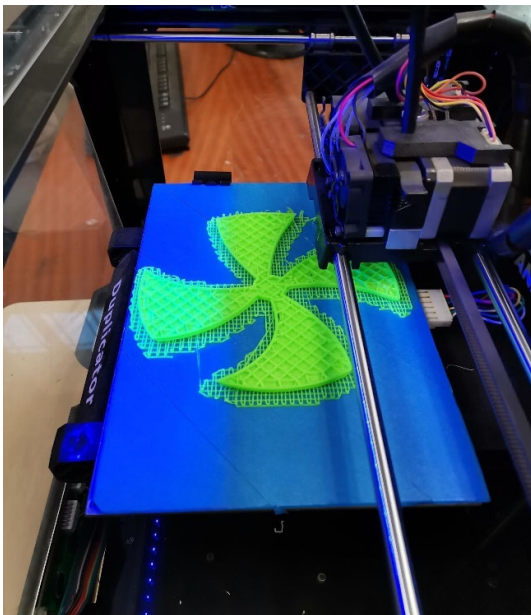
Figure A11 - 3D Printing of Impeller
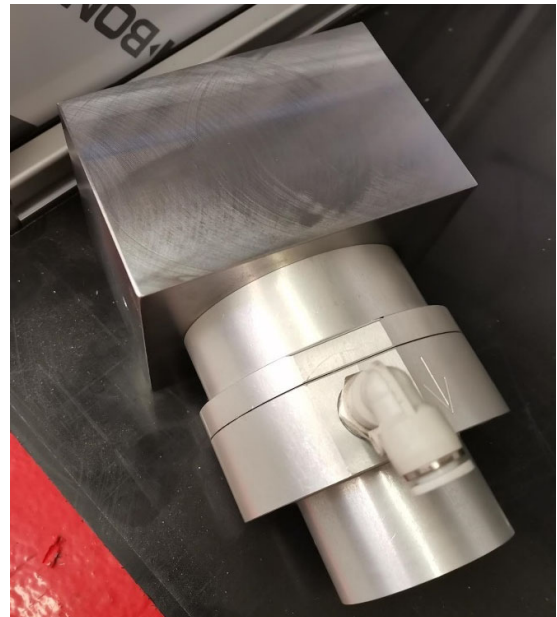
Figure A12 - Feed Ejector and Housing

When designing the hopper and bin, where welds were required, weld calculations were completed to ensure that the hopper could be held properly in the frame, and so that all parts would be held together under the forces of gravity (and so that the bin could properly support the relatively large stirrer motor). The bin calculations (for parts which hold the stirrer motor) are outlined below (these were extended to the hopper as well). The combined motor and support mass is 14.452kg.

$$P = (m_{motor} + m_{support}) * g = 141.726N \qquad \text{(A1)}$$

The distance from the centre of gravity of the support plate to the weld is 100mm (a) and the length of sheet metal pieces is 302mm (b). The sheet metal thickness is 3mm (h).

The bending stress experienced is thus:

$$\sigma_b = \frac{6Pa}{bh^2} \qquad \text{(A2)}$$

For the above stated parameters, the bending stress experienced is 31.286MPa. Based on fluctuating motor loads, a reserve factor of 3 was chosen (meaning that the maximum weld capacity should be greater than $3 * \sigma_b = 93.858MPa$). The lowest maximum weld capacity for the used sheet steel is 462MPa, therefore the weld strength was determined to be more than acceptable for the design. The motor is by far the heaviest component placed on sheet metal with the shortest contact length (least support), and calculations show that the hopper welds hold fine in the frame, thus weld calculations are complete.

Figure A13 - Cardboard Hopper Prototype

The figure above shows a cardboard prototype of the hopper that was made before manufacture of the sheet steel part.

The abrasive transportation system (as well as the internal workings of the machine) is shown in the figure below. The attachment of the end of the hose to the impeller input can be seen.

Figure A14 - Internal Workings of Machine

The three figures below show features of the completed and installed electrical network Single phase electricity was used, and this task enabled me to learn a fundamental new skill on how to work with electrical components.
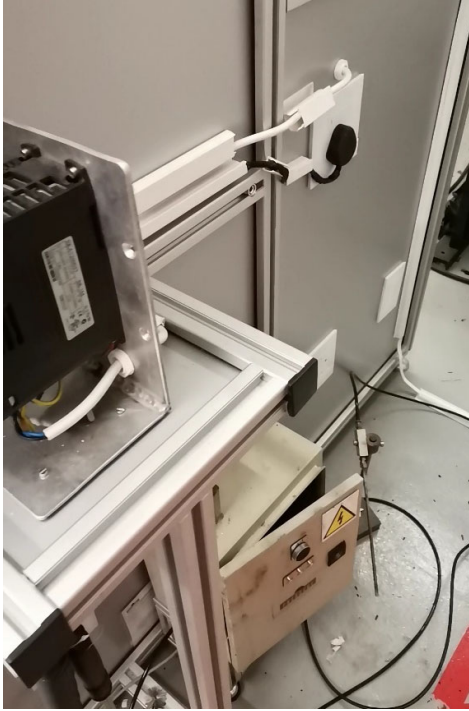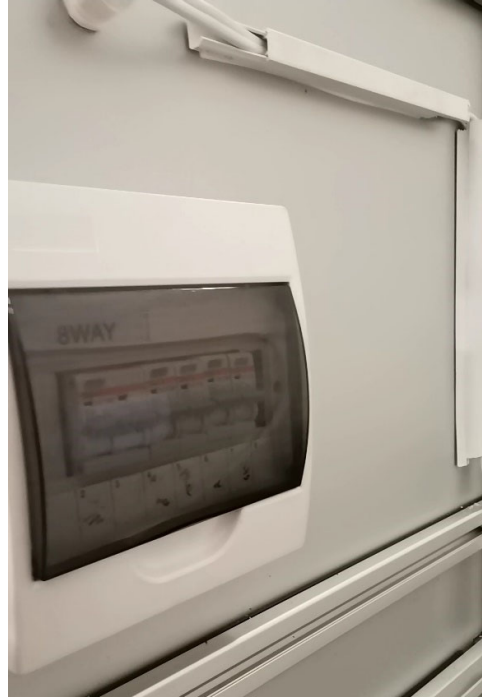

Figure A16 - Wiring and Conduit

Figure A15 - Distribution Board

Figure A17 - Internal Distribution Board

The figures below and on the following page show all the various components of the pneumatic system. The MQH outlet (fed via a mixture of compressed air and water i.e., mist) is shown, while shows the FRL with its control (the knob on top), its outlet (orange pipe) and the inlet (slightly covered by the black fitting). shows the exit of abrasives and compressed air (the open end of the pneumatic system). and show the ball valve controls for the FRL and MQH units as well as the inlet from the compressed air (thicker black pipe). Finally, shows the compressed air inlet to the feed ejector.

Figure A18 - MQH Attached with Stirrer and Abrasives

Figure A20 - FRL

Figure A19 - Inlet to Impeller
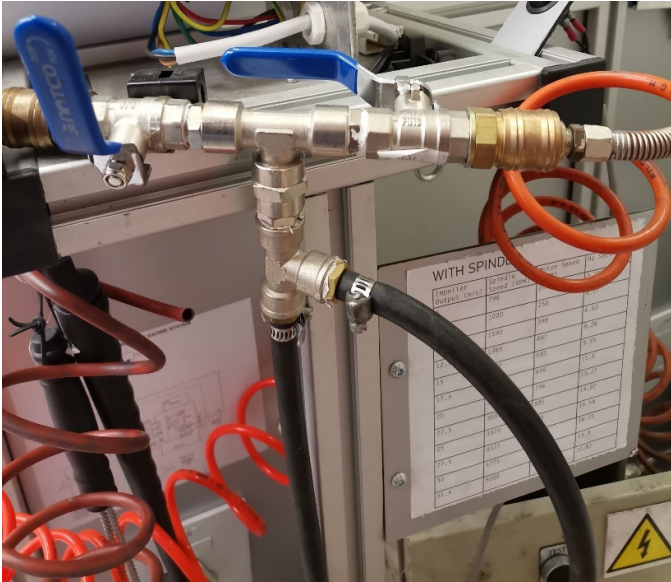
Figure A23 - Pneumatic Control

Figure A21 - Ball Valve

Figure A22 - Compressed Air to Feed Ejector

The figures below and on the following page show images of the partially built machine.

Figure A25- Partially built A

Figure A24 - Flaps

Figure A26- Glove Holes
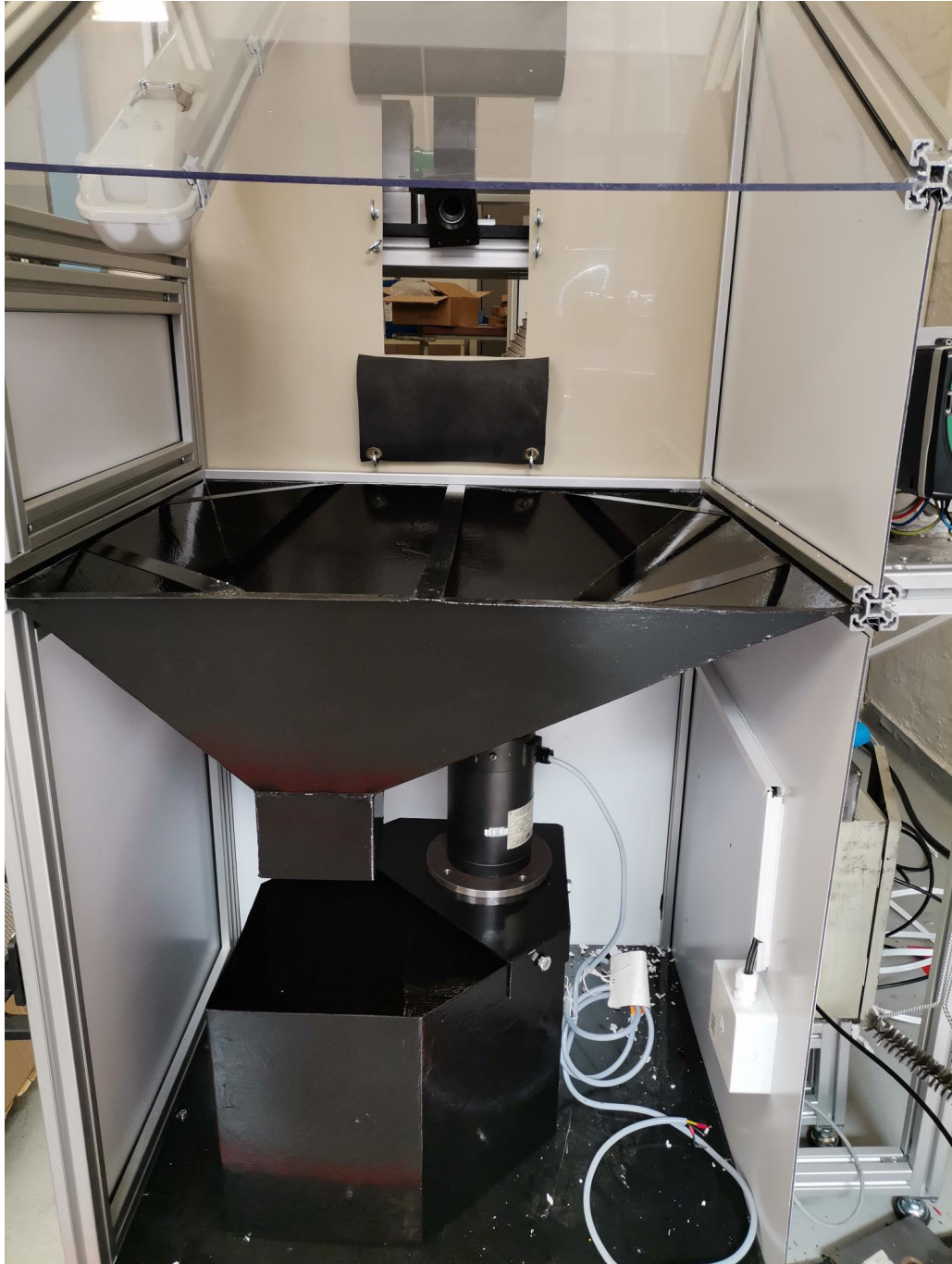
Figure A27- Partially Built B

The drawings on the next two pages show the bin body sheet metal drawing as well as the bin assembly, hopper assembly and abrasive discharge assembly drawings.
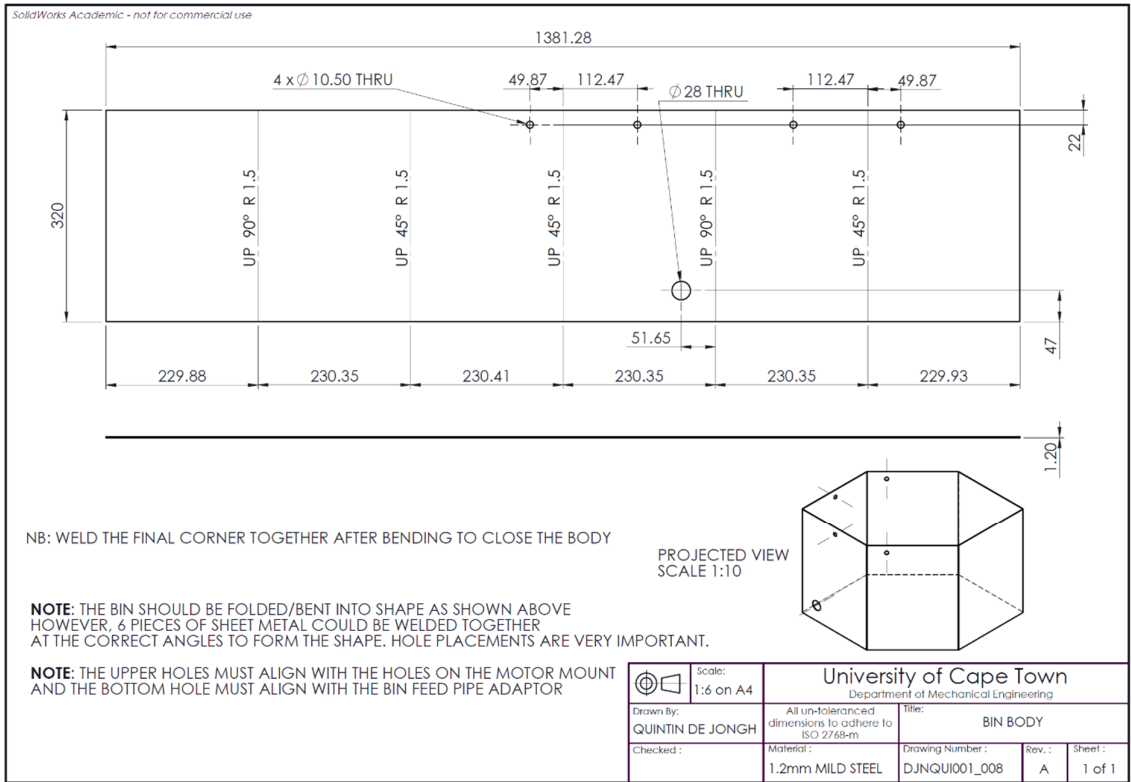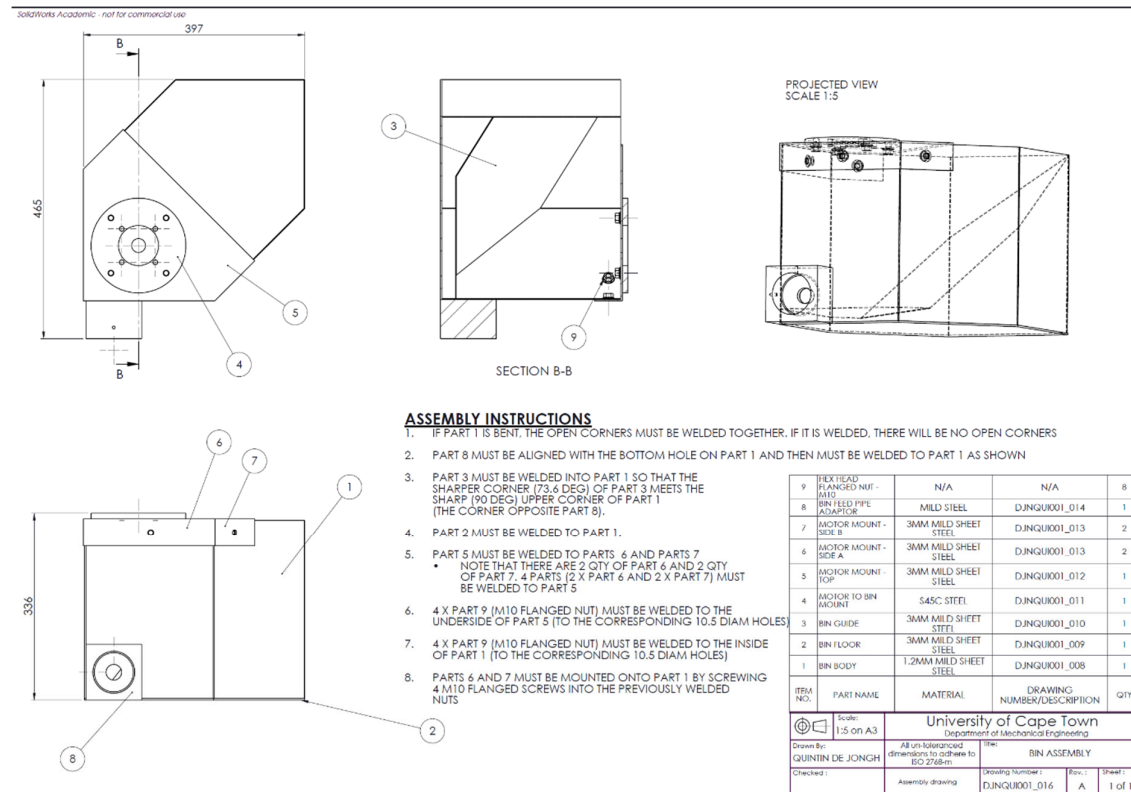
Figure A29 - Bin Body

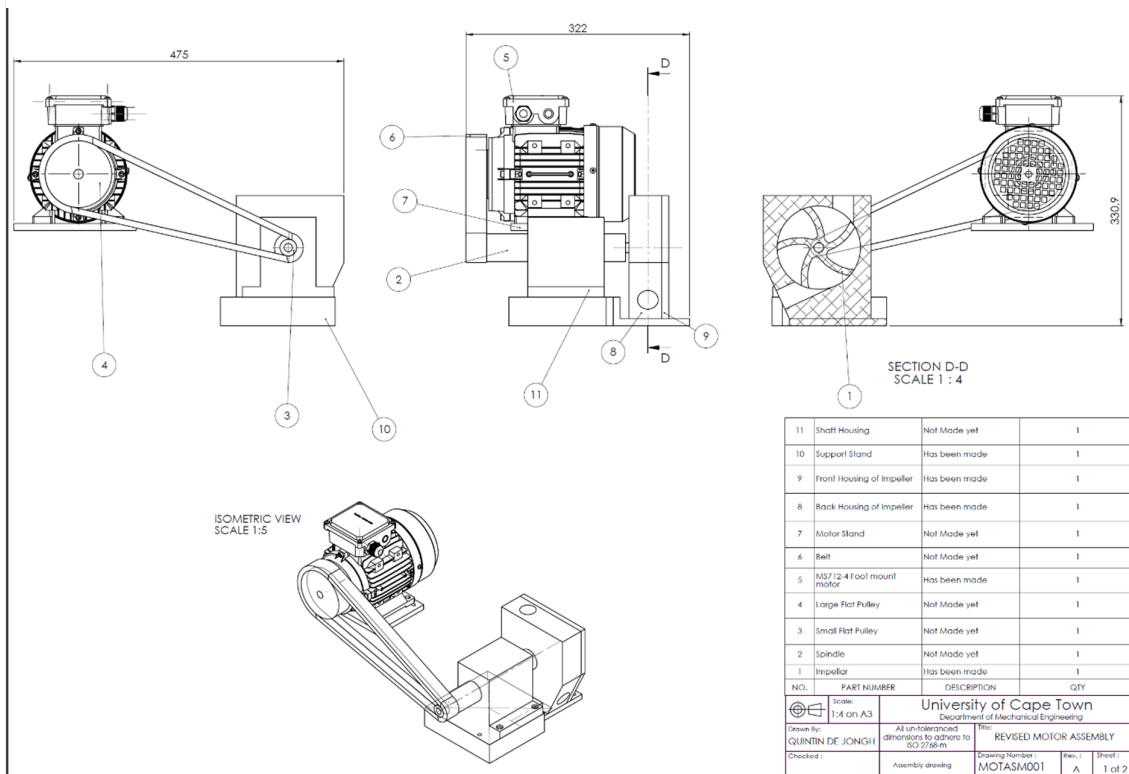*Figure A28 - Bin Assembly*
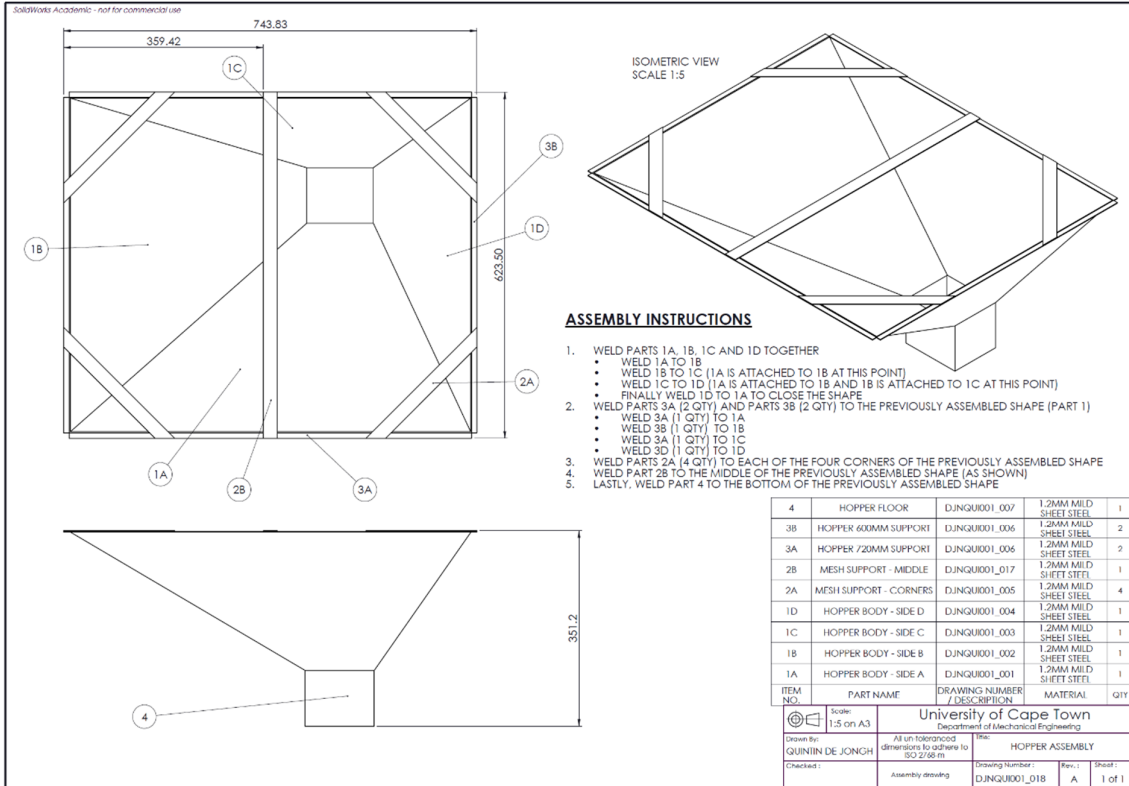
Figure A31 - Hopper Assembly

Figure A30 - Abrasive Discharge Assembly

A guide to use for the machine was created and consists of all the necessary details required to operate the machine (including additional features such as abrasive preparation, emergency stops and maintenance). A snippet of the table of contents can be seen below:

Table of Contents
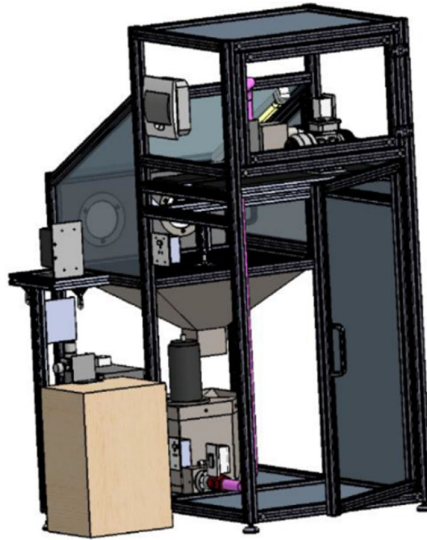
Page **3** of **29**

Figure A32 – Table of Contents for Guide to Use of Flexolap Machine